

# **The Volcanic Development and Petroleum System Evolution of the Faroe-Shetland Basin**

**Benjamin Stephen Allen**

Submitted in accordance with the requirements for the degree of  
Doctor of Philosophy

The University of Leeds  
School of Earth and Environment

October 2016

## **Declaration**

The candidate confirms that the work submitted is his own and that appropriate credit has been given where reference has been made to the work of others.

This copy has been supplied on the understanding that it is copyright material and that no quotation from the thesis may be published without proper acknowledgement.

The right of Benjamin Stephen Allen to be identified as Author of this work has been asserted by him in accordance with the Copyright, Designs and Patents Act 1988.

© 2013 The University of Leeds and Benjamin Stephen Allen

## Acknowledgements

I would first like to express my profound gratitude to Dr Douglas Paton, without whom this project would not have been possible. Your support, guidance and encouragement from the initial project conception through to its final completion has been incalculable. I would also like to thank Dr Dan Morgan for his invaluable scientific contribution, as well as his supreme editing and proof-reading skills and Dr Dave Cornwell for his contribution and continued support throughout the project.

I would like to thank E.ON Ruhrgas for funding this study and giving me the freedom to control the direction of the project. In particular, I would like to thank Dr Ann Watkins, Pablo Palmero, and Neil Sturman for their advice, support and encouragement throughout. I am also grateful to PGS and TGS for the provision of data and to Schlumberger, Badleys and dGB Earth Sciences for providing the data analysis tools.

I would like thank my friends and colleagues within the School of Earth and Environment, especially James Norcliffe, Tobias Dalton, Dave Price, Simon Oldfield, Diego Constantino, Ben Craven, Holly Rowlands, and a huge number of others. Your friendship, advice and scientific input has made the whole PhD experience a rewarding and enjoyable one.

To my sisters Sophie and Jayne Allen, thank you for your support throughout the years and for providing light relief during stressful times.

Finally I would like to thank my parents for their unwavering encouragement, the emotional and financial support you've given during this project and throughout my education has been immeasurable, without you none of this would have been possible. I am eternally grateful for all you have done.

## **Abstract**

The large volume of intrusive igneous material associated with volcanic rift margins introduces significant uncertainty to both hydrocarbon exploration and subsequent prospectivity. Understanding the habit, emplacement and distribution of such material in the context of rift evolution is essential to understanding the evolution of volcanic rift margins. The recent availability of high-quality 3D seismic data from the rift basins of the NE Atlantic Margin has enhanced our understanding of the 3D geometry and emplacement mechanisms of sill intrusions. Although how these intrusions fit within the wider margin context is often overlooked. The West of Shetland area provides an insight into the process of volcanic rift interaction in a petroleum prospective area.

Using multi-client 2D and 3D seismic data this study places reservoir scale observations of sill morphology, distribution and sill-fault interactions within a wider basin context. The study demonstrates that the style and volume of sill intrusion is heavily influenced by the large scale basin structure, the position along the volcanic margin and small scale structural heterogeneities. Given the variations in sill size and frequency there are also implications for the bulk intrusive magma distribution across the margin. Predicting hydrocarbon prospectivity in frontier, or under-explored basins, is inherently uncertain. In order to reduce this uncertainty, sensitivity analysis is performed on key modeling input parameters to define a best practice workflow for undertaking basin modeling in the Faroe-Shetland Basin and similar passive continental margin settings. As the emplacement of igneous intrusions into sedimentary successions has been shown to locally elevate heat flow, the sill complex is incorporated into the regional 2D modeling to investigate the effect sill emplacement has on hydrocarbon prospectivity.

The results highlight the importance of determining the timing of emplacement and the volume of igneous material when assessing the potential impact on maturation and generation of hydrocarbons. The modelling suggests that through an appraisal of sensitivity in areas of poor, limited or even absent data, such as frontier basins we can derive a more constrained basin modeling approach that reduces exploration uncertainty.



# Contents

<b>Chapter 1 – Introduction.....</b>	<b>1</b>
1.1 Research Rationale .....	1
1.2 Study Area .....	3
1.3 Thesis Aims and Objectives.....	4
1.4 Research Questions .....	5
1.4.1 Question 1 - How does regional basin structure and magma supply affect the emplacement of sill complexes along passive margins? .....	5
1.4.2 How can we reduce uncertainty in the interpretation of sill complexes and petroleum system modelling in frontier exploration regions? .....	6
1.4.3 How has the intrusion of the Faroe-Shetland Sill Complex impacted hydrocarbon systems in the Faroe-Shetland Basin? .....	7
1.5 Thesis Layout.....	7
<b>Chapter 2 – Geological Setting &amp; Background .....</b>	<b>11</b>
2.1 Introduction .....	11
2.2 The Tectonic Evolution of the NE Atlantic Margin.....	11
2.3 The North Atlantic Igneous Province .....	14
2.4 The Faroe-Shetland Basin .....	15
2.5 Hydrocarbon History of the Faroe-Shetland Basin .....	17
2.6 Sill Emplacement in Sedimentary Basins .....	20
2.6.1 Sill Emplacement .....	20
2.7 The Impact of Sills on Hydrocarbon Systems.....	24
2.7.1 Thermal Impact .....	24
2.7.1 Physical Impact.....	26
<b>Chapter 3 – Data &amp; Methods .....</b>	<b>29</b>
3.1 Introduction .....	29
3.2 Fundamentals of Seismic Reflection Data .....	30
3.3 Resolution of Seismic Reflection Data .....	31
3.4 Fundamentals of Well Data .....	32
3.5 Data used in this study.....	35

3.5.1	Seismic Data .....	35
3.5.1.1	2D Data .....	36
3.5.1.2	3D Data .....	38
3.5.2	Well Data .....	40
3.6	Software .....	41
3.7	Seismic Interpretation .....	43
3.7.1	Polarity .....	43
3.7.2	Horizon Interpretation .....	44
3.7.3	Sill Interpretation .....	48
3.7.4	Limitations of Seismic Reflection Data.....	50

## **Chapter 4 - Applying Spectral Decomposition to Sill Interpretation... 55**

4.1	Abstract.....	55
4.2	Introduction .....	56
4.3	Data and Methods .....	58
4.3.1	Fast Fourier Transform .....	59
4.3.2	Continuous Wavelet Transform.....	60
4.4	Results.....	61
4.4.1	Fast Fourier Transform .....	61
4.4.2	Interpreting Sills Using Spectral Decomposition .....	63
4.4.2.1	Faulted Sills .....	63
4.4.2.2	Revealing Stacked Sills .....	65
4.4.2.3	Three-dimension Surface Interpretation.....	66
4.5	Discussion.....	69
4.5.1	Magma flow implications.....	69
4.5.2	Fluid flow implications .....	70
4.6	Conclusions .....	73

## **Chapter 5 – The emplacement and distribution of the Faroe-Shetland Sill Complex ..... 74**

5.1	Abstract.....	74
5.2	Introduction .....	75
5.3	Tectonic Setting .....	77

5.4	Data and Methods .....	79
5.5	Resolution and Unresolved Sills.....	81
5.6	Results.....	82
5.6.1	Basin Structure and Regional Distribution of Sills.....	82
5.6.2	Sill Facies .....	86
5.6.2.1	Type I.....	88
5.6.2.1.1	Characteristics .....	88
5.6.2.1.2	Emplacement Environment.....	89
5.6.2.1.3	Source and Flow Direction.....	91
5.6.2.2	Type II .....	92
5.6.2.2.1	Characteristics .....	92
5.6.2.2.2	Emplacement Environment.....	95
5.6.2.2.3	Source and Flow Direction.....	97
5.6.2.3	Type III .....	99
5.6.2.3.1	Characteristics .....	99
5.6.2.3.2	Emplacement Environment.....	101
5.6.2.3.3	Source and Flow Direction.....	102
5.7	Summary of Sill Facies.....	103
5.8	Discussion.....	104
5.8.1	Regional Magma Migration Pathways.....	104
5.8.2	Emplacement of the Faroe-Shetland Sill Complex .....	108
5.8.3	Implications for Hydrocarbon Systems.....	112
5.9	Conclusions .....	112

**Chapter 6 – Controls on Hydrocarbon Generation in the Faroe-Shetland Basin ..... 114**

6.1	Abstract.....	114
6.2	Introduction .....	115
6.3	Petroleum System Elements of the Faroe-Shetland Basin .....	117
6.3.1	Source Rocks .....	117
6.3.2	Reservoirs, Traps and Seals.....	118
6.4	Previous Work.....	120
6.5	Methods.....	121
6.5.1	Seismic Interpretation.....	123

6.5.2	Depth Conversion.....	131
6.5.3	Model Construction .....	131
6.5.3.1	Heat Flow History .....	132
6.5.3.2	Burial History .....	133
6.5.3.3	Stratigraphy .....	136
6.5.3.4	Limitations.....	136
6.6	Part 1 - Sensitivity Analysis .....	139
6.6.1	Lithological Uncertainty .....	139
6.6.2	Heat Flow .....	141
6.6.3	Geometric Uncertainty .....	144
6.6.4	Erosion.....	145
6.6.5	Summary of Sensitivity Analysis.....	147
6.7	Part 2 - Heat Flow Modelling .....	148
6.7.1	Lithospheric Backstripping.....	149
6.7.2	Heat Flow Models .....	154
6.7.3	Heat Flow Calibration.....	154
6.8	Migration Modelling .....	158
6.9	Part 3 – Application to the Faroe-Shetland Basin.....	158
6.9.1	Maturation .....	158
6.9.2	Transformation Ratio (TR).....	169
6.9.3	Overpressure & Temperature.....	174
6.10	Discussion.....	178
6.11	Conclusions .....	180

**Chapter 7 – Controls on Hydrocarbon Generation in the Faroe-Shetland Basin ..... 182**

7.1	Abstract.....	182
7.2	Introduction .....	183
7.3	The Thermal Implications of Sill Intrusion .....	184
7.4	Sill Intrusion in the Faroe-Shetland Basin.....	185
7.5	Methods.....	186
7.5.1	Data .....	186
7.5.2	Intrusion Modelling Workflow .....	189
7.5.3	Uncertainties and Limitations .....	190

7.5.4	Heat Flow Calibration.....	192
7.6	Results.....	196
7.6.1	The Thermal Impact of Sill Intrusion.....	196
7.6.2	The Impact of Sill Intrusion on Maturation.....	202
7.6.3	The Porosity and Permeability Implications of Sill Intrusion .....	212
7.7	Discussion.....	211
7.7.1	The Impact of Sill Intrusion on Hydrocarbon Maturation.....	215
7.7.2	Implications for Hydrocarbon Migration .....	218
7.7.3	Other Factors to Consider .....	220
7.8	Conclusions .....	222
<b>Chapter 8 – Discussion &amp; Conclusion .....</b>		<b>223</b>
8.1	Introduction .....	223
8.2	The Petroleum System Evolution of the Faroe-Shetland Basin.....	223
8.3	Research Questions .....	226
8.3.1	Question 1 – How does regional basin structure and magma supply affect the emplacement of sill complexes along passive-margins? .....	226
8.3.2	Question 2 – How can we reduce uncertainty in the interpretation of sill complexes and petroleum system modelling in frontier exploration regions? ....	227
8.3.3	Question 3 – How has the intrusion of the Faroe-Shetland Sill Complex impacted hydrocarbon systems in the Faroe-Shetland Basin?.....	230
8.4	Applications to Other Areas.....	234
8.5	Conclusions .....	237
8.6	Further Work.....	239
<b>References.....</b>		<b>241</b>

# List of Figures

## Chapter 1

**Figure 1.1** – The global distribution of volcanic passive margins and the occurrence of large scale igneous provinces adapted from Coffin and Eldholm (1992), Courtillot et al. (1999), Menzies (2002), Geoffroy (2005), Ross et al. (2005), Rohrman (2007), Bryan and Ernst (2008), Leroy et al. (2008) & Wright (2012). ..... 2

**Figure 1.2** – Map of the Faroe-Shetland Basin highlighting key structural trends, and sediment depocentres, adapted from Ritchie et al. (2011) and references therein. . 4

## Chapter 2

**Figure 2.1** – Map showing the different orientation of rifting during the evolution of the NE Atlantic Margin, adapted from Ritchie et al. (2011). ..... 12

**Figure 2.2** – Regional map of the Faroe Shetland Basin superimposed with present day bathymetry. The map illustrates the dominant NE-SW trend of the crystalline basement highs which segment the basin into a series of sub-basins, which formed Mesozoic depocentres, adapted from Ritchie et al. (2011). ..... 16

**Figure 2.3** – A summary of the main proven hydrocarbon plays in the Faroe-Shetland Basin, adapted from Ritchie et al. (2011). ..... 19

**Figure 2.4** – 2D seismic section from the Judd Sub-basin showing the variation in sill morphology, including flat, sheet intrusions (SillF) and saucer-shaped bodies (e.g. Sill D & E), from (Thomson and Schofield, 2008). ..... 21

**Figure 2.5** – The components of a typical saucer-shaped sill, from Polteau et al. (2008) ..... 22

**Figure 2.6** – The stages of saucer-shaped sill emplacement, from Thomson and Schofield (2008). Initially sills spread laterally through ductile horizons such as shale, they then exploit weakness or faults in the overburden to climb up stratigraphy before flattening at a suitable horizon..... 23

**Figure 2.7** – A seismic example and schematic formation model of forced folding above a sill intrusion, adapted from Hansen and Cartwright (2006b). The overburden is deformed during sill emplacement, sediments then onlap the structure, which can be used to give a relative timing of intrusion. .... 24

**Figure 2.8** – Schematic illustration showing the impact of sill intrusion on predicted vitrinite reflectance profiles, after Holford et al. (2013). ..... 25

**Figure 2.9** – The potential impacts of sill intrusion of siliciclastic hydrocarbon plays, from Holford et al. (2013). ..... 27

## Chapter 3

- Figure 3.1** – The interaction of a seismic wave at a sub-surface interface and the relationship between velocity, density and the reflection coefficient Wright (2012), adapted from Sheriff and Geldart (1995) and Ashcroft (2011). .....31
- Figure 3.2** – An example of the well logs used this study; the compiled lithology log from TGS was calibrated with the available wireline data. ....35
- Figure 3.3** – Map of the Faroe-Shetland Basin showing the 2D seismic surveys used in this study, selected lines are used to undertake petroleum system modelling in Chapters 6 & 7.....38
- Figure 3.4** – Map of the Faroe-Shetland Basin showing the 3D seismic surveys used in this study. Survey Q214 forms the basis of seismic observations in Chapter 4. Surveys Q213-99, WZ-96/97/08 and TR 7 & 8 are merged into a single cube, a sub-crop of which is used for attribute analysis in Chapter 5. ....39
- Figure 3.5** – Regional map showing the location of commercial wells used throughout this study. ....40
- Figure 3.6** – Schematic illustration of a seismic wavelet (SEG normal convention) and its response to changes in acoustic impedance (Sheriff and Geldart, 1995). An increase in acoustic impedance results in a positive amplitude change and is displayed as a peak; a decrease in acoustic impedance results in a negative amplitude change and is displayed as a trough.....44
- Figure 3.7** – Common seismic reflector terminations after Wright (2012) modified from Emery and Myers (2009) with seismic examples from the surveys FSB99 and NSR006 from the Faroe-Shetland Basin.....45
- Figure 3.8** – Common features of sill intrusions in seismic reflection data; (A) High amplitude, saucer shaped reflections, (b) cross-cutting host stratigraphy, (c) forced folding of overlying sediments and (d) hydrothermal fluid circulation above the tips of intrusion disrupting the overlying sediments.....49
- Figure 3.9** – The use of seismic time-slices can help quickly assess the 3D geometry of high amplitude reflectors in seismic data. Saucer shaped sills produce distinctive circular geometries in plan view, the circumference of which typically decreases with depth.....50
- Figure 3.10** - Map of the Faroe-Shetland Basin showing the location of flood basalts and sill intrusions, adapted from Ritchie et al. (1999). The loss of seismic resolution due to volcanic activity generally increases from SE to NW as the volume and thickness of magmatic material increases.....51
- Figure 3.11** – Seismic section showing a significant loss of resolution below a flood basalt horizon, although reflection events can be identified they are vague and discontinuous, especially when contrasted to the equivalent reflectors above the basalt horizon.....52
- Figure 3.12** – Seismic section showing the loss of resolution below sill intrusions, although resolution is reduced, sedimentary layers are still imaged as coherent, continuous reflectors. ....53

## Chapter 4

**Figure 4.1** - Regional location map highlighting the structural configuration of the basin, the outline of the 3D seismic survey and the size and position of the cropped seismic sub-volume used in this study. ....59

**Figure 4.2** - Application of the Fast Fourier Transform to time-amplitude seismic data. The time gate is set to +/- 28ms and an output frequency of 5Hz and 15Hz respectively. The sill bodies are successfully isolated and lateral discontinuities appear much more prominent (data shown in standard positive polarity).....62

**Figure 4.3** - Application of the Continuous Wavelet Transform to the seismic data, the image shows a range of output frequencies (15Hz, 30Hz, 40Hz, 50Hz & 75Hz), the optimum resolution occurs between 40Hz and 75Hz, discontinuities are well imaged and the top sill reflection appears prominent and sharp. Outputs of 30Hz and 40Hz still produce coherent results however anything below 30Hz is too poor to offer any improvement of the original time-amplitude data.....63

**Figure 4.4** - Identifying faults using spectral decomposition. Areas of disrupted reflectivity in time-amplitude domain seismic (1,2,3,4) are imaged as clear breaks and displacements in the reflection surface when using spectral decomposition making it ideal for identifying and interpreting faults.....65

**Figure 4.5** - Revealing stacked sills using spectral decomposition. In time-amplitude seismic (5 x vertical exaggeration) the sill shows some amplitude variation but remains a single body. However after spectral decomposition (FFT 15 Hz) separation can be seen revealing three stacked sills displaced by post-emplacement faults. ....66

**Figure 4.6** - Main image - 3D interpretation of the top sill reflector using time-amplitude seismic data (left) and spectrally decomposed data (right), the surfaces show the same broad geometry and topographic elevation but spectral decomposition is significantly better at resolving both major and minor features. Inserts – Illustrating the differences between time-amplitude (A1 & B1) and spectral decomposition (A2 & B2) surfaces, the later reveals ridges, geometries and faults previously unseen in time-amplitude data.....68

**Figure 4.7** - Determining magma flow directions from spectral decomposition data. Image A shows a sill surface interpreted using spectral decomposition data (CWT at 50Hz), Image B shows an interpretation of the ridges and furrows on this sill surface which constitute the magma flows and lobe development. Image C deduces the magma flow directions from the interpretation (B) indicating the initial source of the sill in the centre of the deep depression on the SSE edge of the sill. ....71

**Figure 4.8** - Schematic illustration of the potential influence of sills on hydrocarbon migration, adapted from (Rateau et al., 2013). Inset A – Sealing scenario, where the sill acts as an impermeable barrier to fluid flow and thus provides an up-dip seal to the inclined sand horizon. Inset B – Migration scenario, where the sill has undergone deformation producing fault fracture zones capable of inducing permeability significant enough for fluid migration.....73

## Chapter 5

- Figure 5.1** – Schematic model of volcanic facies associated with volcanic passive margins proposed by Planke et al. (2000), the dataset for this study falls within the landward flow facies, in particular the inner flow sub-facies associated with fringe flood basalts, sill intrusion and volcanic vents. ....76
- Figure 5.2** – Location Map of the Faroe-Shetland Basin highlighting the main structural trends and the location of the seismic dataset, adapted from Ritchie et al. (2011). The basin consists of a series of sub-basins segmented by NE-SW trending, basement cored highs, and much of the northeast and central areas of are covered by thick, Early Paleogene flood basalt sequences. ....78
- Figure 5.3** – Chronostratigraphic column showing the lithostratigraphy of the Faroe-Shetland Basin and the corresponding BP T Sequence, the bulk intrusive volcanic activity occurs between T45 and T50 (around 53 Ma to 55 Ma). ....79
- Figure 5.4** – NW-SE trending seismic line from the southwest of the dataset showing the northern splay of the Corona Ridge and wide Sissal Sub-basin.....83
- Figure 5.5** – NW-SE trending seismic from the centre of the dataset, the northern splay of the Corona Ridge has progressed into a crystalline basement high.....84
- Figure 5.6** –NW-SE trending seismic Xline from the northeast of the dataset. The splays of the Corona Ridge have converged, drastically reducing the size of the Sissal Sub-basin. ....85
- Figure 5.7** – (a) Fault array map superimposed on a seismic time slice (-5000 ms TWTT) showing the main structural trends in the area, the geometry of the sub-basins and the approximate emplacement area of the three sill facies. (b) Isochron map of the Cretaceous sediments showing the relative thickness of each sub-basin. ....86
- Figure 5.8** – Opacity rendered images of flood basalt and a Type I sill. The images show how the upper surface of each body has a distinct seismic expression, which helps distinguish between extrusive and intrusive igneous rock.....89
- Figure 5.9** – NW-SE trending seismic line through the Sissal Sub-basin showing the restriction of Type I sills between the northern and southern splays of the Corona Ridge. The sills terminate against the northern splay; most do not reach the southern splay.....90
- Figure 5.10** – Opacity rendered 3D image of the Sissal Sub-basin showing Type I sills. The sills dip north-west towards the northern splay of the Corona Ridge. There is an increase in the angle of dip with increasing depth. ....91
- Figure 5.11** – 3D surface of a Type I sill generated using spectral decomposition (45 Hz Continuous Wavelet Transform). The sill shows it is fed from multiple source points along the northern splay of the Corona Ridge, and flows towards the south-east, developing magma lobes on its outer edges. ....92
- Figure 5.12** –3D surface interpretation of a Type II sill body showing the characteristic saucer shaped morphology. The sills have a flat central base surrounding by steep limbs, which transgress stratigraphy, the flanks of the limbs

are surrounded by either flat outer rims or by the developing magma fingers and lobes .....93

**Figure 5.13** – Seismic time-slices of the Flett Sub-basin illustrating the change in Type II sill emplacement with depth. The deepest sills are emplaced in the centre of a large graben, as they progress up stratigraphy emplacement moves to the flanks to feed smaller, shallow sills. The sills are initiated at a number of discrete points before becoming amalgamated further up stratigraphy as they develop into inter-connecting networks. ....94

**Figure 5.14** – The application of spectral decomposition (as demonstrated in Chapter 4) can be used to delineate stacked sill bodies that are not resolved in conventional seismic data. ....95

**Figure 5.15** – NW-SE trending seismic line through a large graben in the Flett Sub-basin immediately south-east of the southern splay of the Corona Ridge. The graben contains a series of Type II sills that form an inter-connected complex with the deepest sills feeding those higher up stratigraphy. ....96

**Figure 5.16** – A number of vent structures are observed in the Lamba Formation (T38) above the tips of underlying Type II sills. The overlying Flett Formation (T40-T45) thins onto the vents, suggesting their formation preceded deposition, providing a relative timing of sill emplacement. ....97

**Figure 5.17** – Opacity rendered Type II sill showing the development of partial lobes and magma fingers on the fringes of the sill body. Magma is interpreted to flow upwards and away from a singular source at the deepest point of the of the sill body. ....98

**Figure 5.18** – NE-SW trending seismic line showing areas of homogenous, chaotic reflectivity below the base of large Type II sills, interpreted to infer the presence of feeder dykes. The dykes cross multiple sills suggesting they may feed a number of different bodies, which are part of different inter-connecting complexes.....99

**Figure 5.19** – NW-SE orientated seismic line showing the strong segregation of Type III sills by multiple high-angle Mesozoic faults. The limited vertical separation between sills gives them appearance of amalgamated bodies, although internal reflectivity shows them to be individual intrusion events. ....100

**Figure 5.20** – NW-SE seismic line showing the variable relationship between Type III sills and the Cretaceous bounding faults. (a) Intrusion and termination into the fault plane. (b) Intrusion and continuation past the fault plane. (c) Post-emplacement deformation. ....102

**Figure 5.21** – Map showing the inferred areas of magma input into the basin as derived from the flow directions of interpreted sill bodies. Sills are shown as opacity rendered bodies with flow directions marked with arrows, (for clarity not all sills are shown). ....105

**Figure 5.22** – Conceptual Model for the emplacement of the Faroe-Shetland Sill Complex in the Corona Ridge region of the Faroe-Shetland Basin. The splays of the Corona Ridge and other significant Mesozoic faults control magma supply across the area and segregate the different sill facies. The style of intrusion evolves with

distance from the paleo-spreading centre as magma supply and structural style varies. ....111

## Chapter 6

**Figure 6.1** – Flow chart outlining the workflow used in this chapter. The chapter consists of two sub-sections; seismic interpretation and heat flow modelling, which provide input for the main petroleum system modelling workflow. ....122

**Figure 6.2** – Location map of the 2D seismic profiles and commercial wells used to undertake petroleum system modelling in this chapter. ....123

**Figure 6.3** – Generalised stratigraphic column for the Faroe-Shetland Basin summarising the major tectonic events. The horizons interpreted for this study are shown in the ‘Chrono-Strat’ column. Adapted from Holmes et al. (1999). ....124

**Figure 6.4** – Seismic line and geoseismic interpretation of Line A-A’. The line contains no volcanic material and so has excellent imaging down to the Triassic Packages. Thick Upper Cretaceous depocentres are observed in Flett Sub-basin whilst the Cenozoic section is thin to absent towards the southeast of the section. ....126

**Figure 6.5** - Seismic line (top) and geoseismic interpretation (bottom) of Line B-B’. The Flett Sub-basin has significantly thicker Lower Cretaceous packages further southwest on Line A-A’. Both the Flett and Foula Sub-basins form substantial Cretaceous depocentres separated by the Flett Ridge, whilst the Cenozoic package thickens significantly towards the centre of the line. ....127

**Figure 6.6** – Seismic line (top) and geoseismic interpretation (bottom) of Line C-C’, where thick basalt sequences limit the resolution of the Lower Mesozoic section northwest of the Corona Ridge and heavy sill intrusion can be observed southeast of Corona Ridge. There is a significant increase in water depth and Cenozoic thickness from the edges to the centre of the line. ....128

**Figure 6.7** – Seismic line (top) and geoseismic interpretation (bottom) of Line D-D’. Whilst the Upper Cretaceous packages thicken from the Ereland Basin to the Corona Basin, the opposite occurs for the Eocene to Oligocene packages, which thin onto the Pilot Whale Anticline and are substantially thinner in the Corona Basin. ....129

**Figure 6.8** – The sediment-water interface temperature is used to define the upper boundary conditions of the model and is based on the average air surface temperature as defined by Wygrala (1989) and the present day latitude of the basin. ....133

**Figure 6.9** – Reconstruction of erosion events using the model flattening techniques, the missing section is added to model layer to reproduce expected syn-depositional geometries. ....134

**Figure 6.10** – Composition plot for three dominant sedimentary facies illustrating the influence of lithological composition on the peak source rock temperature during petroleum system modelling. The percentage of shale in the system strongly

correlate to increased peak temperatures, with a >60% increase in peak temperature from a sand-dominated to shale dominated system.....	140
<b>Figure 6.11</b> – Time-temperature plots for the three tested heat flow scenarios; (1) constant heat flow, (2) Lithospheric stretching model after McKenzie (1978) with a Cretaceous rift event with a $\beta$ -factor of 3, (3) multi-rift model after (Scotchman et al., 2006) showing three phases of Cretaceous rifting and heat flow spike during the Paleogene volcanic event. ....	142
<b>Figure 6.12</b> – Predicted VR profiles (% Ro) for the heat flow scenarios presented in plotted against measured VR profiles from wells 204/19-1 and 205/21-01A. ....	143
<b>Figure 6.13</b> – Sensitivity analysis of potential geometric uncertainty that may arise during seismic interpretation. The source rock thickness and thickness of underburden have a negligible effect on peak source rock temperature. The depth of the source rock is somewhat more influential.....	145
<b>Figure 6.14</b> – Sensitivity analysis of the three main erosion events and their impact on peak source rock temperature. Only Cenozoic erosion has a noticeable influence on temperature, the earlier events occur before the source rock has been sufficiently buried. ....	146
<b>Figure 6.15</b> – A qualitative ranking of the sensitivity parameters tested, the results indicate that the heat flow model used and the depth of the source rock have the largest impact on the final modelling results. ....	148
<b>Figure 6.16</b> – Flexural backstripping workflow used to determine the depth-dependant $\beta$ -factors for Late Paleocene extension. The Top Paleocene (pre-post-rift) horizon is sequentially restored to 0 m water depth using trial $\beta$ -factors.....	151
<b>Figure 6.17</b> – Whole lithosphere $\beta$ -factors for depth-dependent rifting in the Paleocene derived from flexural backstripping of Line A-A'. $\beta$ -factors show a gradual increase from the southeast to northwest, moving from the shelf towards the basin axis. ....	152
<b>Figure 6.18</b> – Whole lithosphere $\beta$ -factors for depth-dependent rifting in the Paleocene derived from flexural backstripping of Line B-B'. There is a gradual increase in $\beta$ -factor from the Rona High into Flett Sub-basin.....	152
<b>Figure 6.19</b> - Whole lithosphere $\beta$ -factors for depth-dependent rifting in the Paleocene derived from flexural backstripping of Line C-C'. Modelling shows a broadly symmetrical increase in $\beta$ -factor from the flanks of the basin to the centre peaking at $\sim 10$ .....	153
<b>Figure 6.20</b> - Whole lithosphere $\beta$ -factors for depth-dependent rifting in the Paleocene derived from flexural backstripping of Line D-D'. $\beta$ -factors show a significant increase from the Ereland to the Flett Sub-basin, with a maximum $\beta$ -factor of 5.....	153
<b>Figure 6.21</b> – Predicted 2D heat flow profiles for Line A-A' and Line B- B' shown at the End Lower Cretaceous (100 Ma) and End Paleocene (55 Ma). Both lines show an increase in heat flow during the Paleocene towards the northeast of the profile associated with the increased lithospheric mantle stretching observed towards the axis of the basin. ....	155

<b>Figure 6.22</b> - Predicted 2D heat flow profiles for Line C-C' and Line D- D' shown at the End Lower Cretaceous (100 Ma) and End Paleocene (55 Ma). Line C-C' shows an increase in Paleocene heat flow towards the centre of the line where lithospheric mantle stretching is highest, Line D-D' shows greatest heat flow in the Corona Sub-basin towards the northwest.....	156
<b>Figure 6.23</b> – Predicted vitrinite reflectance profiles (solid line) calibrated with measured vitrinite reflectance data (points) for the available wells showing good to excellent correlation. ....	157
<b>Figure 6.24</b> – Present day predicted maturity map (%Ro) of the Upper Jurassic source rock. Data is extrapolated between modelled 2D lines using present day source depth contour maps.....	160
<b>Figure 6.25</b> – Time extraction plots from the Flett Sub-basin, Rona & Corona highs illustrating the maturation evolution of the Upper Jurassic source rock, shown as predicted vitrinite reflectance (%Ro). Plot numbers refer to the localities shown on the map in Figure 6.24. ....	161
<b>Figure 6.26</b> - Time extraction plots from the Flett, Foula and Corona Sub-basins illustrating the maturation evolution of the Upper Jurassic source rock, shown as predicted vitrinite reflectance (%Ro). Plot numbers refer to the localities shown on the map in Figure 6.24. ....	162
<b>Figure 6.27</b> - Time extraction plots from the Flett, Corona and Ereland Sub-basins illustrating the maturation evolution of the Upper Jurassic source rock, shown as predicted vitrinite reflectance (%Ro). Plot numbers refer to the localities shown on the map in Figure 6.24. ....	163
<b>Figure 6.28</b> – Modelled hydrocarbon maturation potential and predicted transformation ratio for Line A-A' . ....	165
<b>Figure 6.29</b> - Modelled hydrocarbon maturation potential and predicted transformation ratio for Line B-B' .....	166
<b>Figure 6.30</b> - Modelled hydrocarbon maturation potential and predicted transformation ratio for Line C-C'.....	167
<b>Figure 6.31</b> - Modelled hydrocarbon maturation potential and predicted transformation ratio for Line D-D' . ....	168
<b>Figure 6.32</b> – Present day predicted transformation ratio (%) of the Upper Jurassic source rock. Data is extrapolated between modelled 2D lines using present day source depth contour maps.....	170
<b>Figure 6.33</b> – Time extraction plots from the Flett and Foula Sub-basins and the Corona High illustrating the hydrocarbon generation history of the Upper Jurassic source rock, shown as predicted transformation ratio (%). Peak oil generation (50% TR) is highlighted. Plot numbers refer to the localities shown on the map in Figure 6.32. ....	172
<b>Figure 6.34</b> - Time extraction plots from the Flett, Foula and Ereland Sub-basins illustrating the hydrocarbon generation history of the Upper Jurassic source rock, shown as predicted transformation ratio (%). Peak oil generation (50% TR) is	

highlighted. Plot numbers refer to the localities shown on the map in Figure 6.32. ....173

**Figure 6.35** – Compiled time extraction plots for the Flett Sub-basin and Rona & Corona Highs illustrating the development of overpressure and heat flow evolution in the Upper Jurassic source rock horizon in relation to burial depth and transformation ratio. Plot localities are shown in Figure 6.24 & Figure 6.32. ....175

**Figure 6.36** - Compiled time extraction plots for the Flett Sub-basin and Rona & Corona Highs illustrating the development of overpressure and heat flow evolution in the Upper Jurassic source rock horizon in relation to burial depth and transformation ratio. Plot localities are shown in Figure 6.24 & Figure 6.32. ....176

**Figure 6.37** - Compiled time extraction plots for the Flett Sub-basin and Rona & Corona Highs illustrating the development of overpressure and heat flow evolution in the Upper Jurassic source rock horizon in relation to burial depth and transformation ratio. Plot localities are shown in Figure 6.24 & Figure 6.32. ....177

**Figure 6.38** – Isochron maps of the Upper Cretaceous and Eocene/Oligocene packages alongside transformation ratio burial plots showing hydrocarbon generation during these periods. The areas of hydrocarbon generation strongly correlate with the areas of deposition. ....181

## Chapter 7

**Figure 7.1** – Schematic illustration of the thermal aureole surrounding a sill intrusion, showing the zone of thermal alteration. Common observations suggest the thickness of the thermal aureole ( $t_a$ ) is related to the thickness of the sill intrusion ( $t_s$ ) (Galushkin (1997) and references therein. ....184

**Figure 7.2** – Map of the Faroe-Shetland Basin showing the location of 2D seismic profiles used for intrusion modelling. The lines are modified from the petroleum system modelling undertaken in Chapter 6.....187

**Figure 7.3** – Line B-B'- 2D seismic profile and petroleum system model showing the location of the modelled sill. The 1D extraction points and individual sills used for analysis in this chapter are highlighted. ....188

**Figure 7.4** - Line C-C'- 2D seismic profile and petroleum system model showing the location of the modelled sills. The 1D extraction points and individual sills used for analysis in this chapter are highlighted. ....188

**Figure 7.5** - Line D-D'- 2D seismic profile and petroleum system model showing the location of the modelled sill(s). The 1D extraction points and individual sills used for analysis in this chapter are highlighted. ....189

**Figure 7.6** – Flowchart illustrating the workflow used to undertake sill intrusion modelling. ....190

**Figure 7.7** – Calibration of sill intrusion modelling using the numerical and analytical solutions of Fjeldskaar et al. (2008). A good match can be observed between the published data and that generated using the techniques of this study.....193

<b>Figure 7.8</b> – Heat flow calibration using measured vitrinite reflectance data from the maturity aureole above the Midland Valley Sill (Scotland). (a) Observed data (Raymond and Murchison, 1988) (b) calculated data (Galushkin, 1997) (c) modelled data from this study using Intrusion Model within Petromod®. An excellent correlation is observed >100 m from the sills, the underestimation <100 m from the sill is attributed to the effects of convective heat flow. ....	195
<b>Figure 7.9</b> – Sequential predicted temperature plots for Line B-B' up to 0.05 Ma after the intrusion event.....	199
<b>Figure 7.10</b> – Sequential predicted temperature plots for Line C-C' up to 0.05 Ma after the intrusion event.....	200
<b>Figure 7.11</b> – Sequential predicted temperature plots for Line D-D' up to 0.05 Ma after the intrusion event.....	201
<b>Figure 7.12</b> – Time – temperature plots from the 1D extraction points (shown in Figure 7.3, Figure 7.4 & Figure 7.5) illustrating the increase in in-situ source rock temperature during the intrusion event.....	202
<b>Figure 7.13</b> – Sequential predicted vitrinite reflectance plots for Line B-B' up to 0.05 Ma after the intrusion event.....	204
<b>Figure 7.14</b> – Sequential predicted vitrinite reflectance plots for Line C-C' up to 0.05 Ma after the intrusion event.....	205
<b>Figure 7.15</b> – Sequential predicted vitrinite reflectance plots for Line D-D' up to 0.05 Ma after the intrusion event.....	206
<b>Figure 7.16</b> – Time – temperature plots from the 1D extraction points (shown in Figure 7.3, Figure 7.4 & Figure 7.5) illustrating the increase in predicted maturity of the source rock during the intrusion event. ....	207
<b>Figure 7.17</b> – Time-temperature plot and predicted vitrinite reflectance profile for a 30 m thick sill intruded at 2050 m depth from Line C-C' (see Figure 7.4 for location). ....	209
<b>Figure 7.18</b> - Time-temperature plot and predicted vitrinite reflectance profile for a 80 m thick sill intruded at 3200 m depth from Line C-C' (see Figure 7.4 for location). ....	210
<b>Figure 7.19</b> - Time-temperature plot and predicted vitrinite reflectance profile for a 110 m thick sill intruded at 3771 m depth from Line B-B' (see Figure 7.3).....	211
<b>Figure 7.20</b> – Porosity and permeability plots for a low (Line B-B'), mid (Line C-C') and high (Line E-E') intrusion scenario (the location of 1D extraction is shown in Figure 7.3, Figure 7.4 & Figure 7.5). The plots illustrate a dramatic reduction in both porosity and permeability between the intruded igneous rock and the host stratigraphy.....	213
<b>Figure 7.21</b> – The effect of sill intrusion on the porosity of the host stratigraphy. Porosity is reduced by up to 20% within the metamorphic aureole of the intrusion. Sandstone lithologies experience greater porosity reduction than shale.....	214

## Chapter 8

- Figure 8.1** – Map showing the present day maturity of the Faroe-Shetland Basin, with maturation and transformation ratio plots illustrating the hydrocarbon generation history in different areas of the basin.....225
- Figure 8.2** – Decision matrix illustrating the level of uncertainty associated with the different data types, methods and software used to undertake key tasks in each chapter of this thesis. The overall level uncertainty is then assessed with regards to its impact on petroleum system modelling. ....230
- Figure 8.3** – Map of the Faroe-Shetland Basin showing the distribution of hydrocarbon plays (after Ritchie et al., 2011) and the distribution of sills as observed in this study and in other published studies (Rateau et al., 2013, Schofield et al., 2015). The spatial correlation suggests the impact of sill intrusion on prospectivity is only a consideration in the Eocene Fan, Paleocene Sands and Commodore Formation Plays. ....232
- Figure 8.4** – A schematic illustration of some of the potential implications of sill intrusion on the Commodore Formation, Paleocene Sandstone and Eocene Fan Plays. ....233
- Figure 8.5** – The global distribution of offshore sill complexes, including East Greenland, West Greenland, Brazil, Angola, Senegal, and China, from Magee et al. (2016). The techniques and workflows established in this thesis are transferable and can be used to study the impact of igneous intrusions on the potential and proven hydrocarbon systems in these regions.....236

## List of Tables

<b>Table 1.1</b> – Summary of chapters within this thesis.....	9
<b>Table 3.1</b> – Table showing the minimum and maximum seismic velocities (V) and dominant frequencies (f) at different stratigraphic levels for the FSB99 and NSR06 2D seismic surveys used in this study, values represent area averages, actual values may vary between individual lines. The velocity of Sub-Volcanic and Mesozoic sections represents a conservative estimate due to the limited well penetration of these formations.....	37
<b>Table 3.2</b> – Table showing the calculated minimum and maximum vertical and horizontal resolution at different stratigraphic levels for the FSB99 and NSR06 2D seismic surveys.....	37
<b>Table 3.3</b> – An overview of the commercial wells used in the study.....	41
<b>Table 3.4</b> – Summary of the software packages used in this study and their application.....	43
<b>Table 3.5</b> – Table illustrating the main seismic horizons used for petroleum system modelling in Chapters 6 & 7.....	46
<b>Table 5.1</b> – Summary of the shared characteristics used to define individual sill facies. Volume calculations are based on an average sill thickness of 40 m, which represents an absolute minimum thickness defined by the limits of seismic resolution, actual volumes may be substantially higher (especially for Type I Sills). .....	84
<b>Table 6.1</b> – Area average interval velocities used for depth conversion based on check shot data from Quads 204, 206 and 214.....	131
<b>Table 6.2</b> – Estimated paleo-water depths for the Rockall Trough and Faroe-Shetland Basin (Clift and Turner 1998). Data is compiled from lithological logs based on drill cuttings, limited recovered core and correlation with land-based outcrops. The post-Tertiary – present day water depths assume a constant deepening from the shelf to basin centre. These numbers represent a 1D area average and must be extrapolated with the aid of seismic reflector geometry to produce 2D paleo-water depths. ....	135
<b>Table 6.3</b> – Summary of model construction .....	138
<b>Table 7.1</b> – The thermal and physical parameters used for intrusion modelling, values are predicted from Robertson (1988), Clauser and Huenges (1995) and are calibrated using published analytical models (Fjeldskaar et al., 2008) and field data (Raymond and Murchison, 1988). .....	196

## Chapter 1 Introduction

### 1.1 Research Rationale

Continental passive margins have been a mainstay of hydrocarbon exploration success for many decades (Levell et al., 2010). They host around 35% of giant field discoveries which in turn constitute 67% of the world's proven hydrocarbon reserves (Mann et al., 2003). Exploration within bathymetrically-deep, offshore basins along such margins can carry high risk and often incurs significant expense to exploit (White et al., 2003); however, as global demand for hydrocarbons increases and our exploration technologies improve, they become increasingly attractive areas for hydrocarbon exploration (Pratsch, 1978, Levell et al., 2010).

Continental passive margins develop adjacent to juvenile oceanic spreading centres (Bond et al., 1995) and represent the transition between oceanic and continental crust which is not currently part of a developing plate margin (Allen and Allen, 2013) (Figure 1.1). They can be divided into two end member models, volcanic and non-volcanic (Eldholm et al., 1995). Volcanic passive margins are associated with break-up over a hotter-than-normal mantle (Geoffroy, 2005), typically due to actively upwelling mantle plumes (Fleitout et al., 1986, Olson et al., 1988, White and McKenzie, 1989, Hill, 1991, Holbrook and Kelemen, 1993, Eldholm et al., 1995). Melt is generated when upwelling asthenosphere decompresses and crosses the solidus at lower pressure; typically, this happens where lithosphere is thinned (McKenzie, 1984). This melt causes significant emplacement of igneous material both within and on top of the continental crust (White and McKenzie, 1989).

Volcanic-passive margins are currently the target of active hydrocarbon exploration in areas such as the NE Atlantic, NW Australia, Brazil, and China (Archer et al., 2005). The presence of voluminous igneous rock, however, strongly influences the thermal, structural and geodynamic evolution of the basin (White and McKenzie, 1989, Coffin and Eldholm, 1994). Therefore understanding the role of igneous rocks in basin development and their impact on hydrocarbon systems is key to successful exploration (Davies et al., 2004, Archer et al., 2005). Furthermore, hydrocarbon

occurrences have been discovered associated with a range of igneous rocks including sills, dykes, laccoliths, tuffs and flood basalts (Schutter, 2003). Sills alone have been linked with discoveries in the USA, Argentina, Brazil, Ghana, Japan, Italy and Russia (Hedberg, 1964, Meyerhoff, 1980, Belotti et al., 1995, Milani and Zalan, 1999, Masters, 2000, Hoshi and Okubo, 2010).

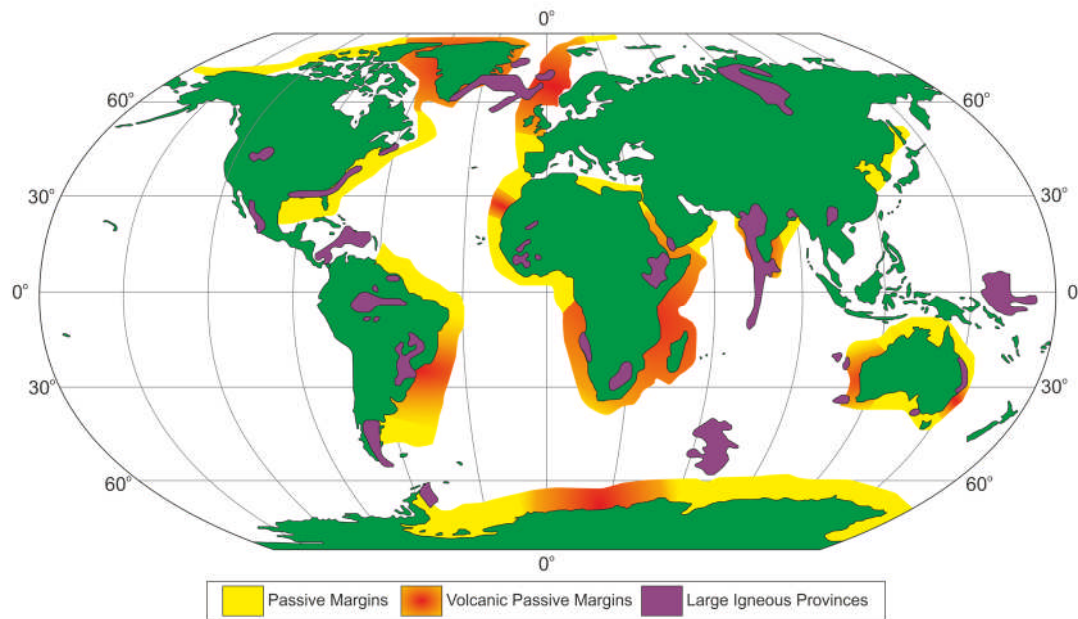


**Figure 1.1** – The global distribution of volcanic passive margins and the occurrence of large scale igneous provinces adapted from Coffin and Eldholm (1992), Courtillot et al. (1999), Menzies (2002), Geoffroy (2005), Ross et al. (2005), Rohrman (2007), Bryan and Ernst (2008), Leroy et al. (2008) & Wright (2012).

This study focuses on the Faroe-Shetland Basin, a region of frontier exploration on the NE Atlantic Margin (Larsen et al., 2010). The basin underwent intense volcanic activity during continental break up in the Early Paleocene (Naylor et al., 1999), including the emplacement of the extensive Faroe-Shetland Sill Complex (FSSC) (Bell and Butcher, 2002). The impact of the volcanic rocks, however, in particular the intrusive sill complex, on hydrocarbon systems in the basin is not uniform and is poorly understood (Holmes et al., 1999).

Over the past two decades the increased availability of 3D seismic reflection data has significantly advanced our understanding of the FSSC (Schofield et al., 2012). Previous studies of the FSSC have been focused on specific aspects of the sill complex, such as the morphology of intrusions (Bell and Butcher, 2002, Smallwood and Maresh, 2002, Thomson, 2004), emplacement mechanisms (Trude, 2004, Thomson, 2007, Schofield et al., 2012), feeding relationships (Hansen et al., 2004) and the formation of vent and fold structures (Hansen and Cartwright, 2006). Others have begun to consider the regional distribution of intrusions and magma sources in the basin (Schofield et al., 2015), however, only a few have considered the impact upon petroleum systems (Rateau et al., 2013, Schofield et al., 2015) and none have fully explored the thermal implications of sill intrusion in the basin.

This thesis looks to develop our current understanding of the Faroe-Shetland Sill Complex and its thermal and physical implications for local hydrocarbon systems. In doing so it demonstrates the value of applying 3D seismic data and predictive forward modelling to understanding the evolution and development of frontier hydrocarbon exploration areas.

## **1.2 Study Area**

The Faroe-Shetland Basin is a confined deep-water basin located between the Faroe and Shetland islands on the NE Atlantic Margin (Mitchell et al., 1993) (Figure 1.2). It comprises a series of segmented Mesozoic to Early Cenozoic rift basins that have a complex poly phase rift history that initiated in the Permo-Triassic and continued sporadically until the final stages of continental break-up during the early Tertiary (Dean et al., 1999, Doré et al., 1999, Jolley and Bell, 2002, Ellis and Stoker, 2014). The North Atlantic Igneous Province formed due to the arrival of the proto-Icelandic plume and the onset of sea floor spreading in the Early Paleogene (Smallwood and White, 2002). It consists of extensive extrusive flood basalts and shallow crustal intrusions across the basin (Saunders et al., 1997, Skogseid et al., 2000, Jolley and Bell, 2002).

The basin provides an excellent case study for the formation of intrusive sill complexes and their impact on hydrocarbon systems, as it has extensive, high-quality 2D and 3D seismic reflection data gathered during various phases of hydrocarbon exploration from the 1970's onwards (Ritchie et al., 2011) and there are numerous proven hydrocarbon plays within the basin (Spencer et al., 1999, Lamers and Carmichael, 1999, Larsen et al., 2010, Ritchie et al., 2011).

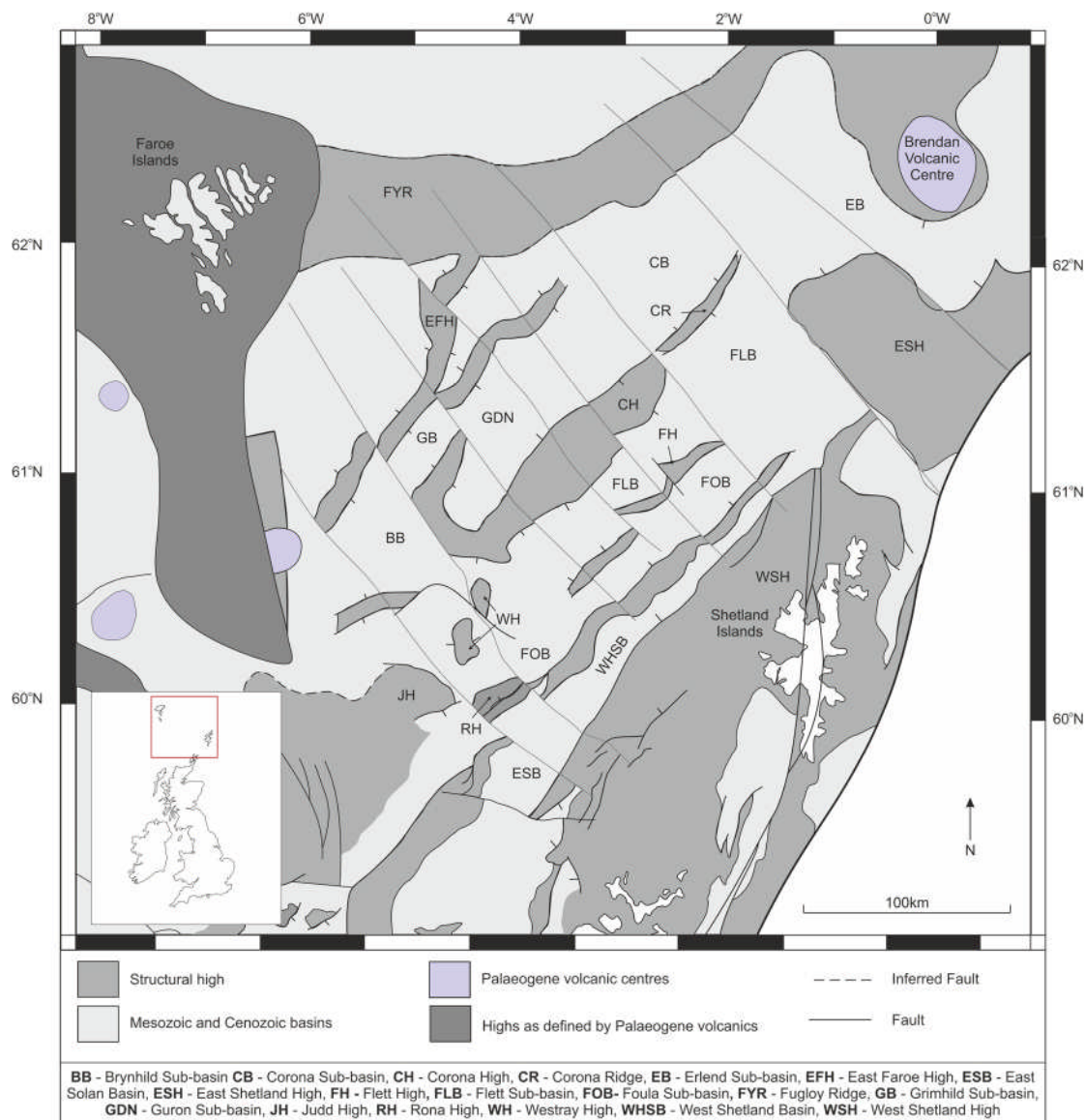


**Figure 1.2** – Map of the Faroe-Shetland Basin highlighting key structural trends, and sediment depocentres, adapted from Ritchie et al. (2011) and references therein.

### 1.3 Thesis Aims and Objectives

The overall aim of this thesis is to understand what controls the distribution and morphology of intrusive sill complexes in the Faroe-Shetland Basin and what impact they have had on local and regional hydrocarbon systems. In order to achieve this, the fundamental objectives of the project are as follows:

- Consider the variation in morphology and distribution of the Faroe-Shetland Sill Complex and how this relates to the structure and magma supply across the basin.
- Assess and quantify the key uncertainties associated with hydrocarbon exploration in frontier volcanic basins.
- Use predictive forward modelling to determine the heat flow history of the Faroe-Shetland Basin, and evaluate the impact that this has on hydrocarbon maturation in the region.
- Assess the thermal impacts of sill intrusion on the regional hydrocarbon system.

### 1.4 Research Questions

The aims and objectives, outlined above will be addressed through a series of research questions that are detailed below. These will be considered in the context of this study in the discussion chapter (Chapter 8) at the end of the thesis.

#### 1.4.1 Question 1 – How does regional basin structure and magma supply affect the emplacement of sill complexes along passive margins?

Since the pioneering field studies of Du Toit (1920) through to modern 3D seismic analysis (Bell and Butcher, 2002, Hansen et al., 2004, Magee et al., 2013), authors have recognised a wide variety in the size, shape and geometry of sill intrusions, indeed even intrusions within the same sill complexes have been shown to vary significantly (Smallwood and Maresh, 2002).

Studies have demonstrated on a local scale how lithological and structural controls play a key role in the emplacement and development of sill bodies (Thomson and Schofield, 2008, Magee et al., 2013). Similarly, on a regional scale, basin structure seems instrumental in the distribution of bulk magma volumes shown by the alignment of igneous complexes with major structural discontinuities (Marsh, 1973, Rumph et al., 1993, Archer et al., 2005, Jolley et al., 2005, Jolley and Morton, 2007, Passey and Varming, 2010, Schofield et al., 2015).

Given the significant variation in the size and morphology of sills observed in the Faroe-Shetland Basin (Thomson, 2004) and the availability of high-fidelity 3D seismic reflection data, the area provides an excellent case study to assess how sills are symptomatic of their emplacement environment and what this can in turn tell us about the emplacement regime and magma supply during formation.

A schematic regional framework for the magmatic seismic facies associated with volcanic rift margins was proposed by Planke et al. (2000) which describes four main magmatic facies, representing a progression from the spreading centre towards the continent. Furthest from the spreading centre is the landward flow facies, which consists of landward lava flows, lava deltas, inner lava flows, sills and vents. The data area of this study falls within the area of inner flows and sills. Through the application of seismic reflection data it should be possible to refine this facies and in so doing explain the transition from inner flows to sills and how sill emplacement evolves with distance from the proto-spreading centre.

#### **1.4.2 Question 2 – How can we reduce uncertainty in the interpretation of sill complexes and petroleum system modelling in frontier exploration regions?**

Although seismic reflection data have significantly enhanced our understanding of sill complexes on both a regional and local scale (Smallwood and Maresh, 2002, Planke et al., 2005, Schofield et al., 2015) interpretation is not, however, without its issues (Roberts et al., 2005). One of the key limitations of seismic reflection data in volcanic basins is the loss of resolution around or below igneous rocks due to the

attenuation of seismic energy (White et al., 2005, Shaw et al., 2008). Not only does this inhibit our ability to study sills (Cartwright and Hansen, 2006) but it also greatly impacts our ability to interpret sedimentary stratigraphy and structures that are located beneath volcanic intervals (Lamers and Carmichael, 1999).

In the Faroe-Shetland Basin, a significant portion of the northeast and central areas of the basin contain thick flood basalts, and extensive sill intrusion (Skogseid et al., 2000). As such, the seismic resolution, particularly in the Mesozoic successions, is typically poor (Nelson, 2010). This can be problematic when considering the structural and thermal evolution of the basin, especially in the context of hydrocarbon prospectivity as the dominant source rock in the area is of Upper Jurassic age (Bailey et al., 1987, Scotchman et al., 1998) and thus poorly imaged across much of the area (Lamers and Carmichael, 1999).

As a consequence, any petroleum system or basin evolution study in this area is inherently uncertain. In order to reduce this uncertainty, it is important to understand as far as possible all of the various factors that could impact any modelling, and how best to resolve these with the data available.

### **1.4.3 Question 3 – How has the intrusion of the Faroe-Shetland Sill Complex impacted hydrocarbon systems in the Faroe-Shetland Basin?**

Existing studies of the area assume that the FSSC has a negligible effect on the regional thermal evolution and hydrocarbon maturation history of the Faroe-Shetland Basin (Holmes et al., 1999). Indeed, published basin modelling studies either dismiss (Holmes et al., 1999, Iliffe et al., 1999) or ignore entirely (Jowitt et al., 1999) the potential impact of sill intrusion on the regional thermal evolution of the basin. In consequence, the impact of the FSSC on local hydrocarbon systems has not been fully explored.

The local effects of magma emplacement on organic matter are well documented in field, experimental and modelling studies (Carslaw and Jaeger, 1959, Jaeger, 1964, Rodnova, 1976, Simonet et al., 1981, Dennis et al., 1982, Hutton and Henstridge, 1985, Clayton and Bostick, 1986, Saxby and Stephenson, 1987, George, 1992,

Galushkin, 1997, Gurba and Weber, 2001, Rimmer et al., 2009, Fjeldskaar et al., 2008). Indeed, even published well data from the Faroe-Shetland Basin demonstrates local alteration of vitrinite reflectance profiles as a direct consequence of sill intrusion (Holmes et al., 1999). Furthermore, studies have suggested that the cumulative effect of multiple intrusions can maintain an elevated geotherm substantially longer than individual intrusions (Aarnes et al., 2011).

Petroleum system modelling in the Vøring Basin, Norwegian Margin, predicts that the thermal impact of multiple sill intrusions can potentially double the fraction of kerogen transformed to petroleum (Fjeldskaar et al., 2008). Given the similarity in structural, lithological and thermal settings between the Vøring and Faroe-Shetland Basins it is not unreasonable to assume that there is potential for similar heating and maturation influences. At the very least, it offers a good rationale to re-evaluate our current understanding of the thermal impacts associated with the FSSC.

## 1.5 Thesis Layout

This thesis comprises of eight chapters (Table 1.1), specifically: three introductory chapters, four data chapters and a final discussion chapter synthesising the findings and conclusions of the work undertaken.

**Chapter 1** - Introduces the project rationale, study area and layout of the thesis.

**Chapter 2** - Provides regional context to the study by summarising the tectonic evolution of the NE Atlantic Margin and Faroe-Shetland Basin. The North Atlantic Igneous Province and the Faroe-Shetland Sill Complex are introduced, along with a brief overview of the exploration history, including the proven and potential petroleum plays in the area.

**Chapter 3** - Presents the data, software and methods used in this thesis. The fundamental concepts of seismic reflection data are described, including its suitability and limitations for the study of igneous intrusions. In addition the coverage, quality and limitations of the available seismic datasets are considered,

specifically the variation in seismic resolution across the basin, which is critical to this study. The distribution, well logs and limitations of the commercial wells that contribute to this study are summarised. An overview is given of the methods and workflows used throughout the thesis, however, specialist workflows such as petroleum system modelling, flexural backstripping (both Chapter 6) and intrusion modelling (Chapter 7) are dealt with within their respective chapters.

**Chapter 4** - Explores the application of spectral decomposition to the interpretation of sill intrusions in seismic reflection data. By converting seismic data from the time-amplitude to frequency-amplitude spectrum, previously unresolvable features can be identified on the intrusion surface. This enhanced imaging reveals both deformation and emplacement features, which are used to gain a better understanding of sill development and the implications for surrounding petroleum plays.

**Chapter 5** - Focuses on the distribution and emplacement of the Faroe-Shetland Sill Complex close to the Corona Ridge. Through the interpretation of 3D seismic data, distinctive sill geometries can be identified that are indicative of their emplacement environment and are related to magma distribution across the basin. Conceptual emplacement models are developed to explain the evolution and development of sill emplacement towards the fringes of the volcanic region developed during passive margin formation.

**Chapter 6** - Aims to enhance our understanding of the petroleum system evolution of the Faroe-Shetland Basin through predictive forward modelling. The chapter first deals with the issue of uncertainty, common in all frontier exploration regions. Quantitative sensitivity analysis is undertaken identifying the most uncertain variables in the workflow and solutions implemented to mitigate their impact. Flexural backstripping is applied to determine the variation in stretching factors across the basins, which are then used to produce heat flow scenarios for modelling. The results of petroleum system modelling are presented highlighting the maturity evolution and key controls on hydrocarbon maturation in the region.

**Chapter 7** – Building on the petroleum system modelling undertaken in Chapter 6, this chapter assesses the implications of sill intrusion on the petroleum system

evolution of the Faroe-Shetland Basin. The models created in Chapter 6 are modified to incorporate sill induced heat flow associated with the North Atlantic Igneous Province during the Early Cenozoic volcanic event. The timing and magnitude of sill induced heat flow is considered with respect to its overall impact on in-situ source rock and early generated hydrocarbons. The secondary effects of intrusions such as porosity and permeability reduction in the country rock are also explored.

**Chapter 8** - Provides a synthesis of the data chapters by discussing the implications of the study in the context of the aims, objectives and research questions before presenting the final research conclusions.

Chapter	Content
Chapter 1	Introduction, aims and background of the study.
Chapter 2	Regional setting of the NE Atlantic Margin and the evolution of the Faroe-Shetland Basin.
Chapter 3	The data and methods used throughout the study.
Chapter 4	Applying spectral decomposition to the study of sill complexes.
Chapter 5	Developing an emplacement model for the Faroe-Shetland Sill Complex.
Chapter 6	Regional petroleum system modelling of the Faroe-Shetland Basin.
Chapter 7	Heat flow implications of sill intrusions.
Chapter 8	Discussion and conclusions integrating the findings of Chapters 4-7.

**Table 1.1** – Summary of chapters within this thesis.

## Chapter 2 Geological Setting & Background

### 2.1 Introduction

The thesis focuses upon the Faroe-Shetland Basin and some of the wider aspects of the North Atlantic Igneous Province. As such, this chapter provides an overview of the tectonic evolution of the North Atlantic Margin and Faroe-Shetland Basin as well as the development of the North Atlantic Igneous Province. To give context to the study the petroleum exploration history of the Faroe-Shetland Basin is introduced. Finally a detailed overview is given of the emplacement of sill intrusions and their impact on petroleum systems, a fundamental underlying process in this study.

### 2.2 The Tectonic Evolution of the NE Atlantic Margin

The Faroe-Shetland basin is an elongate deep-water basin stretching between the Faroe and Shetland Islands on the NE Atlantic Margin (Mitchell et al., 1993). It has a complex poly-phase rift history which initiated in the Permo-Triassic and continued episodically until the final stages of continental break-up during the early Cenozoic (Dean et al., 1999)

The structural evolution of the Atlantic Margin is attributed to an inherited basement structural grain (Coward, 1990), and at its largest scale, the Atlantic Margin represents the oblique re-opening of the Caledonian suture system and fold belt (Doré et al., 1999). There are three, dominant, inherited structural trends in the basin (NE-SW, E-W, NW-SE); in this context, the main NE-SW trend originates from the steeply-dipping shear zones formed during Late Caledonian deformation, which are oblique to the orogeny but parallel to the Cretaceous-Cenozoic basins and the opening of the Atlantic. The N-S trend lies inboard (towards the UK) of the NE-SW trend and accommodated E-W extension during the Jurassic. The NW-SE lineaments appear to have determined the position of transfer zones, which can be

seen as lineament terminations and offsets (Rumph et al., 1993) and segmenting basins (Doré et al., 1997) (see Figure 2.1).

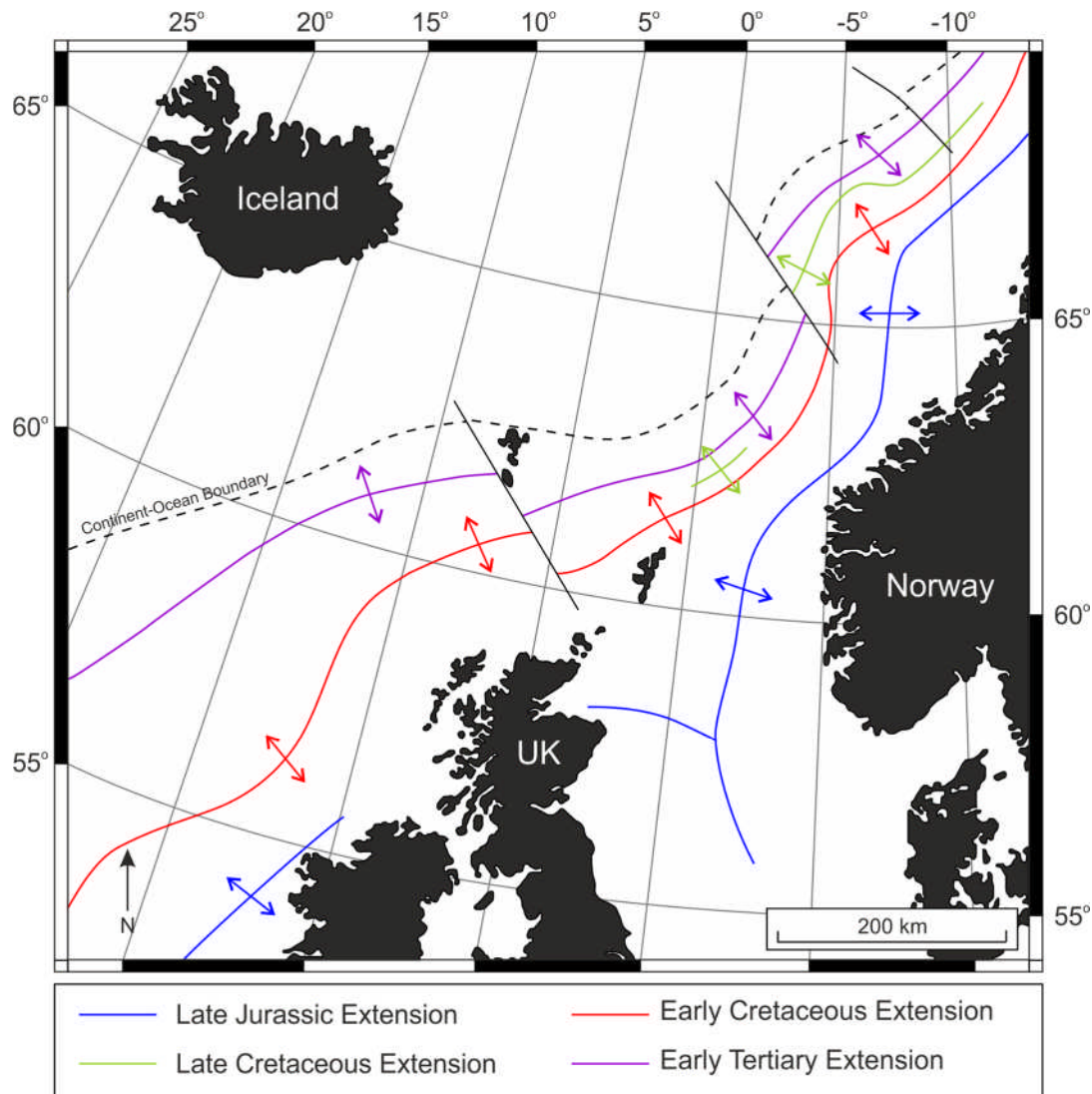


**Figure 2.1** – Map showing the different orientation of rifting during the evolution of the NE Atlantic Margin, adapted from Ritchie et al. (2011).

Extension began in Devonian times (immediately post-Caledonian) with post-orogenic collapse and back-sliding of the nappe pile (Coward et al., 1989). Basins created during Devonian-Carboniferous rifting are seen as important to the Atlantic Margin development, but are poorly-resolved in seismic surveys, largely due to over-printing by younger structural events (Doré et al., 1999).

Extension in the Permo-Triassic represents the mosaic-like fragmentation of the super continent Pangaea. The super-continent split almost immediately after it was formed, however, rather than break-up along a dominant extension vector (Coward, 1995) rifting occurred along the suture lines on which it was fused (Ryan and Dewey, 1997). On the Atlantic margin, this was the northeast-southwest trending Caledonian fold belt (Doré et al., 1999).

The transition from Triassic to Jurassic in the North Atlantic represents a shift to rift tectonics, where rifting was driven by incipient ocean floor spreading in Tethys (to the southeast) and the Proto-Central Atlantic (to the southwest) (Doré, 1992). The Early Jurassic was characterised by mild extension along the north-south inherited grain and by thermal subsidence; however, in the Late Jurassic, the fabric and stress distribution became greatly variable which can be seen in migrating rifts and shifting sediment depocentres across the margin (Dean et al., 1999). This suggests rifting during the Late Jurassic was controlled by seafloor spreading in Tethys rather than central Atlantic spreading (Ziegler, 1988).

Tethyan sea floor spreading had ceased by the Early Cretaceous and was replaced by subduction on the northern margin of the ocean (Ziegler, 1988). At this time, rifting switched from a north-south dominated "Tethyan" rift to a northeast-southwest dominated system. It is widely assumed that Early Cretaceous rifting was a single event which has since been disputed (Doré et al., 1999), the rotation of least principle stress (from E-W to NW-SE) in the early Cretaceous shows two rifting episodes which were almost coincident in time but not in space (Doré et al., 1999). By the end of Cretaceous, landmasses were close to sea level due to reduction in topography and transgressive seas (Doré et al., 1999).

Rifting spanned a period from the latest Cretaceous to the earliest Eocene until break-up around 53 Ma. Widespread volcanism during the late Paleocene-early Eocene formed the North Atlantic Igneous Province, which is believed to have initiated at 62-61 Ma and continued until the early Eocene around 51 Ma (Smallwood and White, 2002). It has been suggested that the bulk of the volcanic activity occurred over 2-3 million years (Skogseid et al., 2000). The igneous activity is associated with the migration of the proto-Icelandic plume, which supplied

considerable volumes of melt into a thinned axis of incipient opening (Eldholm et al., 1989). Extensive flood basalts as well as dyke swarms and sill complexes are associated with the volcanism, the latter of which, are predominantly intruded into mud-rich Upper Cretaceous -Paleocene sediments (Thomson and Schofield, 2008).

The horizontal stress patterns reversed following plate separation in the Early Eocene, thus NW-SE extension was replaced by southeast compression caused by ridge push forces associated with the adjacent ocean; this compressive regime still exists to the present day in NW Europe (Doré and Lundin, 1996). Associated with the compression are inversion structures which record multi-phase inversion (Doré and Lundin, 1996, Davies et al., 2004).

### **2.3 The North Atlantic Igneous Province**

Large Igneous Provinces (LIPs) are associated with volcanic passive-margin formation (White and McKenzie, 1989, Skogseid et al., 2000, Geoffroy, 2005) and involve the emplacement of significant volumes of predominantly mafic igneous rock through processes other than normal seafloor spreading (Morgan, 1983, Coffin and Eldholm, 1992, Coffin and Eldholm, 1994). Volcanic passive-margin formation is associated with thermal anomalies in the upper mantle, which are in turn capable of producing significant volumes of melt (White and McKenzie, 1989). Debate still exists as to the origin of such thermal anomalies with both mantle plume (Campbell and Griffiths, 1990, Callot et al., 2001) and non-plume (Anderson, 1994, King and Anderson, 1995) models proposed.

The North Atlantic Igneous Province formed as a response to continental break-up along the NE Atlantic in the Early Paleocene (Skogseid et al., 2000) and is thought to be associated with the impingement of the proto-Icelandic plume at the base of the lithosphere and the onset of sea-floor spreading (Nadin et al., 1997, Saunders et al., 1997, Smallwood and White, 2002, Passey and Hitchen, 2011). The Province consists of extensive sub-aerial flood basalts, an extensive suite of intrusions, known as the Faroe-Shetland Sill Complex and various volcanic centres (White and McKenzie, 1989, Skogseid et al., 2000, Bell and Butcher, 2002). The total volcanic

products have an estimated areal extent of  $1.3 \times 10^6 \text{ km}^2$  and a potential total crustal volume of  $6.6 \times 10^6 \text{ km}^3$  (Coffin and Eldholm, 1994, Eldholm and Grue, 1994).

#### 2.4 The Faroe-Shetland Basin

The Faroe-Shetland Basin is a NE-SW striking rift basin located between the Faroes and the Shetland Isles on the NE Atlantic Margin (Sørensen, 2003). It is composed of a series of sub-basins, formed during multiple phases of extension (Doré et al., 1999), which are segmented by Lewisian-cored basement highs composed of Lewisian Gneiss (Ritchie et al., 2011) (see Figure 2.2). The basin has substantial present day water depths of up to 2.5 km developed through post-rift subsidence (Fletcher et al., 2013); the present day bathymetry of the basin is shaped by a series of SW-NE trending Cenozoic compression structures (Davies et al., 2004). Sediment input to the basin was dominantly from the east and was sourced from the Scotland-Shetland Platform (Ritchie et al., 1996, Sørensen, 2003).

The basin has a dominant NE-SW structural grain, inherited from Caledonian structures (Coward, 1990), which were utilised during multi-phase rifting throughout the Mesozoic and Early Paleogene (Dean et al., 1999). A series of NW-SE trending lineaments cut the basin perpendicular to the main structural trend, which have been interpreted to form along inherited Caledonian compressional zones (Rumph et al., 1993); although their exact origin is still debated (Moy and Imber, 2009). The lineaments are believed to play a role in sediment channelling and magma emplacement within the basin (Rumph et al., 1993, Jolley et al., 2005, Jolley and Morton, 2007, Ellis et al., 2009, Moy and Imber, 2009, Passey and Varming, 2010).

The basin experienced extensive volcanism during the formation of the North Atlantic Igneous Province in the Late Paleocene, this included suites of both intrusive and extrusive igneous rock (Ritchie and Hitchen, 1996, Naylor et al., 1999, Ritchie et al., 2011). Over  $40\,000 \text{ km}^2$  of flood basalts were emplaced over the northwest and centre of the basin (Schofield et al., 2015), whilst the Faroe-Shetland

Sill Complex was emplaced into the Cretaceous and Paleocene basin fill, over an area of at least 22 500 km<sup>2</sup> (Passey and Hitchen, 2011).

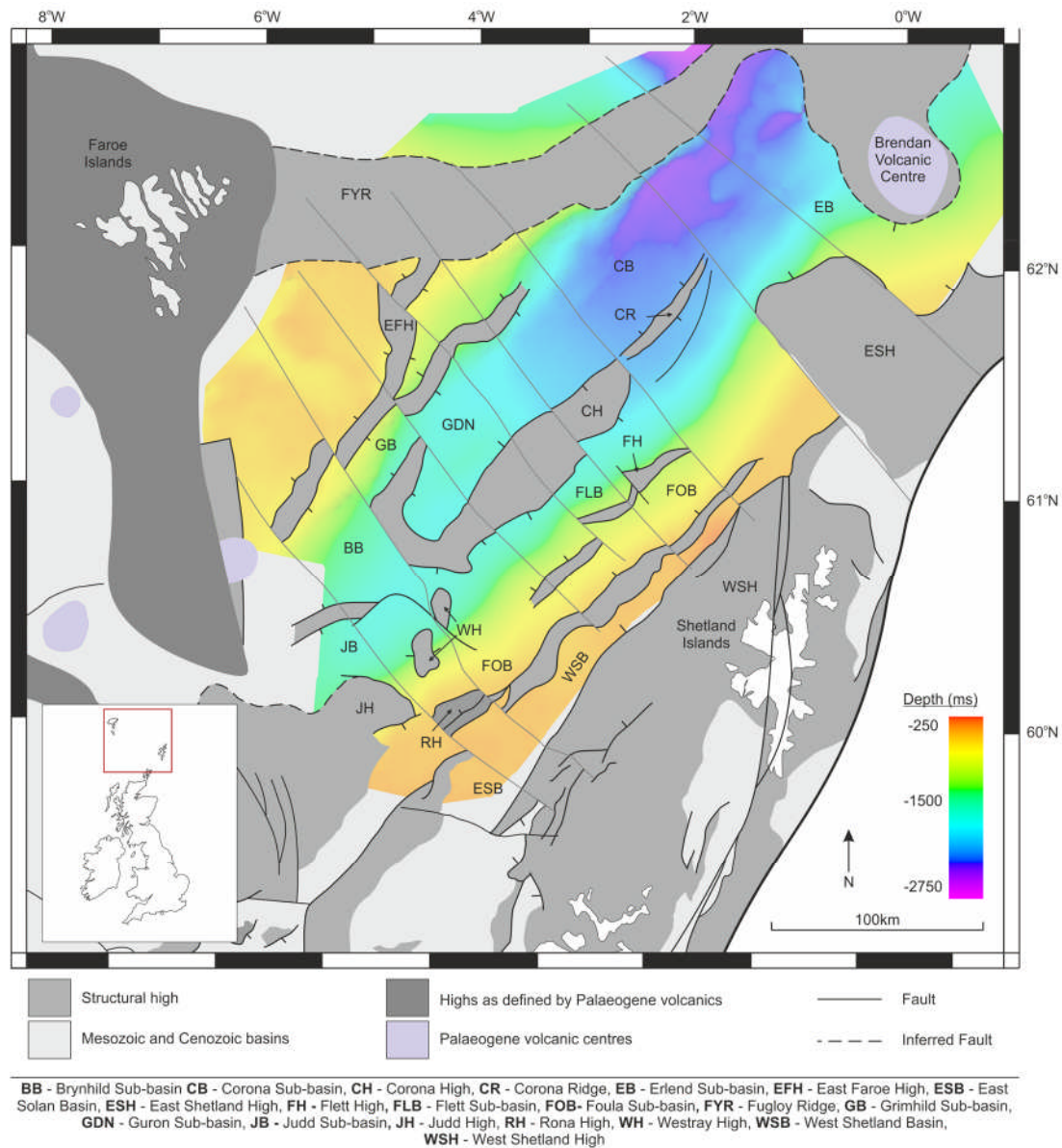


**Figure 2.2** – Regional map of the Faroe Shetland Basin superimposed with present day bathymetry. The map illustrates the dominant NE-SW trend of the crystalline basement highs which segment the basin into a series of sub-basins, which formed Mesozoic depocentres, adapted from Ritchie et al. (2011).

## 2.5 Hydrocarbon History of the Faroe-Shetland Basin

The Faroe-Shetland Basin has been the object of active hydrocarbon exploration since the first geophysical surveys of the 1960's and the early exploration wells of the early 1970's (Larsen et al., 2010). To date, over 150 exploration and appraisal wells have been drilled, along with many thousands of line-kilometres of 2D and 3D seismic data (Ritchie et al., 2011). Exploration has been moderately successful, with a number of currently-producing fields and several significant discoveries with development potential, despite which the margin is still considered to be one of the last remaining frontier regions with potential "big field" discoveries (Schofield et al., 2015).

Early exploration in the 1970s focused on shallow, tilted fault block targets and wells were drilled in the North Rona and West Shetland Basins with little success (Lamers and Carmichael, 1999, Larsen et al., 2010). Later encouraging shows within the Mesozoic succession on the Rona High, Judd and Foula Basins culminated in the discovery of the Clair and Victory fields in 1977. These discoveries occurred within Devonian-Carboniferous and Lower Cretaceous reservoirs, however, technical and economic restrictions meant that neither was developed at this time (Ritchie et al., 2011).

By the 1980's advances in technology allowed exploration to move towards deeper water, and there was a simultaneous shift from the traditional tilted fault block prospects to more complex plays such as stratigraphic traps (Ritchie et al., 2011). Numerous small, uneconomic discoveries were made across the Foula, Flett and East Solan basins (Loizou, 2005) were made throughout the decade and although the discovery of reservoir-quality Paleocene sandstones in the Flett Sub-basin stimulated further interest in the area (Smallwood and Kirk, 2005), nothing significant was found.

Waning exploration and lack of significant, economical discoveries by the late 1980s raised concerns as to the potential of landward basin settings as viable exploration targets (Herries et al., 1999). In the early 1990's, however, discoveries were made in the East Solan Basin, these being the Triassic Strathmore Discovery and the Upper Jurassic Solan discovery (Larsen et al., 2010).

The application of new technology was now improving exploration, with the Foinaven discovery coming through the reprocessing of seismic and amplitude anomaly analysis of older data (Cooper et al., 1999). Similar approaches led to the discovery of the Schiehallion and Loyal fields in the Paleocene sandstones of the Judd Sub-basin shortly after (Loizou, 2005). By the late 1990's the Corona High was an exploration target and after some unsuccessful drilling attempts the Tobermory discovery was made with a gas-bearing reservoir found within Eocene sands (Loizou, 2005). From the early 2000's onwards, exploration wells have continued to be drilled and new seismic data acquired for the appraisal of existing discoveries and further exploration (Ritchie et al., 2011).

The presence of multiple plays, which span stratigraphy provides an excellent case study to investigate the impact of sill intrusion on the hydrocarbon prospectivity of a frontier exploration basin.

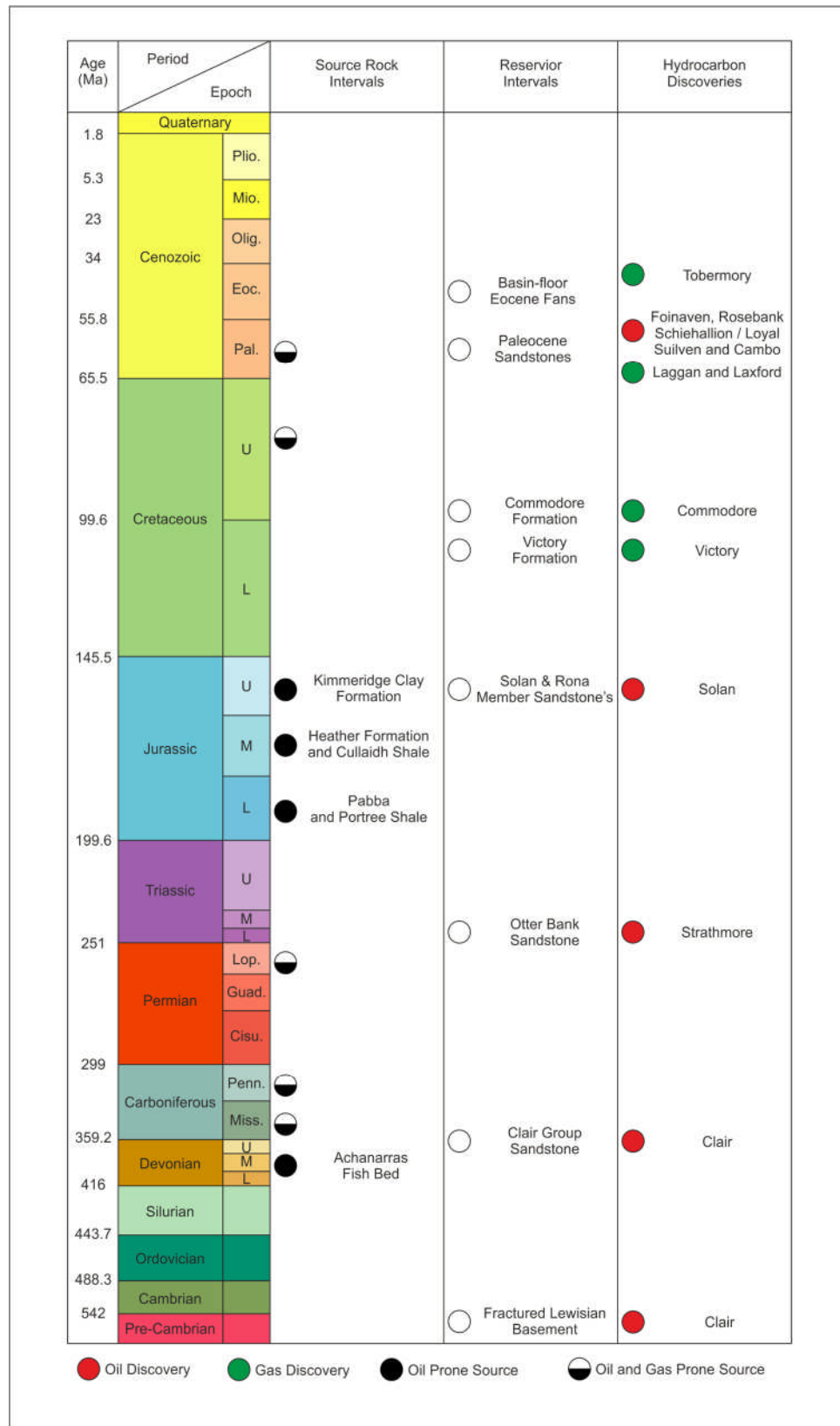


Figure 2.3 – A summary of the main proven hydrocarbon plays in the Faroe-Shetland Basin, adapted from Ritchie et al. (2011).

## 2.6 Sill Emplacement in Sedimentary Basins

### 2.6.1 Sill Emplacement

Large sill complexes are a common feature of LIPs and have been extensively studied in the Karoo-Basin, South Africa (Chevallier and Woodford, 1999), the Møre and Vøring Basin, W Norway (Planke et al., 2005), the Australian NW Shelf (Jackson et al 2013), the Parana Basin, Brazil (Bellieni et al., 1984), the Northern Yellow Sea basin, East China (Lee et al., 2006) and the Faroe-Shetland and Rockall Basins of the NE Atlantic (Smallwood and Maresh, 2002, Magee et al., 2013).

Until recently our understanding of sill emplacement was largely based on field studies (Du Toit, 1920, Bradley, 1965, Francis, 1982, Chevallier and Woodford, 1999), and consequently the partial and often limited exposure of outcrops meant many aspects of emplacement were poorly understood. More recently, however, an increase in experimental studies (Malthe-Sørensen et al., 2004, Menand et al., 2011, Galerne et al., 2011) and the availability of 3D seismic reflection data (Bell and Butcher, 2002, Smallwood and Maresh, 2002) have significantly enhanced our understanding of the 3D geometry, emplacement mechanisms and regional distribution of igneous sill complexes associated with volcanic passive-margins.

Sills are intrusive igneous bodies and vary significantly in width from a few metres to several kilometres (Bell and Butcher, 2002). They form as either sheet intrusions, emplaced parallel to bedding in stratified sedimentary sequences (Francis 1982) or as 'saucer-shaped' intrusions, which have concave-upwards morphologies with peripheral limbs that transgress stratigraphy (Du Toit, 1920, Leaman, 1975). It was not until the application of seismic reflection data, however, that the true complexity and variation of sill morphology was recognised (Smallwood and Maresh, 2002). In reality, the aforementioned geometries probably represent end members, with significant variation in between (Thomson and Schofield, 2008) (see Figure 2.).

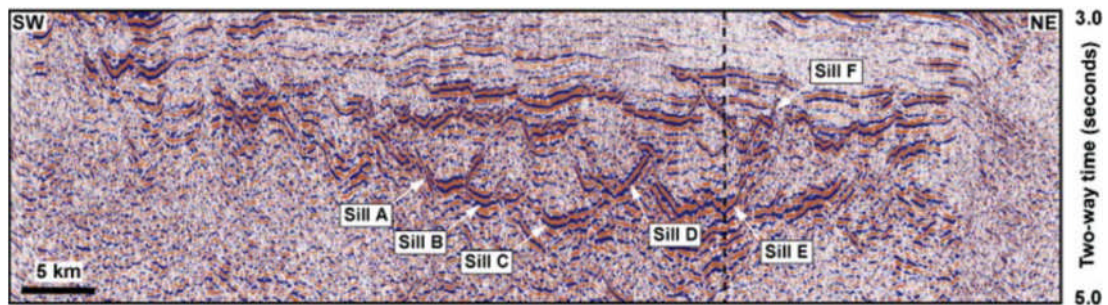


**Figure 2.4** – 2D seismic section from the Judd Sub-basin showing the variation in sill morphology, including flat, sheet intrusions (Sill F) and saucer-shaped bodies (e.g. Sill D & E), from (Thomson and Schofield, 2008).

Sills are typically fed by vertical or steeply-dipping dykes (Gretener, 1969, Kavanagh et al., 2006, Gouly and Schofield, 2008, Menand, 2008, Galerne et al., 2011), however, a debate exists whether this is beneath the base of the inner sill (Pollard and Johnson, 1973, Hansen et al., 2004, Malthe-Sørensen et al., 2004, Hansen and Cartwright, 2006a, Menand, 2008, Polteau et al., 2008, Galerne et al., 2011), or on the flanks of the outer sill (Bradley, 1965, Francis, 1982, Chevallier and Woodford, 1999, Gouly and Schofield, 2008). Seismic observations of in-situ 3D sill geometries suggest they are fed from their deepest but not necessarily most central point (Thomson and Schofield, 2008), with recent modelling studies appearing to confirm this (Galerie et al., 2011). The recognition of magma flow directions, lobes and magma fingers demonstrates that magma typically flows radially away from the feeder and up stratigraphy (Thomson and Schofield, 2008, Schofield et al., 2010, Schofield et al., 2012). It also is possible for sills to be fed by other sills (Thomson, 2004, Cartwright and Hansen, 2006), forming complex, interlinked networks, which transport magma from chambers at depth to the shallower sections of stratigraphy.

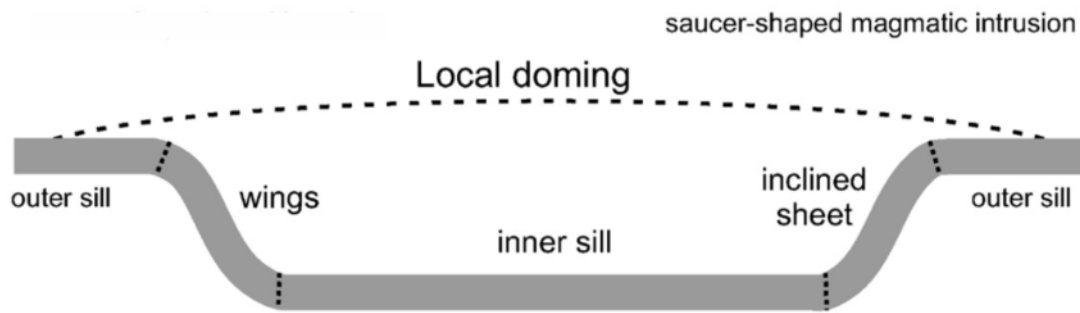


**Figure 2.5** – The components of a typical saucer-shaped sill, from Polteau et al. (2008)

There are two principle requirements for the emplacement of sills, these are: (1) the driving pressure of the magma must exceed the vertical stress of the overburden and the tensile strength of the host rock or a plane of weakness (Menand, 2008). (2) The least compressive stress ( $\sigma_3$ ) must be vertical or sub-vertical (Menand et al., 2011), during dyke emplacement the least compressive stress is horizontal, so in order for a dyke to spread laterally there must be modification of the stress field (Valentine and Krogh, 2006, Maccaferri et al., 2011). Further controls such as magma supply, rigid anisotropy in stratified sequences (Menand, 2008), host rock rheology (Gudmundsson, 2011), the effects of neutral buoyancy (Bradley, 1965, Roberts, 1970) and the structural regime during emplacement (Jackson et al., 2013, Magee et al., 2013) all play a role in the morphology, depth and size of the emplaced sills.

Pre-existing structure and lithology plays a key role on the emplacement of sill bodies, with sills exploiting the path of least resistance either through shales or exploiting fault planes to climb to higher stratigraphic levels (Thomson, 2007, Thomson and Schofield, 2008, Magee et al., 2013). There is also evidence to suggest that orientation of incipient break-up lineaments and other inherited structural trends play a key role in the distribution and emplacement of magma across a region, such as the ENE-WSW lineaments in the North Rockall Trough (Archer et al., 2005) and the NE-SW structural trend of the Faroe-Shetland Basin (Schofield et al., 2015).

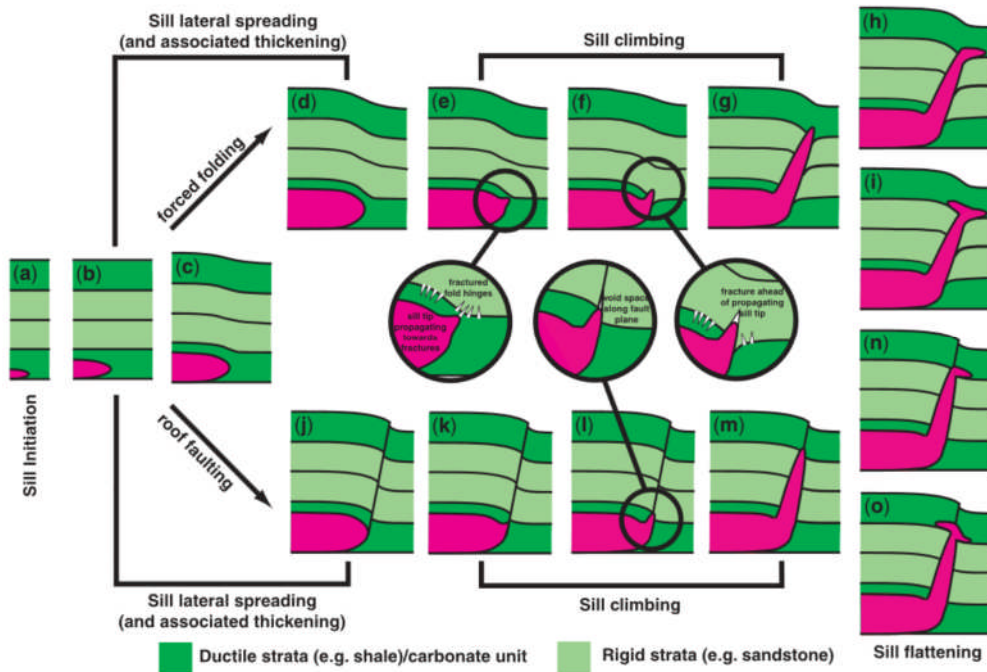


**Figure 2.6** – The stages of saucer-shaped sill emplacement, from Thomson and Schofield (2008). Initially sills spread laterally through ductile horizons such as shale, they then exploit weakness or faults in the overburden to climb up stratigraphy before flattening at a suitable horizon.

Radiometric dating of sills in the subsurface is sparse and often inaccurate (Schofield et al., 2015). The relative timing can, however, be established through the cross cutting relationships with host stratigraphy or older sills (Hansen et al., 2004) and through the deformation caused by local faults (Magee et al., 2013). The process of sill emplacement may form forced folds (Trude et al., 2003, Hansen and Cartwright, 2006b, Jackson et al., 2013) or hydrothermal vent systems (Trude et al., 2003, Davies et al., 2002, Hansen et al., 2004, Svensen et al., 2004, Planke et al., 2005, Cartwright et al., 2007, Magee et al., 2013) within the overlying stratigraphy, such topographic features developing onlap relationships with later sediments and having been used to successfully date the intrusions.

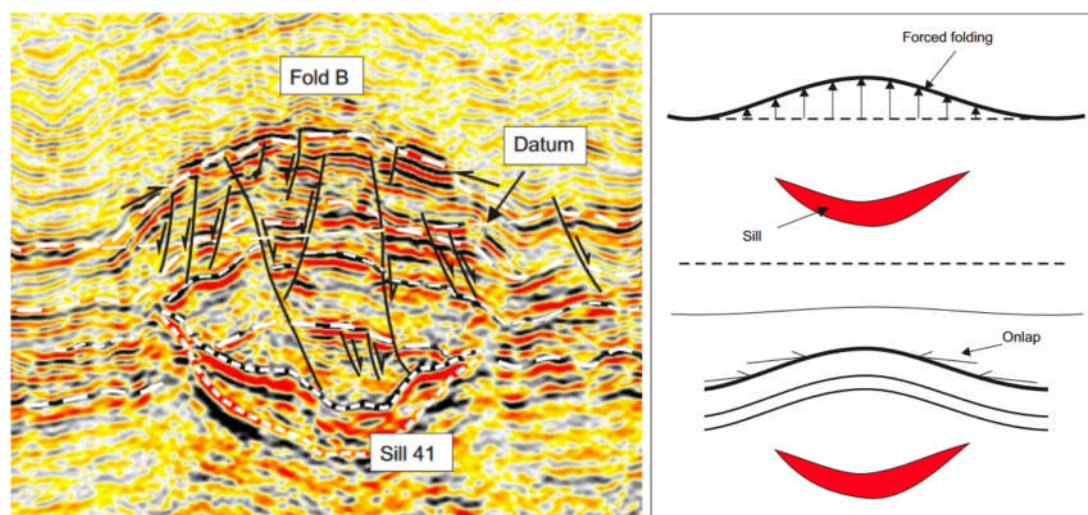


**Figure 2.7** – A seismic example and schematic formation model of forced folding above a sill intrusion, adapted from Hansen and Cartwright (2006b). The overburden is deformed during sill emplacement, sediments then onlap the structure, which can be used to give a relative timing of intrusion.

## 2.7 The Impact of Sills on Hydrocarbon Systems

As hydrocarbon exploration spreads to volcanic margin basins (Archer et al., 2005), it becomes increasingly important to understand the impact intrusive igneous bodies, such as sills, have on prospectivity. Sills have the ability to both enhance and disrupt hydrocarbon plays (Rateau et al., 2013) as well as having thermal implications for hydrocarbon maturation (Fjeldskaar et al., 2008). Studies are beginning to demonstrate the importance of understanding sills and their implications for hydrocarbon prospectivity (Schutter, 2003, Jamtveit et al., 2004, Archer et al., 2005, Lee et al., 2006, Holford et al., 2012, Witte et al., 2012, Holford et al., 2013, Rateau et al., 2013).

### 2.7.1 Thermal Impact

Sill emplacement has been shown to modify the thermal evolution of the sedimentary basins into which they are emplaced (Brown et al., 1994). On a regional scale, the contact metamorphism of organic matter and hydrous minerals produces large volumes of methane, which are released through vent complexes into the atmosphere (Svensen et al., 2004, Svensen et al., 2006, Aarnes et al., 2010). Over a short period of time such volumes of methane can impact the global carbon

cycle (Aarnes et al., 2011). Indeed, climate variations have been attributed to the emplacement of sills within LIPs such as North Atlantic Igneous Province, the Karoo-Ferrar Province, the Siberian Traps and the Emshian Volcanic Province (Pálfy and Smith, 2000, Svensen et al., 2004, Ganino and Arndt, 2009).

On a local scale, contact metamorphism caused by sill intrusion has been shown to enhance the maturation of organic matter (Jaeger, 1964, Peters et al., 1978, Simonet et al., 1981, Hutton and Henstridge, 1985, Clayton and Bostick, 1986, Saxby and Stephenson, 1987, George, 1992, Galushkin, 1997, Gurba and Weber, 2001, Cooper et al., 2007, Jones et al., 2007, Fjeldskaar et al., 2008, Rimmer et al., 2009, Wang and Manga, 2015). The extent of maturation is typically linked to the thickness of the sill, with thermal aureoles ranging between 0.5 and 5 times the sill's thickness (Galushkin, 1997). The thermal impact of sill intrusion has a cumulative effect when sills are emplaced within close vertical proximity as opposed to isolated bodies (Annen and Sparks, 2002, Aarnes et al., 2011). Once emplaced, the low thermal conductivity of sills may have an insulating effect on the surrounding sediments (Chen et al., 1999).

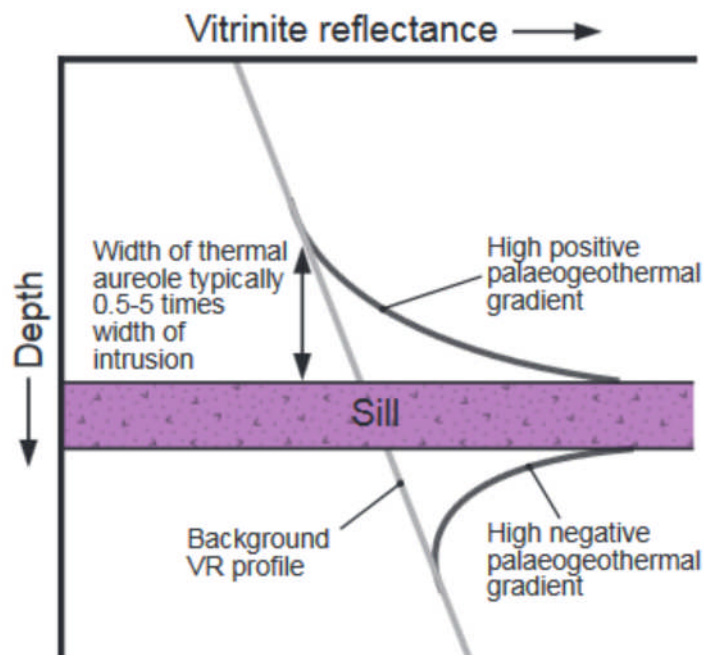


**Figure 2.8** – Schematic illustration showing the impact of sill intrusion on predicted vitrinite reflectance profiles, after Holford et al. (2013).

### 2.7.2 Physical Impact

Given the low porosity, low permeability characteristics of crystalline igneous rock (Robertson, 1988, Clauser and Huenges, 1995) it is reasonable to assume that (where present), sills have a detrimental effect on hydrocarbon migration (Holford et al., 2012). Indeed, sills have been shown to act as impermeable barriers creating compartmentalisation of reservoirs and restricting fluid flow through the subsurface (Holford et al., 2013); they even have the potential to form hydrocarbon traps where they cut inclined or tilted strata (Lee et al., 2006)

In some instances, however, sills may actually have greater porosity and permeability than the surrounding host lithology, given that sills preferentially intrude shales and muds which are themselves low porosity, low permeability rocks (Thomson and Schofield, 2008). The presence of vesicles has been linked to increased sill porosity, as has the hydrothermal and low temperature alteration of sills such as the dolerite sills in the Ayukawa Oil Field, Japan (Hoshi and Okubo, 2010). Additionally, open fractures, such as those caused during cooling, provide secondary porosity and permeability, and have been linked to gas shows in sills drilled within the Faroe-Shetland Basin (Rateau et al., 2013) and may form naturally-fractured reservoirs (Ray, 1989, Masters, 2000, Petford and McCaffrey, 2003, Witte et al., 2012). In such cases it is possible for sills to become the preferential sites of migration, providing a baffled, interconnected migration pathway through otherwise impermeable host rocks (Rateau et al., 2013).

Where sills have been shown to be fed by vertical or steeply dipping dykes (Gretener, 1969, Kavanagh et al., 2006, Valentine and Krogh, 2006, Gouly and Schofield, 2008, Menand, 2008), these feeding systems may act as an impermeable barrier comparative to a sealing fault through stratigraphic layers (Lee et al., 2006).

Hydrothermal pipes and vents have been recognised in volcanic basins worldwide (Jamtveit et al., 2004, Svensen et al., 2004, Planke et al., 2005, Hansen, 2006, Lee et al., 2006). They are contemporaneous with sill emplacement and form distinctive zones of chaotic seismic reflection above the flanks or inclined tips of sill intrusions (Hansen et al., 2004). Such features are predicted to occur in any sedimentary basin where there is a phase of intrusive volcanic activity (Trude et al., 2003, Hansen et

al., 2004, Svensen et al., 2004). The presence of hydrothermal vents results in the heating of groundwater to a supercritical state, making it an excellent solvent for hydrocarbons (Schutter, 2003). This can play an important role in mobilising hydrocarbons through the subsurface, either aiding migration to established reservoirs or losing charge through seepage (Schutter, 2003). The formation of hydrothermal vent systems can compromise overlying seals and the established pipe systems they form may still serve as a conduit to fluid migration long after the initial intrusion event is over and once all hydrothermal activity has subsided (Cartwright et al., 2007).

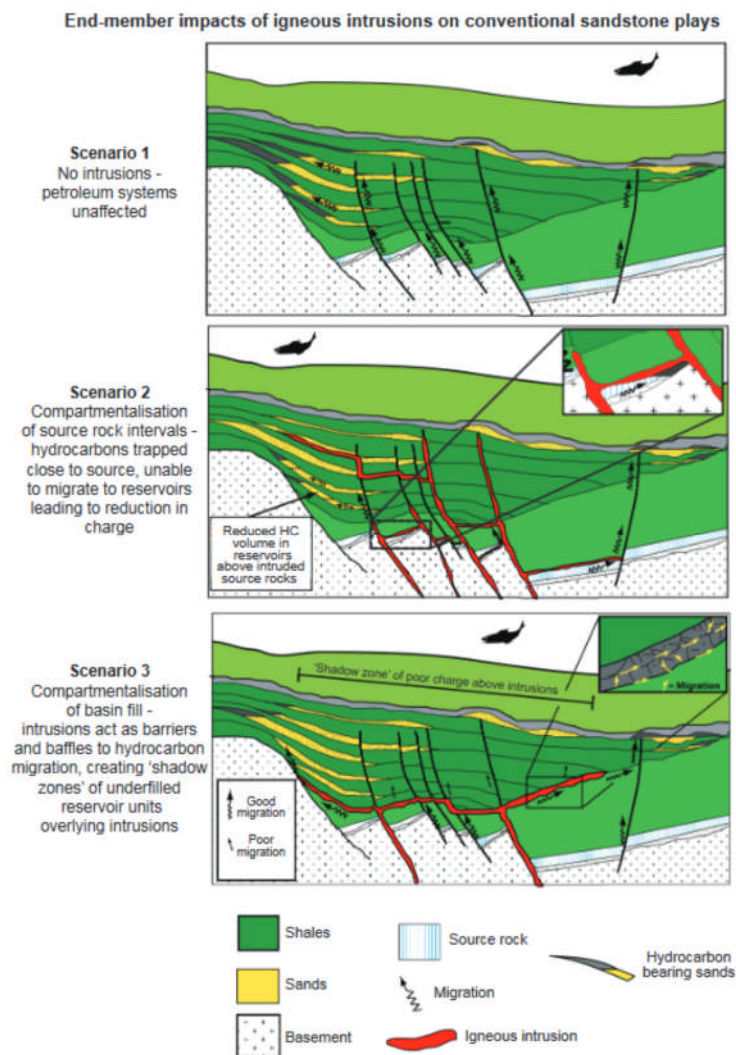


**Figure 2.3** – The potential impacts of sill intrusion of siliciclastic hydrocarbon plays, from Holford et al. (2013).



## Chapter 3 Data & Methods

### 3.1 Introduction

This chapter provides an overview of the data, software and methods used to study the volcanic development and petroleum system evolution of the Faroe-Shetland Basin.

The interpretation of seismic reflection data is a primary tool for the exploration of hydrocarbons, especially in offshore and deep-water settings (Kearey et al., 2013). It is routinely used to image the subsurface, allowing us to study the structural and stratigraphic trends of the area to reduce risk during exploration (Hart, 1999).

Surveys shot over volcanic passive margins (such as the NE Atlantic Margin) inevitably image the widespread igneous material emplaced during margin formation (Smallwood and Maresh, 2002). Whilst this can be problematic from an exploration perspective it provides an excellent opportunity to study large-scale, in-situ intrusions, which are usually only partially exposed at the Earth's surface (Bell and Butcher, 2002, Schofield et al., 2015).

This study utilises industry-acquired seismic reflection surveys and commercial wire-line well log data to study the intrusive volcanic complexes and their impact on hydrocarbon systems. Where necessary, the resolution and limitations of the seismic reflection data are discussed, specifically where issues arise due to the presence of igneous material - a common and persistent problem throughout the basin (Smallwood and Maresh, 2002).

An overview is given on the seismic interpretation methods used throughout this thesis (Section 3.7), however, specific methods and workflows utilised in Chapters 5, 6 and 7 are not detailed here as they represent stand-alone pieces of work. As such, detailed descriptions are best presented within the individual chapters.

### 3.2 Fundamentals of Seismic Reflection Data

Seismic reflection surveying is a geophysical technique used to image the subsurface through the detection of acoustic energy that is reflected from lithological interfaces in the subsurface (Bacon et al., 2007). Seismic reflection data record the changes in acoustic impedance (the resistance to propagation of sound energy) as waves propagate through the sub-surface. Acoustic impedance ( $Z$ ) can be expressed as a function of density ( $\rho$ ) and velocity ( $V$ ):

$$Z = \rho \times V$$

#### Equation 3.1

The density and seismic velocity of a given lithology are controlled by a range of variables including; porosity, pore fluid pressure, composition, burial depth, texture and temperature (Kearey et al., 2013).

Seismic reflection data provide an approximate cross-section of the underlying subsurface geology and is typically displayed in two-way travel time (TWTT). Whilst the data may be a close proxy of underlying subsurface geology it is actually only displaying relative changes in acoustic impedance (density and velocity), which are significant enough to create a reflection response (Sheriff and Geldart, 1995). The resolution of the seismic data controls how representative the seismic reflection profiles are of the true subsurface geology (Bacon et al., 2007).

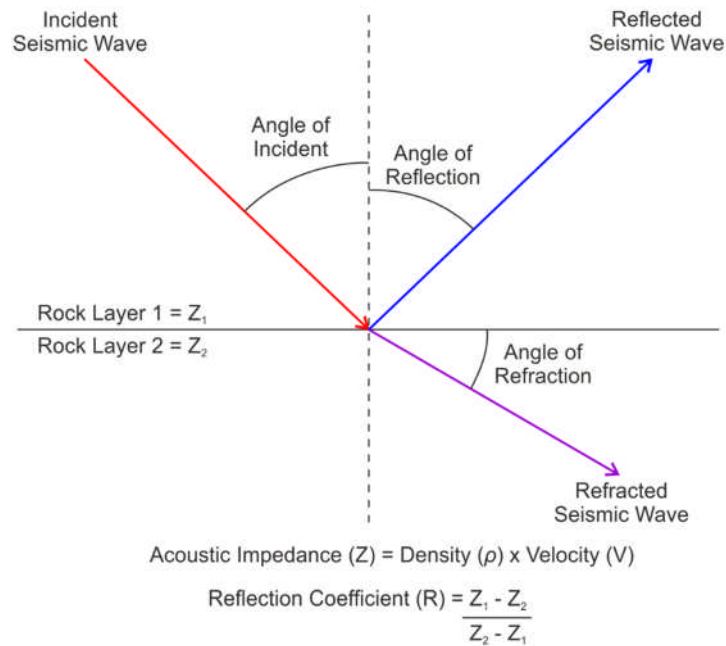


**Figure 3.1** – The interaction of a seismic wave at a sub-surface interface and the relationship between velocity, density and the reflection coefficient Wright (2012), adapted from Sheriff and Geldart (1995) and Ashcroft (2011).

### 3.3 Resolution of Seismic Reflection Data

The resolution of seismic data defines the minimum distance between vertical and horizontal features required for them to be imaged as separate events (Sheriff and Geldart, 1995). Seismic resolution is dependent on the wavelength ( $\lambda$ ) of the seismic signal, which is a function of seismic velocity ( $V$ ) and the dominant frequency ( $f$ ) and can be expressed as:

$$\lambda = \frac{V}{f}$$

**Equation 3.2**

As such, the vertical resolution ( $R_v$ ) of seismic data is a function of wavelength and can be expressed as:

$$R_v = \frac{\lambda}{4}$$

**Equation 3.3**

Similarly the horizontal resolution ( $R_h$ ) can be expressed as:

$$R_H = \frac{\lambda}{2}$$

**Equation 3.4**

The vertical resolution ( $R_V$ ) controls how far apart two objects must be in space to be imaged as separate reflection events such as stratigraphic or sequence boundaries. Horizontal resolution ( $R_H$ ) controls how far apart features must be on a single interface for them to be imaged as separate events such as discontinuities on the reflection surface created by faults (all equations are from Sheriff and Geldart (1995)).

The resolution of seismic reflection data typically decreases with depth due to changes in seismic velocity and dominant frequency (Bacon et al., 2007). Seismic velocities in most settings increase with depth due to the compaction of sediment during burial (Kearey et al., 2013). In contrast, the dominant frequency of the signal is characteristically lower due to the loss of seismic energy through attenuation, scattering and absorption (Sheriff and Geldart, 1995). Where appropriate in this thesis the resolution of the data is stated within individual chapters.

The presence of igneous rocks within sedimentary successions also impacts the resolution of seismic data (Roberts et al., 2005). The high density, high velocity igneous rock accelerates the rate of acoustic scattering and absorption reducing the dominant frequency whilst simultaneously increasing seismic velocity (Shaw et al., 2008, Nelson, 2010). This problem is well documented in the Faroe-Shetland Basin (Nelson, 2010, Schofield et al., 2015), in particular below the thick, Early Cenozoic basalts which reduce resolution such that published seismic interpretations often estimate or neglect completely the interpretation of sub-basalt structures (Lamers and Carmichael, 1999, Ritchie et al., 2011). The problems associated with igneous rocks and seismic resolution are discussed further in Section 3.7.4.

**3.4 Fundamentals of Well Data**

The drilling of exploration wells allows for the collection of high-resolution 1D geophysical data, they also provide physical samples of subsurface formations

through the collection of core, sidewall cores and cuttings (Asquith et al., 2004). Well data has a significantly higher resolution than seismic reflection data, with centimetre-scale wireline logs and millimetre-scale core samples (Rider, 1986), however, these data must be extrapolated over large distances using seismic data, to correlate between 1D well points (Serra, 1983).

Wireline logs are deployed down exploration wells to measure the in-situ physical properties of the rock, such as radioactivity, resistivity, seismic velocity and density (Asquith et al., 2004). The data are converted into continuous, high-resolution geophysical logs and are interpreted as a suite to determine the lithology, age and structure of formations. Further analysis can also help deduce physical properties such as porosity, permeability and the presence of hydrocarbons (Rider, 1986).

Wells also provide physical samples of subsurface formations through the collection of conventional core or sidewall core. Aside from identifying formation lithologies the samples can be analysed using radiometric and biostratigraphic dating, micro-scale deformation analysis and investigated for hydrocarbon presence indicators (Asquith et al., 2004).

The following well logs have been used within this study:

### ***Interval Velocity & Average Velocity***

Velocity logs measure the seismic velocity of a formation by emitting an acoustic wave and recording the time taken for it to return to the receiver (Rider, 1986). Velocity is strongly influenced by lithology, density, porosity and fluid pressure, and generally increases with depth (Asquith et al., 2004).

Interval velocities define the seismic velocity over a particular formation or chronostratigraphic division and are used to construct velocity models for depth conversion. Data from wells in close proximity or that drill through the same formations may be combined to produce average velocities for that area (Serra, 1983).

***Gamma Ray (GR) & Standard Resolution Formation Density (RHOZ)***

Gamma ray logs measure the radioactivity of rock formations through the decay of  $^{40}\text{K}$ ,  $^{238}\text{U}$  and  $^{232}\text{Th}$  isotopes (Asquith et al., 2004). High gamma ray responses (measured in API units) are diagnostic of clay-rich lithologies due to the high natural radioactivity of k-feldspars, micas and clay minerals (Serra, 1983). High gamma ray response may also be an indication the formation has a high organic content (Asquith et al., 2004).

Density logs use back-scattered radiation to measure the density of the rock formation, the value represents the total combined density of the rock particles, pore space and pore fluid (Rider, 1986, Asquith et al., 2004). Density logs can be especially useful in the identification of volcanic rocks in sedimentary sequences (Serra, 1983).

***Vitrinite Reflectance (VR)***

Vitrinite is a common component in sedimentary kerogens and is produced during the diagenesis of organic plant matter such as lignin and cellulose (Dow, 1977). Vitrinite reflectance (%Ro) is a measurement of the percentage of light reflected off a vitrinite maceral at 500X magnification in oil immersion (Cardott, 2014). Vitrinite reflectance values can be calibrated to determine the peak temperature history of the sample, which in turn can be used to reconstruct the thermal evolution of sedimentary basins (Burnham and Sweeney, 1989, Sweeney and Burnham, 1990). As vitrinite reflectance is particularly sensitive over temperatures ranging from 60-120 °C it can be used effectively as a proxy for hydrocarbon maturity (Cardott, 2014).

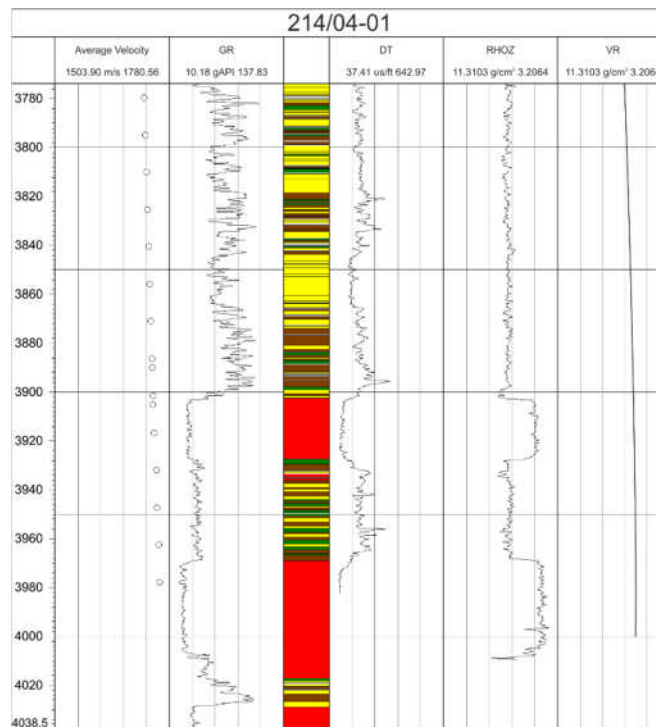


**Figure 3.2** – An example of the well logs used this study; the compiled lithology log from TGS was calibrated with the available wireline data.

### 3.5 Data used in this study

Geophysical surveys were first undertaken in the Faroe-Shetland Basin during the early phases of exploration in the 1960's and were followed shortly after by the drilling of exploration wells in the early 1970's. Since then, many thousand line-kilometres of high quality 2D and 3D seismic reflection data have been acquired and upwards of 150 appraisal wells drilled (Ritchie et al., 2011).

This study uses a combination of commercially acquired seismic reflection surveys supplemented with wireline log data from a series of selected appraisal wells, the location, quality and applications of the data are outlined below.

#### 3.5.1 Seismic Data

All seismic data were provided by E.ON E&P under the license of seismic contractors Petroleum Geo-Services and TGS for academic use at the University of

Leeds. The data arrived processed and ready to interpret; as such, little is known of the processing methods used. All seismic data are supplied and displayed in two-way travel time (TWTT). Depth conversion, when required, was undertaken using the interval velocities obtained from well check shot data.

### 3.5.1.1 2D Data

This study utilises two, 2D seismic reflection surveys (FSB99 & NSR06), which were acquired, processed and licenced by TGS Survey. FSB99 consists of 59 individual lines totalling 5000 line kilometres; the data cover much of the central and northern areas of the basin including the Corona, Flett and Guorun Sub-basins, the Corona High and the Fugloy Ridge. Survey NSR06 consists of 67 lines with a total of 4520 line kilometres and covers the shallow basins immediately west of the Shetland Isles including the West Solan, South Solan, East Shetland and West Shetland Sub-basins (Figure 3.3).

Collated check-shot data from the available commercial wells was used to determine average seismic velocities, which were then employed to calculate vertical resolution of the seismic data (see Table 3.1). Many of the wells are restricted to basin highs and have limited penetration depths so the velocities, especially in the deeper Mesozoic and sub-volcanic sections are likely to be a conservative estimate. The average vertical seismic resolution ( $R_v$ ) is around 10 m in the Cenozoic section and 25 m in the Paleogene section. Resolution increases to around 35 m in the upper parts of the volcanic-free Mesozoic succession, whilst sub-basalt resolution is around 60 m (although as low as 90 m) Table 3.2).

The 2D seismic data provides a basis for petroleum system modelling (Chapter 6) and sill intrusion modelling (Chapter 7).

	FSB				NSR06			
	Velocity (m/s)		Dom. Freq. (Hz)		Velocity (m/s)		Dom. Freq. (Hz)	
	Min V	Max V	Min <i>f</i>	Max <i>f</i>	Min V	Max V	Min <i>f</i>	Max <i>f</i>
Neogene	1600	2000	30	45	1600	1800	30	52
Paleogene	1600	2300	15	30	1700	2000	15	35
Mesozoic	1700	2400	12.5	20	1800	2200	15	25
Sub-Volc.	2000	2800	7.5	15	2500	2700	7.5	22

**Table 3.1** – Table showing the minimum and maximum seismic velocities (*V*) and dominant frequencies (*f*) at different stratigraphic levels for the FSB99 and NSR06 2D seismic surveys used in this study, values represent area averages, actual values may vary between individual lines. The velocity of Sub-Volcanic and Mesozoic sections represents a conservative estimate due to the limited well penetration of these formations.

	FSB				NSR06			
	Horiz. Res. (m)		Vertical Res. (m)		Horiz. Res. (m)		Vertical Res. (m)	
	Min <i>R<sub>h</sub></i>	Max <i>R<sub>h</sub></i>	Min <i>R<sub>v</sub></i>	Max <i>R<sub>v</sub></i>	Min <i>R<sub>h</sub></i>	Max <i>R<sub>h</sub></i>	Min <i>R<sub>v</sub></i>	Max <i>R<sub>v</sub></i>
Neogene	17	33	9	16.5	15	30	7.5	15
Paleogene	26	76	13	38	24	66	12	33
Mesozoic	43	96	22	48	36	73	18	36
Sub-Volc.	66	186	33	93	56	180	28	90

**Table 3.2** – Table showing the calculated minimum and maximum vertical and horizontal resolution at different stratigraphic levels for the FSB99 and NSR06 2D seismic surveys.

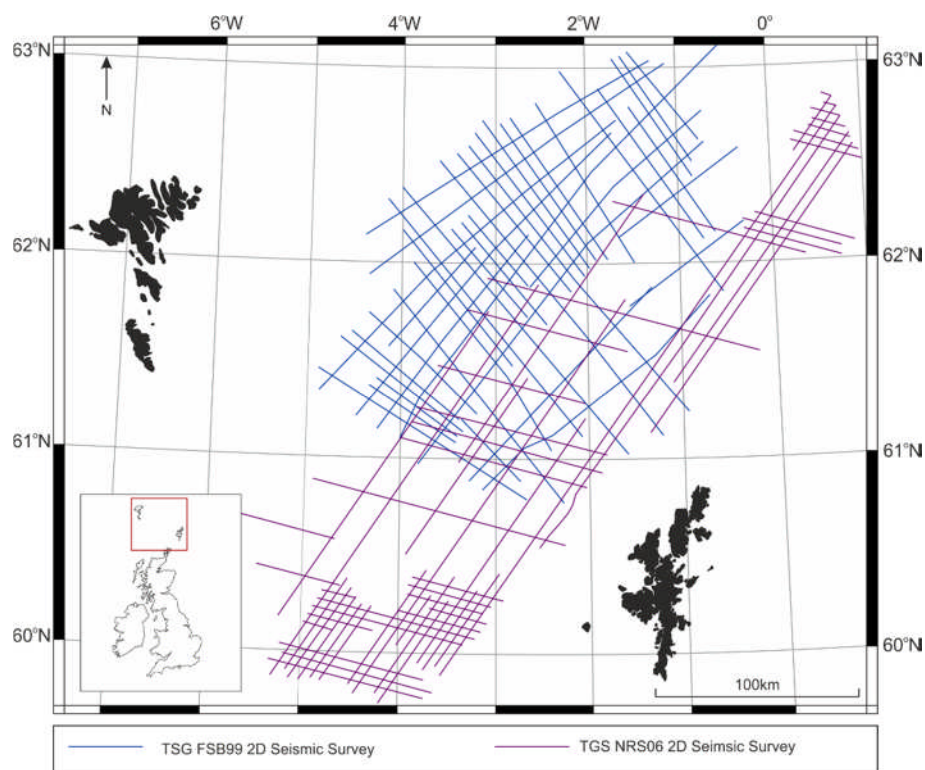


**Figure 3.3** – Map of the Faroe-Shetland Basin showing the 2D seismic surveys used in this study, selected lines are used to undertake petroleum system modelling in Chapters 6 & 7.

### 3.5.1.2 3D Data

This study also utilises 3D seismic reflection dataset, this consists of two sub-sections of the MegaSurveyPlus 3D survey, acquired by PGS in the late 1990's. This high-resolution dataset covers upwards of 8,000 km<sup>2</sup> across the central section of the basin and images to 10 s TWTT with a water depth of up to 1600 m (Figure 3.4).

The Q214 survey (Figure 3.4 – Green) has an area of 2,365 km<sup>2</sup>, it overlies the Corona and Flett Sub-basins with the Corona Ridge trending NE-SW through the centre of the dataset. The dataset provides excellent imaging of the Faroe-Shetland Sill Complex and the overlying post-rift basin fill, image quality below the sills and flood basalt is substantially less (Discussed in Section 3.7.4). This dataset is used for the interpretation and analysis of the Faroe-Shetland Sill Complex in Chapter 4.

The second survey is a merged cube comprised of smaller sub-sections Q213-99, WZ-98, WZ-96/97 and TR 7&8 covering a total area of 5,574 km<sup>2</sup> and runs through

the central axis of the basin over the Corona high and Guron Sub-basin (Figure 3.4 – Red). A small, cropped sub-section of this survey is used to undertake spectral decomposition analysis of sill intrusions in Chapter 5 (Figure 3.4 – Blue).

At the base of the Cenozoic succession, the seismic resolution of the data is around 40 m (average velocity 2800 m/s, average dominant frequency 17 Hz), this decreases to between 50 – 80 m (average velocity 3000 - 4500 m/s, average dominant frequency 14 Hz) in the Cretaceous succession, depending on the depth and density of sill intrusion.

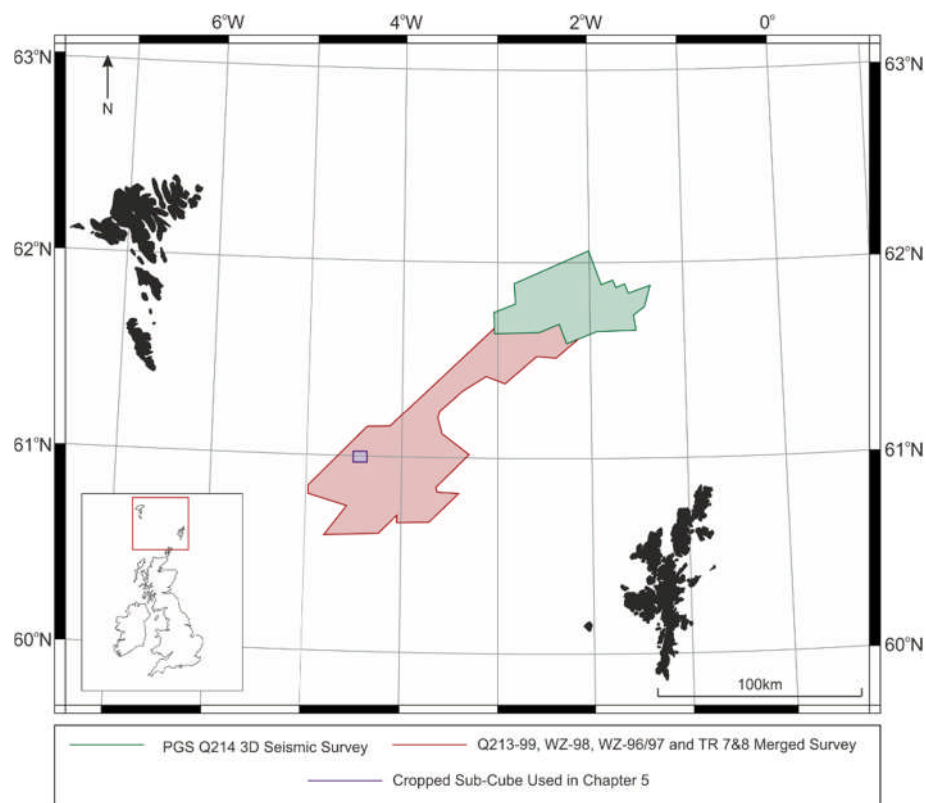


**Figure 3.4** – Map of the Faroe-Shetland Basin showing the 3D seismic surveys used in this study. Survey Q214 forms the basis of seismic observations in Chapter 4. Surveys Q213-99, WZ-96/97/08 and TR 7 & 8 are merged into a single cube, a sub-crop of which is used for attribute analysis in Chapter 5.

### 3.5.2 Well Data

Although over 150 exploration wells have been drilled in the Faroe-Shetland Basin, they are largely restricted to basin margins and structural highs (Holmes et al., 1999). Consequently, there is limited well control of the deeper Mesozoic succession, including the prolific Kimmeridgian source rock in the central and deeper regions of the basin. A number of commercial wells are used in this study (Figure 3.5 & Table 3.3), the wells were pre-loaded with formation and chrono-stratigraphic well tops compiled by TGS; where possible these well tops were used for the identification and correlation of the main stratigraphic horizons used throughout the thesis. Lithological logs were also provided, compiled by TGS. These logs combined all geophysical and core data to determine formation lithologies, the lithological interpretations were calibrated using available gamma-ray and density logs, before being used to populate the petroleum system models in Chapters 6 & 7. Interval velocities are used to depth-convert regional 2D seismic profiles from TWTT to depth (Chapter 6) a pre-requisite for petroleum system modelling (Chapters 6 & 7). Vitrinite reflectance profiles are used to calibrate the heat flow models during petroleum system modelling (Chapter 6).

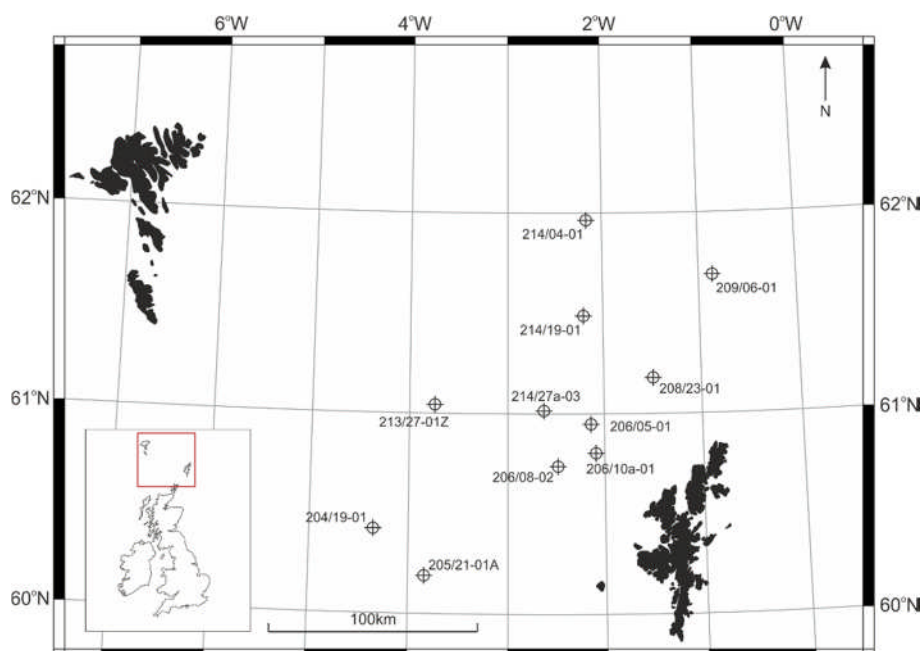


**Figure 3.5** – Regional map showing the location of commercial wells used throughout this study.

Well Name	Latitude	Longitude	Measured Depth
204/19-01	060 25 14.200N	004 20 52.500W	15280
205/21-01A	060 10 57.000N	003 50 35.000W	4406
206/05-01	060 56 26.000N	002 10 14.300W	13515
206/08-02	060 44 08.550N	002 28 52.010W	6200
206/10a-01	060 48 20.670N	002 08 58.700W	9725
208/23-01	061 10 13.900N	001 30 53.500W	6697
209/06-01	061 41 18.960N	000 52 13.740W	12719
213/27-01Z	061 03 06.900N	003 43 34.100W	12153
214/04-01	061 57 53.130N	002 14 02.210W	14175
214/19-01	061 48 15.630N	002 12 03.200W	15580
214/27a-03	061 00 35.930N	002 39 00.460W	14412

**Table 3.3** – An overview of the commercial wells used in the study.

### 3.6 Software

A number of commercial software packages were used throughout this study and provide the platform for a variety of data analysis and modelling workflows, including but not limited to: seismic interpretation, depth conversion, well correlation, flexural back-stripping and petroleum system modelling. All work was undertaken using a workstation running Windows® operating system under academic licences at the University of Leeds.

#### ***Petrel® (Ver. 2014.5, Schlumberger)***

*Petrel®* is a seismic interpretation, geo-cellular modelling and reservoir simulation software platform, which enables the integration of multiple data types for various and widespread applications.

For the purposes of this study, *Petrel*<sup>®</sup> was primarily used as a seismic and well-interpretation platform, producing the basis of observations used in Chapter 4 and the inputs for workflows in Chapters 5, 6 & 7.

***OpendTect*<sup>®</sup> (Ver. 5.0.8, dGB Earth Sciences)**

*OpendTect*<sup>®</sup> is an open source seismic interpretation platform; with a similar basic functionality to *Petrel*<sup>®</sup>, however, it contains specific volume attribute algorithms, which *Petrel*<sup>®</sup> does not; this software was therefore used to generate spectral decomposition attribute cubes for the analysis of sill intrusions in Chapter 5.

3D seismic dataset are imported from *Petrel* into *OpendTect*<sup>®</sup> where Discrete Fourier Transform and Continuous Wavelet Transform algorithms are used to generate spectral decomposition attribute cubes, the cubes are then returned to *Petrel*<sup>®</sup> for re-interpretation; more detail is presented in Chapter 5.

***Flexural Decomposition*<sup>®</sup> (Badley Geoscience)**

*Flexural decomposition*<sup>®</sup> is a reverse-modelling software package used to establish the  $\beta$ -factors of present day geological cross sections through the sequential back-stripping and decompaction of post-rift sedimentary layers.

In this study, *Flexural Decomposition*<sup>®</sup> was used to determine whole-crustal  $\beta$ -factors from regional 2D seismic profiles (imported from in *Petrel*). The computed  $\beta$ -factors were used to construct 2D heat flow models, which were applied during petroleum system modelling (Chapter 6).

***Petromod*<sup>®</sup> (Ver. 2014.1, Schlumberger)**

*Petromod*<sup>®</sup> is a predictive forward-modelling software package used to study the petroleum system evolution of sedimentary basins. The structural, thermal and depositional history of the basin can be reconstructed through time in order to simulate the maturation, migration and trapping of hydrocarbons.

The software was used for the petroleum system modelling undertaken in Chapters 6 and for the modelling of sill intrusions in Chapter 7.

Software	Application	Used In
Petrel®	Seismic interpretation, depth conversion, horizon generation, wireline well log interpretation/correlation.	Chapters 4, 5 & 6
OpendTect®	Geophysical attribute generation.	Chapter 5
Flexural Decompaction®	Lithospheric backstripping to determine stretching factors.	Chapter 6
Petromod®	Petroleum system modelling and intrusion modelling.	Chapter 6 & 7

**Table 3.4** – Summary of the software packages used in this study and their application.

### 3.7 Seismic Interpretation

Seismic interpretation was the primary method of data analysis used throughout this thesis, it forms the basis of the observations made in Chapters 4 & 5 and provides the inputs for the modelling undertaken in Chapters 6 & 7.

This section briefly highlights the theory, techniques and limitations of seismic interpretation in the Faroe-Shetland Basin.

#### 3.7.1 Polarity

All seismic data in this study are presented using the Society of Exploration Geophysicists normal convention (positive standard polarity). The polarity of seismic data is dependent on the change in acoustic impedance at a given reflection interface (Sheriff and Geldart, 1995).

Negative acoustic impedance is displayed as a trough (red) and represents the transition of a seismic wavelet from a higher velocity, higher density lithology into a lower velocity, lower density lithology. In contrast positive acoustic impedance is displayed as a peak (black) and represents the transition of the seismic wavelet from lower velocity, lower density lithology into a higher velocity, higher density lithology (Figure 3.6).

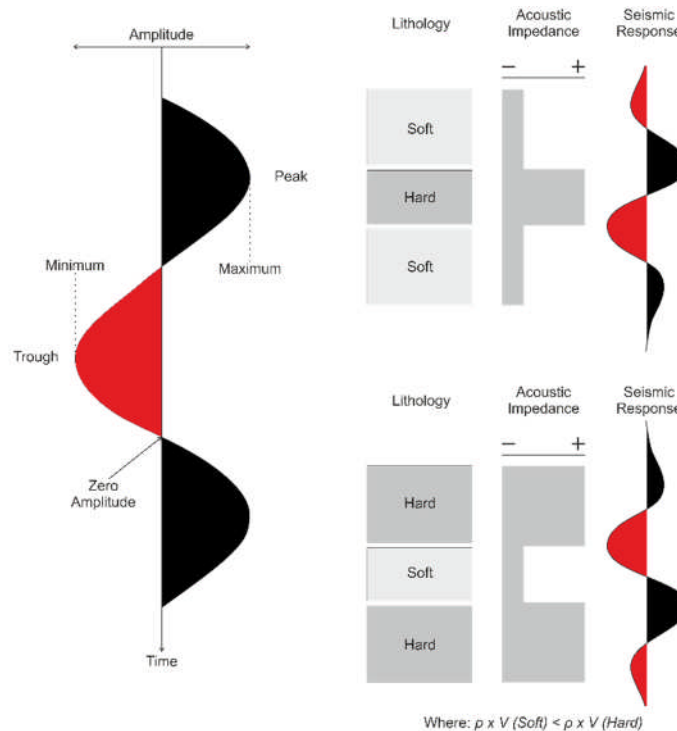
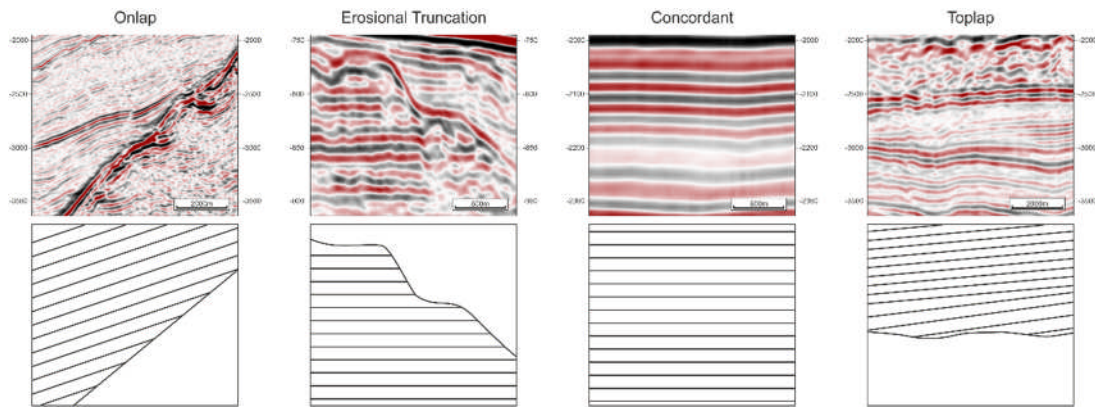


**Figure 3.6** – Schematic illustration of a seismic wavelet (SEG normal convention) and its response to changes in acoustic impedance (Sheriff and Geldart, 1995). An increase in acoustic impedance results in a positive amplitude change and is displayed as a peak; a decrease in acoustic impedance results in a negative amplitude change and is displayed as a trough.

### 3.7.2 Horizon Interpretation

Seismic reflection data provide an approximate 2D cross-section of the underlying subsurface; through horizon interpretation, individual seismic reflectors can be mapped across a region to establish their stratigraphic and structural context within the seismic data (Sheriff and Geldart, 1995).

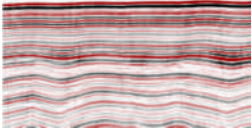
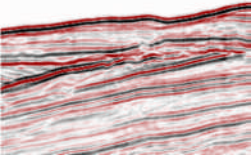
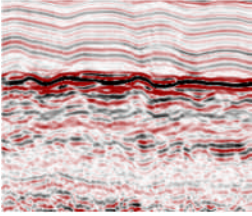
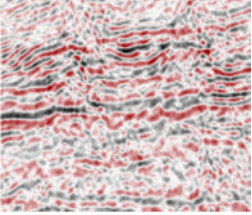
Ideally, seismic horizons are correlated with wireline log data, providing robust, confident, age-constrained interpretations (Ashcroft, 2011). In cases, however, where wireline log correlation is not possible, reflectors may also be identified by their distinctive seismic facies, internal reflector geometries or reflector termination patterns (Table 3.5 & Figure 3.7).

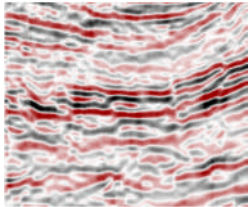
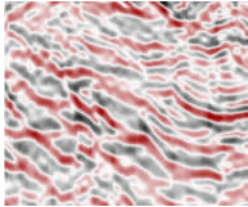
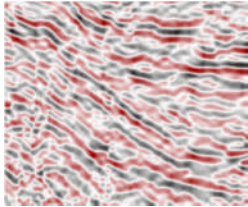
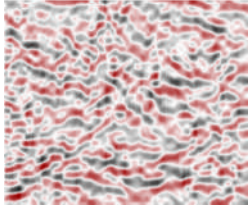


**Figure 3.7** – Common seismic reflector terminations after Wright (2012) modified from Emery and Myers (2009) with seismic examples from the surveys FSB99 and NSR006 from the Faroe-Shetland Basin.

Regional horizon interpretation was undertaken for key chrono-stratigraphic horizons representative of the complex structural and tectonic evolution of the basin. Initial horizon identification and interpretation was undertaken in the southwest of the area using the NSR06 2D seismic survey, due to the excellent seismic imaging and well correlation to the basement. Horizon interpretations were progressively developed towards the northeast through a combination of crossline correlation and loop tie methods, using further well data where possible. The confidence in horizon interpretation decreases from the southeast shelf towards the deeper northwest portion of the basin where well correlation is poor and seismic resolution decreases due to the extensive Paleogene volcanics.

In this study, interpretation of seismic horizons is undertaken to establish the regional structural and stratigraphic context of the basin and to provide geometrical inputs for petroleum system modelling and flexural backstripping workflows. The main seismic horizons are interpreted in this study are summarised in Chapter 6.

Horizon	Age	Type	Well Correlation	Characteristics	Confidence	Seismic Expression
Seabed	0 Ma	Erosional	Excellent	The Seabed appears as a strong prominent reflector throughout the dataset and is well constrained by all available wireline data points.	V. High	
Mid Miocene Unconformity	13 Ma	Erosional	Excellent	One of a series of unconformities driven by Cenozoic inversion (e.g. Davies et al., 2004), the Mid-Miocene unconformity can be correlated across much of the central and northwest basin and is marked by its strong onlap relationships.	V. High	
Near Top Oligocene	23 Ma	Erosional	Excellent	In areas the reflector is obscured by the high amplitude Opal C/T horizon, a Late Miocene diagenetic event. Where visible the reflector often marks the transition from chaotic reflectors below to concordant reflectors above.	High	
Top Paleocene	55 Ma	Depositional	Good	The Top Paleocene reflector is obscured by Paleogene flood basalts across much of the central and northwest portions of the basin. Where it is visible it is a moderate amplitude reflector often overlain by strongly concordant reflectors.	Good	

Top Upper Cretaceous	65.5 Ma	Erosional	Moderate	The Base Tertiary Unconformity is used as a proxy for the Top Upper Cretaceous reflector; it often has marginally higher amplitude than the underlying Upper Cretaceous succession and is marked by onlap of concordant Paleocene reflectors in most areas.	Moderate	
Top Lower Cretaceous	99.6 Ma		Poor	The seismic expression of the Top Lower Cretaceous reflector varies across the basin, where it is well imaged in the south it has a distinct onlapping relationship with the overlying Upper Cretaceous sediments, elsewhere in the basin it is extremely vague, with few distinctive characteristics.	Low	
Top Jurassic	145 Ma	Erosional	Poor	The Base Cretaceous Unconformity is used as a proxy for the Top Triassic horizon; in areas of poor well control the reflector can be identified by its high amplitude and is often onlapped by overlying Lower Cretaceous reflectors.	Moderate to Low	
Basement	> 155 Ma	Unconformity	Poor	The basement displays highly chaotic, homogeneous internal reflectivity. The transition from basin fill to basement is often vague at depth and below volcanics.	Very Low	

**Table 3.5** – Table illustrating the main seismic horizons used for petroleum system modelling in Chapters 6 & 7.

### 3.7.3 Sill Interpretation

The application of seismic data to study the geometry and emplacement of sills is a relatively recent innovation, that has seen a rapid increase in popularity over the past decade due to the increased availability of high quality 3D seismic data acquired by hydrocarbon exploration companies (Bell and Butcher, 2002). The use of such seismic data allows us to interpret in-situ sill bodies and visualise them in 3D, a significant advance over the partially-exposed field examples on which previous sill studies were largely based (Du Toit, 1920, Bradley, 1965, Roberts, 1970, Francis, 1982).

Although sills have been drilled by a significant number of wells in the Faroe-Shetland Basin (Schofield et al., 2015), this still only represents a small percentage of the total number of intrusions across the area. As such, the vast majority of intrusions have no well control and must be identified using seismic data alone (Thomson, 2004). Igneous intrusions, however, can display distinctive characteristics in seismic data, which aids in their identification.

Sills are imaged as high amplitude reflectors in seismic reflection data, due to the large impedance contrast between the high-velocity crystalline igneous rock and the surrounding, lower-velocity, lower-density sediments (Smallwood and Maresh, 2002) Figure 3.8. This contrast is usually enhanced due to the preferential intrusion of sills into softer mudstone and shale horizons (Thomson and Schofield, 2008).

In addition to the reflection characteristics, there are a number of common geometric features that help identify sills in seismic data. It is common for sills to form as saucer-shaped bodies (Figure 3.8 – A), often with a flat or cusped base and moderate to steeply-dipping limbs, which cross-cut host stratigraphy (Figure 3.8 – B) (Magee et al., 2013). Forced Folds (see Figure 3.8 – C) are another distinctive feature commonly associated with sill emplacement (Pollard and Johnson, 1973, Trude et al., 2003, Hansen et al., 2004, Jackson et al., 2013), these sub-circular folds form due to bulk vertical uplift of the overburden during emplacement (Pollard and Johnson, 1973, Kerr and Pollard, 1998, Goult and Schofield, 2008) and directly overlay the sills to which they are genetically correlated (Jackson et al., 2013).

Heat transfer from the sill to surrounding country rock during emplacement has been shown to sustain hydrothermal systems within pore fluid (Einsele et al., 1980, Cathles et al., 1997). These systems create a distinctive, chaotic, disrupted reflector pattern, which is commonly focused at the tips of the sill (Figure 3.8 – D).

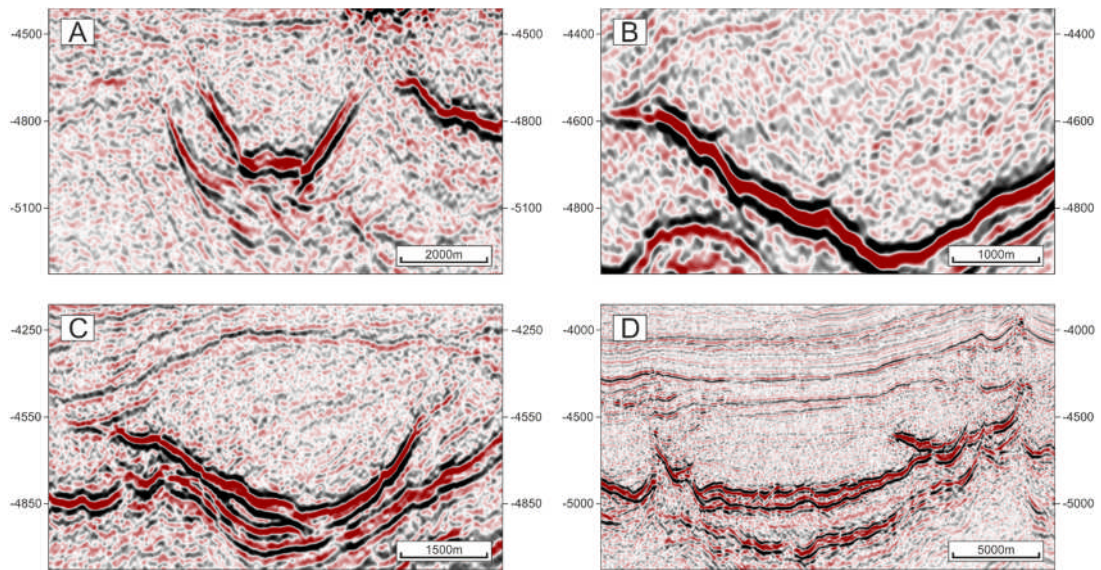


**Figure 3.8** – Common features of sill intrusions in seismic reflection data; (A) High amplitude, saucer shaped reflections, (b) cross-cutting host stratigraphy, (c) forced folding of overlying sediments and (d) hydrothermal fluid circulation above the tips of intrusion disrupting the overlying sediments.

Seismic visualisation techniques are also useful to identify sills, time-slices provide a plan view of the seismic data at a particular time or depth (Z axis) (Bacon et al., 2007). In time-slices sills often appear as circular or sub-circular bodies, with decreasing circumference with depth (Figure 3.9).

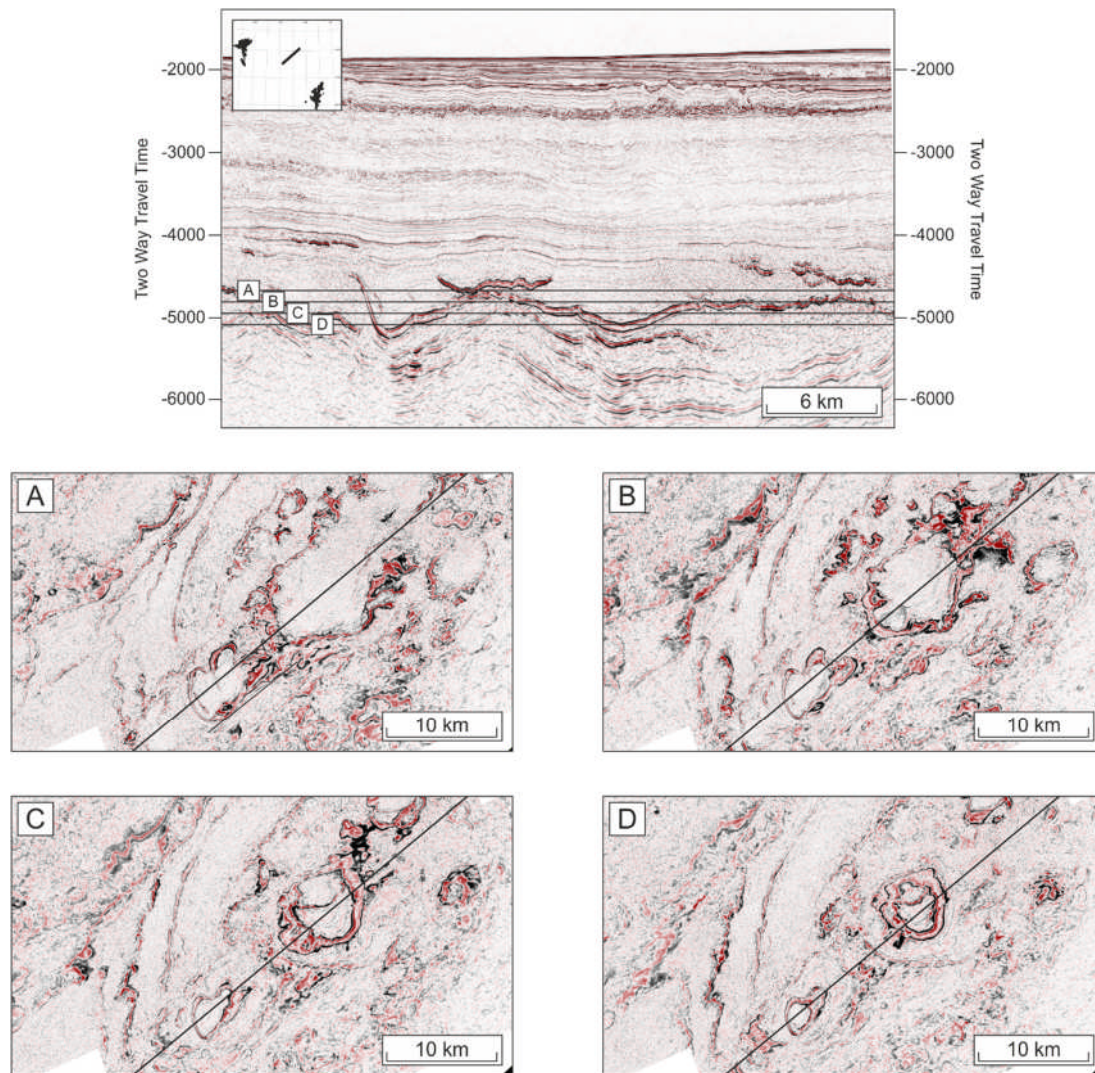


**Figure 3.9** – The use of seismic time-slices can help quickly assess the 3D geometry of high amplitude reflectors in seismic data. Saucer shaped sills produce distinctive circular geometries in plan view, the circumference of which typically decreases with depth.

### 3.7.4 Limitations of Seismic Reflection Data

As discussed previously (Section 3.3) the presence of igneous rocks can severely impact the resolution of seismic data (Roberts et al., 2005). Volcanic rocks typically have higher densities and seismic velocities than the surrounding sedimentary rock, particularly in the case of sills, which tend to preferentially intrude softer mudstone horizons (Thomson and Schofield, 2008). This produces a significant impedance contrast and accelerates the attenuation, scattering and absorption of seismic energy, notably the higher frequencies, resulting in a reduction in both vertical and

horizontal resolution (White et al., 2005, Shaw et al., 2008, Nelson, 2010). Up to 40,000 km<sup>2</sup> of thick flood basalt sequences were extruded across the Faroe-Shetland Basin during the Cenozoic volcanic events (Naylor et al., 1999, Schofield and Jolley, 2013), these deposits cover much of the northeast and central parts of the basin (Ritchie et al., 1999). In addition, the Faroe-Shetland Sill Complex formed during the same period of volcanic activity (Smallwood and Maresh, 2002), the thickness and distribution of this complex varies across the basin (Schofield et al., 2015). As a result of this basaltic volcanism and intrusion, seismic reflection data from the Faroe-Shetland Basin exhibits many of the imaging problems associated with presence of igneous rock. The distribution of volcanic rocks in the Faroe-Shetland Basin is shown in Figure 3.10.

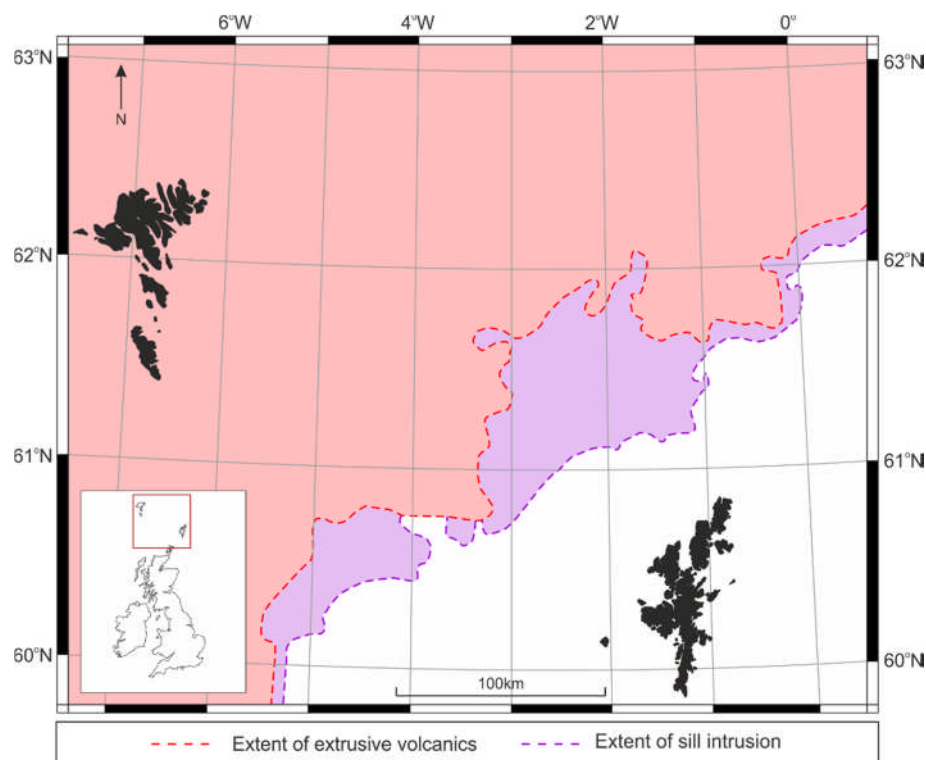


**Figure 3.10** - Map of the Faroe-Shetland Basin showing the location of flood basalts and sill intrusions, adapted from Ritchie et al. (1999). The loss of seismic resolution due to volcanic activity generally increases from SE to NW as the volume and thickness of magmatic material increases.

The extent to which igneous rocks impact seismic resolution strongly depends on the type and nature of the volcanic material present. Thick flood basalt sequences composed of inter-bedded lava flows can produce a number of internal reflections (Maresh and White, 2005), which reduce resolution to the point that no further reflectors are imaged below (White et al., 2003) (see Figure 3.11). By contrast, sill intrusions are typically thinner and although they reduce seismic resolution, sedimentary reflectors may still be imaged around or below them (see Figure 3.12).

Data from the Faroe-Shetland Basin suggests that seismic resolution can be up to three times lower below igneous material compared to the non-volcanic equivalent (see discussion Section 0). During sill interpretation, therefore we consider the application of additional imaging techniques such as spectral decomposition (Chapter 4), which can be used to aid the interpretation of the Faroe-Shetland Sill Complex (Chapter 5). The loss of resolution also increases uncertainty when interpreting the Mesozoic horizons required for basin modelling (Chapter 6), the impact of this uncertainty on the modelling results is assessed through sensitivity analysis.

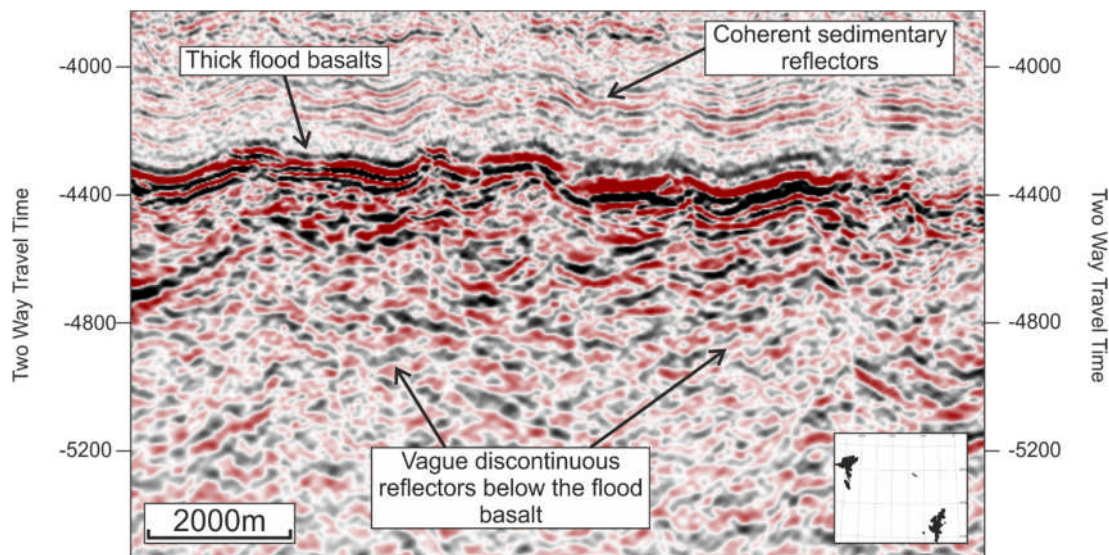


**Figure 3.11** – Seismic section showing a significant loss of resolution below a flood basalt horizon, although reflection events can be identified they are vague and discontinuous, especially when contrasted to the equivalent reflectors above the basalt horizon.

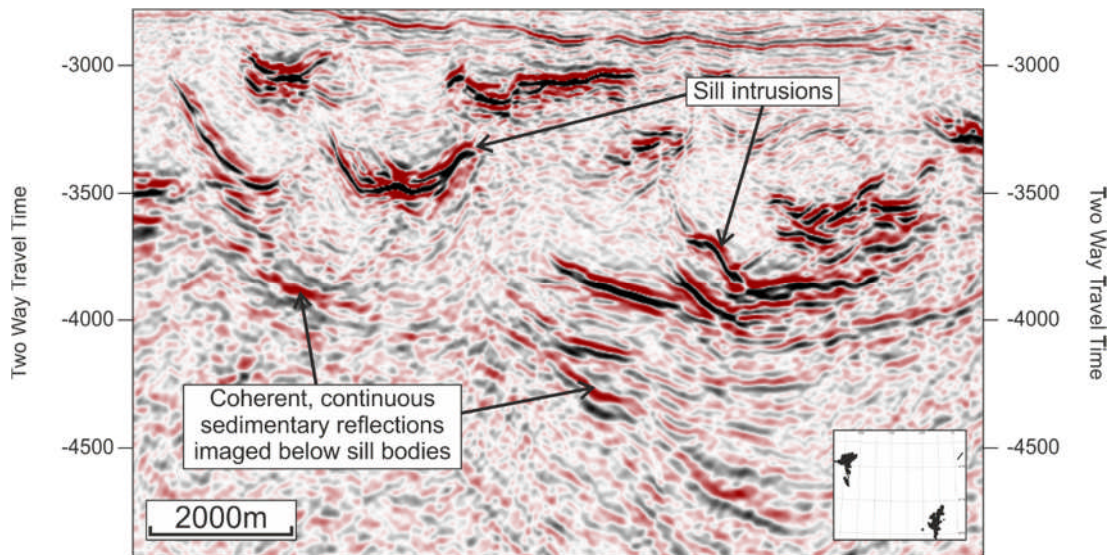


**Figure 3.12** – Seismic section showing the loss of resolution below sill intrusions, although resolution is reduced, sedimentary layers are still imaged as coherent, continuous reflectors.



## Chapter 4 Applying Spectral Decomposition to Sill Interpretation

### 4.1 Abstract

The presence of intrusive igneous bodies in sedimentary basins introduces significant risk and uncertainty for hydrocarbon exploration. With implications for fluid migration, trap formation and seal integrity it is essential to understand the emplacement, distribution and deformation of these bodies to mitigate this risk. 3D seismic data have improved our understanding of sub-surface igneous bodies significantly over the last decade; however, there are still substantial limitations. Of particular note is that seismic resolution is greatly reduced through the intrinsic attenuation of seismic energy caused by a large impedance contrast between crystalline igneous bodies and the surrounding sediments. This greatly impacts our ability to resolve both sills at depth as well as the detailed architecture of stacked sill complexes.

Spectral decomposition is an established seismic attribute used to convert data from the time-amplitude domain into the frequency-amplitude domain; the tuning of specific frequencies in the latter domain can increase vertical and horizontal resolution.

This study applies two common spectral decomposition techniques (Fast Fourier Transform & Continuous Wavelet Transform) to a 3D seismic data volume from the Faroe-Shetland Basin, NE Atlantic, with the aim of enhancing the fidelity of the seismic image, thereby allowing us to improve the imaging of the sill bodies. Our results show that spectral decomposition successfully increases our ability to resolve sills in seismic data, the increase in vertical resolution helps identify individual bodies in closely stacked sill complexes whilst the horizontal resolution allows for the identification of faults and lobe geometries on the sill surface.

The ability to interpret lobes on the sill surface allows for the deduction of magma flow directions and source localities, whilst the interpretation of previously unseen faults has implications for permeability and migration in hydrocarbon systems.

## 4.2 Introduction

It has been shown that sills can have a significant impact on surrounding hydrocarbon plays (Rateau et al., 2013, Schofield et al., 2015, Holford et al., 2013) whilst conventional seismic data is prone to imaging and resolution issues (Wood et al., 2015, Thomson, 2004). Conversion of seismic data into the frequency-amplitude domain can help address some of the key data issues allowing us to better understand the role of sills in hydrocarbon systems.

Sills commonly appear as high amplitude reflections in seismic data due to the large impedance contrast between the high velocity and density crystalline igneous rocks and the surrounding softer sediments (Thomson, 2004). However, geometric spreading, scattering and intrinsic attenuation of seismic energy are all accelerated by such lithologies causing a significant reduction in resolution below a given sill body (Pujol and Smithson, 1991). Intrinsic attenuation reduces the frequency content of the signal; as such the higher frequencies are reduced below the sill interface and are often drowned out by lower frequencies causing a significant drop off in time-amplitude resolution (Aki and Richards, 2002).

One method to address this is to consider the application of seismic attributes, specifically spectral decomposition in order to extract further information from the seismic signal beyond the time-amplitude response. Spectral decomposition in its simplest form is the conversion of seismic data into its constituent frequencies which enables us to see amplitude and phase tuned to specific wavelengths (Hall and Trouillot, 2004). Successfully applied, spectral decomposition can provide quantitative information on bed thickness and lateral discontinuities (Gridley and Partyka, 1997, Partyka et al., 1999) and is routinely used in stratigraphic and sedimentary data interpretation.

The reflection of seismic energy from a single impedance contrast boundary in the subsurface produces a predictable response on the amplitude spectrum of the reflection; however any given seismic signal is composed of a collection of reflections, refractions, diffractions and noise from a range of sub-surface interfaces creating a complex tuned reflection which has a unique response in the frequency domain (Partyka et al., 1999). Spectral decomposition breaks down the survey into its component frequencies, and once isolated the amplitude spectrum of a given frequency represents vertical variation whilst the phase of the signal can delineate spatial variation (Praptono et al., 2003). By extracting the data at key frequencies it is possible to enhance visualisation of reflection events which would otherwise be masked by dominant low frequency signals.

If applied successfully, spectral decomposition has the ability to enhance the visualisation of sills at depth, particularly those emplaced beneath other sills; potentially aiding both identification and interpretation. The ability of spectral decomposition to detect lateral discontinuities also has the potential to reveal details on the sill surface previously undetectable by conventional seismic. Trude (2004) demonstrated the ability to delineate flow patterns from ridges on a sill surface. These large ridges on a shallow sill were visible in conventional seismic; however, with the enhanced visualisation and ability to delineate subtle lateral discontinuities using spectral decomposition there is potential to assess flow patterns in the sills observed at depth.

The Faroe-Shetland Basin is a confined deep-water basin located between the Faroe and Shetland Islands on the NE Atlantic Margin (Mitchell et al., 1993, Rateau et al., 2013). It overlies a Mesozoic to Early Cenozoic rift basin that has a complex poly-phase rift history which initiated in the Permo-Triassic and continued sporadically until the final stages of continental break-up during the early Tertiary (Dean et al., 1999). The North Atlantic Igneous Province formed during this time (Late Paleocene to Early Eocene), emplacing extensive sill complexes into Cretaceous and Paleocene mudstones (Sørensen, 2003).

Significant exploration interest in the area has led to the acquisition of extensive high quality 3D seismic data; the application of this data to the study of sills is

relatively recent yet has already provided fresh insights into the emplacement and development of sill complexes (Bell and Butcher, 2002, Smallwood and Maresh, 2002, Hansen et al., 2004, Hansen and Cartwright, 2006b, Thomson and Schofield, 2008, Magee et al., 2013). The presence of intrusive igneous bodies in sedimentary basins can introduce significant uncertainty in the exploration and production of hydrocarbons, but by studying the geometry, shape and deformation of these bodies it is possible to understand and minimise the risk they pose.

This study applies two common methods of spectral decomposition, the Fast Fourier Transform and the Continuous Wavelet Transform to 3D seismic data from the Faroe-Shetland Basin, to demonstrate its application in aiding the identification and interpretation of igneous sills and the potential implications of such findings.

### 4.3 Data and Methods

This study utilises a 356 km<sup>2</sup> sub volume cropped between -4.5 and -6.5s TWT from the PGS Megamerge WZ 97-99 3D seismic survey immediately NE of the Mid Faroe High (see Figure 4.1). The constraints of the cropped volume were defined temporally and spatially to encompass a stacked complex of three large (~5 km long) sills within mudstones of a Cretaceous age (see Figure 4.1).

The average interval velocity at the base of Well 214/04-01 (-3.9 s TWT) is 4800 m/s whilst the dominant frequency between -4.5 and -6.5 s TWT is 15 Hz. This gives a minimum vertical resolution of 80 m, although true is resolution is likely to be lower than this given the potential increase in interval velocity from -3.9 s to -6.5 s TWT.

Spectral decomposition was performed using the dGB OpendTect software platform, with further analysis and interpretation of the data was undertaken using Schlumberger's Petrel 2014.1.

There are numerous workflows for performing spectral decomposition on seismic data (Sinha et al., 2005). This study focuses on two common methods, the Fast Fourier Transform (FFT) and the Continuous Wavelet Transform (CWT), the advantages and drawbacks of both methods are outlined below. These techniques

are fully appraised in previous studies including Partyka et al. (1999), Xia (1999), Sun et al. (2002), Sinha et al. (2005).

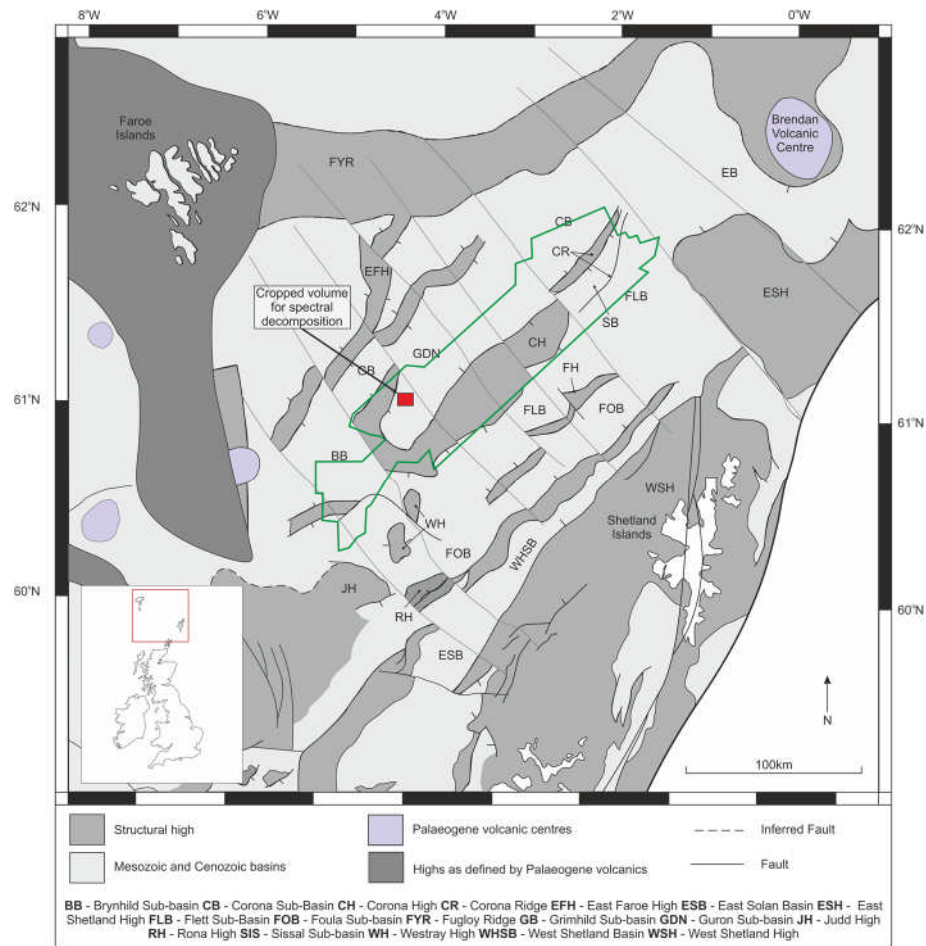


**Figure 4.1** - Regional location map highlighting the structural configuration of the basin, the outline of the 3D seismic survey and the size and position of the cropped seismic sub-volume used in this study.

#### 4.3.1 Fast Fourier Transform

The FFT algorithm computes the Discrete Fourier Transform (DFT) of a signal, transforming it from the time domain into the frequency domain (Gridley and Partyka, 1997) using a fixed window approach to data sampling. The user specifies a time-gate over which the data will be sampled, the length of which strongly influences how the acoustic properties and bed thicknesses are represented in the final attribute (Sinha et al., 2005).

Whilst a longer time window offers a more accurate representation of the entire frequency spectrum it largely overlooks finer scale events. Similarly a shorter time window can accurately resolve high-frequency events and even delineate between events with similar dominant frequencies but misses large portions of the amplitude spectrum (Gridley and Partyka, 1997).

The phase of the signal is the key to identifying lateral discontinuities; in the context of sills this provides the potential to image rugosity on the sill surface and/or faults close to the resolution of the seismic data. Phase responds to subtle changes in seismic character becoming unstable across lateral discontinuities, the effectiveness of phase depends on the size of the time window. Across a longer time window the reflections are likely to be laterally stable, keeping the phase stable, however, a shorter time-gate is more likely to image discontinuities creating a phase response (Partyka et al., 1999).

FFT offers high precision control over the data transformation through the specification of the time-gate and output frequency allowing the user to adapt the process and focus on the reflections, areas or frequencies of interest. However, by doing so it limits the resolution of the entire time-frequency spectrum, omitting large sections of the spectrum (Xia, 1999, Sun et al., 2002). As the focus of this study is in isolating and increasing the resolution of sills from the surrounding reflections and noise a short window approach to the FFT algorithm is applied.

#### **4.3.2 Continuous Wavelet Transform**

Unlike FFT, the CWT algorithm does not require a predefined window length (Sinha et al., 2005), instead it samples the seismic signal using a movable, scalable time window in the form of a wavelet (Chopra and Marfurt, 2007). As the wavelet moves along a given signal the correlation between the wavelet and the signal are recorded producing the wavelet coefficient (Chopra and Marfurt, 2007). The user defined frequency (output frequency) corresponds to the central wavelet frequency which defines the resolution of the final output, it is therefore essential the

selected output frequency is capable of capturing the object of interest, in this case the sills.

CWT provides a method of adaptive sampling, whereby the window size automatically changes with frequency; as such it is able to represent the source data more accurately in the final output. Consequently CWT is far superior at preserving reflection events than the FFT method, particularly at higher frequencies.

#### **4.4 Results**

Spectral decomposition was performed on 2D profiles extracted from the cropped seismic volume using both the FFT and the CWT methods. The parameters defined for each technique strongly influence the ability of the attribute to resolve the target, in this case sills, greater than the 80m time-amplitude seismic resolution.

As such, a range of output frequencies and time gates were adjusted for the FFT to find the optimal resolution. For the CWT a range of frequencies were also applied although the wavelet type (Gaussian) remained constant. Once the optimal parameters on the 2D profile were defined the attribute settings were tested on further 2D profiles to ensure consistency before they were computed for the entire 3D volume.

##### **4.4.1 Fast Fourier Transform**

As the image resolution produced by the FFT relies heavily on user defined parameters a range of time-gates and output frequencies were tested to obtain the optimal values for imaging the sills; these were selected at 10 discrete intervals between +/- 1 ms and +/- 100 ms (time-gate) and 5 Hz and 100 Hz (frequency).

The results show that a time-gate below +/- 15 ms was too finely tuned to encompass all the sills, the final images were chaotic, and the image included unwanted sections of the stratigraphy whilst poorly resolving the sills. Time-gates above +/- 35 ms successfully isolated the sill bodies, but the boundaries of the

reflections were vague and diffuse, offering no improvement on the original seismic image. The results also show that the final image was less sensitive to output frequency with values between 5 Hz and 50 Hz showing little variation; anything above 50 Hz proved detrimental to resolution. A comparison of 2D time-amplitude seismic section with the results of the FFT using a time-gate of  $\pm 25$  ms and output frequencies of 5 Hz and 15 Hz respectively is shown in Figure 4.2.

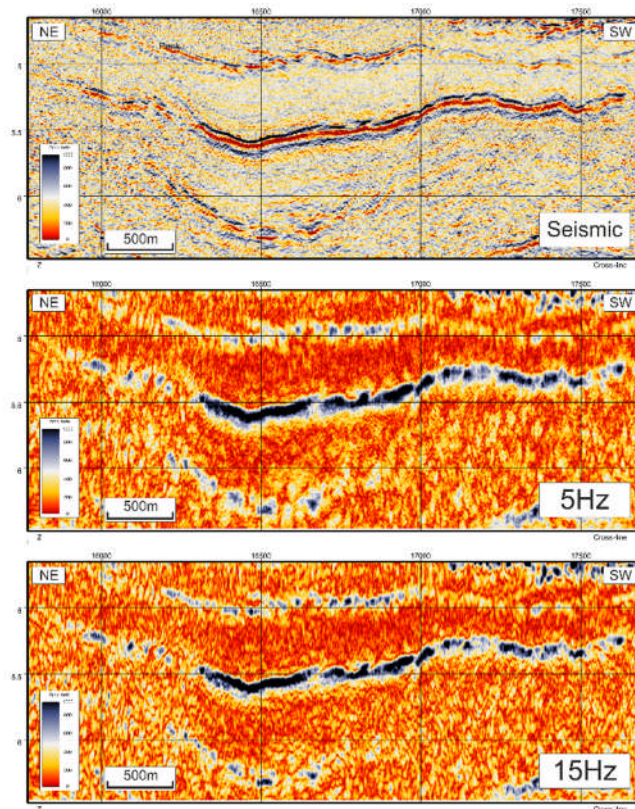


**Figure 4.2** - Application of the Fast Fourier Transform to time-amplitude seismic data. The time gate is set to  $\pm 28$ ms and an output frequency of 5Hz and 15Hz respectively. The sill bodies are successfully isolated and lateral discontinuities appear much more prominent (data shown in standard positive polarity).

The CWT was run using a Gaussian wavelet and a range of output frequencies between 5 Hz and 100 Hz (See Figure 4.3). The resolution and quality of the results varies significantly with frequency and reveal an optimal image between 40 Hz and 100 Hz. This range produces clearly defined sill boundaries, sharp horizontal terminations and separation between stacked reflections. With a decrease in

frequency (20 Hz to 30 Hz) the sills are clearly imaged but the boundaries are more diffuse. The resolution below 20 Hz is poor and offers little or no improvement over the original time-amplitude data.

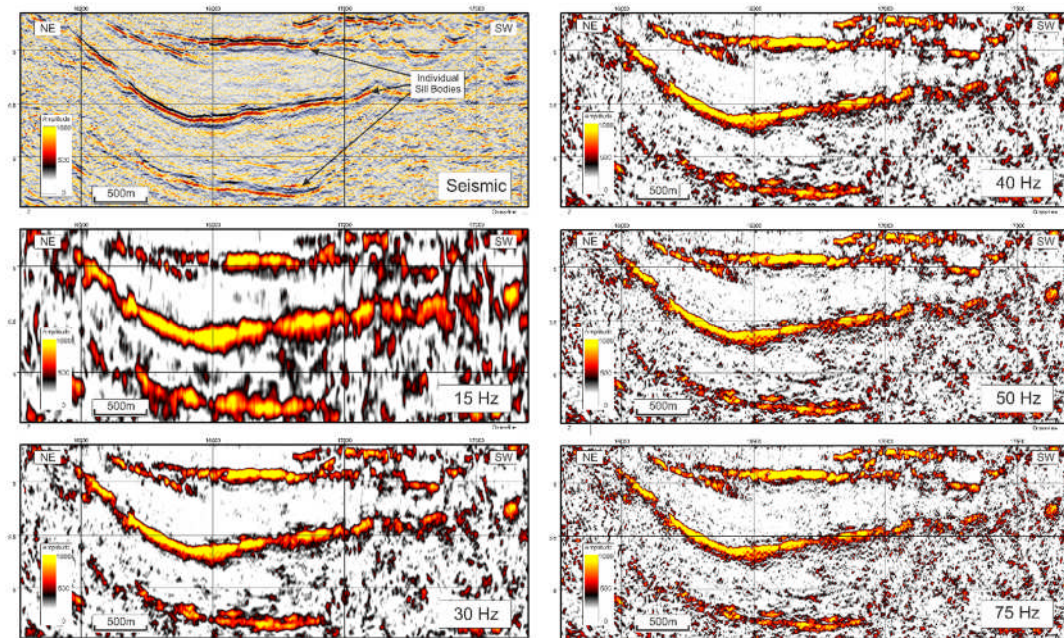


**Figure 4.3** - Application of the Continuous Wavelet Transform to the seismic data, the image shows a range of output frequencies (15Hz, 30Hz, 40Hz, 50Hz & 75Hz), the optimum resolution occurs between 40Hz and 75Hz, discontinuities are well imaged and the top sill reflection appears prominent and sharp. Outputs of 30Hz and 40Hz still produce coherent results however anything below 30Hz is too poor to offer any improvement of the original time-amplitude data.

#### 4.4.2 Interpreting Sills Using Spectral Decomposition

##### 4.4.2.1 Faulted Sills

The sharp boundaries and spatial discontinuities that are apparent in the spectral decomposition data become extremely powerful for identifying faults along the sill surface. Whilst major faults are easy to identify in time-amplitude domain seismic, smaller faults (<80 m) are often lost as they are below conventional seismic resolution. In the spectrally decomposed data however small faults can appear as

sharp discontinuities, clear displacements and often full breaks in the reflector surface. To compare fault imaging between the two, Figure 4.4 shows the same sill in time-amplitude domain seismic and spectrally decomposed data (using the CWT at 40 Hz). In the amplitude-domain seismic it is clear that the sill is not a single coherent reflection with local amplitude minima highlighted (1,2,3 & 4) and variations in local dip that could potentially indicate the presence of faults. However when the same highlighted areas are viewed in the spectral decomposition data these variations show up as clear, well defined terminations in the reflections allowing the interpretation of well-defined fault planes.

Of particular note, area 3 shows some subtle undulations in the top sill surface in the time-amplitude domain while the base is much more diffuse and lacks any clear definition. These small features could be interpreted as faults, albeit with a low degree of confidence. In the spectral decomposition data, however, both the top and the base of the sill are seen to have clear, discrete displacements that would result in much higher confidence fault pick.

Areas 2 and 4 show areas of poor resolution in the time-amplitude domain, the top sill reflector transitions from a coherent, high amplitude response on either side to a lower amplitude, vague reflector in the centre. Spectral decomposition removes the ambiguity of the poorly imaged sections, defining clear, distinct reflections with clear breaks along the surface indicative of faults.

These results demonstrate how spectral decomposition can be used both to increase the confidence of fault picking of seismically resolvable terminations and to identify areas of faulting not observable within the time-amplitude domain.

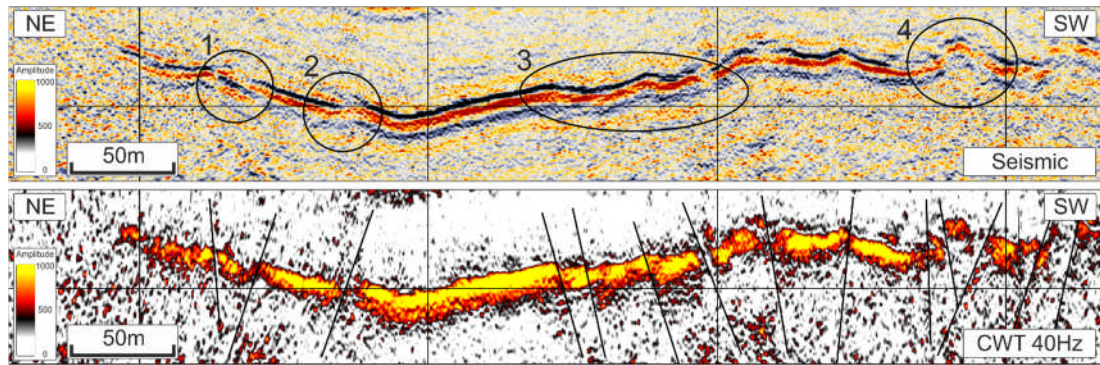


**Figure 4.4** - Identifying faults using spectral decomposition. Areas of disrupted reflectivity in time-amplitude domain seismic (1,2,3,4) are imaged as clear breaks and displacements in the reflection surface when using spectral decomposition making it ideal for identifying and interpreting faults.

#### 4.4.2.2 Revealing Stacked Sills

In Figure 4.5 A, a single coherent reflection within the time-amplitude domain implies that there is a single sill, although there are small amplitude variations, indicated by the varying intensity of the black (trough) wavelet, across the reflection. When the same sill is viewed after applying spectral decomposition using the FFT (+/- 25 ms time-gate & 15 Hz) it is apparent that the small amplitude variations correspond to three individual stacked sills (Figure 4.5 B). The upper sill, S1, can be seen extending to the data edge and terminating at a fault plane (F1) while the middle sill, S2, extends from the data edge for at least 1 km and shows minor faulting by F1. Below S2 the third sill, S3 extends across the entire length of the initial sill imaged on the time-amplitude section and is displaced by a further normal fault (F2). It is hard to determine the timing of the faults relative to sill emplacement although it is likely F1 occurred post sill emplacement as it displaces both S1 and the underlying S2, whose formation was unlikely to be synchronous given how typical stacked sill complexes evolve. F2 may have occurred pre or post emplacement as the sill extends across the fault plane with no clear cut-off there is no definitive way to tell which it is.

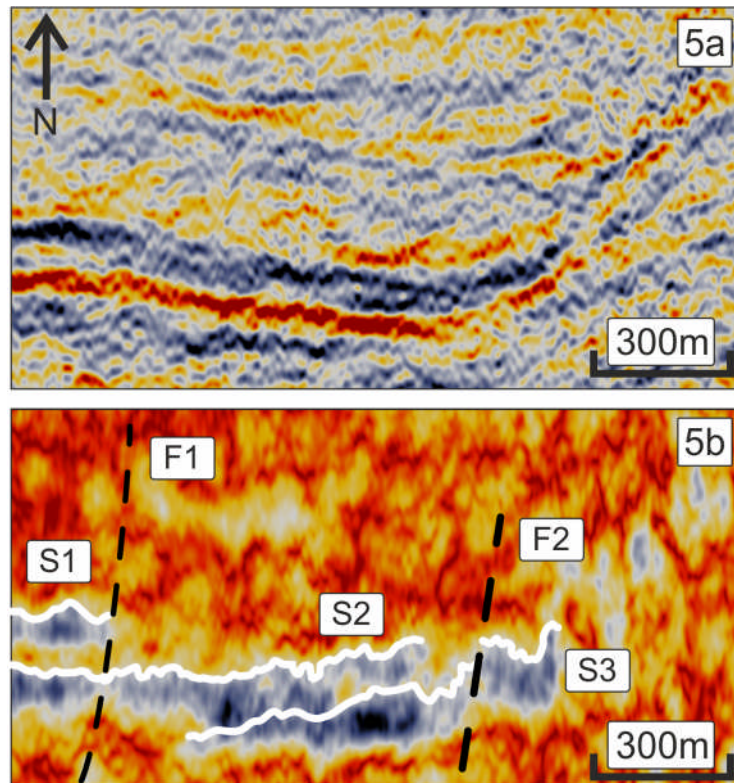


**Figure 4.5** - Revealing stacked sills using spectral decomposition. In time-amplitude seismic (5 x vertical exaggeration) the sill shows some amplitude variation but remains a single body. However after spectral decomposition (FFT 15 Hz) separation can be seen revealing three stacked sills displaced by post-emplacment faults.

#### 4.4.2.3 Three-dimension surface interpretation

One of the most striking differences between amplitude domain seismic and spectrally decomposed data is the definition of the top sill boundary, especially when the CWT method is used (Figure 4.3). In the CWT data the sill boundaries are sharp, well defined and prominent, showing small undulations and ridges across the surface. In comparison the time-amplitude domain data shows a smooth but highly variable surface, which ranges from moderately prominent to diffuse.

The resolution of the top sill reflector has a significant impact on the quality of the 3D surface interpretation that can be produced. Figure 4.6 shows a sill interpreted first using time amplitude-domain seismic (left) and then CWT data (right). Both

were picked using a coarse seed grid (10 inlines by 10 crosslines) completed using a 3D auto-tracking algorithm. The two surfaces show the same broad geometry and topographic variation of the large scale features, however, the resolution of the spectral decomposition derived surface is significantly higher adding substantially more detail.

Inserts A1 & A2 (Figure 4.6) highlight the difference in resolution between the two methods. A1 (time-amplitude domain) shows a flat plateau on the sill surface flanked either side by smooth areas of rapid topographic change which most likely represent simple faults. However, when viewed using spectral decomposition (A2) the flat plateau has a significant ridge running across the centre and the edges of the plateau are seemingly more complex, formed by interlinked faults connected by a relay ramp, the difference in fault complexity between field outcrops and seismic data has been demonstrated by Wood et al. (2015). Aside from revealing new features and geometries, the spectrally decomposed data (A2) also offers enhanced imaging of minor features such as ridges, which although visible in time-amplitude data (A1), are much less apparent and subtle features.

Similar differences can be observed between inserts B1 (time-amplitude) and B2 (spectral decomposition). Areas which appear smooth or featureless in B1 are shown to have topographic variation in B2. Similarly features appear simplified in B1, such as the highlighted ridge which has a relatively smooth curved expression; however, in B2 it is much more complex with significant indentations running perpendicular to the original curve.

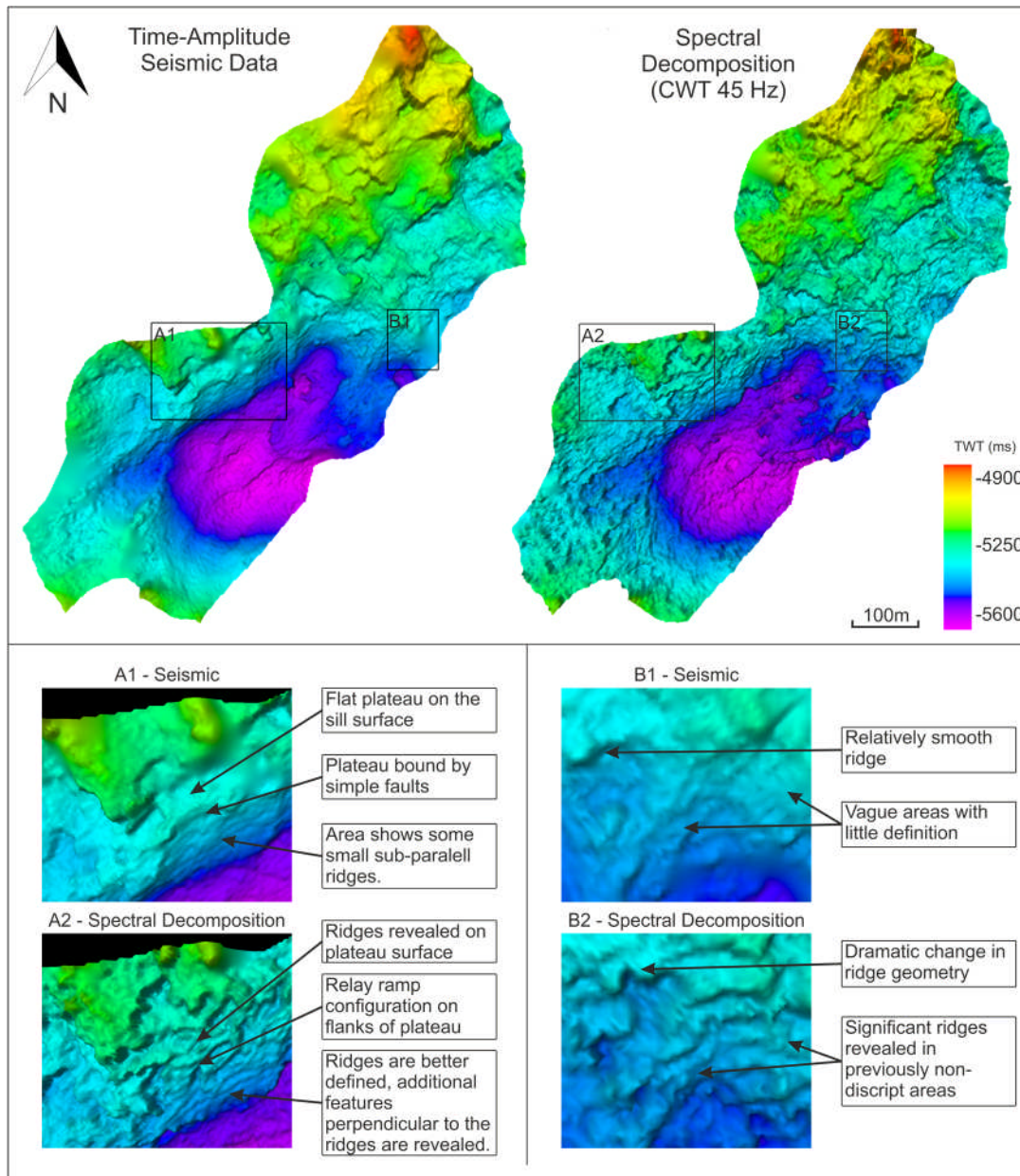


**Figure 4.6** - Main image - 3D interpretation of the top sill reflector using time-amplitude seismic data (left) and spectrally decomposed data (right), the surfaces show the same broad geometry and topographic elevation but spectral decomposition is significantly better at resolving both major and minor features. Inserts – Illustrating the differences between time-amplitude (A1 & B1) and spectral decomposition (A2 & B2) surfaces, the later reveals ridges, geometries and faults previously unseen in time-amplitude data.

## 4.5 Discussion

It has been shown that spectral decomposition when combined with conventional time-amplitude domain seismic can help significantly enhance the imaging, and therefore interpretation, of sill bodies. This enhancement allows for the identification of faults and stacked sills as well as drastically increasing the detail and definition of surfaces produced from the top sill reflector. The potential exploration implications of the interpretations made using the frequency-amplitude data are now considered.

### 4.5.1 Magma flow implications

The ability of spectral decomposition to enhance the resolution of the top sill reflection and reveal previously unattainable features makes it ideal for investigating the size, shape and distribution of the surface ridges that form during magma lobe emplacement.

The sill surface shown in Figure 4.6 is enhanced using spectral decomposition (CWT at 50 Hz; Figure 4.7 – A and the interpretation of ridges and furrows on the sill surfaces is shown in Figure 4.7 – B. This interpretation shows a series of lobes defined by semi-concentric ridges. Lobe geometry varies significantly with those in the south-southeast showing a typically broad circular shape, these rounded lobes can be up to 300 m wide and 150 m long, in contrast to those in the north-northwest of the sill which are typically thinner, smaller and more elongate with most being no wider than 100 m and no longer than 150 m.

Previous interpretations of sill lobes in seismic data (Trude, 2004, Hansen and Cartwright, 2006a, Schofield et al., 2012) identify broadly concentric ridges parallel to the front lobe perimeter as indicative of flow direction, in this example there are multiple flows of different sizes and geometries emanating from a single point close to the south-southeast edge of the sill (marked on Figure 4.7 – C) suggesting this is the main source, it also happens to be the deepest part of the sill which is consistent with the established theory that sills are fed from their deepest point and flow upwards and outwards from the source (Malthe-Sørensen et al., 2004).

Previous authors have noted the tendency of a sill to form strong linear edges if the flow is restricted by either vertical dyke emplacement (Tweto, 1951) or structural heterogeneity such as elevated basement blocks (Hansen and Cartwright, 2006a). In this instance the sill has smooth curved edges parallel to the surface ridges suggesting the external limit of the sill is defined by the outer perimeter of the individual lobes which have been allowed to flow freely with no local restriction.

#### **4.5.2 Fluid flow implications**

Sills are typically relatively thick, laterally extensive bodies composed of low porosity, low permeability crystalline igneous rock (Schutter, 2003); as such if they are emplaced in or around an exploration prospect they have the potential to restrict sub-surface hydrocarbon flow. Impermeable sills have been shown to act as hydrocarbon traps, for example in the Phetchabun Basin, Thailand (Schutter, 2003) and the Solimões Basin Brazil (Filho et al., 2008).

In contrast, sills also have the potential to act as conduits to flow. Fractures and joints associated with the cooling and contraction of the igneous material after emplacement can provide pathways for fluid migration (Rateau et al., 2013) although permeability in this scenario is considered low (Matter et al., 2006). However secondary permeability may provide a valid mechanism for fluid flow through sills. This can be achieved either through the faulting and fracturing of solidified, brittle igneous bodies or through the expansion of pre-existing joints and fractures due to decompression associated with overburden removal in areas of uplift (Rateau et al., 2013). Tectonically induced permeability in sills has been demonstrated in the northern Neuquén Basin, Argentina (Witte et al., 2012).

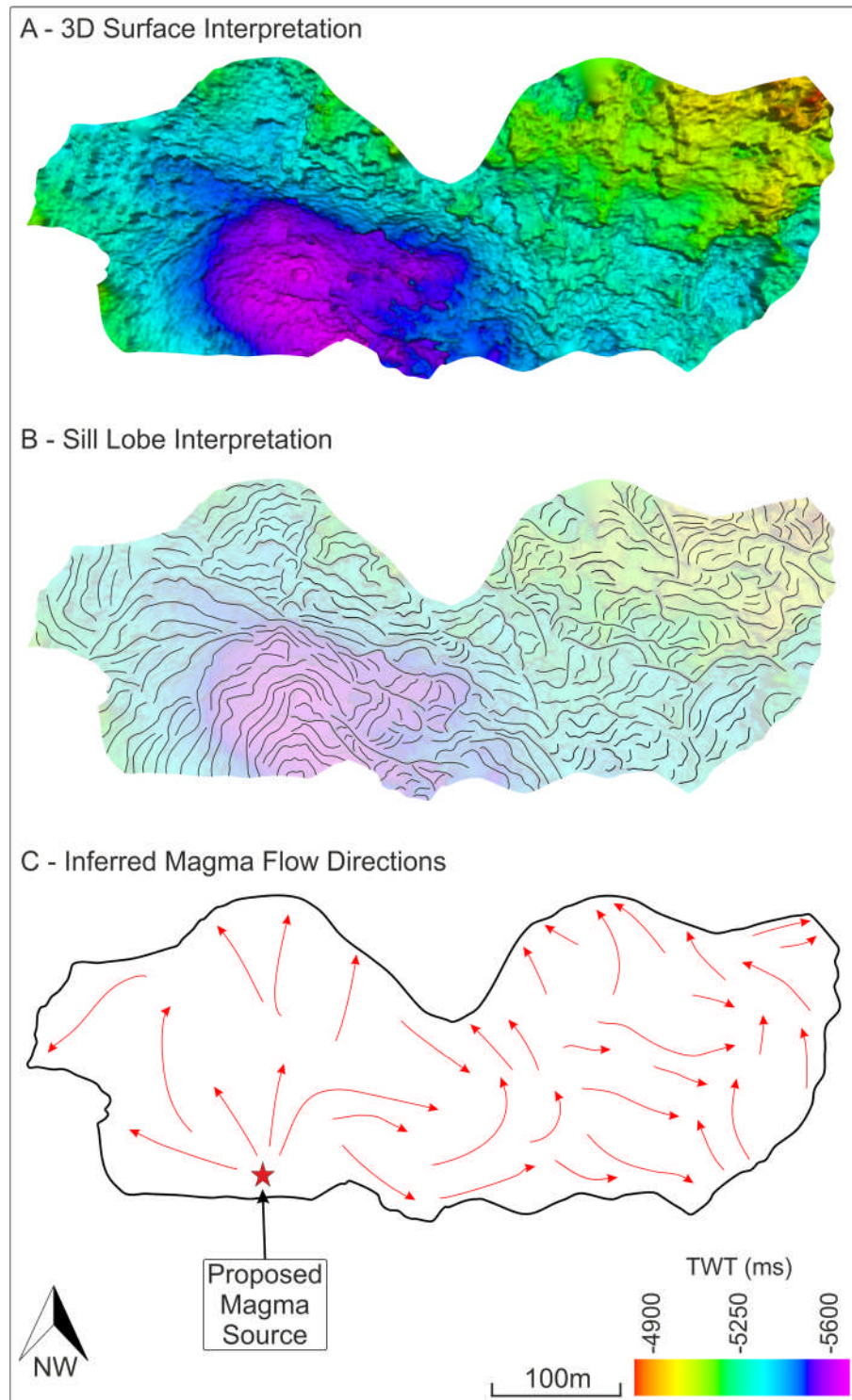


**Figure 4.7** - Determining magma flow directions from spectral decomposition data. Image A shows a sill surface interpreted using spectral decomposition data (CWT at 50Hz), Image B shows an interpretation of the ridges and furrows on this sill surface which constitute the magma flows and lobe development. Image C deduces the magma flow directions from the interpretation (B) indicating the initial source of the sill in the centre of the deep depression on the SSE edge of the sill.

One of the most significant factors in determining a sill's permeability is the tectonic regime post-emplacment; areas with significant deformation, uplift or erosion are more likely to have sills with induced permeability. In the FSB there are numerous inversion events throughout the Cenozoic (Sørensen, 2003) introducing significant potential for the development of permeability within sills. The two end members of migration through sills are schematically represented in Figure 4.8 including a low permeability sealing scenario (Insert A) and a high permeability migration scenario (Insert B). In the low permeability scenario there is no deformation of the sill and it remains deeply buried mitigating both fault induced permeability and decompression induced permeability, as such the sill acts as a seal allowing the accumulation of hydrocarbons below. The high permeability scenario illustrates a much shallower sill which has been extensively faulted thus providing potential for both fault and expansion related migration into the high permeability sands above.

This study has shown previously (Figure 4.4) that frequency-amplitude data produced through spectral decomposition of the original time-amplitude data can help identify faults which are either unclear or not present in the original data. In addition to this, the surfaces produced from the interpretation of the top sill reflector (Figure 4.6) show what may appear to be simple normal faults in time-amplitude seismic are actually complex poly-fault systems that form either isolated segments or are linked through relay ramps. The addition of previously unseen faults and increased fault density subsequently increases fracture density and introduces the potential for greater migration through the sills. Without well data or core samples through such a sill body we cannot quantify the fracture density or the migration potential, however it can tentatively be suggested that with the application of spectral decomposition data we have the ability to predict greater than anticipated sill permeability than with time-amplitude data alone.

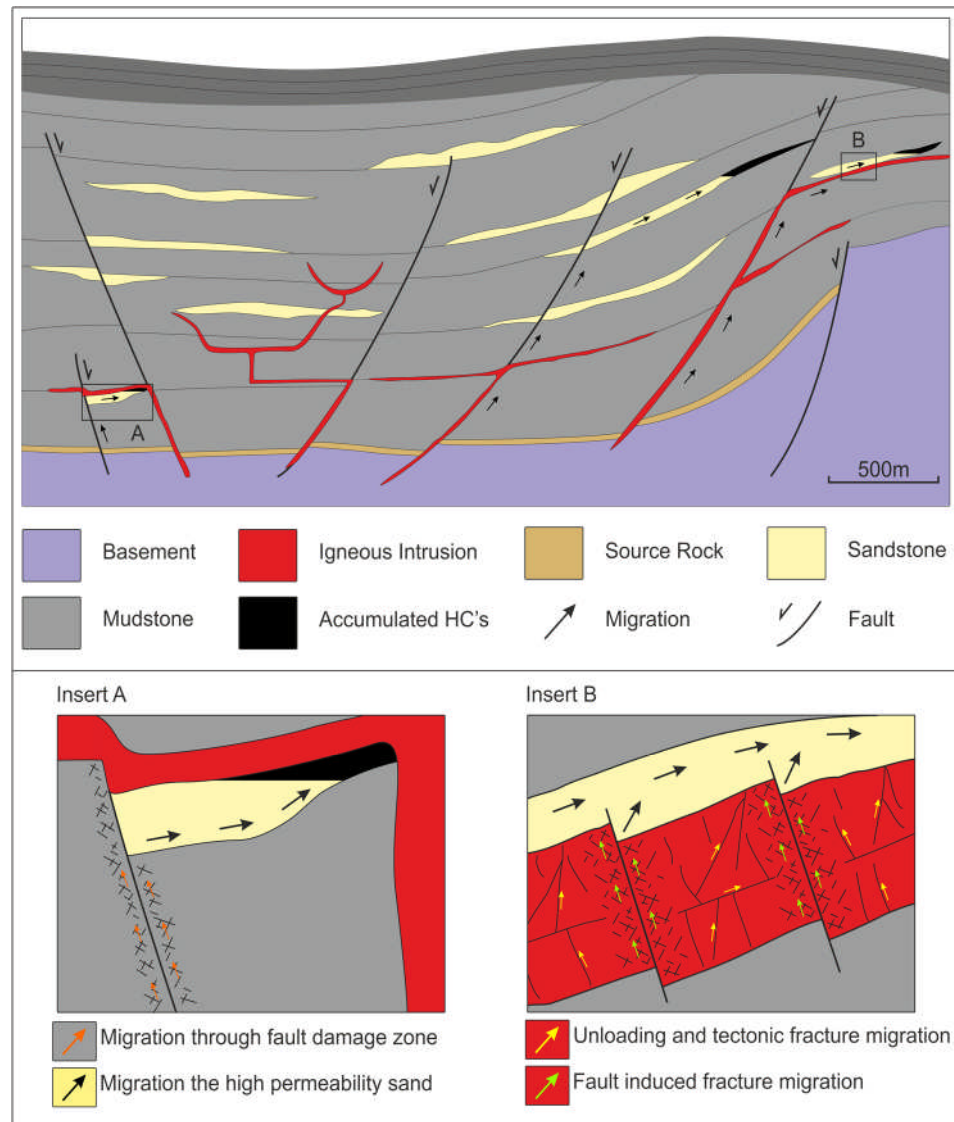


**Figure 4.8** - Schematic illustration of the potential influence of sills on hydrocarbon migration, adapted from (Rateau et al., 2013). Inset A – Sealing scenario, where the sill acts as an impermeable barrier to fluid flow and thus provides an up-dip seal to the inclined sand horizon. Inset B – Migration scenario, where the sill has undergone deformation producing fault fracture zones capable of inducing permeability significant enough for fluid migration.

#### 4.6 Conclusions

Spectral decomposition is an established tool for seismic interpreters working in sedimentary and stratigraphic settings. The ability to view amplitude tuned to specific frequencies has a multitude of applications including but not limited to:

boosting thin bed resolution, defining lateral terminations, suppressing noise, and quantitative bed thickness prediction.

This study has demonstrated that the spectral decomposition attribute also has value in settings where intrusive igneous rocks are widespread. Its application in isolating and identifying sill bodies is significant to the interpretation and identification of sill bodies. Furthermore the increased resolution and definition of lateral terminations helps us to identify the geometry and distribution of faults, and lobes on the sill surface which have important implications for the emplacement and deformation of the sill body. Combined, the increased interpretational ability of spectral decomposition on igneous intrusions can help us mitigate the uncertainty and risk associated of such intrusions in areas of potential hydrocarbon accumulation and migration.

- Both the FFT and CWT methods produce valuable results when applying spectral decomposition to seismic data, although CWT yields a greater resolution and is a more robust method, mitigating most user error.
- With regard to sills, spectral decomposition significantly increases the definition of the top reflector surface allowing for better identification of sill geometries, deformation and lobes.
- Spectral decomposition can increase vertical resolution allowing for the identification of closely stacked systems.
- The enhanced ability of spectral decomposition to highlight lateral discontinuities makes it ideal for identifying faults on the sill surface.
- Reinterpretation of the top sill reflector using the spectrally decomposed data reveals ridges and furrows which are below conventional seismic resolution; careful interpretation of these features shows the shape and distribution of the magma lobes which form the sill. This information can be used to deduce the initial source point of the intrusion.

The ability to identify faults previously below seismic resolution has the potential to increase the predicted permeability of the sill which has implications for potential migration pathways, seals and traps.

## Chapter 5 The emplacement and distribution of sill facies in the Faroe-Shetland Sill Complex

### 5.1 Abstract

To understand the potential impact of intrusive volcanic complexes on petroleum systems, it is first essential to understand what controls their emplacement and development. Establishing a relationship between intrusion style, magma supply and structural setting is key to understanding how these complexes develop, why they vary across volcanic passive margins and the heat flow implications.

The Faroe-Shetland Sill Complex covers an area in excess of 20,000 km<sup>2</sup> within the Faroe-Shetland Basin (Passey and Hitchen, 2011) and was emplaced during the Early Paleocene as a response to the final stages of continental break-up along the NE Atlantic Margin (Skogseid et al., 2000). The area has extensive, high-fidelity 3D seismic reflection data acquired during decades of active hydrocarbon exploration (Ritchie et al., 2011). 3D seismic reflection data has been shown to be a valuable tool in studying in-situ sill complexes (e.g. Bell and Butcher, 2002) and has significantly enhanced our understanding of the emplacement and regional distribution of sills across volcanic passive-margins.

In this chapter, detailed interpretation of 3D seismic reflection data from the NE Corona Ridge region of the Faroe-Shetland Basin reveals three distinct facies of sill intrusion, whose formation was defined by their emplacement environment and magmatic supply. Through detailed analysis of common geometric features, flow directions, feeding relationships and their interaction with basement structure, it is possible to establish what controls the development of each sill facies and how magma emplacement evolves across the margin.

The area is strongly segmented by a series of NE-SW trending Mesozoic faults and crystalline basement highs. The large basement bounding faults and structural highs, such as the splays of the Corona Ridge, play a key role in the distribution of magma across the area, whilst the smaller, Cretaceous-Paleocene faults strongly

influence emplacement style and sill development. This chapter demonstrates how the reduction in magma supply away from the palaeo-spreading centre and the variation in Mesozoic rift structure strongly influences the style of sill emplacement observed in the Faroe-Shetland Basin.

## **5.2 Introduction**

Increased interest from hydrocarbon exploration companies in deep water sedimentary basins has led to the acquisition of high-quality 3D seismic data from a growing number of the world's volcanic passive margins. Seismic reflection data can offer a unique perspective on sill morphology, providing 3D visualisation of in-situ sill complexes (Polteau et al., 2008). The quality and availability of 3D seismic data have led to an increase in seismic-based sill studies (Smallwood and Maresh, 2002, Hansen et al., 2004, Lee et al., 2006) from areas such as the NE Atlantic Margin, Norwegian Margin and offshore SW Australia (Bell and Butcher, 2002, Planke et al., 2005, Magee et al., 2013), which have significantly advanced our understanding of sill emplacement and their influence on petroleum systems (Holford et al., 2013).

Previous seismic-based sill studies have demonstrated how lithological and structural factors control sill emplacement (Thomson and Schofield, 2008), and how sill junctions (Hansen et al., 2004) and interconnected sills (Marsh, 2004, Cartwright and Hansen, 2006) can be used to determine the feeding relationships and magma sources within large sill complexes. Analysis of overlying forced folds and hydrothermal vents have been used as tools for the relative dating of intrusions (Hansen and Cartwright, 2006b, Jackson et al., 2013). Whilst regional interpretation has recognised the development of different sill facies (Planke et al., 2005) and allowing inference of the magma plumbing system across a large areas (Schofield et al., 2015), no study to date has combined these elements to describe the detailed evolution and timing of a sill complex across a margin. Such a study would potentially enhance our understanding of magmatic plumbing systems and the bulk distribution of intrusive magma in volcanic passive-margin settings.

Previous work by Planke et al. (2000) developed a schematic regional framework for the magmatic facies associated with volcanic rift margins (Figure 5.1). Using seismic reflection data from the NE Atlantic and Australia, they distinguished four main magmatic facies (outer seaward dipping reflectors, outer high, inner seaward dipping reflectors and landward flows), which progress from the spreading centre towards the continent. They further refined the landwards flow facies to include landward flows, lava deltas, inner flows, sills and vents. The data area of this study falls within the inner flow, sill and vent facies and therefore offers an opportunity to first test this model and then consider a kilometre-scale refinement.

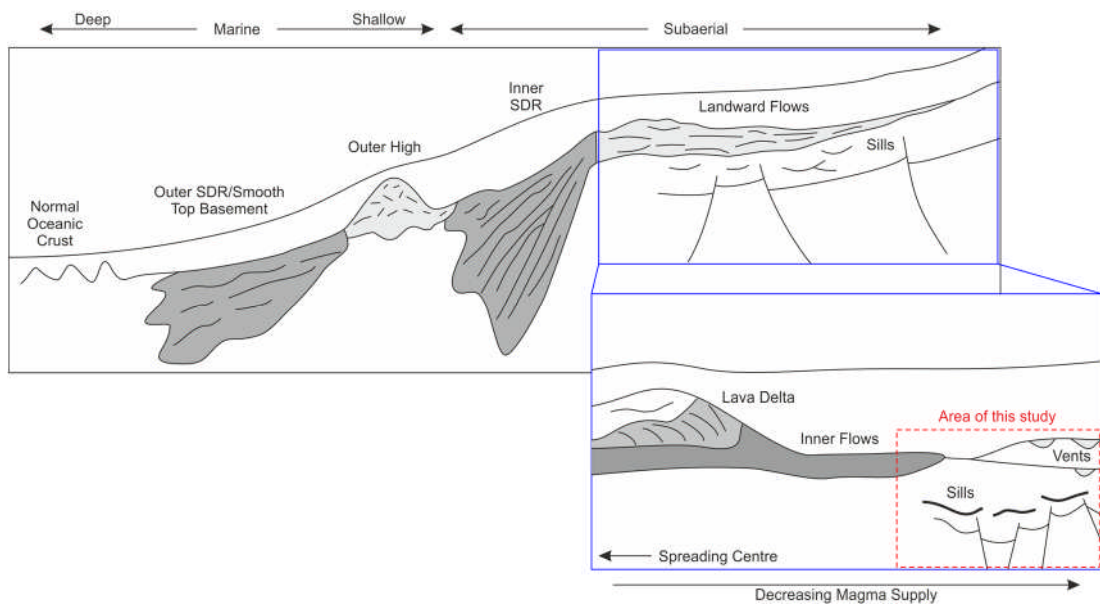


**Figure 5.1** – Schematic model of volcanic facies associated with volcanic passive margins proposed by Planke et al. (2000), the dataset for this study falls within the landward flow facies, in particular the inner flow sub-facies associated with fringe flood basalts, sill intrusion and volcanic vents.

This study focuses on the Faroe-Shetland Basin, NE Atlantic Margin specifically the Faroe-Shetland Sill Complex which formed in the Early Paleogene as a response to continental break-up along the NE-Atlantic Margin (Skogseid et al., 2000) and covers an area of at least 20,000 km<sup>2</sup>. The sills are intruded into thick Cretaceous and Early Paleocene mudstones (Thomson and Schofield, 2008), which were

deposited in a series of segmented Mesozoic rift basins, separated by basement-cored structural highs (Ritchie et al., 2011).

This chapter describes three distinct sill facies observed in the Corona Ridge region of the Faroe-Shetland Basin. Each facies has distinct characteristics, which are indicative of their emplacement environment. This study aims to combine the techniques and observations of previous seismic sill studies with those developed in Chapter 4 to describe the emplacement and evolution of the sill complex, providing a valuable insight into the processes and controls on the development of sill complexes and how they vary away from palaeo-spreading centres.

### **5.3 Tectonic Setting**

#### ***Regional Evolution***

The Faroe-Shetland Basin is a deep-water NE-SW trending, segmented rift basin located between the Faroes and the Shetland Isles on the NE Atlantic Margin (Dean et al., 1999) (Figure 5.2). It has a complex tectonic history spanning several phases of rifting, extensive volcanism and late-stage regional inversion (Doré and Lundin, 1996). The region underwent protracted, multi-phase rifting during the Mesozoic and Early Paleogene along inherited Caledonian structural trends (Doré et al., 1999), forming a series of segmented sub-basins, which are bound by crystalline basement highs (Ritchie et al., 2011). Rifting culminated with continental break-up during the Paleocene-Eocene transition (White, 1988, Coffin and Eldholm, 1992, Smallwood and White, 2002), during which time the arrival of the proto-Icelandic plume at the base of the lithosphere resulted in extensive extrusive and intrusive volcanism (Nadin et al., 1997, Smallwood and White, 2002).

Rifting was followed by extensive post-rift thermal subsidence creating a deep-water basin, which accumulated thick, sand rich Paleogene and Neogene successions (Sørensen, 2003). Subsidence was punctuated by multiple inversion events during the Mid to Late Cenozoic, which occurred along reactivated rift trends to produce the basin configuration seen today (Doré and Lundin, 1996, Davies et al., 2004, Stoker et al., 2005).

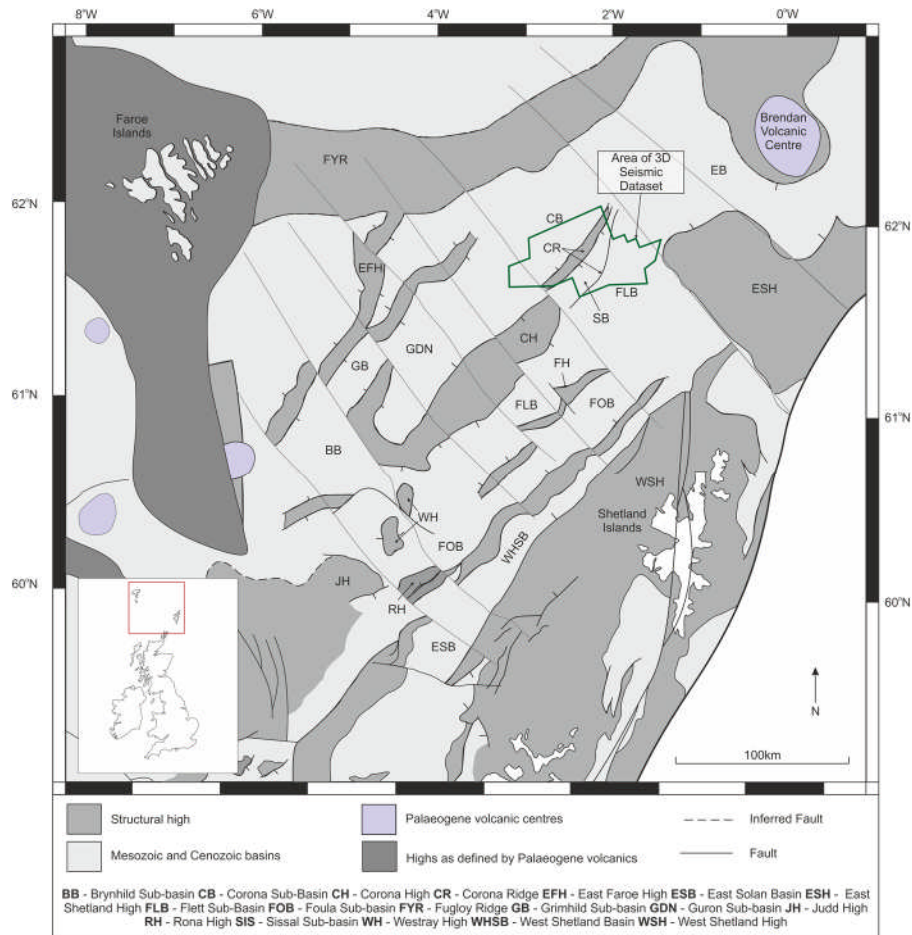


**Figure 5.2** – Location Map of the Faroe-Shetland Basin highlighting the main structural trends and the location of the seismic dataset, adapted from Ritchie et al. (2011). The basin consists of a series of sub-basins segmented by NE-SW trending, basement cored highs, and much of the northeast and central areas of are covered by thick, Early Paleogene flood basalt sequences.

### Timing of Volcanism

The onset of volcanism within the North Atlantic region is believed to have occurred between 62 – 61 Ma (Smallwood and White, 2002) and continued until the Early Eocene around 53 Ma, although radiometric dating of sill intrusions suggests the earliest sills may have been emplaced around 80 Ma (Ritchie and Hitchen, 1996). Extrusive flood basalt volcanism covers an area of 40,000 km<sup>2</sup> across much of the central and northeast portions of the Faroe-Shetland Basin; this consists primarily of the Faroe Islands Basalt Group, which has been dated to around 57 Ma (Passey and Jolley, 2008) (Figure 5.3). Younger flood basalts have also been noted in the area, including T36 (59 Ma) flows in the Foula Sub-basin (Schofield et al., 2015).

In addition to the flood basalts the area also underwent significant intrusive activity, with the Faroe-Shetland Sill Complex covering an area of 22,500 km<sup>2</sup> (Passey and Hitchen, 2011). Published radiometric dating of the Faroe-Shetland Sill Complex suggest that intrusions were emplaced between 80-50 Ma (Ritchie and Hitchen, 1996), although it is thought that the bulk intrusion occurred over 2-3 Ma years (White, 1988, Smallwood and Maresh, 2002) between 55-52 Ma (Passey and Hitchen, 2011) (Figure 5.3).

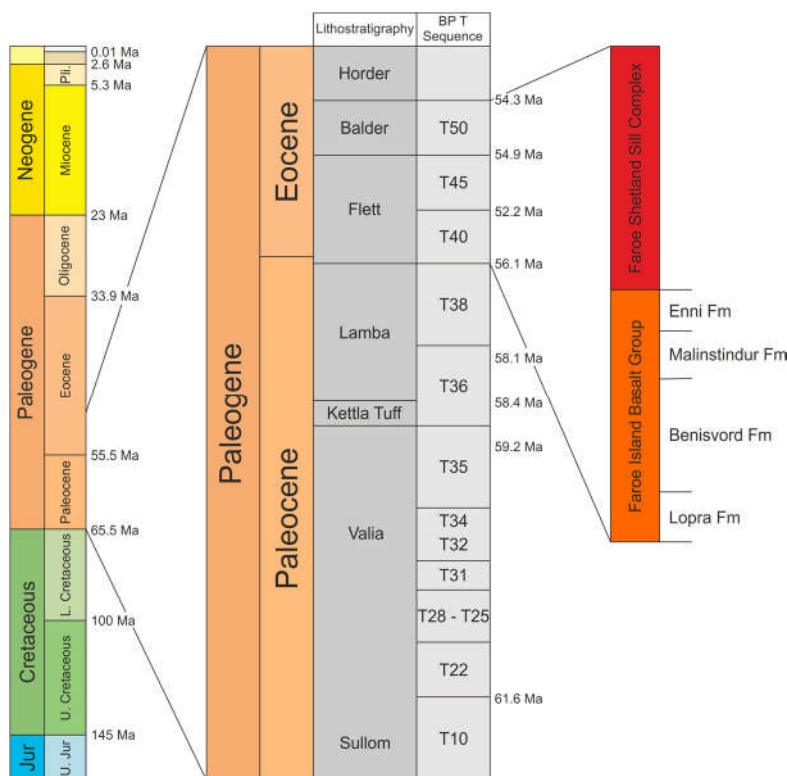


**Figure 5.3** – Chronostratigraphic column showing the lithostratigraphy of the Faroe-Shetland Basin and the corresponding BP T Sequence, the bulk intrusive volcanic activity occurs between T45 and T50 (around 53 Ma to 55 Ma).

#### 5.4 Data and Methods

The study was conducted on a portion of the PGS MegaSurvey Plus 3D seismic survey, which covers the upper north-eastern area of the Corona Ridge in the Faroe-Shetland Basin (Figure 5.2). The seismic dataset is 75 km by 45 km and images the Cretaceous syn-rift strata up through the Palaeogene and Neogene

post-rift basin fill, the bulk volcanic activity and the focus of this study is between -4 and -6 s TWTT.

Sills can be recognised in seismic data due to their high amplitude, which is a consequence of the large impedance contrast between crystalline igneous rocks and the surrounding sedimentary layers (Thomson, 2004). In addition, sills are typically discordant with host stratigraphy and have abrupt reflection terminations (Magee et al., 2013). Seismic interpretation was undertaken using Petrel® (Schlumberger ver. 2014.1); the sills were picked using manual interpretation techniques, with an auto-picking algorithm utilised in areas of high confidence. Opacity rendering techniques were also applied to help visualize the 3D distribution and geometry of the sill bodies during interpretation.

All observations and interpretations were made using time-domain seismic data, this has implications for the geometry and morphology of the sills, as their seismic expression may not necessarily represent their true geometry due to variations in seismic wavespeed. Smallwood (2009) have, however, demonstrated that the key geometric shapes and inter-sill relationships remain largely constant between both time and depth domains and so depth conversion is not considered necessary. Furthermore, with the lack of deep well penetration and the added velocity complications associated with igneous rocks, depth-converted sections may not necessarily provide greater accuracy.

In order to understand fully the controls on magma distribution across the margin it is essential to know where the sills are sourced from and the direction magma traveled through the intrusive bodies. The development of magma lobes formed during the emplacement and propagation of sill bodies (Hansen and Cartwright, 2006a, Schofield et al., 2012) have been successfully used to infer direction of magma transport through igneous intrusions (Thomson, 2004, Hansen and Cartwright, 2006a, Miles and Cartwright, 2010). Magma lobes can be identified on the upper surface of sill intrusions by the broadly concentric ridges which form parallel to front lobe perimeter (Trude, 2004, Hansen and Cartwright, 2006a, Schofield et al., 2012). Late-stage lobes can be identified as individual features on the propagating flanks of an intrusion as they episodically break out along the sill

periphery (Schofield et al., 2010). Detailed analysis of lobe formation can be used to infer the point from which a sill is sourced and thus develop an understanding of the magma sources across the basin (Schofield et al., 2015). Chapter 4 has demonstrated that the value of spectral decomposition in identifying magma lobes and determining flow direction on the surface of sill bodies, the techniques established in Chapter 4 are applied to this dataset to aid analysis and interpretation.

The presence of igneous rocks in sedimentary basins can result in the attenuation of seismic energy (Pujol and Smithson, 1991), which has the effect of reducing the reflection quality of sedimentary marker horizons as well as fault planes below and around igneous intrusions. The impact of attenuation in the dataset is significant, in particular below the Paleogene flood basalts in the northwest of the dataset. Because of this, such stratigraphic and structural interpretation was supplemented with the published structural trends (Moy and Imber, 2009) and inferences made from the position and geometry of interpreted sills.

### **5.5 Resolution and Unresolved Sills**

As the findings and conclusions of this chapter are based primarily on observations made using seismic reflection data, it is important to establish the resolution of the dataset and any implications this may have on the accuracy of the findings.

Vertical seismic resolution defines how thick an object (in this case a sill) must be to image as a discrete reflection event and is a function of the dominant frequency and average velocity of the seismic data (Sheriff and Geldart, 1995). The average dominant frequency in the area is ~17 Hz and drops to as low as 11 Hz in the deeper Cretaceous successions below the flood basalts. The lack of deep well penetration within the data area means average velocities cannot be directly measured, however studies conducted on other parts of the dataset suggest average seismic velocities within the Cretaceous succession range between 3000 and 4500 m s<sup>-1</sup> (Schofield et al., 2015). This gives a best case vertical resolution of 40 m and a worst case resolution of 100 m under perfect conditions (see Section 3.3 for equations).

Such conditions, however, are rarely achieved due to offset-dependent tuning, velocity increases around complex 3D sill bodies and their associated metamorphic aureoles, and structural or stratigraphic variations in the overburden (Planke et al., 2005). Therefore, the predicted resolution represents a best-case scenario.

Well analysis conducted by Schofield et al. (2015) demonstrated that 88% of sills drilled in the Faroe-Shetland Basin are between 0 – 40 m thick with 73 % of the total measured sills less than 15 m thick; this has significant implications when using seismic reflection data to study intrusive igneous rocks. Given that the average vertical seismic resolution within the Cretaceous succession is ~40 m, 88 % of sill intrusions within the basin are below seismic resolution and will not be imaged as discrete reflection events.

Given that the overall aim of this study is to assess the source and distribution of the bulk intrusive magma volume across the area it must be recognised that a significant volume of the intruded magma cannot be accounted for using seismic data alone. However the observations made from the seismically resolved sills are still valuable in identifying intrusion styles, feeding relationships and flow directions, all of which can be used to define the characteristics of the sill complexes in the area and ultimately the process which form them.

## **5.6 Results**

### **5.6.1 Basin Structure and Regional Distribution of Sills**

Structural interpretation shows that the area is highly segmented by northeast-southwest trending normal faults forming a series of thick Cretaceous sub-basins, which have been heavily intruded by the Faroe-Shetland Sill Complex.

The most significant structure in the area is the Corona Ridge, a basement-cored structural high which is composed of two separate splays that extend northeast-southwest through the northwestern and central sections of the dataset, referred to as the northern and southern splays respectively (Figure 5.5). Between the two splays of the Corona ridge is the Sissal Sub-basin which is up to 18 km wide in the

southwest and tapers to around 3 km in the northeast as the two splays begin to converge. The basin fill is predominantly Cretaceous sediments which are typically 1500-2000 ms TWTT thick.

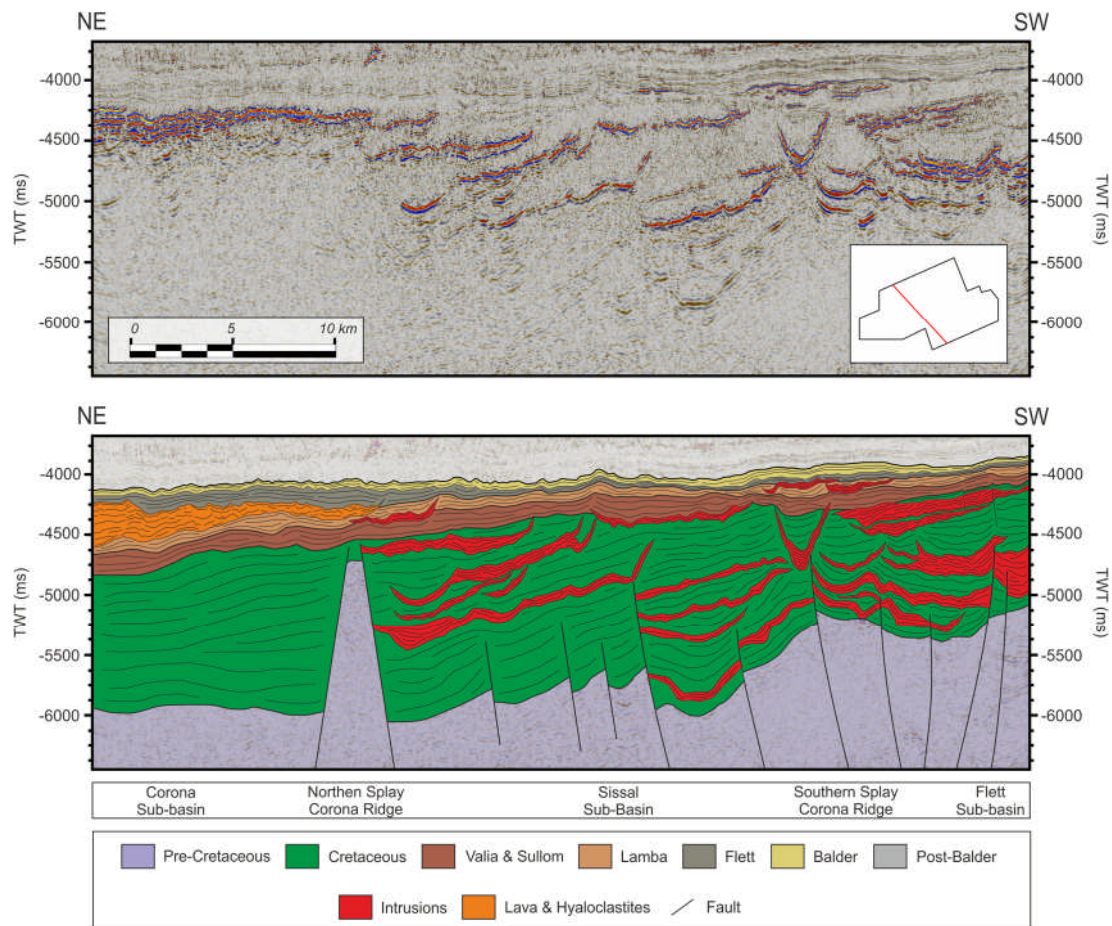


**Figure 5.4** – NW-SE trending seismic line from the southwest of the dataset showing the northern splay of the Corona Ridge and wide Sissal Sub-basin.

The north-western portion of Sissal Sub-basin is overlapped by the fringes of the overlying flood basalts. To the northwest of the northern splay sits the Corona Sub-basin. Few sills are observed here, although the overlying thick flood basalt sequences may be drastically reducing resolution.

Southeast of the southern splay is the Flett Sub-basin, this sub-basin is highly segmented by a series of northeast-southwest trending normal faults (Figure 5.5). There are two main segments of the Flett Sub-basin, the first is a 10 -15 km wide graben running the length of the dataset which is bound by the southern splay to

the northwest and a large basin bounding fault to the southeast, sediment thickness in the centre of the graben is up to 2500 ms TWTT.

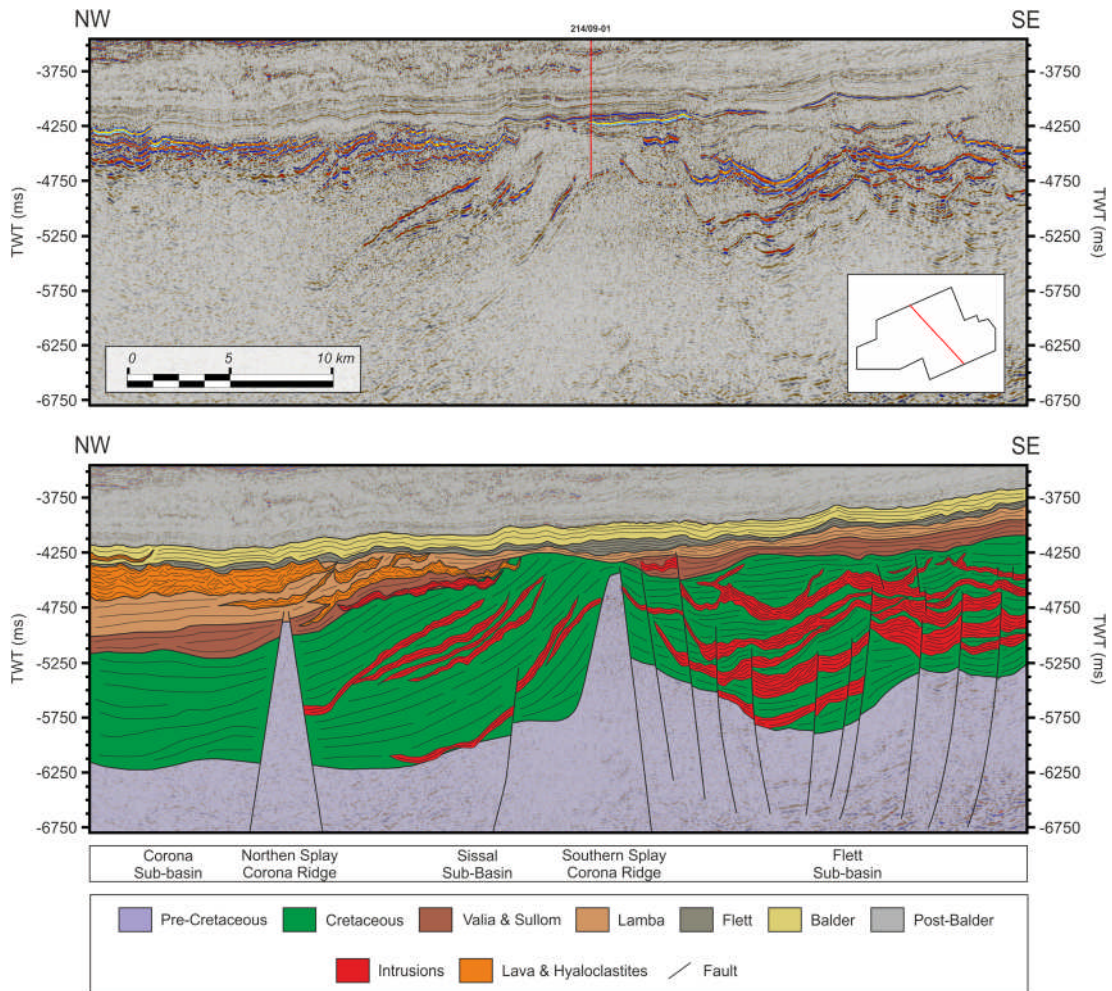


**Figure 5.5** – NW-SE trending seismic from the centre of the dataset, the northern splay of the Corona Ridge has progressed into a crystalline basement high.

The second segment occurs southeast of the large basin bounding fault and is composed of a series of tilted Cretaceous fault blocks compartmentalised by large, high angle normal faults (Figure 5.6). Sediment accumulation is much thinner in this area (<1500 ms TWTT) owing to the shallow depth of the basement.

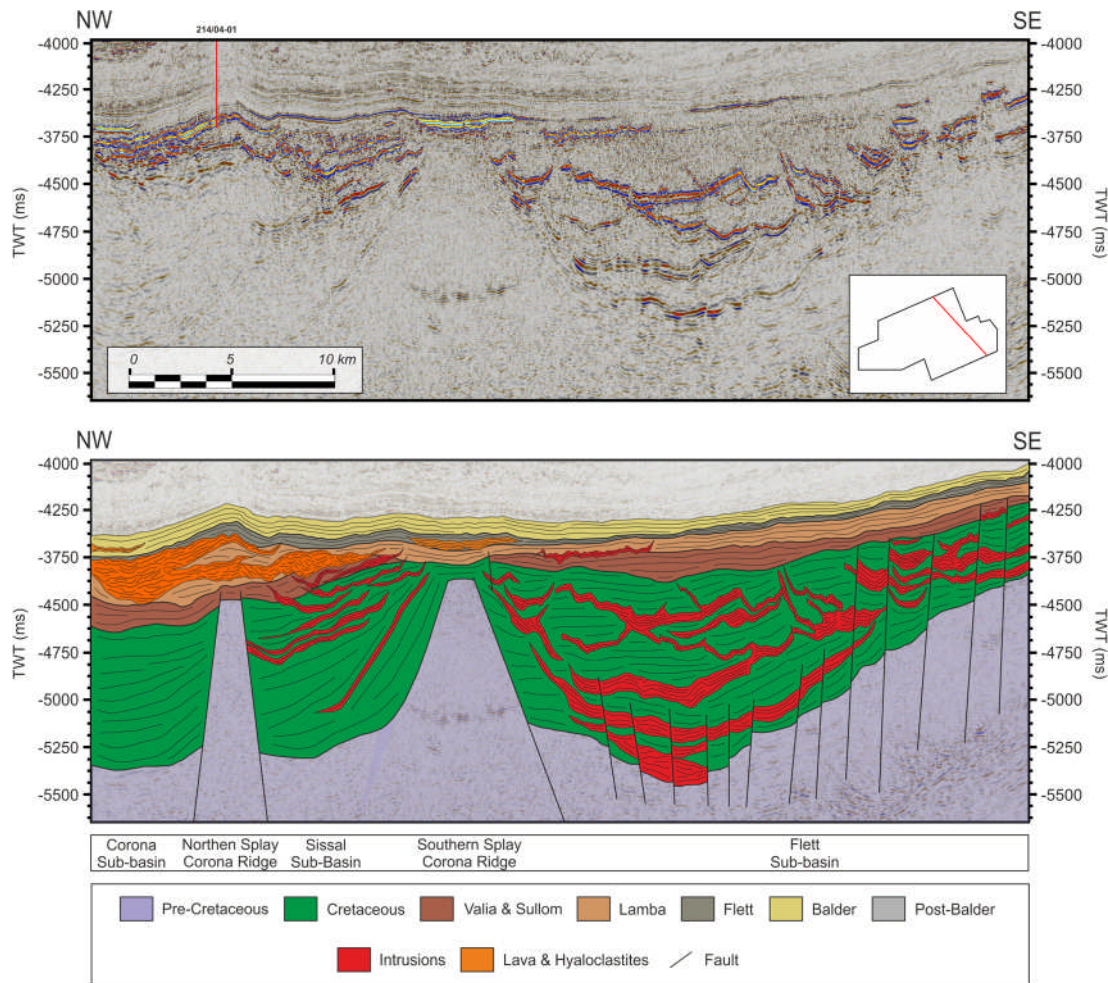


**Figure 5.6** –NW-SE trending seismic Xline from the northeast of the dataset. The splays of the Corona Ridge have converged, drastically reducing the size of the Sissal Sub-basin.

The sub-basins described above provide three discrete areas of sill emplacement, with each area characterised by a distinctive style of sill intrusion. The first is the Sissal Sub-Basin, bound either side by splays of the Corona Ridge, the area features long tabular intrusions, which typically dip to the northwest (Type I sills). The second area is the un-segmented portion of the Flett Sub-basin, bound to the northwest by the northern Splay of the Corona Ridge and to the southeast by the large basin-bounding fault. Here intrusions consist of large, dish-like structures, which form branched, interconnected systems (Type II Sills). The final area is the heavily segmented portion of the Flett Sub-basin in the far southeastern corner of the dataset, which contains a series of small, laterally discontinuous intrusions emplaced between the faults (Type III Sills) (Figure 5.7).

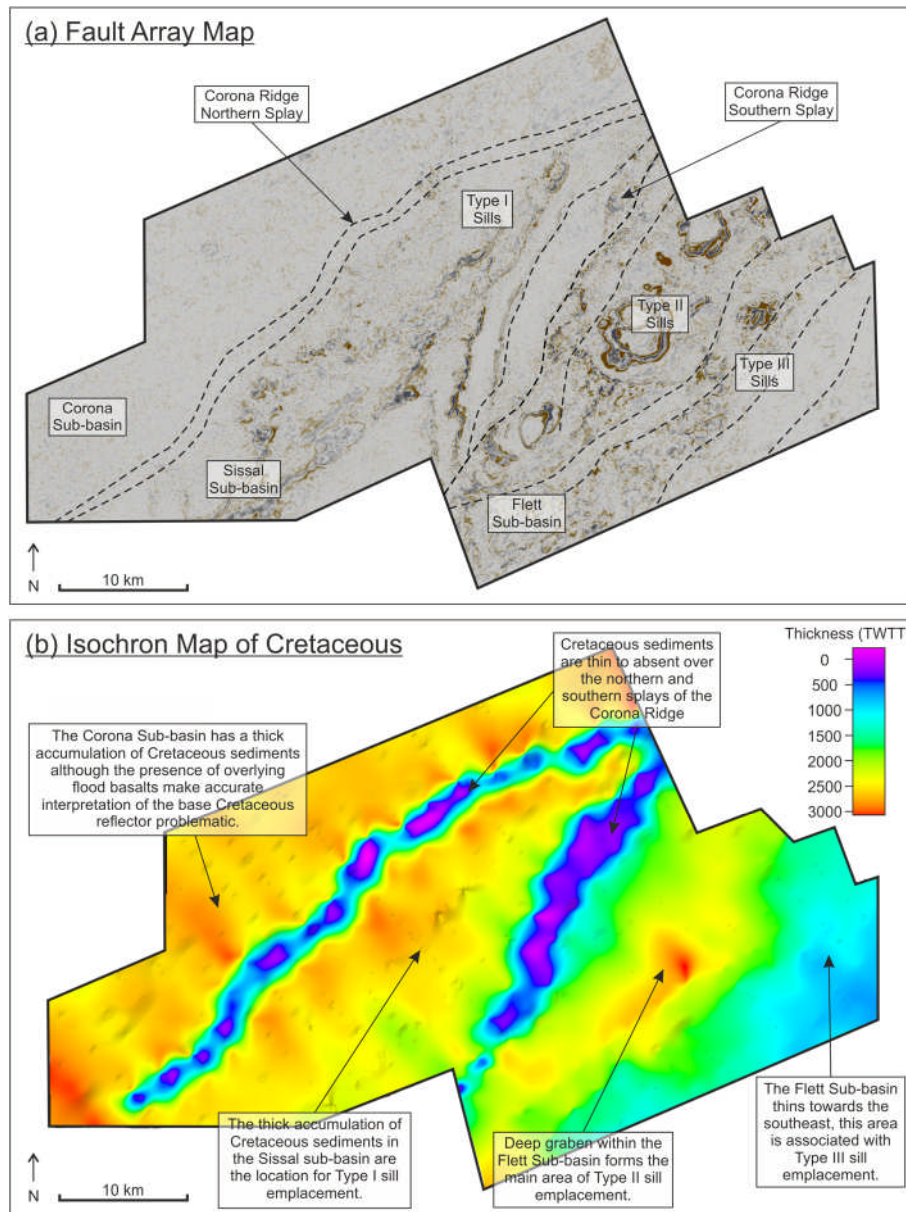


**Figure 5.7** – (a) Fault array map superimposed on a seismic time slice (-5000 ms TWTT) showing the main structural trends in the area, the geometry of the sub-basins and the approximate emplacement area of the three sill facies. (b) Isochron map of the Cretaceous sediments showing the relative thickness of each sub-basin.

### 5.6.2 Sill Facies

Over 75 individual sill bodies were mapped using the 3D seismic data; the sills were then grouped into distinctive facies based on a number of shared characteristics, which are summarised in Table 5.1 below.

	Sill Facies		
	Type I	Type II	Type III
Major Axis (km)	15.6 (Range: 35.4 – 4.5)	4.8 (Range: 14.1 – 0.8)	3.3 (Range: 7.1 – 0.8)
Minor Axis (km)	5.4 (Range: 11.1 – 1.7)	2.9 (Range 13.4 – 0.5)	1.8 (Range: 2.3 – 0.4)
Mean Surface Area (km <sup>2</sup> )	71.5 (Range: 180.7 – 17.2)	14.0 (Range: 53.9 – 0.4)	6.9 (Range: 18.1 – 0.3)
Mean Volume (km <sup>3</sup> )	4.3 (Range: 11.1 – 0.8)	0.57 (Range: 3.3 – 0.03)	0.30 (Range: 0.54 – 0.13)
Location	Sissal Sub-basin	Flett Sub-basin	Flett Sub-basin
Morphology	Flat, tabular, sheet intrusions.	Circular / sub-circular saucer-shaped intrusions.	Small, discontinuous, saucer-shaped intrusions.
Feeding Relationships	Mainly individual bodies, some inter-sill feeding higher up stratigraphy.	Complex network of inter-sill feeding relationships. Dyke fed at base.	Some inter-sill feeding, many fed from the fault planes.
Structural Interaction	Bound between northern and southern splays of the Corona Ridge.	Between the southern splay of the Corona Ridge and basement bound fault.	Emplaced in a strongly segmented area of the Flett-Sub basin.
Stratigraphic Interaction	Layer parallel, some transgressions at shallow depths.	Layer parallel at base, transgressive limbs higher up stratigraphy.	Largely layer parallel within individual fault blocks, some transgression.
Seismic Character	Strong, high impedance reflectors poorly resolved at depth.	High amplitude well imaged shallow intrusions, moderate amplitude at depth.	Moderate amplitude, well imaged due to shallow present day depths.

**Table 5.1** – Summary of the shared characteristics used to define individual sill facies. Volume calculations are based on an average sill thickness of 40 m, which represents an absolute minimum thickness defined by the limits of seismic resolution, actual volumes may be substantially higher (especially for Type I Sills).

The characteristics, emplacement environment and proposed source of each sill facies are discussed in detail below.

### **5.6.2.1 Type I**

#### **5.6.2.1.1 Characteristics**

Type I sills are the most aerially extensive intrusions recognised in the area and typically form elongate bodies, ranging in length from 5 - 35 km and in width from 2 – 11 km. They form tabular sheet intrusions, which are layer-parallel and rarely cross-cut stratigraphy unlike the saucer shaped intrusions observed elsewhere in the basin.

There is a general trend of increasing surface area and thus inferred volume with depth, with the largest, deepest intrusions exceeding 150 km<sup>2</sup>. The upper Type I sills are strong, prominent reflectors and whilst reflection amplitudes generally decrease with depth, they can still be imaged clearly at -6.5s TWTT (~ 6 km). The number of Type I sills decreases with depth, although this may be a function of deteriorating seismic resolution and not indicative of emplacement.

The uppermost Type I sills are within close proximity to and have a similar geometry to the overlying flood basalts. In order to distinguish between the two, opacity rendering was undertaken to highlight the distinct differences in seismic expression of their top surface reflectors (Figure 5.8). Flood basalts typically exhibit highly chaotic, rugose top surfaces caused by the rapid cooling and brittle nature of sub-aqueous emplacement (Schofield 2013), in contrast, sills are characteristically smoother, forming concentric ridges in the direction of flow (Trude 2004). The seismic analysis of the two types of reflector can be used to confidently state that both are formed through different emplacement mechanisms.

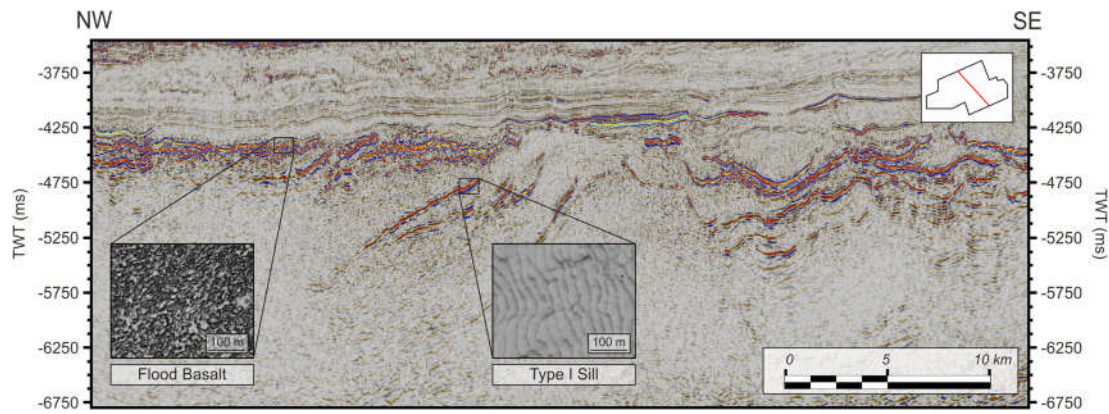


**Figure 5.8** – Opacity rendered images of flood basalt and a Type I sill. The images show how the upper surface of each body has a distinct seismic expression, which helps distinguish between extrusive and intrusive igneous rock.

#### 5.6.2.1.2 Emplacement Environment

Type I sills are confined to a single, large, northeast-southwest trending fault block in the far north-western corner of the dataset (Figure 5.9). The fault block forms the Sissal Sub-basin, which is flanked by the northern splay of the Corona ridge to the northwest and the southern splay of the Corona Ridge to the southeast. The sub-basin is partially overlapped by the aerial extent of the overlying flood basalt sequence.

Type I sills terminate abruptly against the northern splay of the Corona Ridge and typically do not reach the southern splay, however, they can be observed intruding into the fault plane of the southern splay in some areas (Figure 5.9). A series of small normal faults can be observed in the shallower Type I sills, with some evidence of reverse reactivation, which are likely the result of later Cenozoic compression (Ritchie et al., 2003). The shallow faults form clean cut offs in the sill bodies and there is little evidence of intrusion into the fault planes suggesting the small, shallow faults formed post-emplacment and so are not considered important in the context of Type I sill emplacement.

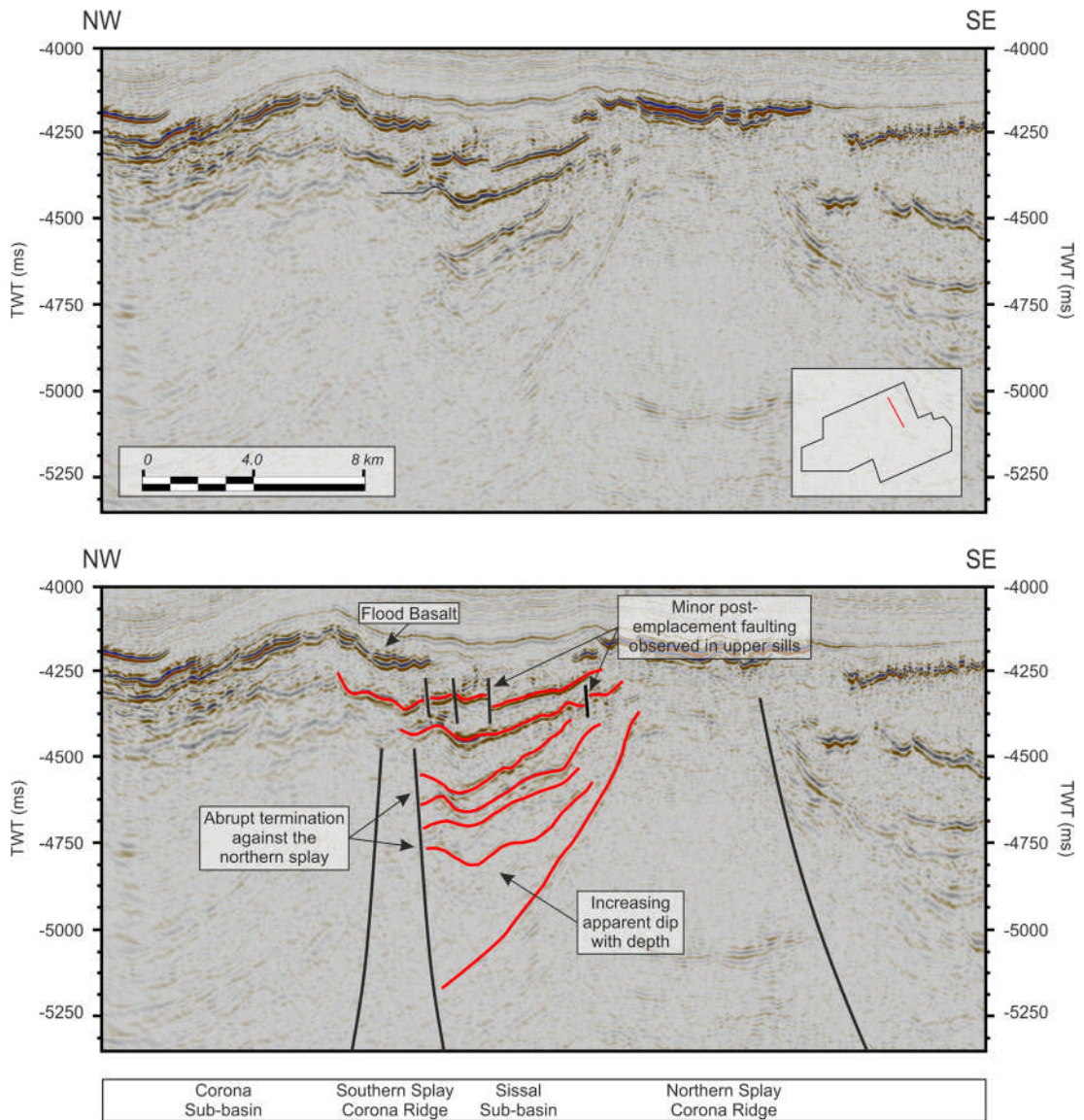


**Figure 5.9** – NW-SE trending seismic line through the Sissal Sub-basin showing the restriction of Type I sills between the northern and southern splays of the Corona Ridge. The sills terminate against the northern splay; most do not reach the southern splay.

When viewed as a complete suite of intrusives the Type I sills form a broad fan-shaped package, which dips to the northwest (Figure 5.9 & Figure 5.10). Based on the apparent dip, the lowest stratigraphic sills appear to be more steeply inclined in contrast to the near horizontal sills higher up stratigraphy. This configuration is interpreted to be the result of intrusion of magma parallel to host stratigraphy, which has been previously been rotated during Cretaceous rifting and subsidence along the northern splay of the Corona Ridge.

It is difficult to constrain the timing of Type I sill emplacement, as there is no well control and the presence of thick flood basalts, shallow faults and inversion obscure any potential forced folding relationships with the overlying sediments.

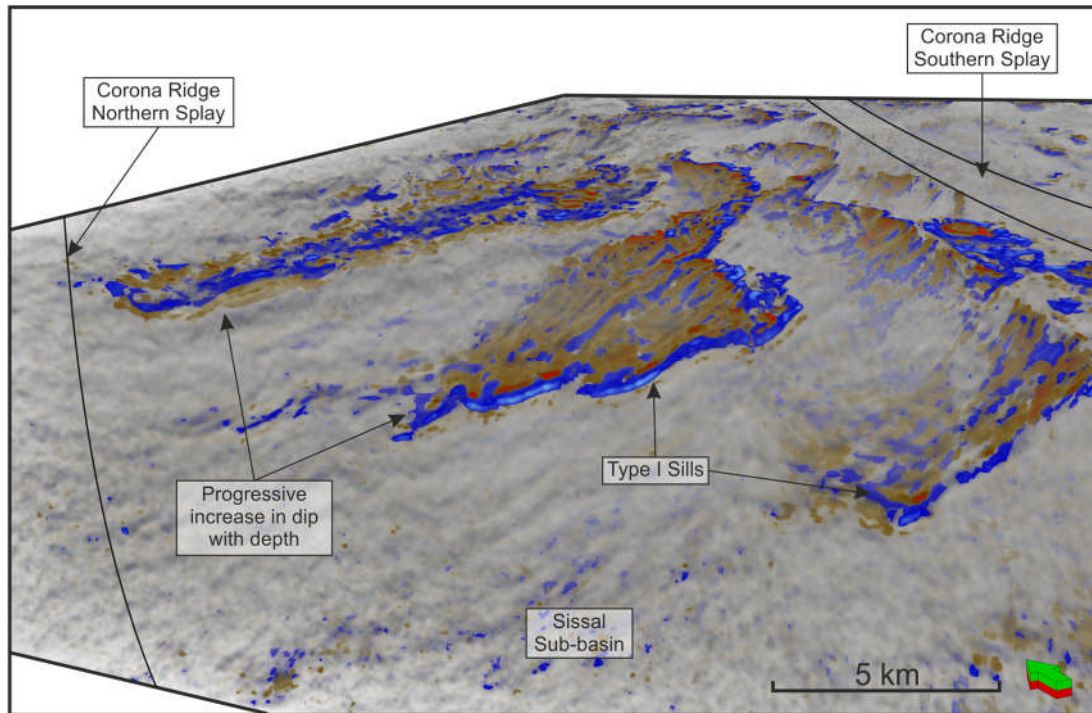


**Figure 5.10** – Opacity rendered 3D image of the Sissal Sub-basin showing Type I sills. The sills dip north-west towards the northern splay of the Corona Ridge. There is an increase in the angle of dip with increasing depth.

### 5.6.2.1.3 Source and Flow Direction

Spectral decomposition was applied to the seismic volume (45 Hz using the Continuous Wavelet Transform, see Chapter 4 for details) to help delineate flow directions on the sills' surface (Figure 5.11). Analysis of the generated surface shows sills are not fed from a single location but rather a series of points along a fault plane, before coalescing into a single competent body. The pattern of flow ridges on the sills' surface and the development of magma lobes on the southeast flank of the sill body suggests that Type I sills are fed from the northwest and flow to the southeast. Where the sills terminate abruptly against the northern splay of the Corona Ridge they are in direct contact with crystalline basement, providing a

viable conduit for magma transportation. The shallower, smaller Type I sills which are not in contact with the basement faults form inter-sill junctions with the shallower, larger sills, suggesting that the larger sills are acting as conduits, transferring magma from the basement to a shallower stratigraphic level.

The elongation of Type I sills in a NE-SW orientation indicates that the splays of the Corona Ridge have restricted their ability to spread NW-SE, perpendicular to the fault planes and so intrusion has preferentially occurred parallel to the main structural trend.

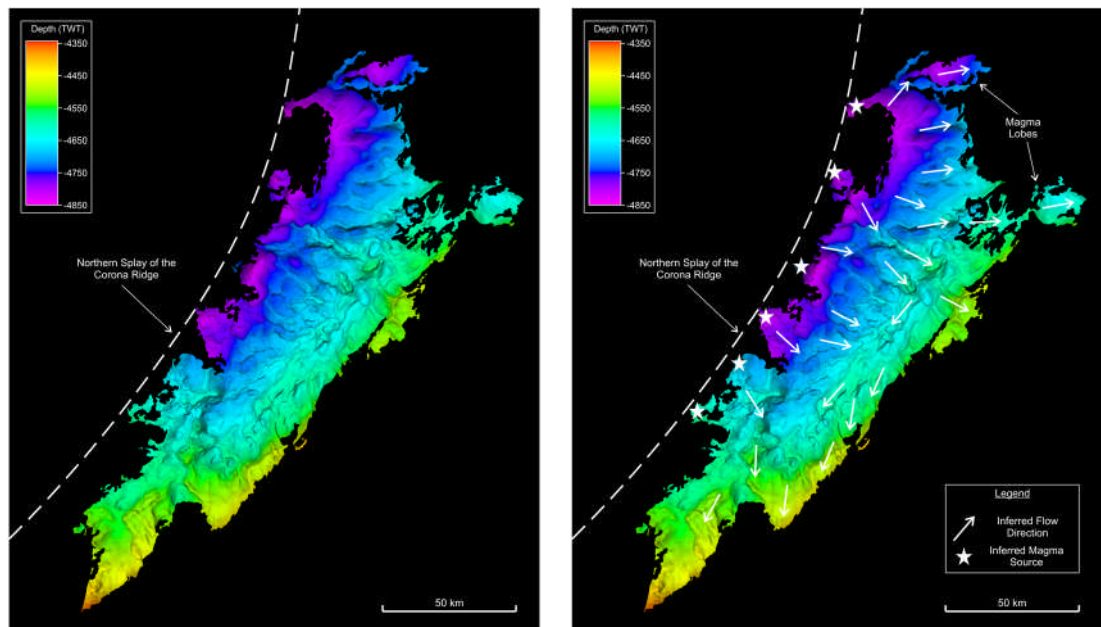


**Figure 5.11** – 3D surface of a Type I sill generated using spectral decomposition (45 Hz Continuous Wavelet Transform). The sill shows it is fed from multiple source points along the northern splay of the Corona Ridge, and flows towards the south-east, developing magma lobes on its outer edges.

## 5.6.2.2 Type II

### 5.6.2.2.1 Characteristics

In seismic time-slices Type II sills form broadly circular or oval shaped intrusions with an average diameter of 5-8 km and have approximate bilateral or radial symmetry (Figure 5.13). In seismic cross-section the intrusions are saucer-shaped

with convex bases, steep limbs, which transgress stratigraphy and flat outer rims (Figure 5.15).

The deepest intrusions are interpreted to be basin-parallel, they form saucer shaped bodies with a convex base and ascending limbs that follow the shape of the Cretaceous graben into which they are emplaced and do not cross cut host stratigraphy. The shallower sills also form saucer-shaped bodies however the ascending limbs are typically transgressive before forming a flat, layer-parallel outer rim (Figure 5.15).

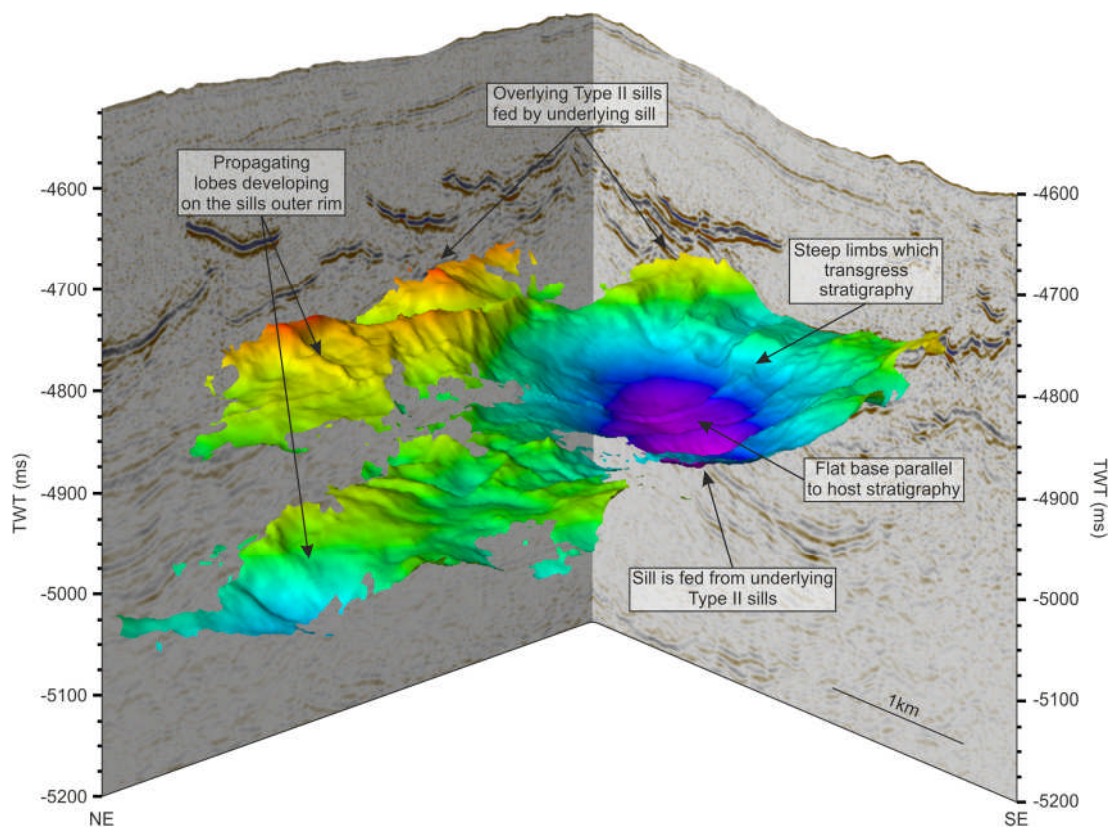


**Figure 5.12** –3D surface interpretation of a Type II sill body showing the characteristic saucer shaped morphology. The sills have a flat central base surrounding by steep limbs, which transgress stratigraphy, the flanks of the limbs are surrounded by either flat outer rims or by the developing magma fingers and lobes.

The sills form a network of interconnected bodies; these branching sill complexes are initiated at depth and gradually progress to shallower levels of emplacement with the underlying sills acting as feeders for those above them (Figure 5.13). They form intricate systems, which can contain up to 10 inter-sill junctions between the oldest base sill to the youngest, upper most sill. A broad decrease in sill diameter is observed (12 km for 1st order sills compared to <1 km for 10th order sills) and thus a decrease in inferred volume as the order of sill interconnectivity increases.

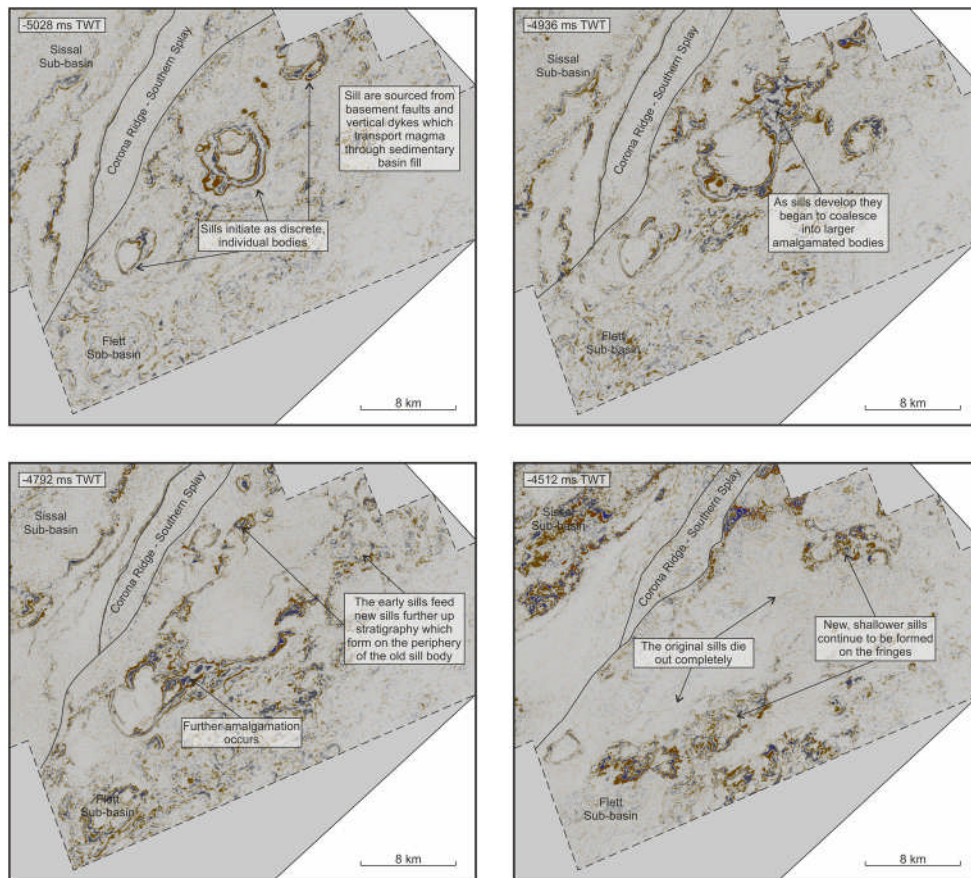


**Figure 5.13** – Seismic time-slices of the Flett Sub-basin illustrating the change in Type II sill emplacement with depth. The deepest sills are emplaced in the centre of a large graben, as they progress up stratigraphy emplacement moves to the flanks to feed smaller, shallow sills. The sills are initiated at a number of discrete points before becoming amalgamated further up stratigraphy as they develop into inter-connecting networks.

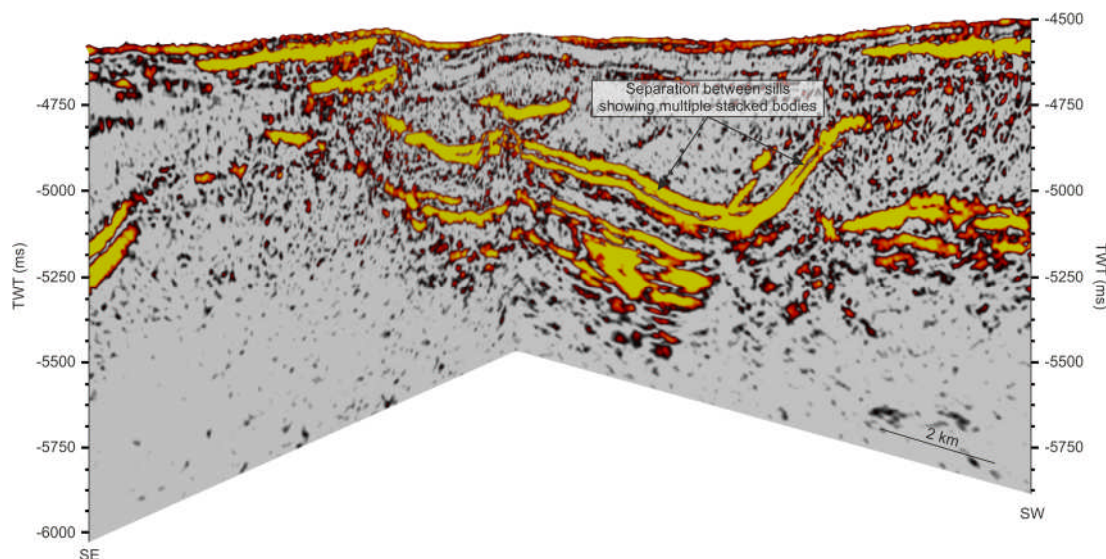


**Figure 5.14** – The application of spectral decomposition (as demonstrated in Chapter 4) can be used to delineate stacked sill bodies that are not resolved in conventional seismic data.

#### 5.6.2.2 Emplacement Environment

The Type II sills are contained within a 10-15 km wide graben in the Flett Sub-basin, immediately southeast of the southern splay of the Corona Ridge (Figure 5.7). The graben is bound to the northwest by the southern splay of the Corona Ridge and to the southeast by a major, basement-bound normal fault. At the base of the Cretaceous succession the graben has a series of high angle, low throw normal faults; however, these have a limited vertical extent. The remainder of the Cretaceous succession has very little deformation, meaning the sills have been emplaced within a stratified sedimentary sequence with limited influence from pre-existing or post-emplacement deformation.

The deepest, largest sills typically initiate in the centre of the graben; as they begin to develop into interconnecting networks and progress up stratigraphy, emplacement begins to shift towards the basin flanks (Figure 5.13).

A series of mounds can be observed in the Top Lamba Formation (T40 – 56.1 Ma) onto which the Flett Formation onlaps (T40 – T45, 56.1 – 54.9 Ma) (Figure 5.16).

The mounds sit directly above the tips of the upper most Type II sills, with zones of chaotic seismic reflection in the zone between. Previous authors have attributed

this spatial correlation to a genetic link between the vent and the underlying sill (Bell and Butcher, 2002, Jamtveit et al., 2004, Planke et al., 2005, Hansen, 2006) which can be used to define a relative time of intrusion (Jackson et al., 2013). As such it is suggested that the uppermost Type II intrusions were emplaced during the deposition of the Flett formation, between 56.1 and 54.9 Ma.

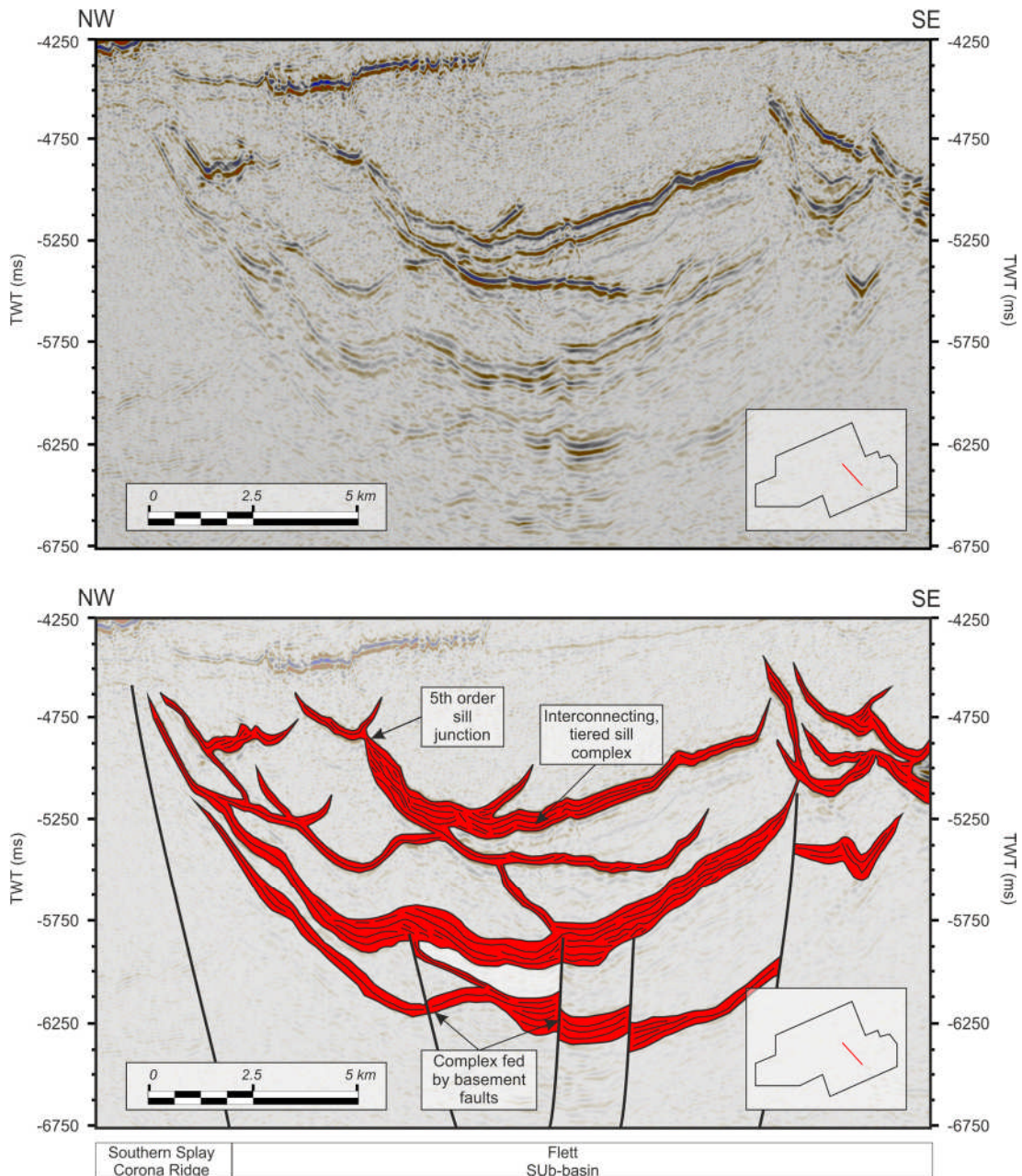


**Figure 5.15** – NW-SE trending seismic line through a large graben in the Flett Sub-basin immediately south-east of the southern splay of the Corona Ridge. The graben contains a series of Type II sills that form an inter-connected complex with the deepest sills feeding those higher up stratigraphy.

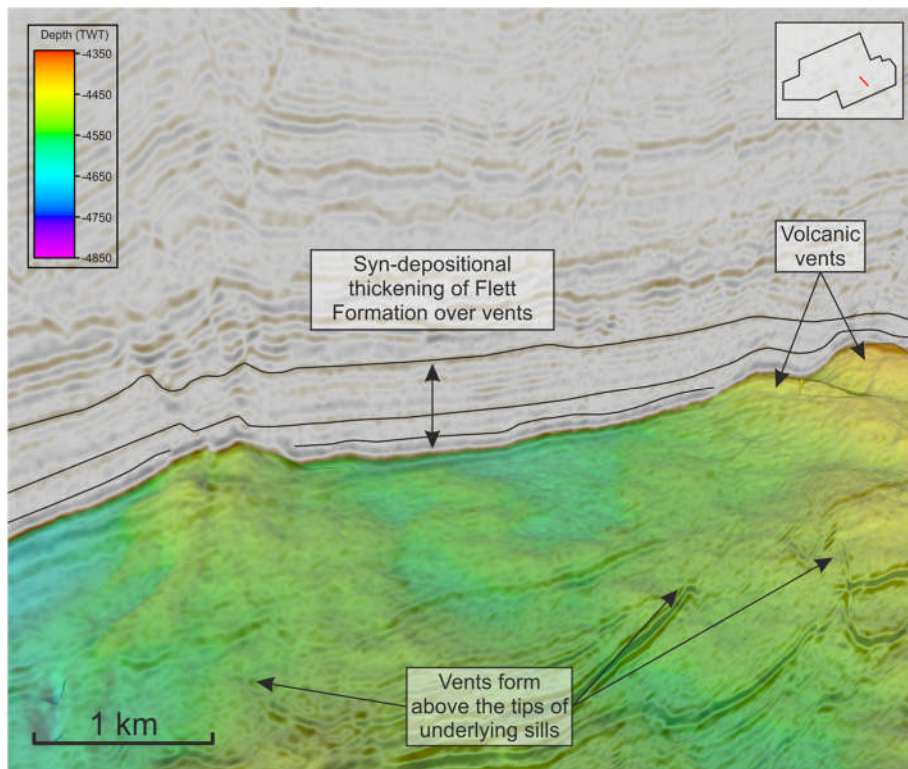


**Figure 5.16** – A number of vent structures are observed in the Lamba Formation (T38) above the tips of underlying Type II sills. The overlying Flett Formation (T40-T45) thins onto the vents, suggesting their formation preceded deposition, providing a relative timing of sill emplacement.

### 5.6.2.2.3 Source and Flow Direction

The observed inter-sill feeding relationships show that Type II sills are typically fed at their deepest, but not necessarily most central, point. Opacity-rendered images (Figure 5.17) show flow lines on the inclined limbs and the development of magma fingers and partial lobes on the outer fringes, which are indicative of magma flowing upwards and away from a singular source.

The majority of Type II sills are fed through inter-sill feeding relationships as part of an interconnected network, which typically progresses upwards and away from the centre of the graben with decreasing depth. The large intrusions, which form the base of the interconnected sill complexes, are connected to the underlying basement via numerous small Cretaceous faults in the centre of the graben,

providing a viable conduit for magma transportation from potential chambers below.

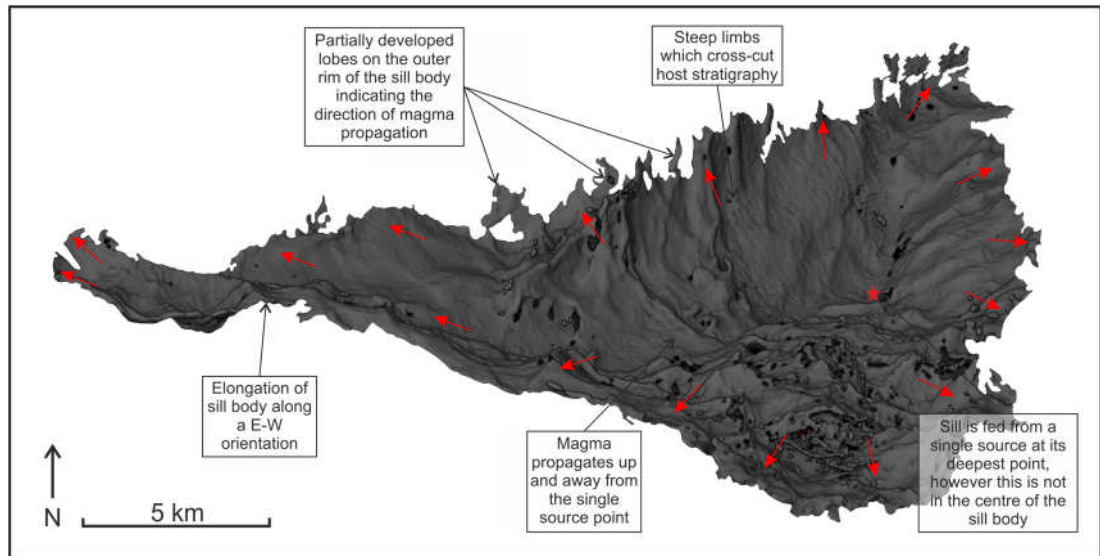


**Figure 5.17** – Opacity rendered Type II sill showing the development of partial lobes and magma fingers on the fringes of the sill body. Magma is interpreted to flow upwards and away from a singular source at the deepest point of the of the sill body.

There are a number of large Type II sills which are not connected to underlying basement, instead there is a significant thickness of Cretaceous basin fill between them and the crystalline rocks below. Beneath the central and deepest point of these sills are vertical zones of chaotic or poor seismic reflectivity (Figure 5.18). Although this may be predicted below a large sill due to the expected attenuation effects (Maresh and White, 2005) the zones are narrow and do not extend across the entire base of the sills. Furthermore, the zones sharply cross-cut underlying well-imaged intrusions. These zones have been interpreted to represent feeder dykes, providing conduits for magma transportation from underlying magma chambers in the basement to the point of emplacement. This seismic response is typical of dykes as conventional seismic reflection data are not acquired or processed to image steep or vertical structures (Kearey et al., 2013). Given the size of the sill complexes, which have been fed by these dykes, the amount of magma transported through them is significant in the context of total Type II sill volume.

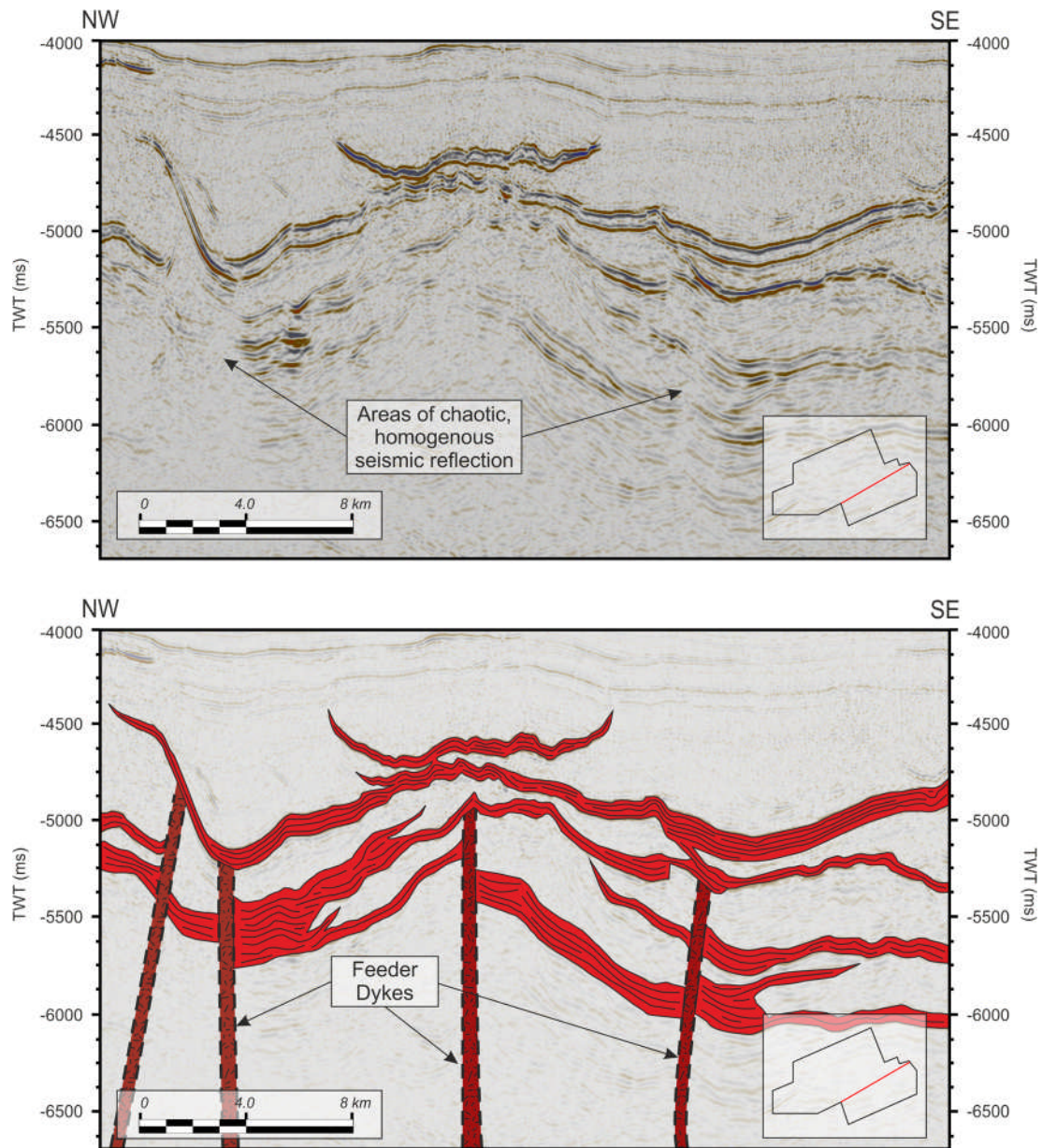


**Figure 5.18** – NE-SW trending seismic line showing areas of homogenous, chaotic reflectivity below the base of large Type II sills, interpreted to infer the presence of feeder dykes. The dykes cross multiple sills suggesting they may feed a number of different bodies, which are part of different inter-connecting complexes.

### 5.6.2.3 Type III

#### 5.6.2.3.1 Characteristics

Type III sills are the smallest of the three types observed in the area and form small, concave-up, dish-like structures, which are sub-circular or ellipsoidal in plan view.

They are typically <3 km long and <2 km wide, with the largest up to 8 km long and

the smallest <0.5 km. The sills characteristically possess a sub-horizontal base, which is parallel with host stratigraphy, with ascending limbs extending from the periphery and transgressing stratigraphy, unlike Type II sills they rarely form complete saucer shaped geometries. Type III sills are the most common sill facies in the area, with more individual bodies than the other two sill facies combined, however, their size means they actually represent the smallest total inferred volume of all the facies. Based on an average thickness of 40 m, the total emplaced volume of Type III sills is approximately 15-20 km<sup>3</sup>, this amounts to the volume of just two or three individual Type I sills.

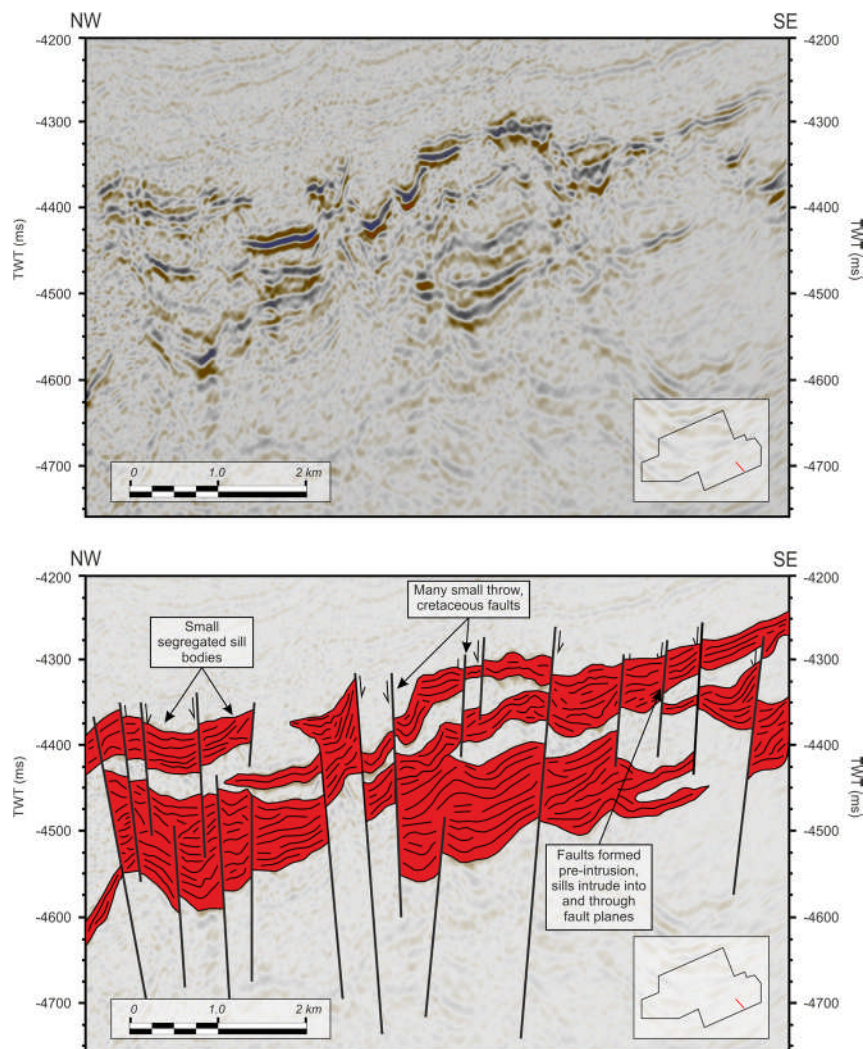


**Figure 5.19** – NW-SE orientated seismic line showing the strong segregation of Type III sills by multiple high-angle Mesozoic faults. The limited vertical separation between sills gives them appearance of amalgamated bodies, although internal reflectivity shows them to be individual intrusion events.

The sills are well-imaged owing to their relatively shallow present-day depth, however their close spatial relationship and the limited vertical separation between intrusions make it difficult to distinguish between individual sill bodies. Indeed, many intrusions appear amalgamated, although internal reflectivity can often be used to delineate the presence, size and shape of the individual bodies (Figure 5.19).

#### **5.6.2.3.2 Emplacement Environment**

Type III sills are emplaced within Flett Sub-basin towards the south-eastern edge of the dataset. A large basement-bound normal fault separates Type III sills from the Type II sills in the centre of the basin. The fault creates a relative structural high, with the Cretaceous stratigraphy between 500 - 2000 ms TWTT, shallower here than in the central areas of the basin (Figure 5.7). The area is heavily segmented by series of normal faults, which extend down to the basement, interspersed with a series of smaller, low throw, normal faults contained entirely within the Cretaceous succession.

It is evident that the relatively high density of faults compared to other areas of the basin has played a significant role in the emplacement and morphology of Type III sills. There is a noticeable trend of elongation within sill bodies along a NE-SW axis, parallel to the fault trend, indicating that the faults have restricted lateral emplacement of magma perpendicular to fault trend. The magma feeding these sills has trouble propagating across fault planes due to its small volume.

The relationship between the Type III sills and the faults suggests the timing of fault activity with respect to sill emplacement is highly variable (Figure 5.20). It is clear that in the majority of cases, fault activity pre-dates sill emplacement, this can be demonstrated by the elongation of sill bodies parallel to fault trend, the intrusion of sills into the fault planes and the abrupt termination of sills against fault planes. However, there are examples of sill bodies, which have been displaced by fault

movement post-emplacment suggesting that a number of faults remained active some time after emplacement.

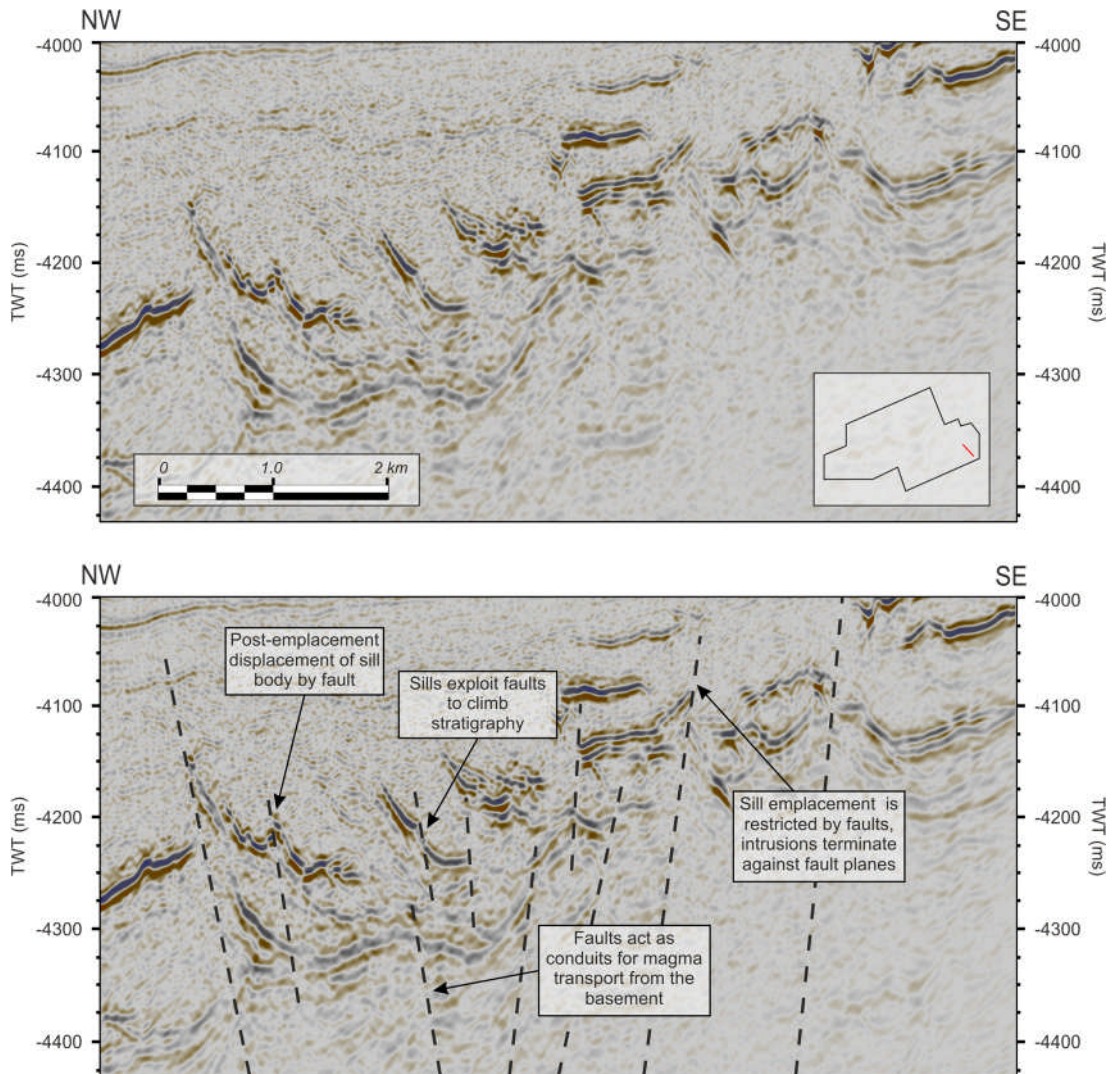


**Figure 5.20** – NW-SE seismic line showing the variable relationship between Type III sills and the Cretaceous bounding faults. (a) Intrusion and termination into the fault plane. (b) Intrusion and continuation past the fault plane. (c) Post-emplacment deformation.

### 5.6.2.3.3 Source and Flow Direction

Unlike Type I and Type II sills there are no obvious feeding mechanisms for Type III sills. The structurally restricted emplacement of the sills means there are few propagating lobes on the fringes of the sill bodies to help determine flow direction.

Where lobes are present there does not appear to be a single dominant orientation, with lobes observed on the southeast, east, northeast and southwest flanks of different bodies. In addition, the discontinuous nature and close vertical spacing between individual Type III sill bodies makes it hard to establish any dominant flow direction on the surface of the sill bodies using opacity rendering or spectral decomposition techniques.

There are no observed or inferred vertical dykes in the area and the sill bodies are many kilometres from the nearest crystalline basement high, therefore it is proposed that Type III sills are primarily sourced from magmas channelled within basement-bound Cretaceous rift faults which segregate the area. Given the size and discontinuous nature of the sills it is suggested that the magma supply is greatly reduced in comparison to the that which fed the Type I and Type II sills.

## **5.7 Summary of Sill Facies**

The three variations of sill intrusion observed in the area all illustrate that the structural regime and accommodation space into which they are emplaced strongly influences the style, size and shape of the intrusion body. Both Type I and Type III sills demonstrate how structurally-restricted emplacement preferentially produces bodies elongated parallel to the strike of the fault plane. This also serves to illustrate how sills will preferentially spread laterally through sedimentary successions rather than exploit fault planes to be emplaced further up stratigraphy. Similarly, the rounded saucer-shaped Type II intrusions demonstrate that with sufficient space for emplacement sills will spread laterally until they find a suitable horizon for lateral emplacement.

### ***Type I***

- Flat, tabular intrusions, elongated in a NE-SW orientation.
- Typically the largest individual bodies and the overall largest volume of any sill facies.

- Emplaced layer-parallel into inclined Cretaceous stratigraphy within the Sissal Sub-basin.
- Fed from the northern splay of the Corona Ridge with magma flowing from NW to SE.
- They were the first of the sill facies to be emplaced.

***Type II***

- A series of interconnected, saucer-shaped intrusions forming branched networks which progress up stratigraphy.
- Vary significantly in size, but generally get smaller with decreasing depth.
- Emplaced in a large graben within the Flett Sub-basin, bound by the southern splay of the Corona Ridge and a large basement-bounding fault.
- Fed from below, predominantly by dykes, but also through a series through dykes exploiting small faults at the base of the Cretaceous succession.
- Emplaced after the Type I sills.

***Type III***

- A number of small discontinuous intrusions, emplaced at shallow depths.
- Intruded into a heavily-segmented area in the southeast of the Flett Sub-basin.
- Fed by a greatly reduced magma supply through basement-bounding Cretaceous age faults.
- They were the latest three sill facies to be emplaced.

**5.8 Discussion**

**5.8.1 Regional Magma Migration Pathways**

Based on the 3D seismic interpretation of feeding relationships, sill surface flow directions and magma lobe orientation, the source point(s) for each sill facies can be identified. There are three distinct migrational pathways for magma input into the basin, which are shown on the regional structure map in Figure 5.21. Given the observed changes in sill morphology, size and frequency between the three sill

facies it is proposed that the bulk volume of intrusive magma supply decreases from northwest to southeast. Each migration pathway is discussed below.

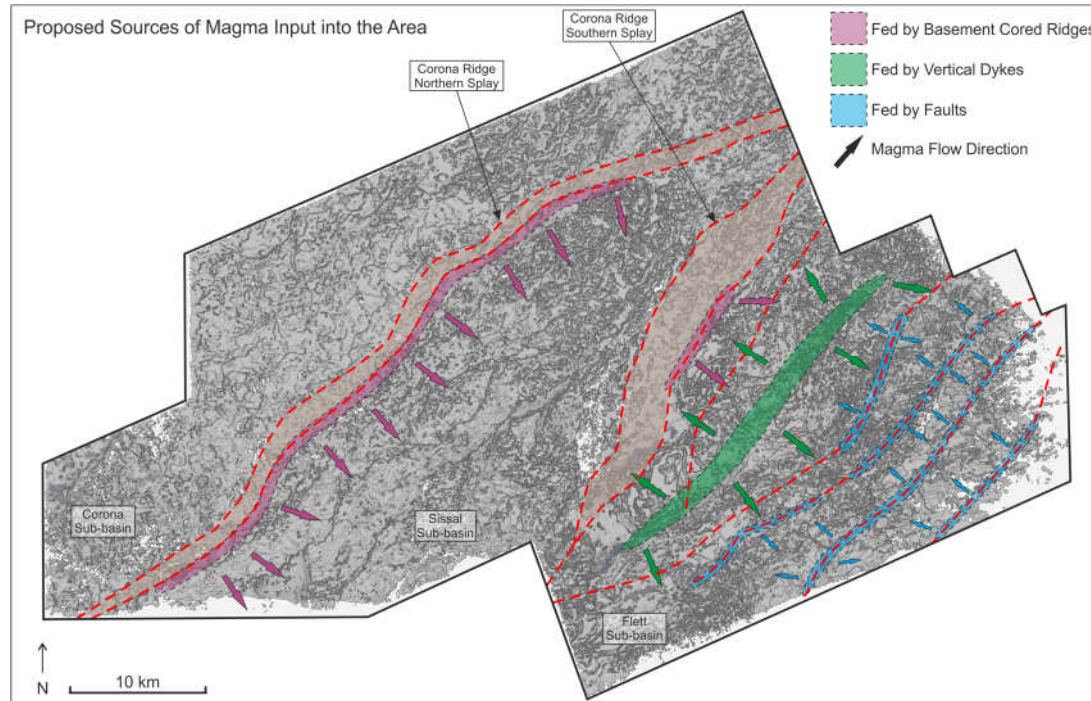


**Figure 5.21** – Map showing the inferred areas of magma input into the basin as derived from the flow directions of interpreted sill bodies. Sills are shown as opacity rendered bodies with flow directions marked with arrows, (for clarity not all sills are shown).

### ***Basement Cored Structural Highs***

The first and volumetrically most significant pathway of magma transport into the basin was along the margins of the crystalline basement highs, which form the Corona Ridge. In the northwest of the data area the northern splay of the Corona Ridge appears to directly feed the large Type I sills, which propagate from northwest to southeast, through the Sissal Sub-basin towards the southern splay of the ridge.

The southern splay also acts a magma source, however this is limited to a few small Type II sills high up stratigraphy within the Flett sub-basin. The total volumetric contribution of the southern splay therefore is significantly less than that of the northern splay.

This suggests that the basement channels magma to flow around it, and instead of the intruding through the basement, the magma preferentially enters the basin at the basement-sediment interfaces.

### ***Dykes***

The true extent and influence of dykes as conduits for magma transport input into the basin is hard to establish. The progressive decline in seismic resolution at depth and the issues associated with the conventional seismic imaging of steep or vertical features makes the detection of feeder dykes problematic and uncertain.

Where dykes have been interpreted they occur in the central areas of the thick Cretaceous graben within the Flett Sub-basin, immediately southeast of the southern splay of the Corona Ridge. They typically feed the sills that form the base of inter-connected Type II sill networks, with single dykes often feeding more than one complex. Even though only a few dykes have been identified, there are likely to be many more, which are not observed due to data resolution issues. They make a significant contribution to the total emplaced magma volume, and it is likely that others exist both within this region and throughout other areas of the basin.

### ***Basement-Bounding Faults***

Basement-bound faults are considered to be the primary mechanism for feeding Type III sills, through channelling dykes within the fault plane. They are also significant contributory pathways for type II sills. They predominantly occur in the Flett Sub-basin and become more common towards the southeast of the area.

Basement-bound faults act as conduits to transport magma from the crystalline basement and below to the Cretaceous sediments above. There is no dominant flow direction in the sills fed in this way, although magma largely flows upwards and away from the faults. The sills they feed contribute a substantial portion of the total emplaced volume in the area and typically provide the dominant magma transport conduit in areas associated with reduced magma supply. They may in fact contribute to the background transport of magma throughout the basin, however, they are only seen in areas of reduced magma supply as the other mechanisms are not active.

### ***Other feeding mechanisms***

The three mechanisms described above account for the bulk magma input into the basin, however a large number of sills, especially those higher up stratigraphy are fed by other mechanisms. The first and most common is inter-sill feeding in which sills are fed by other sills lower down in the stratigraphy, this is common within the shallowest Type I sills, and within the interconnected Type II sill networks but is less common within Type III sills. The second is through faults which do not penetrate the basement, these shallow, high-angle, low-throw faults are typically found in the southeast of the area (Flett Sub-basin), and are most common amongst the small, highly segregated Type III sills. Where faults feed sills they are typically acting as conduits for magma transportation from other sills lower in the stratigraphy.

### ***Summary of Magma Transport into the Basin***

- There are three main transport pathways for magma input into the basin, crystalline basement highs, vertical dykes and basin-bounding faults.
- The different magma transport pathways are more prevalent in different areas of the basin.
- The faults bounding the crystalline basement highs are the primary pathways in the Sissal Sub-basin where the northern splay of the Corona Ridge feeds Type I sills.
- Vertical dykes are predominantly found in the centre of the Flett Sub-basin feeding Type II sills.
- Basement-bound faults are observed across the sub-basins but are the primary pathway for magma input in the highly segmented area in the southeast of the Flett Sub-basin, where they feed Type III sills.
- Sills are also fed by through inter sill relationships and through shallow and non-basement bound faults.

### **5.8.2 Emplacement of the Faroe-Shetland Sill Complex**

The following section compiles the observations made in this chapter to describe the magmatic and tectonic evolution of the Corona Ridge region of the Faroe-Shetland Basin. The area's evolution is illustrated through a series of schematic models shown in Figure 5.22.

#### ***Stage 1 – Basement Grain***

The dominant NE-SW trending structural grain was established during the Caledonian Orogeny and re-activated during a series of rift events in the Permo-Triassic and Jurassic (Doré et al., 1999). Details of these early rift events are limited due to the poor seismic resolution at depth and the over-printing by later tectonic events; however, they develop the early basin configuration and structural grain along which Cretaceous rifting occurs (Ritchie et al., 2011).

#### ***Stage 2 – Cretaceous rifting and basin development***

Protracted, multi-phase rifting during the Early and mid-Cretaceous followed by post-rift thermal subsidence in the Upper Cretaceous established thick mudstone depocentres in the Corona, Sissal and Flett Sub-basins which were segmented by the splays of the Corona Ridge, forming significant basement highs (Dean et al., 1999). Movement on the northern splay of the Corona Ridge during deposition created a steeply inclined syn-depositional geometry within the Cretaceous stratigraphy of the Sissal Sub-basin. The Flett sub-basin is characterised by a series of high-angle, low-throw normal faults, which become more frequent towards the southeast.

#### ***Stage 3 – Paleocene Deposition***

Continued subsidence and further rifting during the Early Paleocene created the accommodation space for the deposition of the Sullom, Valia and Lamba formations 65 – 56 Ma (T10 – T38), which drape over the Cretaceous rift architecture (Lamers and Carmichael, 1999).

#### ***Stage 4 – Type I Sill Emplacement***

The first emplacement of intrusive igneous material (Type I Sills) is considered to have occurred around the start of T40 (56 Ma). Magma travels along the margins of the crystalline basement highs and exploited the northern splay of the Corona Ridge; large volumes of magma were emplaced into the inclined Cretaceous strata, flowing towards the southeast. The deepest and largest Type I sills formed first whilst the magma supply was high.

#### ***Stage 5 – Flood Basalt Emplacement***

Shortly afterwards the first sign of extrusive volcanic activity occurred. Thick sequences of flood basalts and Hyaloclastites were sub-aerially extruded across the Corona and Sissal Sub-basins and above the northern splay of the Corona Ridge. The volcanism was sourced from the northwest and represents the very fringes of a much larger sequence, which probably initiated substantially earlier, closer to the palaeo-spreading centre. The volcanic packages thin from southwest to northeast and do not extend beyond the southern splay of the Corona Ridge.

#### ***Stage 6 Type II Sill Emplacement***

Magma continued to travel southeast through the crystalline basement, to the southern splay of the Corona Ridge and the Flett Sub-basin. Here the magma predominantly entered the basin through a series of vertical feeder dykes along the centre of a large graben, as well as the southern splay of the Corona Ridge and some smaller basement bound faults. The magma formed a series of interconnected branched sill complexes (Type II sills), which gradually progressed from depth to shallow stratigraphic levels. It is difficult to constrain the timing of these complexes although the uppermost sills create vents in the overlying Lamba Formation onto which Flett Formation onlaps, suggesting their formation was around the time of the deposition of the Flett Formation (T40 – T45, 56 -54 Ma).

During this time there was a continuation of Type I sill emplacement, which becomes progressively shallower and the sills progressively smaller due to a reduction in magma supply as it was preferentially emplaced into the Flett Sub-basin.

#### ***Stage 7 Type III Sill Emplacement***

Magma continued to travel southeast through the crystalline basement beneath the Flett Sub-basin; by this point the magma supply was greatly reduced and began to exploit a series of basin-bound faults in a highly segmented area of the basin. A series of small, discontinuous intrusions were emplaced (Type III sills).

Emplacement of the sills within this facies was near simultaneous. Field data from central Greenland shows that Mesozoic faults acted as conduits for magma emplacement were able to feed several layers simultaneously (Planke et al., 1999, Planke et al., 2005). This is considered to be the final stages of sill emplacement and towards the end of the main phase of volcanic activity in the area. The emplacement of Type III was the latest intrusive activity observed (T50 54 Ma) and potentially continues further into the Early Eocene.

***Summary of the Emplacement of the Faroe-Shetland Sill Complex***

- The model explains the three main phases of sill intrusions in the Faroe-Shetland Basin.
- Type I sills were the first to be emplaced (around 56 ma) and are fed from the northern splay of the Corona Ridge during a period of high magma supply.
- Type II sills followed shortly afterwards (56-54 Ma) when the magma had reached the Flett Sub-basin, they are fed by a series of vertical dykes.
- Type III sills were the last to be emplaced (54 – 52 Ma) and occurred in the far southeast of the area under consideration within the heavily-faulted region of the Fett Sub-basin.
- The model presented in this study represents the transition from magma rich to magma poor emplacement with increasing distance from the palaeo-spreading centre.
- The model suggests that there is significant variance within the *sill facies* proposed by Planke (2000) and that intrusion size decreases with waning magma supply away from the spreading centre within their broadly defined facies.

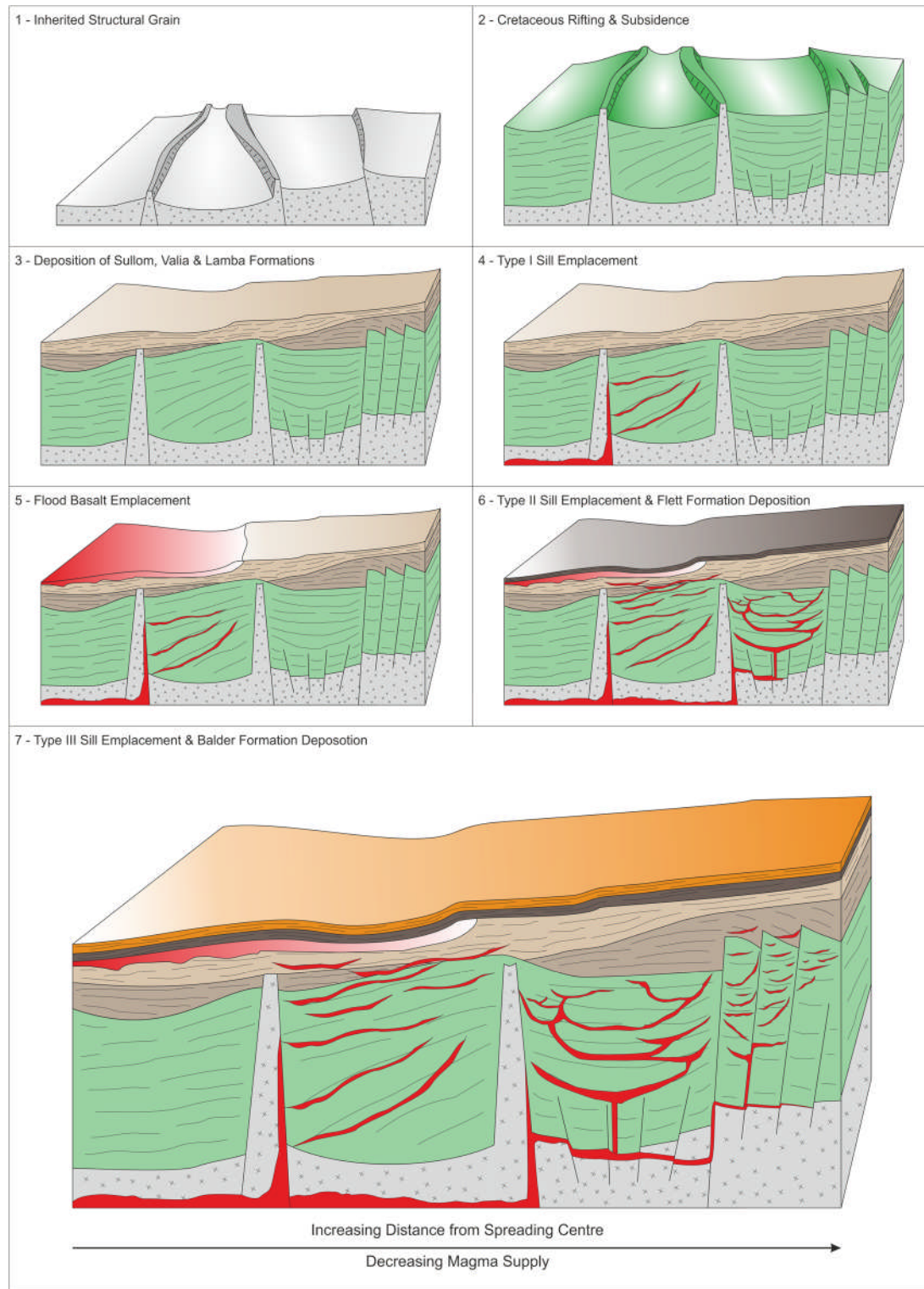


**Figure 5.22** – Conceptual Model for the emplacement of the Faroe-Shetland Sill Complex in the Corona Ridge region of the Faroe-Shetland Basin. The splays of the Corona Ridge and other significant Mesozoic faults control magma supply across the area and segregate the different sill facies. The style of intrusion evolves with distance from the paleo-spreading centre as magma supply and structural style varies.

### **5.8.3 Implications for Hydrocarbon Systems**

The emplacement of the Faroe-Shetland Sill Complex and the observations of sill geometry, distribution and emplacement mechanisms have important implications for potential hydrocarbon systems in the area.

The size, shape and distribution of the sill bodies will impact to what extent they are able to compartmentalise the host stratigraphy and inhibit migration from the underlying Upper Jurassic source rocks at the base of the Cretaceous succession to the Paleocene reservoirs above (e.g. Holford et al., 2012, Rateau et al., 2013). The heavily interlinked Type II sills have the greatest connectivity of all sill facies and also cross-cut stratigraphy, which makes them particularly problematic for migration. They are also fed by vertical dykes, which will add further segregation to the underlying host stratigraphy (e.g. Lee et al., 2006). The layer-bound Type I sills despite their size and large areal extent are considered to be significantly less of a risk.

Faults are considered to act as migration pathways for numerous plays in the area (Ritchie et al., 2011), the exploitation of fault planes by ascending magmas to feed overlying sills, particularly those associated with Type III sills have the potential to restrict possible migration pathways (Jerram et al., 1999).

There are important heat flow implications to consider, both from the sills and from the underlying systems which feed them. The thermal aureoles of the sills themselves are more likely to affect the migration pathways, porosity and permeability in the surrounding Cretaceous host stratigraphy, whereas the deeper feeding systems are closer to potential source rock horizons and so are more likely to affect the rate and extent of maturation. The heat flow implications of sill intrusion will be considered in greater detail in Chapter 7.

## **5.9 Conclusions**

- The sills within the NE Corona Ridge region of the Faroe-Shetland Basin can be categorised into three distinct facies based on their morphology and distribution.

- The style, size and geometry of the intrusive bodies were strongly influenced by magma supply, accommodation space and the structural regime into which they are emplaced.
- There is a broad trend of decreasing sill size and volume from northwest to southeast representing a reduction in magma supply with distance from the future spreading centre.
- Bulk magma transport is around crystalline basement and enters the sedimentary basin fill either through crystalline basement highs, vertical dykes or basement-bound normal faults.
- There are two main points of magma input into the area, the Northern Splay of the Corona Ridge and the Flett Sub-basin.

## Chapter 6 Controls on Hydrocarbon Generation in the Faroe-Shetland Basin

### 6.1 Abstract

In order to establish the impact of the Faroe-Shetland Sill Complex (discussed in chapters 4 & 5) on the petroleum system of the Faroe-Shetland Basin, it is first essential to understand the controls on the evolution of petroleum generation and the development of hydrocarbon maturation in the area.

This chapter undertakes 2D petroleum system modelling to establish the timing, extent and controls on hydrocarbon generation from the Upper Jurassic source rocks in the basin. Quantitative sensitivity analysis is undertaken to establish the impact of data limited variables in the modelling process. The sensitivity analysis identifies heat flow as a key parameter, therefore, variable heat flow scenarios are defined through the application of lithospheric stretching models and flexural backstripping workflows.

The results of petroleum system modelling suggest the Upper Jurassic source rock across much of the basin is mature for oil or gas generation with maturity increasing towards the deepest, central areas of the Flett and Foula Sub-basins. Transformation ratios indicate that much of the central basin is overmature; however, there are significant areas still with generation potential, particularly on the flanks of the basin, over structurally-elevated areas such as the Rona and Corona Highs, and in the shallower sub-basins such as the Ereland and NE Corona.

Modelling suggests that hydrocarbon generation in the Faroe-Shetland basin is predominantly controlled by the timing of source rock burial, which is linked to the rate of post-rift subsidence following Early Cretaceous and then Paleocene rift events. Source rocks in areas of significant Late Cretaceous subsidence reach maturity first but are overmature by the end Late Cretaceous. Areas which were still immature or partially mature at this time underwent a significant increase in maturity due to the pulse in heat flow associated with lithosphere stretching during

Paleocene rifting. Maturity then progressed further during the significant post-Paleocene subsidence that occurred throughout the Eocene and Oligocene.

Although substantial overpressure developed as a response to rapid subsidence, it was not significant enough to retard maturation in the deepest areas of the Flett, Foula and Corona Sub-basins, where burial depth and heat flow are highest. In the Ereland and far NE Corona Sub-basins, however, the development of overpressure during post-Paleocene subsidence slowed the rate of maturation until Late Cenozoic uplift reduced overpressure and peak oil generation could be attained.

## 6.2 Introduction

The complex tectonic and volcanic evolution of the Faroe-Shetland Basin makes reconstructing its hydrocarbon generation history challenging. The area has undergone protracted multi-phase rifting (Doré et al., 1999) whilst significant expanses of thick flood basalts covered much of the central and northeast parts of the region (Sørensen, 2003). Consequently, the basin exhibits many of the common data limitations prevalent within frontier exploration basins (Rose, 1987, Pettingill and Weimer, 2002, Kearey et al., 2013). This chapter focuses on petroleum system modelling constrained by quantitative sensitivity analysis to determine the temporal and spatial controls on maturation of the Upper Jurassic source rock.

Petroleum system modelling is the temporal reconstruction of basin history (Welte et al., 2012) which simulates the thermal history and petroleum generation of a region for a given geologic and depositional history (Welte and Yalçin, 1988). The accuracy and reliability of petroleum system modelling is largely dependent on the quality and extent of the data available. As a minimum, petroleum system modelling requires high-resolution seismic reflection data and well logs with stratigraphic information (Al-Hajeri et al., 2009).

Like many other frontier exploration regions, the Faroe-Shetland Basin has extensive high quality 2D and 3D seismic reflection data available as this is typically gathered in the early phases of exploration (Kearey et al., 2013). Well coverage, however, particularly that which penetrates the Upper Jurassic source rock, is

restricted to the basin margins and structural highs, meaning that the deepest, central and northwest portions remain undrilled (Ritchie et al., 2011). Furthermore, seismic resolution deteriorates significantly with depth and in areas with extensive Paleogene volcanics (White et al., 2005, Shaw et al., 2008, Nelson, 2010), introducing significant uncertainty during seismic interpretation. The data issues associated with the Faroe-Shetland Basin highlight why predicting hydrocarbon prospectivity in frontier, or under-explored basins is inherently uncertain. What can be stated, however, is that as global exploration increasingly steps-out to deep water or ultra-deep water settings, these issues will become commonplace (Qingping, 2006).

In order to minimise the impact of data limitations, this chapter first addresses the inherent uncertainty by undertaking quantitative sensitivity analysis on key input parameters of the petroleum system modelling workflow. Through the appraisal of sensitivity in areas of poor, limited or even absent data, it is possible to derive a more constrained basin modelling approach that reduces exploration uncertainty. The outcome of this sensitivity analysis is transferable to other frontier or data-limited exploration regions.

Once uncertainty has been established, 2D petroleum system modelling is undertaken using representative lines across the basin to determine the timing and extent of maturation of the Upper Jurassic source rocks. Lithospheric stretching models are used to predict rift-related heat flow during basin evolution. The rift history of the Faroe-Shetland basin is complex (Dean et al., 1999) and simple depth-uniform stretching models (McKenzie, 1978) do not apply (Fletcher et al., 2013). To reconstruct the heat flow evolution of the basin, both depth-uniform (McKenzie, 1978) and depth-dependent (Royden and Keen, 1980, Clift and Lin, 2001, Davis and Kusznir, 2004, Kusznir and Karner, 2007) stretching models are applied and flexural backstripping is used to estimate variable stretching factors ( $\beta$ -factors) across each 2D transect.

Overall, this chapter aims to define the petroleum generation history of the Faroe-Shetland Basin, in particular how the temporal and spatial changes in deposition and subsidence influence hydrocarbon maturation. The chapter also aims to

quantify and resolve the uncertainty associated with undertaking petroleum system modelling in data-limited or frontier exploration regions.

### 6.3 Petroleum System Elements of the Faroe-Shetland Basin

A successful hydrocarbon play requires the presence of a suitable source, reservoir, trap and seal (Welte and Yalçin, 1988). Furthermore, a delicate balance between the timing of hydrocarbon maturation, expulsion, migration and trap formation is critical to prospectivity (Hantschel and Kauerauf, 2009). There are a number of commercially-producing fields in the Faroe-Shetland Basin as well as further proven, but as yet undeveloped, discoveries (Ritchie et al., 2011). In this context, this section summarises the key petroleum system elements of the basin.

#### 6.3.1 Source Rocks

Although nine potential source rock horizons have been identified in the Faroe-Shetland Basin (Scotchman and Doré, 1995, Scotchman et al., 1998), only Middle Devonian (Bailey et al., 1990), Lower Jurassic (Scotchman and Thomas, 1995) and Middle and Upper Jurassic (Bailey et al., 1987) source rocks have been genetically correlated to hydrocarbons extracted from commercial wells.

Geochemical and well data indicate that Upper Jurassic – Early Cretaceous (Kimmeridgian-Ryazanian) source rocks are most important to the Faroe-Shetland Basin (Holmes et al., 1999) and have been genetically linked to numerous major discoveries including the Clair, Foinaven, Schiehallion and Strathmore fields (Scotchman et al., 1998, Herries et al., 1999).

The Kimmeridgian source rocks are typically fully marine, organic-rich mudstones (Type II kerogen) which can be rich, with over 10 wt% total organic content (TOC) and hydrocarbon indices (HI) up to 600 mg/g. Average values are in the order of 6 wt% TOC and a HI of 350 mg/g (Iliffe et al., 1999). The formation also includes some terrestrial Type III and restricted Type I kerogens (Iliffe et al., 1999).

The Kimmeridge Clay Formation is considered to be relatively widespread across the basin, especially in graben areas (Dean et al., 1999) and has a maximum drilled thickness of 295.5m (Well 206/05-1) (Ritchie et al., 1996), although typical deposits are considerably thinner.

### **6.3.2 Reservoirs, Traps and Seals**

Viable hydrocarbon plays have been proven in reservoirs ranging from fractured Lewisian Basement through to basin-floor Eocene fans. A wide variety of trapping styles are observed, which often combine stratigraphic and structural elements whilst competent seals range from Triassic through to Paleocene in age (Ritchie et al., 2011).

#### ***Producing Fields***

The Foinaven field overlies the Westray Ridge; significant hydrocarbon accumulations have been discovered within Paleocene age, stacked basin floor fans, which are separated by thin mudstone units (Carruth, 2003). A faulted anticlinal trap, with both dip closure and stratigraphic pinch-out supports oil accumulations; additional gas caps are formed through the biodegradation of early-generated oils (Cooper et al., 1999).

The Schiehallion development consists of the Schiehallion and Loyal fields, both have oil accumulations in Mid Paleocene sandstone reservoirs. Gently dipping beds provide up-dip closure to the north, west and south, which is sealed by structurally juxtaposed mudstones. To the east, stratigraphic pinch-outs form, here reservoir units are sealed both above and below by Mid Paleocene Mudstones (Leach et al., 1999).

The Clair Field overlying the Rona Ridge has a hydrocarbon column of over 800 m and two separate gas caps contained within Carboniferous to Devonian red beds sealed beneath thick, Upper Cretaceous mudstone (Coney et al., 1993). Initial extraction was problematic, with slow flow rates due to low-porosity reservoirs and heavy oil accumulations, however, after appraisal of fracture networks, hydraulic

fracturing was implemented and in its first year of production the field produced over 5 million barrels of oil (Barr et al., 2007).

### ***Undeveloped Discoveries***

The Rosebank/Lochnagar discovery consists of large, anticlinal traps overlying the Corona high, with oil and gas-bearing Upper Paleocene to Lower Eocene deltaic sandstones reservoirs interbedded with volcanoclastic sediments and sills (Loizou, 2005, Helland-Hansen, 2009).

Within the East Solan Basin, the Lower Triassic Strathmore and Upper Jurassic Solan discoveries overlap one another. The Strathmore field consists of oil-bearing Triassic sandstones held in a three-way closure with the Upper Jurassic Kimmeridge Clay Formation resting unconformably above. The Upper Jurassic Sandstones of the Solan field are entirely enclosed by the Kimmeridge Clay Formation, which provides both the source and seal (Herries et al., 1999).

On the south-western end of the Flett High, the Laggan discovery consists of gas-bearing, Late Paleocene sandstones which are trapped in truncated hanging wall blocks with up-dip stratigraphic pinch-outs and sealed by Upper Paleocene mudstones (Ritchie et al., 2011).

Towards the NE end of the Rona Ridge, gas discoveries are trapped in a south-easterly dipping fault block consisting of Lower Cretaceous Sandstones, which are sealed by Upper Cretaceous Mudstones to form the Victory Field (Goodchild et al., 1999). Further prospects include the Cambo discovery, which consists of oil-bearing and gas-bearing Upper Paleocene deltaic sands on the southwest edge of the Corona High (Ritchie et al., 2011) and the Laxford discovery, which tested gas from Paleocene sandstones in the Foula Sub-basin (Loizou, 2007).

There are a number of other prospects in the Faroe-Shetland Basin including Alligin, Arkle, Cuillin and Tobermory; however, there is limited published information available for these discoveries (Ritchie et al., 2011, Loizou, 2014).

#### 6.4 Previous Work

Studies indicate that at present, the majority of the basin is post-mature for hydrocarbon generation. Kerogen transformation ratios are >80% in the Flett, Judd and Brynhild Sub-basins and around 60-80% in Corona Basin (Ilfiffe et al., 1999). Source rocks overlying structural highs such as the Judd Platform, Westray Ridge, Mid Faroe High and Corona High are significantly less-mature, with transformation ratios typically <50% (Ilfiffe et al., 1999).

Basin modelling studies suggest that Upper Jurassic source rocks underlying significant Cretaceous depocentres began generating oil in the Mid Cretaceous where oil production peaked by the Late Cretaceous and gas generation commenced by the Paleocene (Holmes et al., 1999). In contrast, the equivalent source rocks beneath Paleocene depocentres began generating oil by the Late Cretaceous, with production not peaking until the Mid-Late Paleocene (Holmes et al., 1999, Jowitt et al., 1999). It is thought that much of the Cretaceous charge has either been lost through seepage or is contained within reservoirs in a biodegraded state (Jowitt et al., 1999).

The present day burial depths and the predicted maturity of the Upper Jurassic source rock suggest that gas should be the dominant hydrocarbon discovered in the Faroe-Shetland Basin, however this is not observed to be the case, with the majority of Paleocene reservoirs containing oil (Scotchman et al., 2006). Various mechanisms have been proposed to account for this including the 'motel' (Lamers and Carmichael, 1999) and 'whoopie cushion' (Ilfiffe et al., 1999) models, which propose that early oils generated during the Cretaceous were held in Cretaceous reservoirs before being released during the Tertiary after the formation of shallow Paleocene reservoirs and traps. There is little seismic evidence, however, to show Cretaceous reservoirs, volumetrically capable of holding oil to feed present day hydrocarbon discoveries (Scotchman et al., 2006).

Scotchman et al. (2006) suggest that high pressures developed during Late Cretaceous and Paleocene subsidence events could help delay some oil generation until the Early Tertiary. They propose three, discrete phases of hydrocarbon charge, the first phase of generation occurring during the Cretaceous, all charge from this

phase being now completely biodegraded. Generation was then switched off during Cretaceous uplift.

A second phase of generation occurred following rapid subsidence and associated with volcanic-related heat flow due to the Paleogene volcanic event; this charge bypassed the Cretaceous reservoirs and entered the shallow Paleocene reservoirs where it partially biodegraded until burial during the Eocene. Overpressure developed through rapid burial during the Cretaceous and Paleocene preventing complete conversion of kerogens to hydrocarbons, and allowing for a third, and final, phase of generation during the Oligocene-Miocene, when a reduction in overpressure due to regional inversion caused generation, charging the present day oil-rich reservoirs.

## 6.5 Methods

To assess the hydrocarbon generation history of the Faroe-Shetland Basin, 2D regional petroleum system modelling was undertaken using Petromod® (Ver. 2014.1 by Schlumberger). The workflow consists of three major elements, seismic interpretation, heat flow modelling and petroleum system modelling (Figure 6.1).

A key aspect of this study is the application of sensitivity appraisal to the modelling workflow in order to identify and reduce uncertainty. The sensitivity analysis undertaken is outlined in Section 6.6, the results of which are used to inform the three main workflows outlined below.

**Seismic interpretation** is used to define the geometric constraints of the petroleum system model, specifically the chrono-stratigraphic layers, source rock depth and erosional events. Four, 2D regional seismic lines were selected to incorporate the along-axis variation within the basin; descriptions of line selection and seismic interpretation are covered in Section 6.5.1.

**Heat flow modelling** defines the thermal evolution of the basin, which has been shown to have a significant influence on organic maturity (Section 6.6.2). Flexural backstripping was undertaken to establish variable  $\beta$ -factors for each of the 2D profiles. Using these  $\beta$ -factors the timing and magnitude of rift-related heat flow

anomalies were calculated using both depth-uniform and depth-dependent lithospheric stretching models (McKenzie, 1978, Davis and Kusznir, 2004). The backstripping workflow and resultant heat flow models are presented in section 6.7.

**Petroleum system modelling** is used to reconstruct the temporal evolution of the basin, simulating the thermal history and hydrocarbon generation. Through petroleum system modelling it is possible to define main controls on hydrocarbon maturation. The results of petroleum system modelling are shown in Section 6.9.

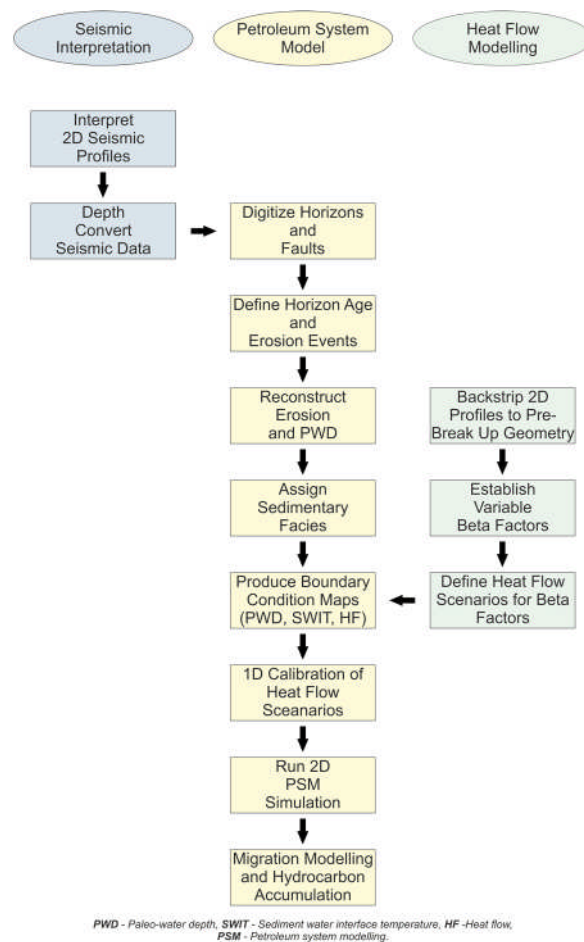


**Figure 6.1** – Flow chart outlining the workflow used in this chapter. The chapter consists of two sub-sections; seismic interpretation and heat flow modelling, which provide input for the main petroleum system modelling workflow.

### 6.5.1 Seismic Interpretation

Four, 2D seismic lines were selected from the TGS NSR and FSB99RE09 regional seismic surveys to form the basis of petroleum system modelling. The four lines run perpendicular to the axis of the basin (Figure 6.2).

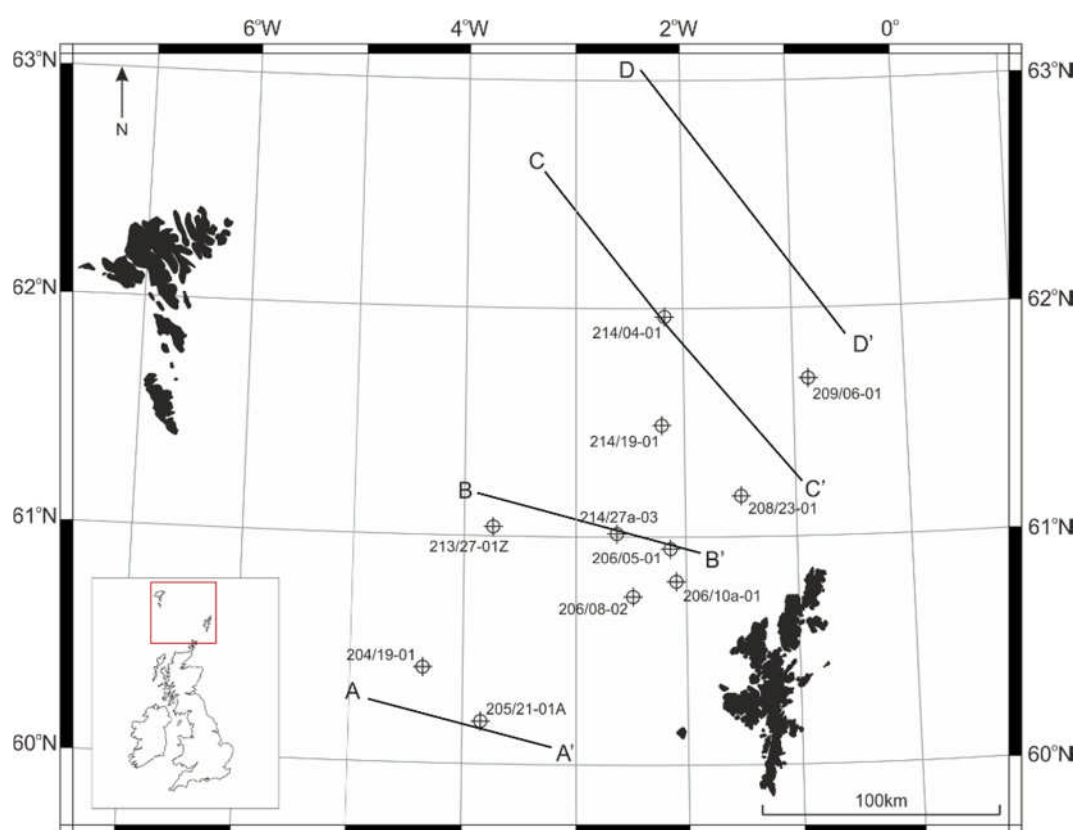


**Figure 6.2** – Location map of the 2D seismic profiles and commercial wells used to undertake petroleum system modelling in this chapter.

Seismic interpretation was undertaken using Petrel® (Ver. 2014.5 by Schlumberger). Interpretation of major chronostratigraphic horizons was guided by operator well tops and published regional interpretations (Lamers and Carmichael, 1999, Dean et al., 1999, Ritchie et al., 2003, Sørensen, 2003). The horizons selected for seismic interpretation are shown on the stratigraphic column in Figure 6.3 and the layers of the final model are shown in Table 6.3.

Age (Ma)	Period / Epoch		Chrono-Strat	Tectonic Events
	Period	Epoch		
1.8	Quaternary			
5	Neogene	Plio.	<b>M</b>	Major compression events from Paleocene to present day.
22		Mio.	<b>PG</b>	
34	Palaeogene	Olig.		
56		Eoc.	<b>TP</b>	★ Uplift related to Paleocene rifting, intense plume related magmatism
65		Pal.	<b>BTU</b>	Three major rifting events in the Cretaceous
96	Cretaceous	Upper		Campanian - Maastrichtian
			<b>LC</b>	Cenomanian - Santonian
				Valanginian-Barremian
145	Jurassic	Lower		Major structural relief developed over 80 Ma
		Upper	<b>BCU</b>	Possible oblique extension indicated by the thinning of Jurassic sediments on flanks and thickening in Cretaceous depocentres
		Upper	<b>BS</b>	
210	Triassic		<b>TT</b>	Marine Incursion

**M** - Mid Miocene Unconformity, **PG** - Top Paleogene, **TP** - Top Paleocene, **BTU** - Base Tertiary Unconformity, **LC** - Top Lower Cretaceous, **BCU** - Base Cretaceous Unconformity, **BS** - Base Source Rock, **TT** - Top Triassic.

**Figure 6.3** – Generalised stratigraphic column for the Faroe-Shetland Basin summarising the major tectonic events. The horizons interpreted for this study are shown in the ‘Chrono-Strat’ column. Adapted from Holmes et al. (1999).

**Line A-A'** (Figure 6.4) extends from the southwest edge of the Corona High, across the Flett and Foula sub-basins and on to the Rona High. The line crosses one of the

few areas of the basin which is free from any volcanic material; consequently, the line has excellent imaging down to the thick Triassic sediments (Figure 6.4 Insert C). The excellent resolution of the seismic data at depth allows robust interpretation of the Upper Jurassic source rock which is clearly defined clearly by the prominent Base Cretaceous Unconformity reflector. Both the Flett and Foula Sub-basins contain thick Mesozoic sequences particularly the Upper Cretaceous packages, which fill significantly the depocentres created through post-rift thermal subsidence following Early Cretaceous rifting (Figure 6.4 Insert A). The Cenozoic packages are thin to absent above the Flett and Rona Highs, owing to erosion during Late Cenozoic uplift.

**Line B-B'** extends from the central area of the Corona High through the Central Flett Sub-basin over the Flett High and into the Foula Sub-basin before terminating on the Rona High (Figure 6.5). Unlike Line A-A', Line B-B' shows evidence of Cenozoic volcanism: flood basalt can be seen imaged as a thin package of high-amplitude, continuous reflectors at Upper Paleocene level (Figure 6.5 Insert A) and a single sill has been intruded into the Upper Cretaceous sediments of the Flett Sub-basin (Figure 6.5 Insert B). Whilst there is some loss of imaging immediately below the sill, the relatively thin layers of volcanic material mean imaging of the underlining Mesozoic section is still good. The presence of Triassic sediments across the entire section is inferred from previous interpretations (Lamers and Carmichael, 1999) and although clear reflection events can be seen at depth, there are no other age constraints at this level (Figure 6.5 Insert C). The Cenozoic sequence thickens towards the centre of the transect and is up to twice as thick in the centre of the Flett Sub-basin as it is on the Corona or Rona Highs. Present day sea level increases substantially from the southeast to northwest, reaching 1500 m over the Corona High.

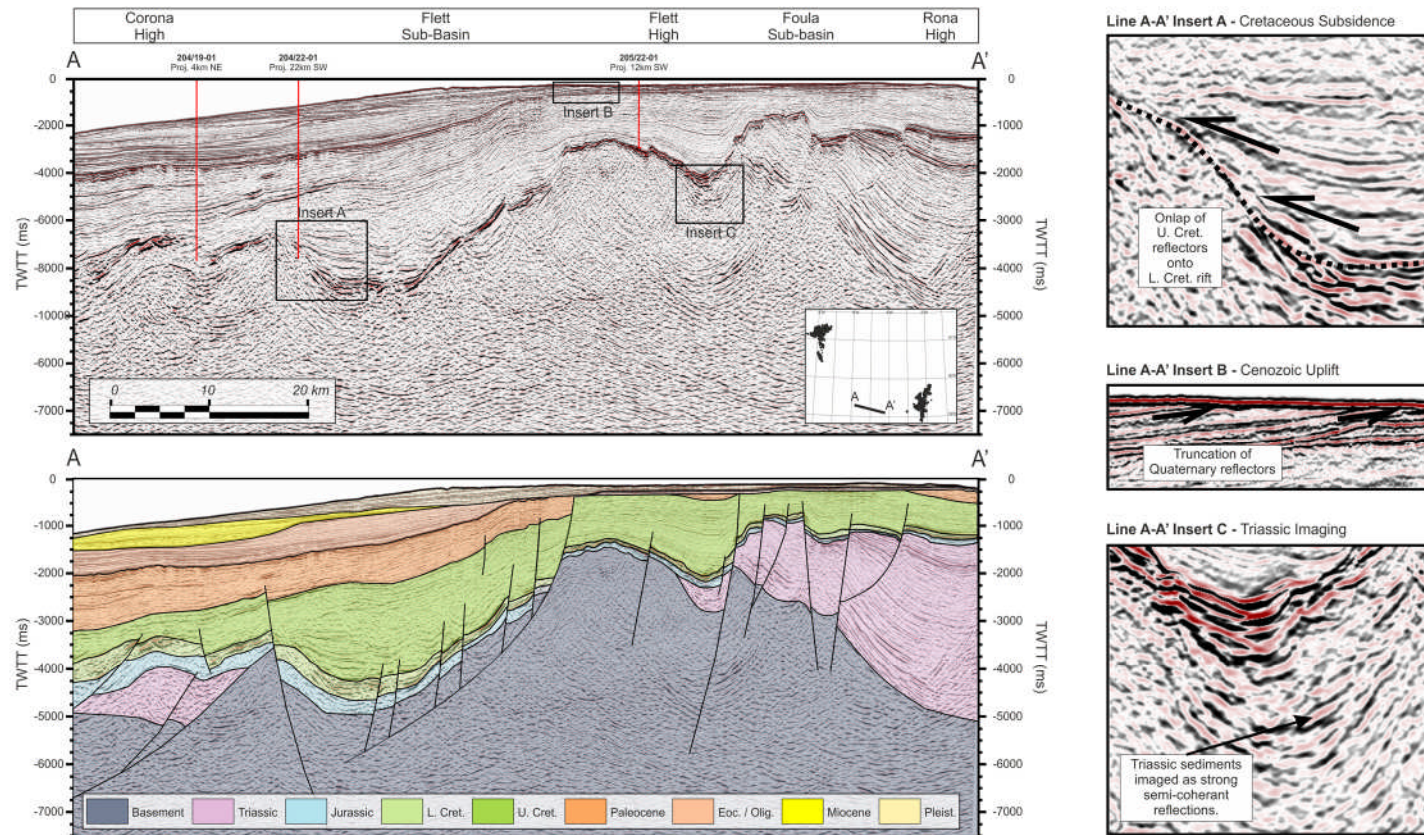


**Figure 6.4** – Seismic line and geoseismic interpretation of Line A-A'. The line contains no volcanic material and so has excellent imaging down to the Triassic Packages. Thick Upper Cretaceous depocentres are observed in Flett Sub-basin whilst the Cenozoic section is thin to absent towards the southeast of the section.

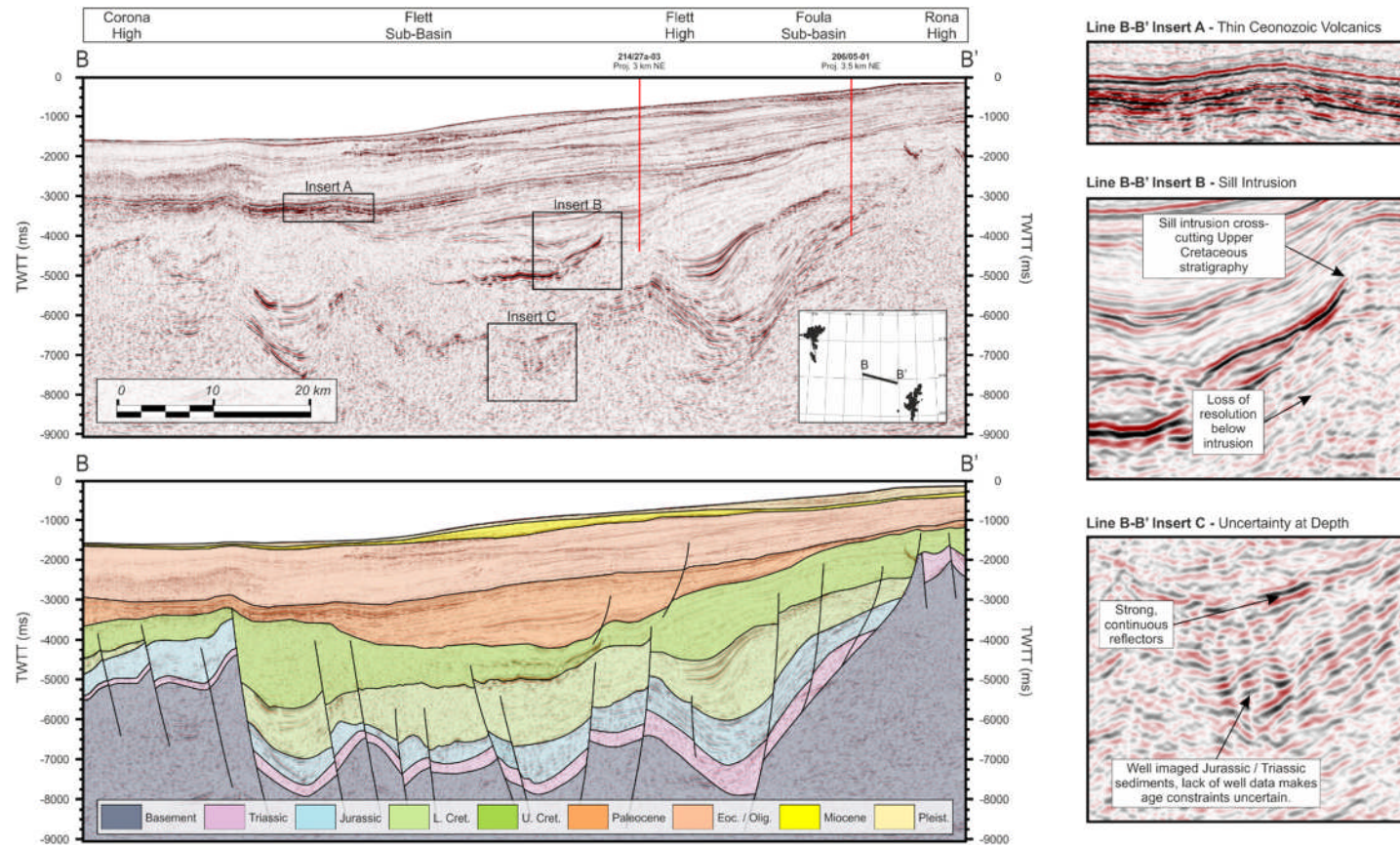


**Figure 6.5** - Seismic line (top) and geoseismic interpretation (bottom) of Line B-B'. The Flett Sub-basin has significantly thicker Lower Cretaceous packages further southwest on Line A-A'. Both the Flett and Foula Sub-basins form substantial Cretaceous depocentres separated by the Flett Ridge, whilst the Cenozoic package thickens significantly towards the centre of the line.

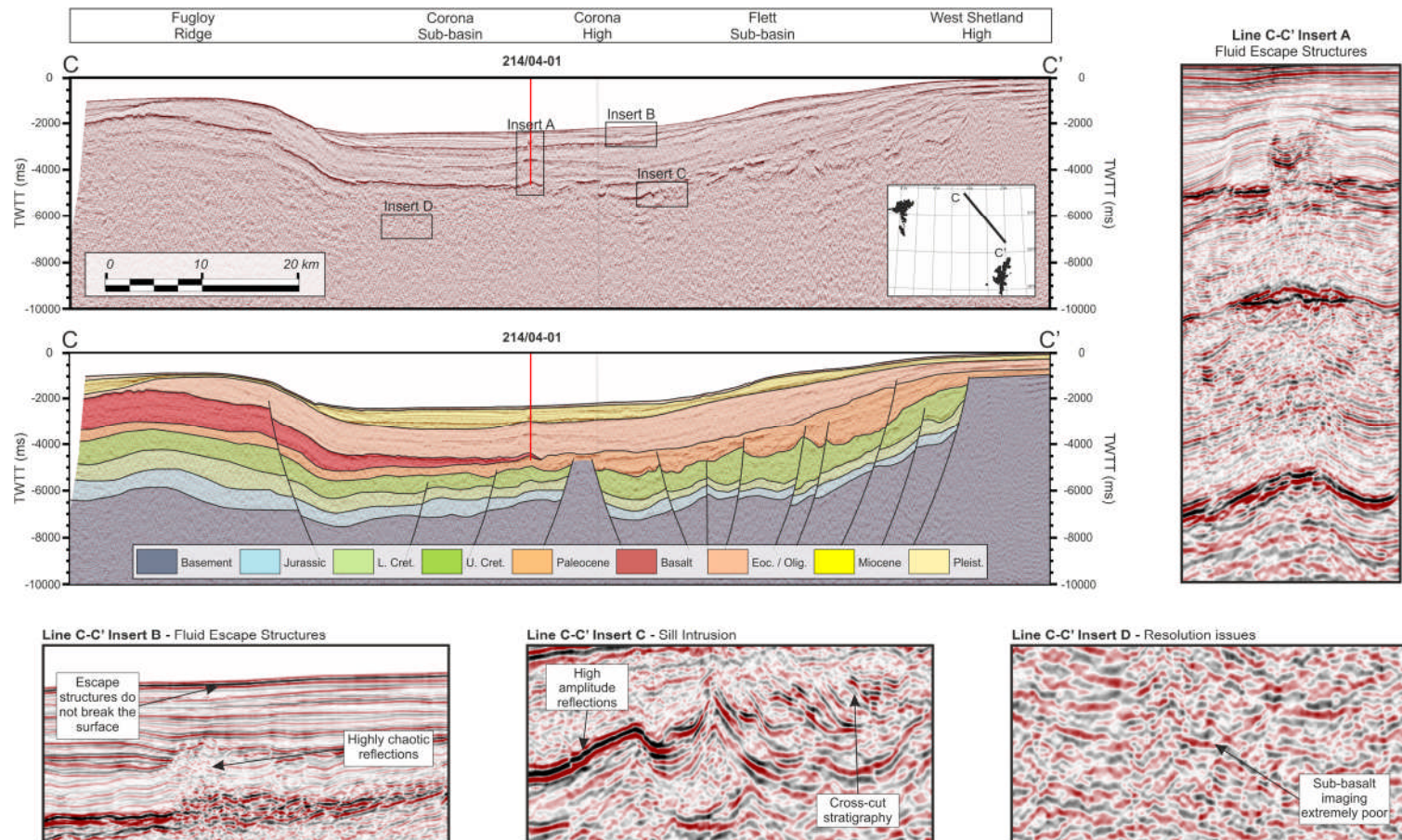


**Figure 6.6** – Seismic line (top) and geoseismic interpretation (bottom) of Line C-C', where thick basalt sequences limit the resolution of the Lower Mesozoic section northwest of the Corona Ridge and heavy sill intrusion can be observed southeast of Corona Ridge. There is a significant increase in water depth and Cenozoic thickness from the edges to the centre of the line.

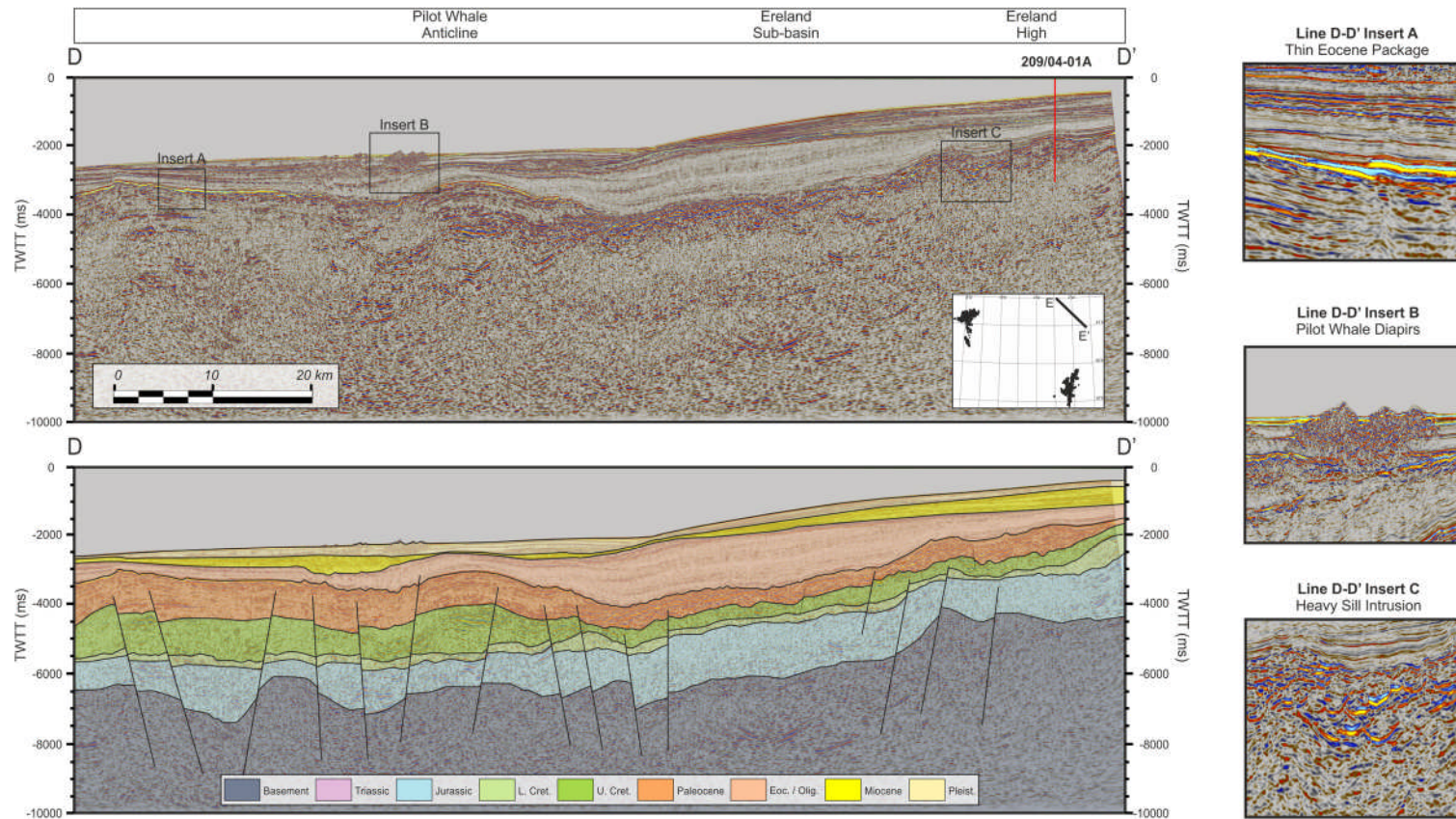


**Figure 6.7** – Seismic line (top) and geoseismic interpretation (bottom) of Line D-D'. Whilst the Upper Cretaceous packages thicken from the Ereland Basin to the Corona Basin, the opposite occurs for the Eocene to Oligocene packages, which thin onto the Pilot Whale Anticline and are substantially thinner in the Corona Basin.

**Line C-C'** extends from the Fugloy Ridge in the northwest, through the Corona and Flett Sub-basins and onto the West Shetland High in the southeast (Figure 6.6). A thick flood basalt package extends from the northwest and thins towards the centre of the basin at top Paleocene level. There are also a number of intrusive sills throughout the Upper Cretaceous and Paleocene packages (Figure 6.6 Insert C). Imaging below the flood basalt is extremely poor (Figure 6.6 Insert D) and has no well control; therefore, much of the Mesozoic interpretation is based on published interpretations (Lamers and Carmichael, 1999, Ritchie et al., 2011) and other Mesozoic trends in the area. Extensive post-rift thermal subsidence following Paleocene rifting has produced thick Cenozoic depocentres in the centre of the basin, however, the Cenozoic packages thin drastically over the Fugloy Ridge due to inversion during the Tertiary. Fluid escape structures are common (Figure 6.6 Insert A & B) within the Upper Cenozoic package suggesting some late stage fluid migration, although they do not break the surface.

**Line D-D'** extends from the northwest Corona Basin, over the Pilot Whale Anticline and into the Ereland Sub-Basin before terminating on the Ereland High (Figure 6.7). The area has undergone intensive sill intrusion (Figure 6.7 Insert C), which significantly impedes interpretation of the Lower Mesozoic sediments. Upper Cretaceous packages are generally thicker in the Corona Basin than the Ereland Basin, however, the opposite is true for the Eocene to Oligocene packages, which thicken significantly in the Ereland Basin and thin drastically over the Pilot Whale Anticline and into the Corona Basin (Figure 6.7 Insert A). Formation of the Pilot Whale Anticline during the Late Paleogene and Early Neogene is likely to have controlled sediment distribution at this time. (Ritchie et al., 2003). A series of seabed mounds known as the Pilot Whale Diapirs (Long et al., 2003) can be observed (Figure 6.7 Insert B), they form as mud volcanoes which are sourced from mobilised muds within the Eocene to Oligocene succession (Ritchie et al., 2003).

### 6.5.2 Depth Conversion

In order to undertake petroleum system modelling, the seismic data must be domain-converted from two-way travel time to depth. A velocity model was constructed using average interval velocities derived from compiled check-shot data across Quads 204, 206 and 214 (Table 6.1). Horizon interpretation provided geometrical constraint for the model and constant interval velocities were applied.

To ensure the validity of the velocity model, depth-converted sections were calibrated against available operator well tops. An excellent correlation between the depth-converted seismic sections and well tops could be observed from the seabed to the Paleocene horizon. Sparse well penetration below the Paleocene horizon means the model is less-constrained at this level, although where available, well tops correlated well with the depth-converted sections.

Interval	Interval Velocity (km/s)
Water Column	1.5
Seabed – Top Paleocene	2.0
Basalt	3.5
Paleocene – Lower Cretaceous	2.6
Lower Cretaceous – Basement	3.5
Basement	4.5

**Table 6.1** – Area average interval velocities used for depth conversion based on check shot data from Quads 204, 206 and 214.

### 6.5.3 Model Construction

The maturation of organic matter is dependent on the thermal and tectonic evolution of the basin (Welte and Yalçin, 1988), which is controlled by the heat flow

history, burial history (subsidence, uplift and erosion) and thermal conductivity of the sediments (Allen and Allen, 2013). The following section summarises how the thermal and tectonic evolution of the basin are reconstructed during petroleum system modelling.

#### **6.5.3.1 Heat Flow History**

Simulating the thermal history of the basin requires the designation of upper and lower boundary conditions; in petroleum system modelling these are defined by the sediment-water interface temperature (SWIT) and basal heat flow, respectively (Hantschel and Kauerauf, 2009).

Here, SWIT is modelled using the global average air surface temperatures, proposed by Wygrala (1989) and the present day latitude of the basin (Figure 6.8).

Basal heat flow represents a highly influential, yet poorly-constrained, parameter (Holmes et al., 1999) that can be modelled using a variety of techniques. The suitability of these techniques is dependent on the type and quality of data available. In order to produce the most accurate basal heat flow model, sensitivity analysis of the different techniques is undertaken (see Section 6.6.2). The results of sensitivity analysis are applied during the construction of the final basal heat flow models used for petroleum system modelling (Section 6.7).

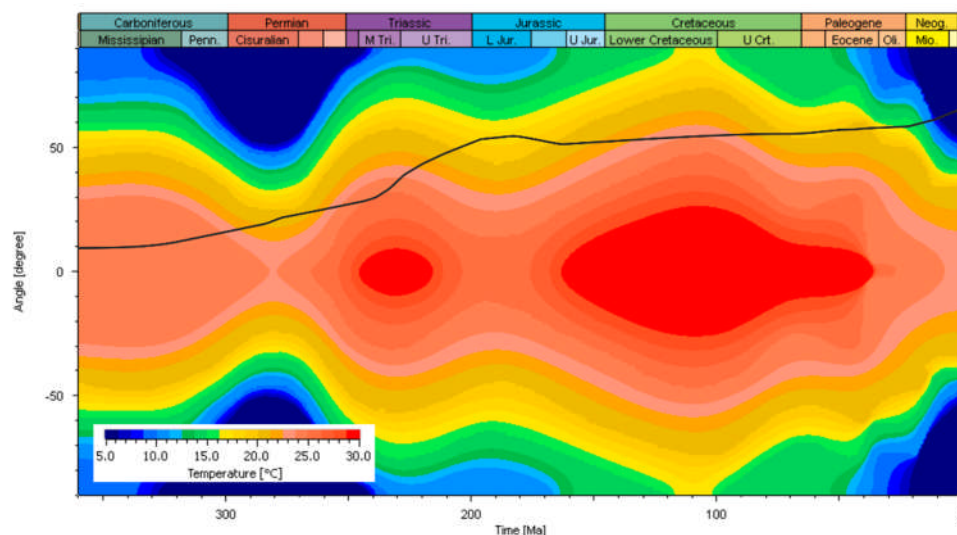


**Figure 6.8** – The sediment-water interface temperature is used to define the upper boundary conditions of the model and is based on the average air surface temperature as defined by Wygrala (1989) and the present day latitude of the basin.

### 6.5.3.2 Burial History

#### *Erosion*

Erosion events can change the depth at which the source rock has been buried through time. As burial history plays a critical role in the maturation of hydrocarbons, it is important to reconstruct such erosion events to account for any changes in source rock depth brought about by the uplift events, which initiate erosion (Hantschel and Kauerauf, 2009). It may also alter the compaction of sediments, which has important implications for thermal conductivity. There are a number of erosion events in the Faroe-Shetland Basin, however the most significant are considered to be the Base Cretaceous, Base Tertiary and Late Cenozoic events (Dean et al., 1999), all three are considered here.

Erosion events can be modelled by restoring the affected layers within the petroleum system model to their syn-depositional geometries, this can be done by reconstructing the missing section using flattening techniques (Figure 6.9). The layer below the affected horizon is flattened which reveals the geometry, thickness

changes and missing section of the eroded layer. The layer can then be reconstructed to a realistic pre-erosional geometry by projecting the layer across the missing section, guided by published estimates (Doré and Lundin, 1996, Dean et al., 1999, Sørensen, 2003)

In order to assess the impact of erosion and any potential errors during erosion reconstruction sensitivity analysis is undertaken (see section 6.6.4).

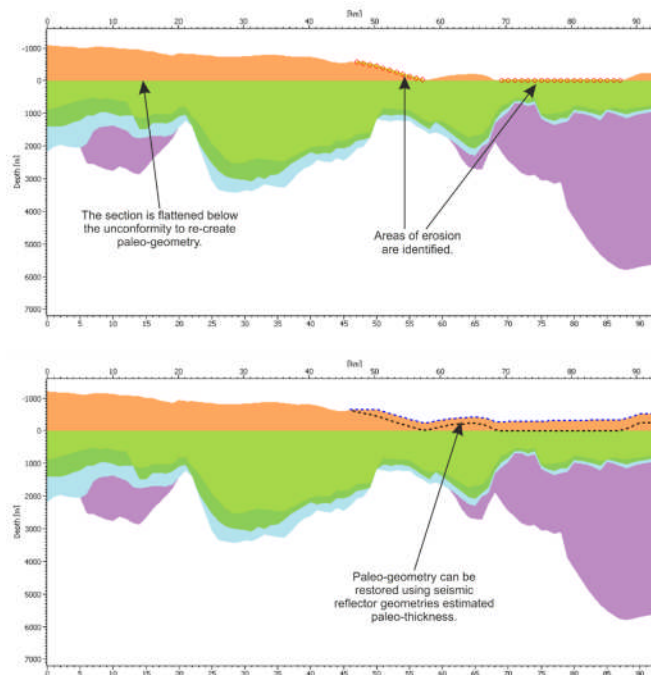


**Figure 6.9** – Reconstruction of erosion events using the model flattening techniques, the missing section is added to model layer to reproduce expected syn-depositional geometries.

***Paleo-bathymetry***

Whilst paleo-bathymetry has been shown to have no thermo-dynamic implications for hydrocarbon maturation, it strongly influences the paleo-geometry of the model layers (Ben-Awuah et al., 2014). This can have important implications for the expulsion, migration and trapping of hydrocarbons (Adda, 2012). Paleo-bathymetry was reconstructed based on seismic reflector geometry, published global sea level curves (Haq et al., 1987) and compiled regional data (Clift and Turner, 1998).

Period	Age From (Ma)	Age To (Ma)	Facies	Minimum Water Depth (m)	Maximum Water Depth (m)	Average Water Depth (m)
Permo-Triassic	250	230	Predominantly red sandstones, some marine incursions suggesting deposition close to sea level.	-200	200	0
Early Jurassic	230	190	Shallow water carbonates, characteristic of deposition within the photic zone.	0	100	50
Late Jurassic	190	145.5	Marine shales, deposited in quiet shelf conditions.	0	250	125
Valanginian - Ryazanian	145.5	130	Shallow marine carbonates, deposition within the photic zone.	0	100	50
Barremian - Albian	130	99.6	Deeper shelf deposits.	100	500	300
Late Cretaceous	99.6	70.6	Mid to outer shelf muddy carbonates.	0	250	125
Maastrichtian	70.6	65.5	Outer shelf deposition, suggestion of deepening.	100	500	300
Danian - Thanetian	65.5	55.8	Coals suggest deposition close to sea level, reddened lava tops indicate some sub-aerial exposure.	0	100	50
Post Tertiary Basalts – Present Day	55.8	0	Rapid deepening of sea levels to present day.	130	1500	200

**Table 6.2** – Estimated paleo-water depths for the Rockall Trough and Faroe-Shetland Basin (Clift and Turner 1998). Data is compiled from lithological logs based on drill cuttings, limited recovered core and correlation with land-based outcrops. The post-Tertiary – present day water depths assume a constant deepening from the shelf to basin centre. These numbers represent a 1D area average and must be extrapolated with the aid of seismic reflector geometry to produce 2D paleo-water depths.

### 6.5.3.3 Stratigraphy

The stratigraphy of the layers within the model controls important physical parameters such as porosity, permeability and thermal conductivity, all of which can have a major influence on hydrocarbon maturation and migration (Alsulami, 2014). In this study, stratigraphy is extrapolated from nearby wells. Interpreted lithological logs are calibrated against available gamma ray and density logs, which are then used to populate the model layers. Each lithology is assigned standard physical parameters pre-defined by the software, the source rock horizon is assigned published parameters, based on area average characteristics, including a total organic content of 6 wt% and hydrocarbon indices of 350 mg/g (Scotchman et al., 1998). For the purposes of modelling, it is assumed that the source rock is laterally extensive across the basin and where seismic resolution is poor, maintains a constant thickness of 100 m, this is representative of the source rock observations made by Ritchie et al. (2011).

The sensitivity of the model to changes stratigraphic composition is tested in Section 6.6.1 and the final lithological compositions used for each model layer are listed in Table 6.3.

### 6.5.3.4 Limitations

There are a number of limitations associated with the petroleum system modelling undertaken in this chapter, these limitations typically arise due to restrictions with the data or that they fall beyond the remit of this study. The main limitations are as follows:

- Faults are not modelled. Whilst it is recognised that faults may have important fluid flow implications (Barton et al., 1995, Hindle, 1997, Aydin, 2000), this study is focused primarily on hydrocarbon maturation on which faults have limited impact.
- There are no available data for physical rock properties such as porosity, permeability and fluid pressure. Therefore, standard lithological parameters within the software are used.

- There is continued debate as to the influence of volcanism on regional heat flow, previous. Some authors have suggested it has no influence (Dean et al., 1999, Green et al., 1999, Holmes et al., 1999), whilst others indicate that volcanism may be capable of raising heat flow (Iliffe et al., 1999, Parnell et al., 1999, Green, 2002, Scotchman et al., 2006). In this chapter, the heat flow implications of both the extrusive flood basalt and intrusive sills are ignored; however, the impact of sills on hydrocarbon maturation is considered in Chapter 7.
- The study does not model hydrocarbon accumulations, volumetrics or flow rates as these require well-constrained source rock thickness, geochemistry and kinetics, which are not possible with the data available.
- Source rock properties are defined by area average characteristics, despite there being basin-wide variation of between 2 – 15 % TOC (Scotchman and Doré, 1995). This is due to the limited well data which makes incorporating accurate lateral facies variations difficult.

Model Horizon	Age	Layer Age	Event Type	Dominant Lithology	Petroleum System Element	TOC (%)	HI (mgHC/gTOC)	Kinetics	Max Time Step (Ma)
Sea Bed	0		Erosion						10
		Quaternary		Sandstone	Overburden	-	-	-	
Top Pliocene	3.6		Erosion						10
		Pliocene		Sanstone	Overburden	-	-	-	
Top Miocene	6.3		Deposition						10
		Miocene		Sandstone	Overburden	-	-	-	
Top Oligocene	23		Deposition						10
		Eocene - Oligocene		Sandstone	Overburden	-	-	-	
Top Paleocene	55		Deposition						10
		Paleocene		Sandstone	Overburden	-	-	-	
BTU	65		Erosion						10
		Upper Cretaceous		Shale	Overburden	-	-	-	
Albian	89		Deposition						10
		Lower Cretaceous		Siltstone	Overburden	-	-	-	
BCU	100		Erosion						10
		Upper Jurassic Source Rock		Shale	Source Rock	8	350	Burnham TII (1989)	
Base Kim. Clay	157		Deposition						10
		Jurassic		Siltstone	Underburden	-	-	-	
Top Triassic	201		Deposition						10
		Triassic		Sandstone	Underburden	-	-	-	
Basement	237		Deposition						10
		Basement		Gneiss	Underburden	-	-	-	

Table 6.3 – Summary of model construction

## 6.6 Part 1 - Sensitivity Analysis

As highlighted previously, there are a number of data issues and uncertainties associated with petroleum system modelling in the Faroe-Shetland Basin, as is common with many frontier regions. In this section, sensitivity analysis is undertaken to quantify the potential influence of these uncertainties on the final modelling results. The results of sensitivity analysis can then be used to reassess and modify the petroleum system model to consider the cause of the likely outcome on the final results.

All sensitivity analysis is undertaken on Line A-A' as it is the most data-constrained line available, with close calibration wells and excellent seismic imaging at depth.

### 6.6.1 Lithological Uncertainty

The lithological information used to populate petroleum system models is typically derived from well data, predominantly wireline logs and core (Paton et al., 2007). Whilst this provides high-resolution, accurate representations of the subsurface, it is only 1D and therefore data must be extrapolated between well points. In frontier regions, the number of wells is typically small or non-existent and the spacing between wells is likely to be large, therefore, lithologies must be extrapolated over large distances.

To test the impact of lithological variations on petroleum system modelling, multiple scenarios were run for varying lithological compositions. The analysis focuses on the three dominant siliclastic lithologies, sand, shale and silt. Overall model composition was varied to provide scenarios ranging from 0 – 100% for each lithology type. The modelling results (Figure 6.10) show that peak source rock temperature is most sensitive to the percentage of shale or sand in the system, with shale increasing peak temperatures and sandstone reducing them. Data from Eppelbaum et al. (2014) show that increasing the amount of quartz (i.e. sandstone) in the system increases the thermal conductivity of the model. In the case of petroleum system modelling, an increasing the thermal conductivity accelerates the

basal heat flow away from the base of the model (close to the source rock) and out of the system, which results in lower peak source rock temperatures.

In order to account for these affects when extrapolating well data, it is important to assimilate the relative quantities of each lithology into each model layer rather than using single values as is prevalent in other studies (Jowitt et al., 1999, Iliffe et al., 1999).

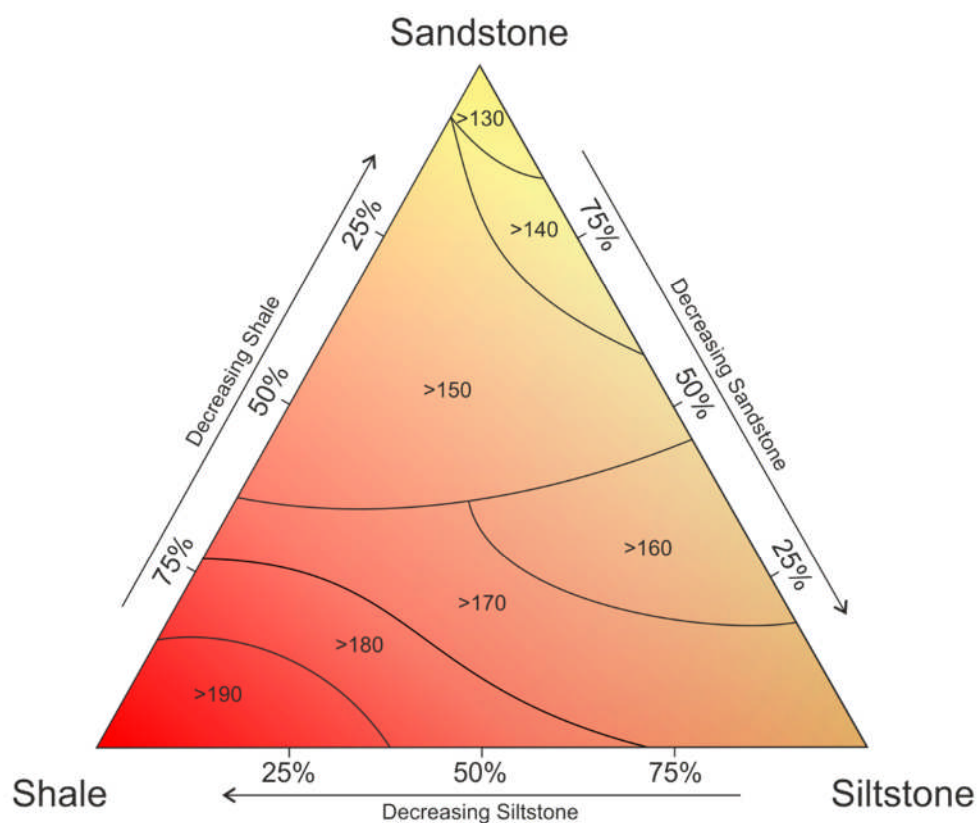


**Figure 6.10** – Composition plot for three dominant sedimentary facies illustrating the influence of lithological composition on the peak source rock temperature during petroleum system modelling. The percentage of shale in the system strongly correlate to increased peak temperatures, with a >60% increase in peak temperature from a sand-dominated to shale dominated system.

### 6.6.2 Heat Flow

Heat flow is considered to be one of the most influential, yet unconstrained, variables in petroleum system modelling (Holmes et al., 1999). There are a number of techniques used to reconstruct the thermal history of sedimentary basins; the suitability of which is strongly influenced by the type, quality and extent of data available.

The simplest technique is to simulate a constant heat flow through time by extrapolating present day heat flow throughout the burial history (Holmes et al., 1999, Iliffe et al., 1999, Lamers and Carmichael, 1999). Whilst this technique can produce viable models, it is not geologically realistic as it fails to account for the heat flow implications of rifting or volcanism (Scotchman et al., 2006).

Lithospheric stretching models demonstrate the link between rifting and heat flow (McKenzie, 1978, Keen, 1985, Wernicke, 1985, Davis and Kusznir, 2004, Péron-Pinvidic et al., 2007). The thinning of continental lithosphere during rifting causes mantle upwelling of the asthenosphere, increasing heat flow in the lithosphere (McKenzie, 1978). The duration of the heat flow anomaly is linked to the relative rate of crustal stretching and subsequent thermal re-equilibration (Jarvis and McKenzie, 1980). The magnitude of the heat flow anomaly is linked to the amount of stretching ( $\beta$ -factor), which can be estimated through the sequential backstripping of the post-rift stratigraphy (Fletcher et al., 2013). Crustal stretching models can be used to estimate rift-related heat flow in areas with limited or poor well data (Paton et al., 2007, Alsulami, 2014).

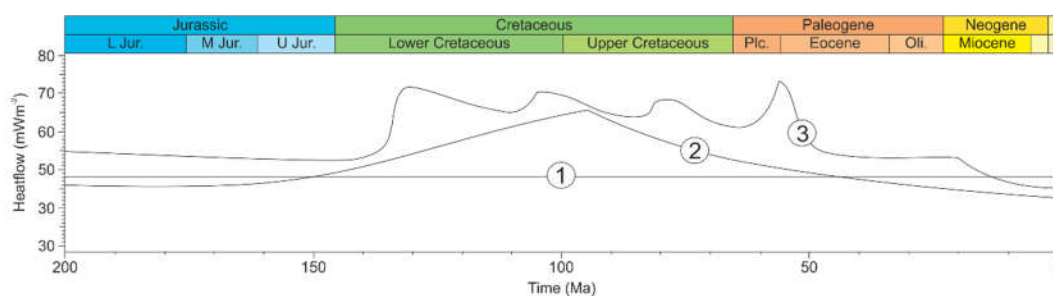


**Figure 6.11** – Time-temperature plots for the three tested heat flow scenarios; (1) constant heat flow, (2) Lithospheric stretching model after McKenzie (1978) with a Cretaceous rift event with a  $\beta$ -factor of 3, (3) multi-rift model after (Scotchman et al., 2006) showing three phases of Cretaceous rifting and heat flow spike during the Paleogene volcanic event.

As the Faroe-Shetland Basin has a complex tectonic and volcanic evolution a simple lithospheric stretching model does not account for the multiple phases of rifting or the heat influx caused by volcanism (Scotchman et al., 2006). Heat flow scenarios can be derived from the burial and tectonic histories obtained from well data to produce 1D models, which account for each rift and volcanic event (Scotchman et al., 2006).

Sensitivity analysis was undertaken to determine the influence of different heat flow scenarios on predicted vitrinite reflectance profiles (See Chapter 3 – Section 3.4). Three heat flow scenarios were tested (6.11). The first is a constant heat flow of  $48 \text{ mWm}^{-2}$  taken from the calibrated models of Holmes et al. (1999). The second is derived from a depth-uniform lithospheric stretching model (McKenzie, 1978) with a  $\beta$ -factor of 3, proposed by Dean et al. (1999). The third is a reconstruction of the multi-phase rift model of Scotchman et al. (2006).

Simulations were run using Line A-A. For each heat flow scenario, a 1D extraction was taken adjacent to wells 204/19-1 and 205/21-01A. Using the kinetics of Burnham (1989), predicted vitrinite reflectance profiles (%Ro) are compared to those measured, the results are shown in Figure 6.12.

Calibration of the tested heat flow scenarios with measured vitrinite reflectance data shows that all three are capable of producing realistic simulations of the

basin's heat flow history. It is, however, apparent that incorporating rift-related heat flow either through a lithospheric stretching model or a multi-rift model produces better correlation with the measured vitrinite data than the constant heat flow scenario, which typically underestimates heat flow.

Whilst the multi-rift model arguably offers the best correlation with the observed data, it represents a complex 1D model that would be hard to replicate in the deeper, data-limited areas of the basin. By contrast, lithospheric stretching models can be produced using the available seismic data, creating a custom, data constrained heat flow scenario for each section the basin. Therefore lithospheric stretching models are considered most suited to heat flow modelling in this study. The application of stretching models to this study and resultant heat flow scenarios are discussed in Section 6.7.

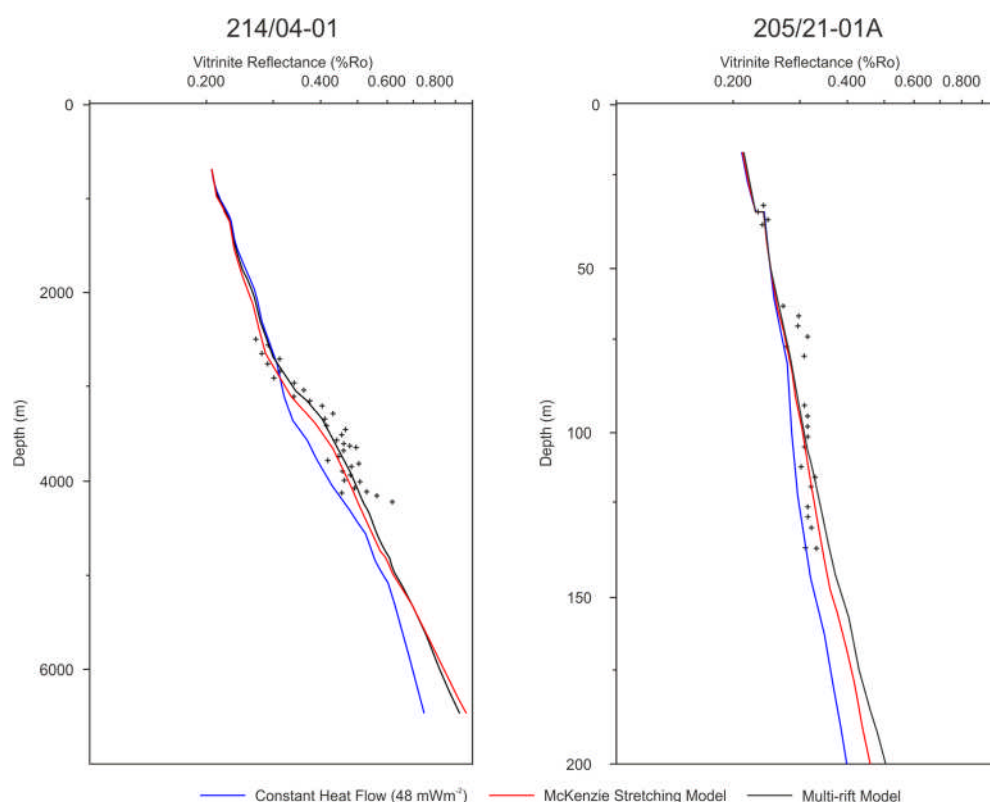


**Figure 6.12** – Predicted VR profiles (% Ro) for the heat flow scenarios presented in plotted against measured VR profiles from wells 204/19-1 and 205/21-01A.

### 6.6.3 Geometric Uncertainty

Interpretation of seismic reflection data provides the geometric constraints of the petroleum system model, therefore the quality and resolution of the seismic data and the accuracy of depth conversion strongly influences how representative the model is of geological reality. In areas with strong well ties, prominent reflectors and good cross-line correlation, the risk of geometric uncertainty is small; this is particularly true of the Neogene and Upper Paleogene succession. A lack of deep well penetration and poor seismic imaging at depth can however, introduce uncertainty in to the interpretation of Lower Paleogene and Mesozoic sediments. To consider the impact of geometric uncertainty on the modelling results, three possible misinterpretations are simulated within the Mesozoic sediments.

First, the thickness of the underburden is tested, this represents all sedimentary strata between the basement and the source rock horizon, which in this instance is the remaining Middle and Lower Jurassic section and some Triassic sediments.

Second the thickness of the source rock is assessed and thirdly the source rock depth is considered (Figure 6.13).

All variables are expressed as a percentage increase from the original interpretation, with 0% representing no change and 100% doubling the original depth and/or thickness. The impact of the variables is measured against changes in peak source rock temperature.

The results of sensitivity analysis suggest that the model is largely resistant to changes in the underburden and source rock thickness. A 100% increase in underburden thickness produces a <1% change in peak source rock temperature, this is even lower for source rock thickness with the same uncertainty causing a <0.5% change. In contrast, the model is however highly sensitive to source rock depth, only a 6% change in depth can elevate peak source rock temperatures by up 5%, making accurate interpretation of the top source rock horizon (Base Cretaceous Unconformity) vital in producing an accurate model.

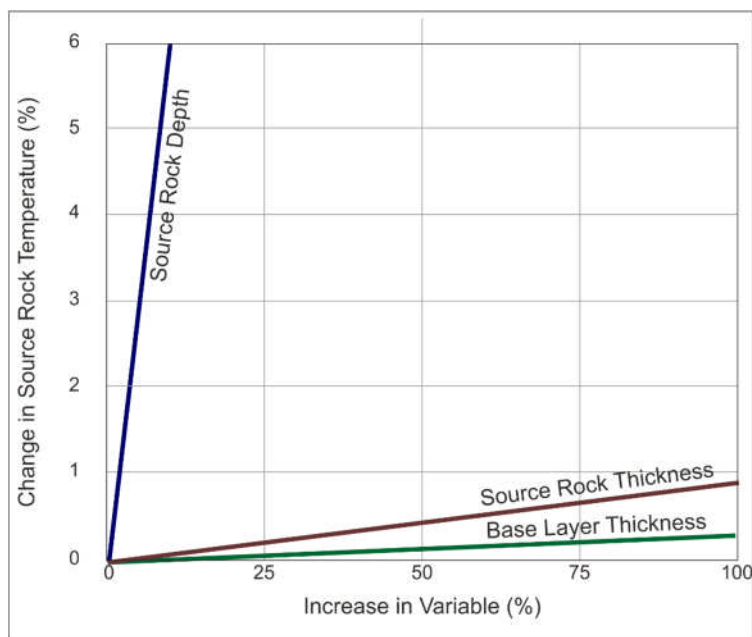


**Figure 6.13** – Sensitivity analysis of potential geometric uncertainty that may arise during seismic interpretation. The source rock thickness and thickness of underburden have a negligible effect on peak source rock temperature. The depth of the source rock is somewhat more influential.

#### 6.6.4 Erosion

Erosion of sedimentary stratigraphy occurs when relative sea level falls, either through regional uplift or eustatic fluctuations (Emery and Myers, 2009, Coe, 2003). With no erosion, petroleum system modelling assumes that each depositional layer progressively buries the source rock. Should erosion occur, however, the burial history of the source rock changes either through increased burial by the previously-eroded section or through the uplift events, which initiate erosion.

To account for the impact of erosion on source rock burial, such events can be reconstructed within the petroleum system model. Stratigraphic horizons are typically restored through the projection of seismic reflector terminations and the incorporation of well data or published trends (Paton et al., 2007, Alsulami, 2014).

In the Faroe-Shetland Basin there are three main periods of erosion to consider, being Base Cretaceous, Base Tertiary and Cenozoic (Dean et al., 1999). To test the sensitivity of the model to erosion, each event is modelled individually, the events are reconstructed from 0% (i.e. no erosion has occurred) to 100% (i.e. the pre-

erosion layer is 100% thicker than the post-erosion layer). The impact is measured as the effect on peak temperature of the Upper Jurassic source rock (Figure 6.14).

Sensitivity analysis shows that the Base Cretaceous and Base Tertiary erosion events have little impact on source rock temperature. Both events occur too early in basin evolution for them to significantly impact maturation of the source rock, which has not been buried sufficiently at this point. The scale of these events would have to be an order of magnitude larger than that modelled to significantly impact Upper Jurassic maturation; even then, the impact is only short-term and would have little impact on the long-term thermal profile of the system.

The model is significantly more sensitive to Cenozoic erosion, with peak source rock temperatures changing by up to 10%, this owes largely to the depth and thermal maturity of the source rock at this time. Such drastic changes would however, require a large margin of error in the modelling process. As the Cenozoic sequence is well constrained by seismic data, such significant misinterpretation is highly unlikely.

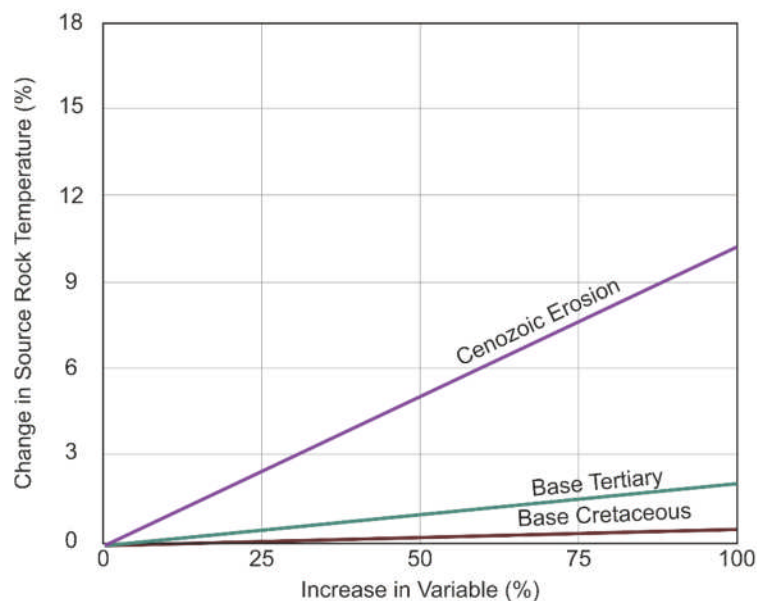


**Figure 6.14** – Sensitivity analysis of the three main erosion events and their impact on peak source rock temperature. Only Cenozoic erosion has a noticeable influence on temperature, the earlier events occur before the source rock has been sufficiently buried.

### 6.6.5 Summary of Sensitivity Analysis

Sensitivity analysis shows that the thickness of the underburden and source rock has least impact on the final modelling result. This is reassuring, as these are often highly uncertain parameters - especially in the deeper areas of the basin and below the volcanic sequences.

The impact of erosion typically depends on the age of the event; results indicate that Base Cretaceous and Base Tertiary erosional events occur too early in basin evolution to have a significant influence on source rock temperatures, as a consequence they will not be included in the final model. Cenozoic erosion is slightly more influential and is included in the final model, although the potential margin of error is considered to be low given the excellent seismic constraints at shallow depths.

Lithological variation modelling indicates that the composition of each siliciclastic layer can have a significant impact on the predicted peak source rock temperature. In order to account for this, each model layer will incorporate the lithological variation seen in the well data by including approximate percentages of each lithology rather than using a single lithology per layer. Layers will also be split into sub-layers to help incorporated this variation.

Source rock depth has a significant impact on petroleum system model; it also represents one of the largest uncertainties during the modelling workflow. Whilst little can be done to improve the accuracy of the interpretation, constant model simulations and calibration during model construction can be used to ensure the risk of a major misinterpretation is kept low.

Heat flow models are considered to be the most influential variable on peak source rock temperature and thus hydrocarbon maturation. Calibration with measured vitrinite reflectance data shows incorporating rift related heat flow anomalies produces more realistic simulation. Heat flow models are therefore constructed using lithospheric stretching models and flexural backstripping (see Section 6.7).

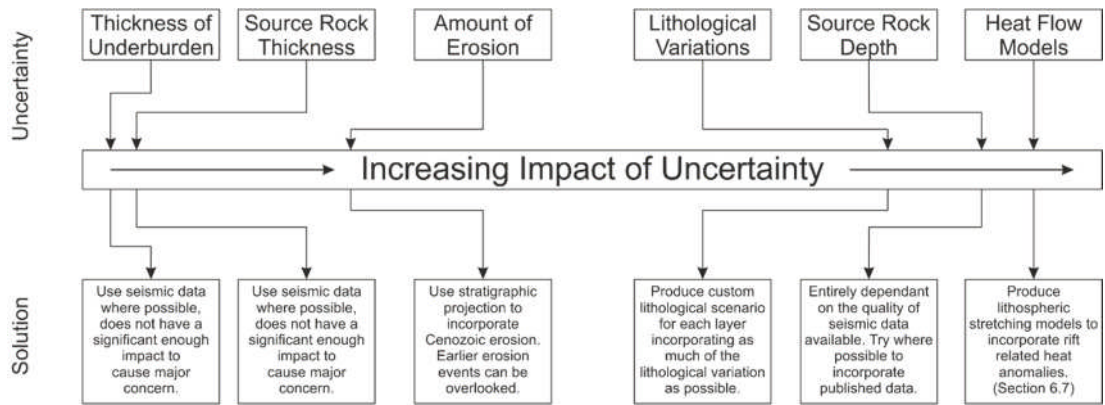


**Figure 6.15** – A qualitative ranking of the sensitivity parameters tested, the results indicate that the heat flow model used and the depth of the source rock have the largest impact on the final modelling results.

## 6.7 Part 2 - Heat Flow Modelling

The sensitivity analysis undertaken in Section 6.6.2 suggests that incorporating rift-related thermal anomalies into heat flow modelling produces the closest correlation with the observed vitrinite reflectance data. Therefore, lithospheric stretching models are here used to derive custom heat flow scenarios for each modelled line.

The Faroe-Shetland Basin formed through multiple, protracted rift events during the Mesozoic and Early Paleogene (Doré et al., 1999). The restoration of seismic profiles (Fletcher et al., 2013) show that Upper Cretaceous post-rift subsidence can be accounted for by modelling Lower Cretaceous rifting using a depth-uniform stretching model (McKenzie, 1978) with a  $\beta$ -factor of  $\sim 1.4$  (Fletcher et al., 2013).

The subsidence rates following Paleocene rifting, however, are anomalously high, and far exceed those predicted from standard McKenzie (1978) depth-uniform stretching models (Turner and Scrutton, 1993, Nadin et al., 1997, Clift and Turner, 1998, Fletcher et al., 2013). Post-rift subsidence following the Paleocene rifting can exceed 1.5 km in some areas of the basin which would require  $\beta$ -factors of 1.4 or greater (Fletcher et al., 2013), however, the seismic evidence suggests that Paleocene  $\beta$ -factors are rarely exceed 1.1 (Lamers and Carmichael, 1999, Dean et

al., 1999, Smallwood and Kirk, 2005), with fewer faults and less displacement than the Mesozoic sections.

Depth-dependent stretching occurs when the lithospheric mantle has been thinned to a greater extent than the upper crust (Royden and Keen, 1980, Clift and Lin, 2001, Davis and Kusznir, 2004, Kusznir and Karner, 2007) and can account for the observed high post-Paleocene subsidence rates of the Faroe-Shetland Basin (Fletcher et al., 2013).

Therefore, the lithospheric stretching model that will be used to define the heat flow scenario in this study combines depth-uniform stretching during the Early Cretaceous with depth-dependent stretching during the Paleocene. To determine the  $\beta$ -factors required for stretching models, flexural backstripping is undertaken on each of the modelled transects.

### 6.7.1 Lithospheric Backstripping

The methods and rationale of reverse post-rift subsidence modelling (here referred to as flexural backstripping) are described in detail by Kusznir et al. (1995), Roberts et al. (1998), Kusznir et al. (2005) and Fletcher et al. (2013). The technique sequentially removes overburden layers to restore the section to its pre-post-rift horizon, the remaining layers are decompacted and the flexural isostatic rebound applied (Figure 6.16). In this study an inherited  $\beta$ -factor of 1.4 (from Fletcher et al., 2013) is applied to account for Mesozoic rifting before the Top Paleocene horizon of each section is restored to 0 m water depth which is consistent with previous observations (Fletcher et al., 2013) using trial  $\beta$ -factors (Figure 6.16).

A vertical shift of 500 m is applied to account for the maximum possible water-loaded tectonic subsidence. Flexural backstripping produces a variable 2D  $\beta$ -factor profile unique to each modelled transect which can then be used during heat flow modelling.

Line A-A' (Figure 6.17) shows a gradual increase in  $\beta$ -factor from southeast to northwest as it moves from the West Shetland High into the Flett Sub-basin, close

to the main central axis of the Faroe-Shetland Basin with the highest  $\beta$ -factor of around 2.6. A similar pattern is observed along Line B-B' (Figure 6.18), although as the line is closer to the centre of the basin where Paleocene subsidence is greater,  $\beta$ -factors are generally higher, peaking at 3.5 in the Flett Sub-basin. Line C-C' shows a broadly symmetrical increase in  $\beta$ -factor from the edges of the line to the centre (Figure 6.19). Substantial stretching of the lithospheric mantle has seen upwards of 1.5 km of post-Paleocene subsidence with  $\beta$ -factors  $>10$  modelled for the centre of the basin.  $\beta$ -factors of  $\sim 7.5$  towards the northwest of the line are likely to be an anomaly due to the Paleogene volcanic section being modelled as sediments during the backstripping workflow. Line D-D' shows low  $\beta$ -factors are modelled for the Ereland Sub-basin ( $\sim 1.5$ ), however these increase dramatically into the Corona Sub-Basin ( $\sim 5$  Figure 6.20).

Overall modelling indicates there is an increase in  $\beta$ -factor from the flanks of the Faroe-Shetland Basin to the centre and from the southwest corner to the north-eastern extent.

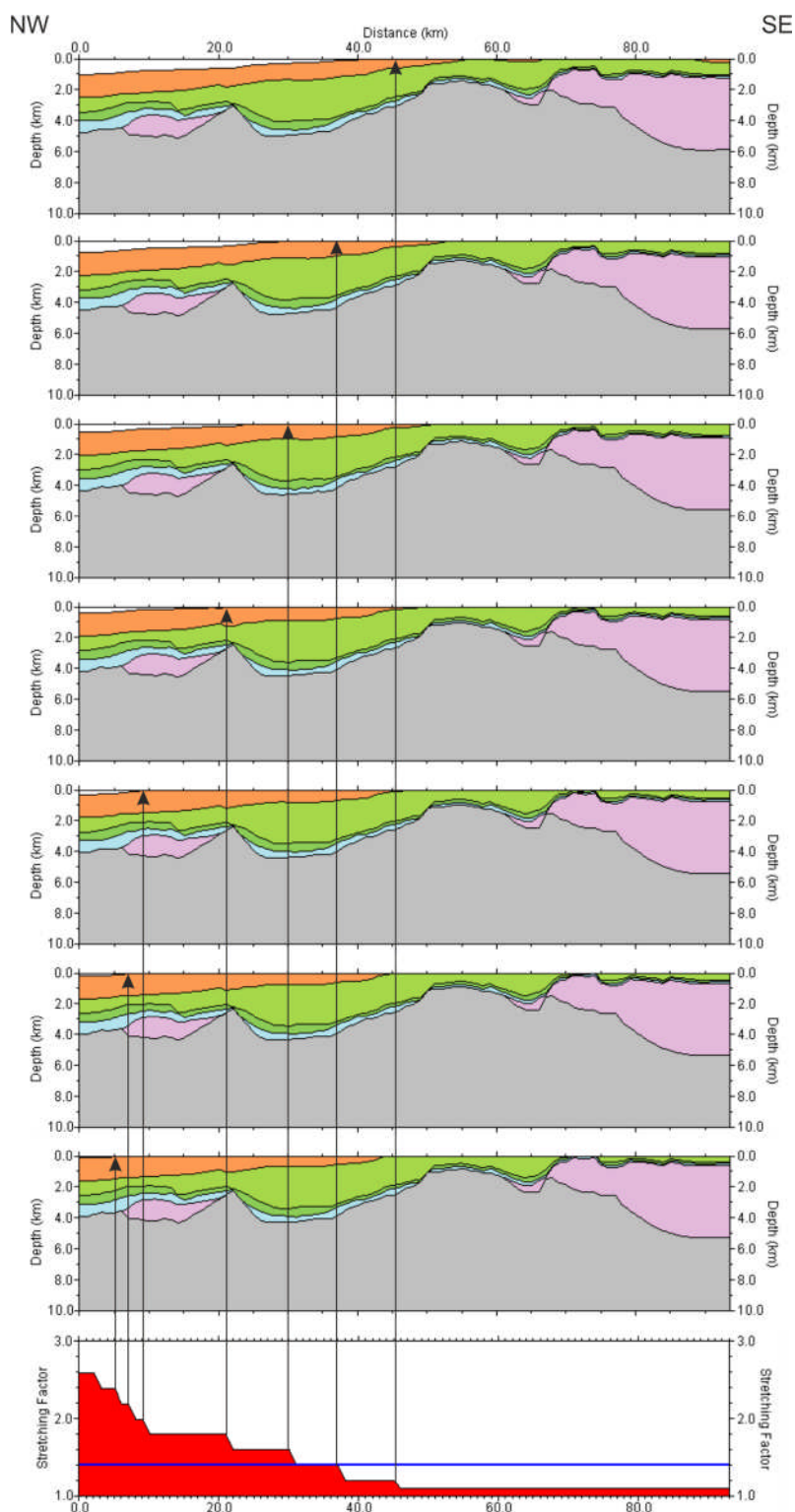


**Figure 6.16** – Flexural backstripping workflow used to determine the depth-dependant  $\beta$ -factors for Late Paleocene extension. The Top Paleocene (pre-post-rift) horizon is sequentially restored to 0 m water depth using trial  $\beta$ -factors.

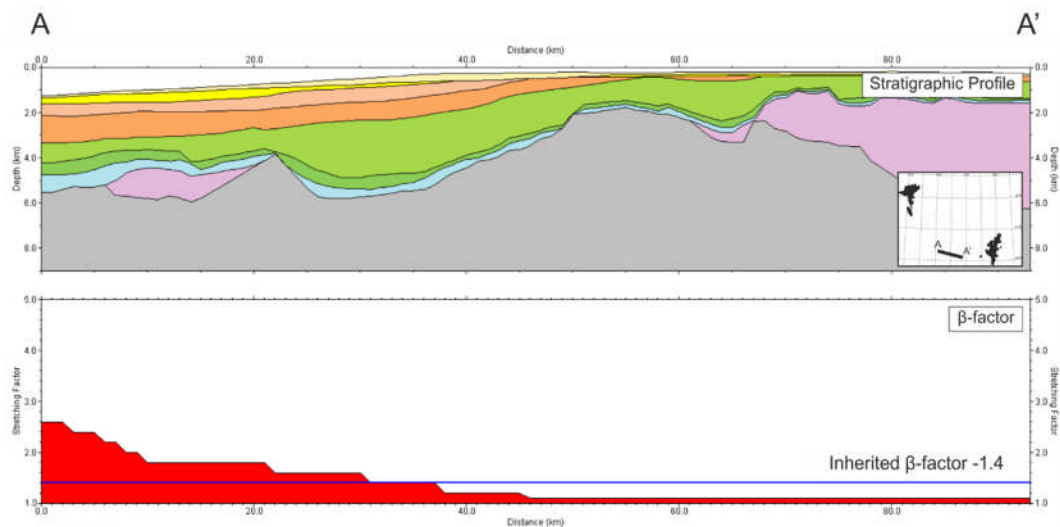


**Figure 6.17** – Whole lithosphere  $\beta$ -factors for depth-dependent rifting in the Paleocene derived from flexural backstripping of Line A-A'.  $\beta$ -factors show a gradual increase from the southeast to northwest, moving from the shelf towards the basin axis.

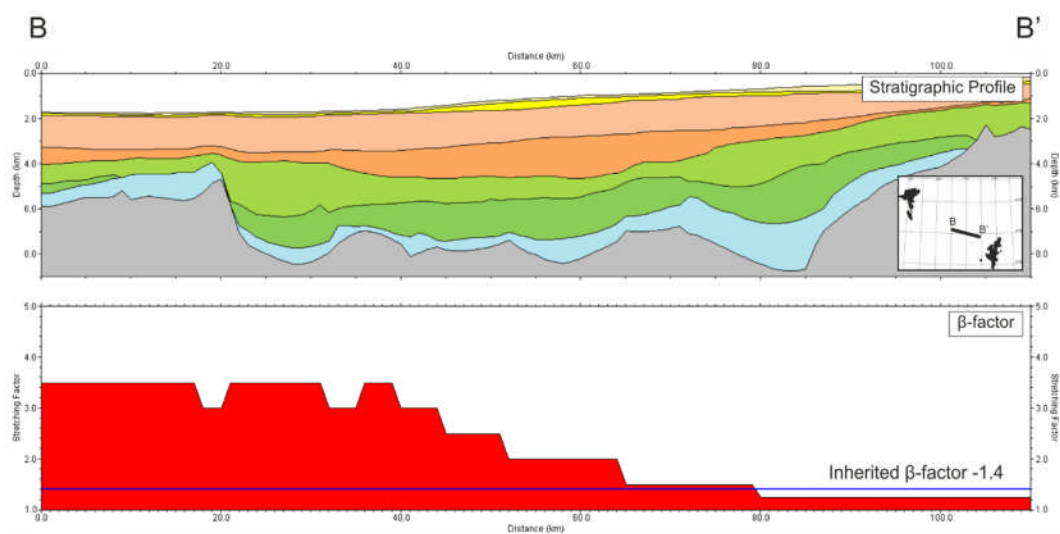


**Figure 6.18** – Whole lithosphere  $\beta$ -factors for depth-dependent rifting in the Paleocene derived from flexural backstripping of Line B-B'. There is a gradual increase in  $\beta$ -factor from the Rona High into Flett Sub-basin.

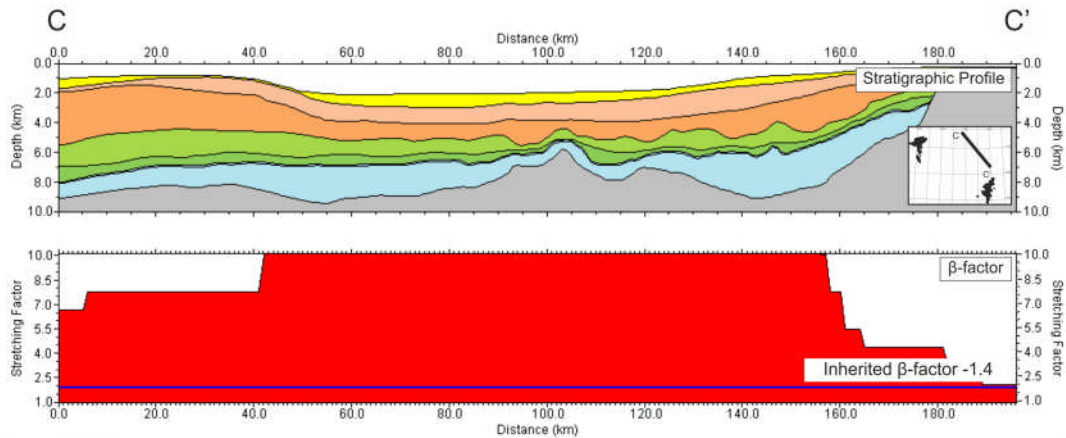


**Figure 6.19** - Whole lithosphere  $\beta$ -factors for depth-dependent rifting in the Paleocene derived from flexural backstripping of Line C-C'. Modelling shows a broadly symmetrical increase in  $\beta$ -factor from the flanks of the basin to the centre peaking at  $\sim 10$ .

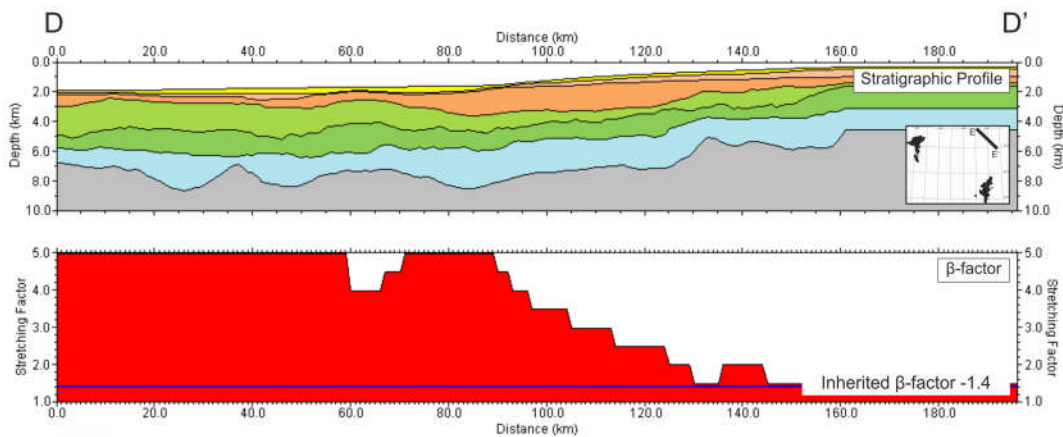


**Figure 6.20** - Whole lithosphere  $\beta$ -factors for depth-dependent rifting in the Paleocene derived from flexural backstripping of Line D-D'.  $\beta$ -factors show a significant increase from the Ereland to the Flett Sub-basin, with a maximum  $\beta$ -factor of 5.

### 6.7.2 Heat Flow Models

Using the  $\beta$ -factors established in Section 6.7.1, individual heat flow models were constructed for each profile, the results of heat flow modelling are shown in Figure 6.21 & 6.22). By using a standard depth-uniform stretching model for Cretaceous rifting the resultant heat flow is generally constant throughout the Jurassic and Cretaceous at around 47 mW/m<sup>2</sup>. Using a uniform value across the results in no variation in heat flow between depocentres and structural highs. There is a substantial increase heat flow during the Paleocene rift event, which exceeds 60 mW/m<sup>2</sup> in the Flett, Foula and Corona Sub-basins at the end Paleocene. Heat flow correlates closely with the stretching factors established through flexural backstripping and so areas that have undergone greater stretching generally experience higher heat flow than less stretched points on the same line.

The influence of the heat flow models on source rock temperature are discussed in more detail in Section 6.9.3.

### 6.7.3 Heat Flow Calibration

In order to test the validity of the heat flow models, predicted vitrinite reflectance profiles (%Ro) were calibrated with measured vitrinite reflectance data (%Ro) from the available wells (Figure 6.23). Simulations were run for each 2D profile using the Type II kerogen kinetics of Burnham (1989) and the heat flow scenarios as defined in Section 6.7.2. Where wells intersect the modelled lines, 1D extractions were taken for calibration; wells that do not intersect the modelled lines were projected to the nearest adjacent line. Overall, a good correlation is observed between the predicted and measured vitrinite reflectance data (Figure 6.23) suggesting that the heat flow model and other petroleum system model parameters are capable of accurately reproducing basin evolution. There are a number of areas in which the predicted data deviates slightly from the measured data; this could be attributed to a number of factors and most likely represents minor variations in lithology, erosion or kinetics between the well location and the projected extraction point on the modelled line.

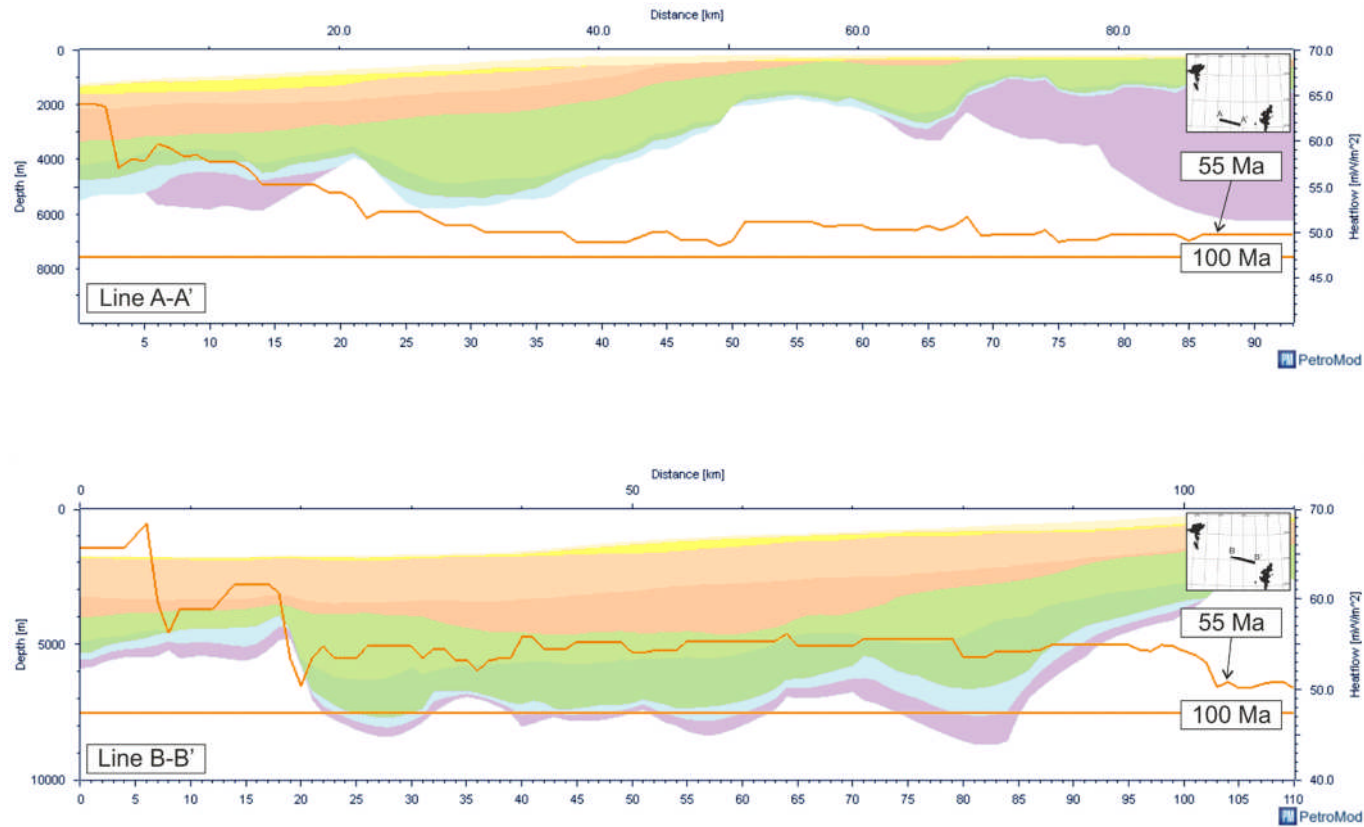


**Figure 6.21** – Predicted 2D heat flow profiles for Line A-A' and Line B-B' shown at the End Lower Cretaceous (100 Ma) and End Paleocene (55 Ma). Both lines show an increase in heat flow during the Paleocene towards the northeast of the profile associated with the increased lithospheric mantle stretching observed towards the axis of the basin.

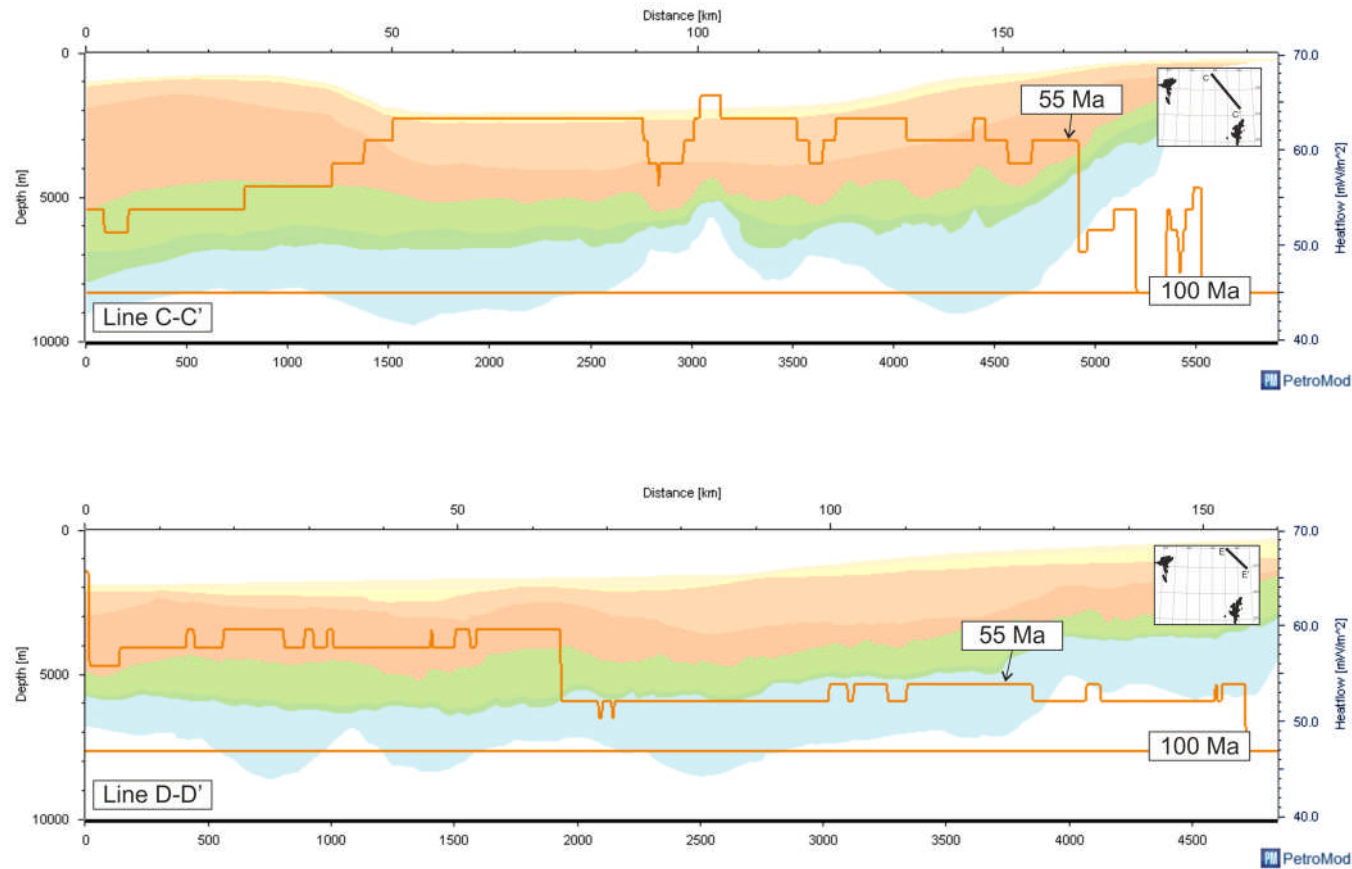


**Figure 6.22** - Predicted 2D heat flow profiles for Line C-C' and Line D- D' shown at the End Lower Cretaceous (100 Ma) and End Paleocene (55 Ma). Line C-C' shows an increase in Paleocene heat flow towards the centre of the line where lithospheric mantle stretching is highest, Line D- D' shows greatest heat flow in the Corona Sub-basin towards the northwest.

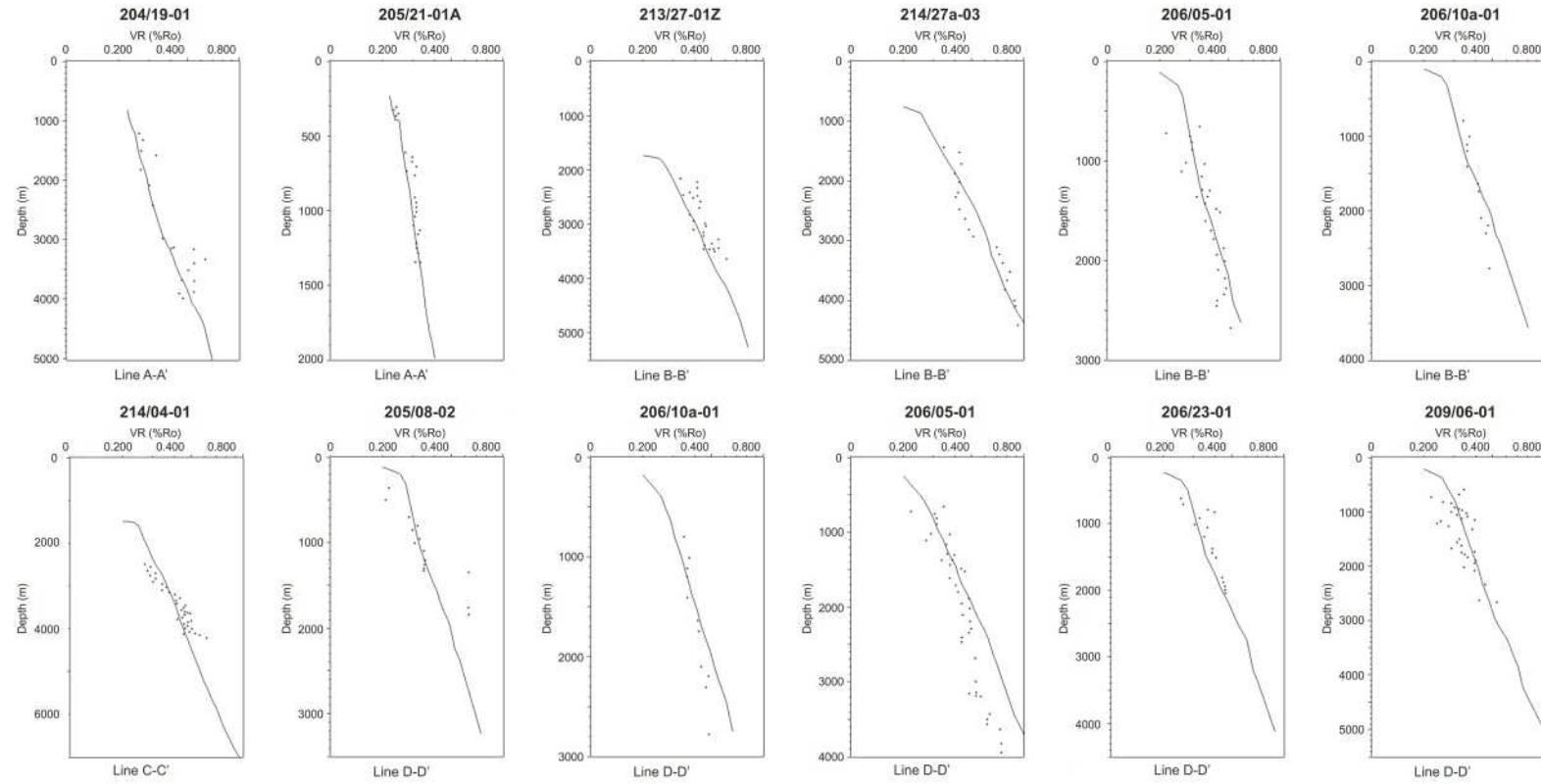


**Figure 6.23** – Predicted vitrinite reflectance profiles (solid line) calibrated with measured vitrinite reflectance data (points) for the available wells showing good to excellent correlation.

## 6.8 Migration Modelling

To better understand the timing of hydrocarbon expulsion and the potential migration pathways in the basin, migration modelling is incorporated into each simulation run. Two types of migration modelling available within the software, *Darcy Flow* and *Flowpath*, these can be used individually or combined together using the *Hybrid* function. *Darcy Flow* assumes flow velocity is controlled by rock permeabilities and fluid viscosity functions; in contrast *Flowpath* uses buoyancy as the principle mechanism for migration (Welte et al., 2012). The application of each method is dependent on the data available, size of the model and objectives of the simulation (Welte and Yalçin, 1988, Hantschel and Kauerauf, 2009). For the purposes of this study, the *Hybrid* function is used to combine both methods.

All migration modelling undertaken in this chapter qualitative, as there are a number of parameters, which are not possible to define with the data available, including detailed lateral facies variations, fault permeability and fracture networks.

## 6.9 Part 3 – Application to the Faroe-Shetland Basin

The main aim of this chapter is to establish the timing and controls of hydrocarbon maturation in the Faroe-Shetland Basin; this section presents the results of petroleum system modelling, focusing on the maturation, transformation ratio and development of overpressure in the source rock horizon as well as regional heat flow variations and hydrocarbon migration modelling. The data are presented as a series of model transects, 1D time plot extractions and extrapolated 2D maps.

### 6.9.1 Maturation

The extent of maturation for the Upper Jurassic source rock can be inferred from the predicted vitrinite reflectance values (%Ro) obtained during petroleum system modelling. The present-day maturation map of the Upper Jurassic source rock (Figure 6.24) shows the NE-SW trending structural highs in the southeast of the basin, such as the West Shetland and Rona Highs are immature with respect to hydrocarbon generation (<0.55 %Ro). Much of the central basin axis is within the

main oil window (0.70 – 1.00 %Ro) including the Guorun and Ereland Sub-basins and the south-western and north-eastern areas of the Flett Sub-basin. Basement ridges within these basins such as the Mid Faroe and Corona Highs are slightly less mature and remain in the early oil window (0.55 – 0.70 %Ro). The deeper areas towards the northeast of the Corona Basin have entered the late oil window (1.00 – 1.30 %Ro). The central Flett and Foula Sub-Basins are within either the Wet Gas (1.30 – 2.00 %Ro) or the Dry Gas (2.00 – 4.00 %Ro) windows and represent the most mature areas of the basin. There is a general trend of increasing maturity from the shelf to the basin axis and from the flanks to the centre of the basin.

In order to assess the evolution of hydrocarbon maturation, a series of 1D time extraction plots are taken from representative points along the modelled transects (Figure 6.25, Figure 6.26 & Figure 6.27) the localities of which are shown on the map in Figure 6.24.

The Flett Sub-basin shows significant variation in the timing of maturation. Source rocks in the southwest corner of the basin (Plot 1 - Figure 6.25) experienced early oil generation in the Late Cretaceous (~74 Ma) and entered the main oil window by the end Late Cretaceous (~65 Ma). The source rock remained in the oil window and did not produce gas. A similar maturation pattern can be observed in the far northeast of the basin (Plot 7 - Figure 6.27), however, hydrocarbon generation here occurred much later, taking until the Early Eocene (~50 Ma) to enter the early oil window and the Late Eocene (~35 Ma) to enter the main oil window.

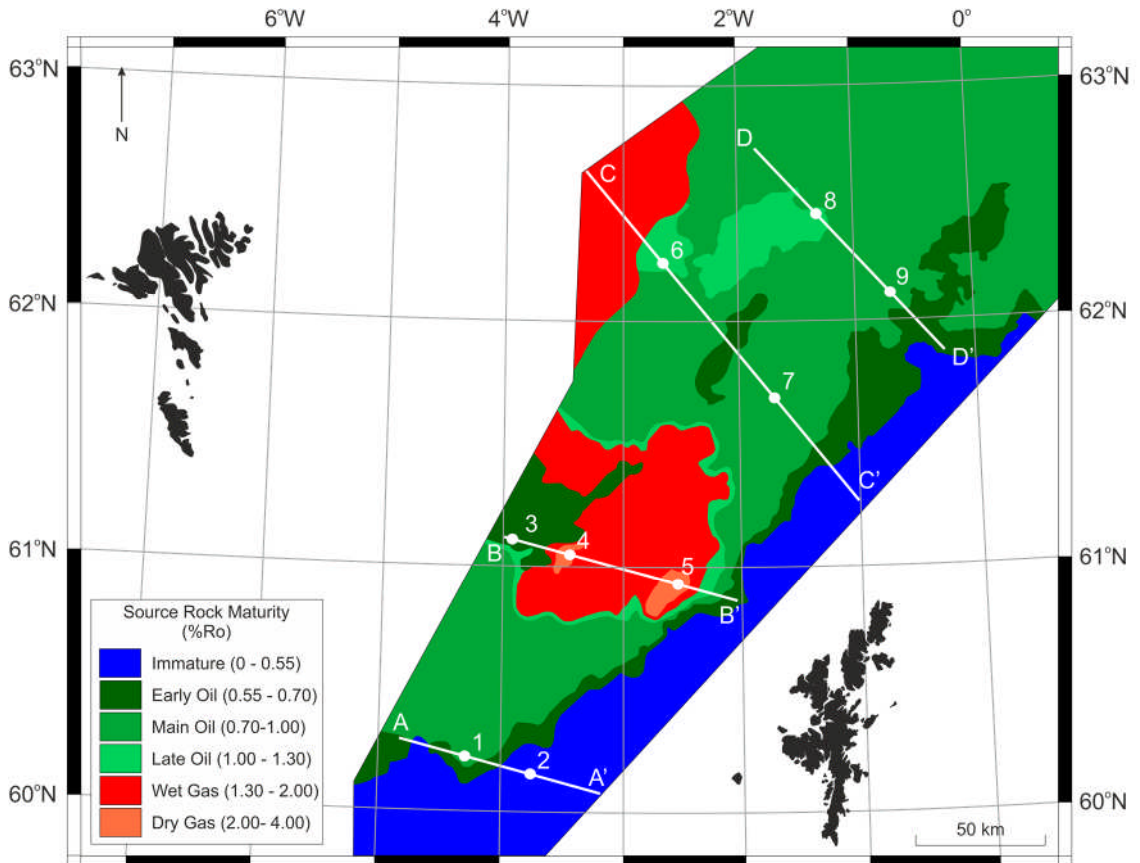


**Figure 6.24** – Present day predicted maturity map (%Ro) of the Upper Jurassic source rock. Data is extrapolated between modelled 2D lines using present day source depth contour maps.

This is a major contrast to the deeper, more central areas of the Flett Sub-basin which went early oil generation in the late Early Cretaceous to early Late Cretaceous (~115 – 94 Ma, Plot 4 – Figure 6.26) and were generating wet gas towards the end of the Late Cretaceous (~70 -65 Ma) and dry gas by the Late Oligocene (~25 Ma). Similarly, the adjacent central Foula Sub-basin also began to generate oil by the late Early Cretaceous (~96 Ma), wet gas by the Late Cretaceous (~68 Ma) and dry gas by the Early Eocene (~48 Ma, Plot 5 Figure 6.26). To the northwest of these basins the Corona High is significantly less mature; it entered the early oil window by the end Paleocene (~55 Ma), progressing to the main oil window by the Early Oligocene (~33 Ma) where it remained until the present day (Plot 3 Figure 6.25).

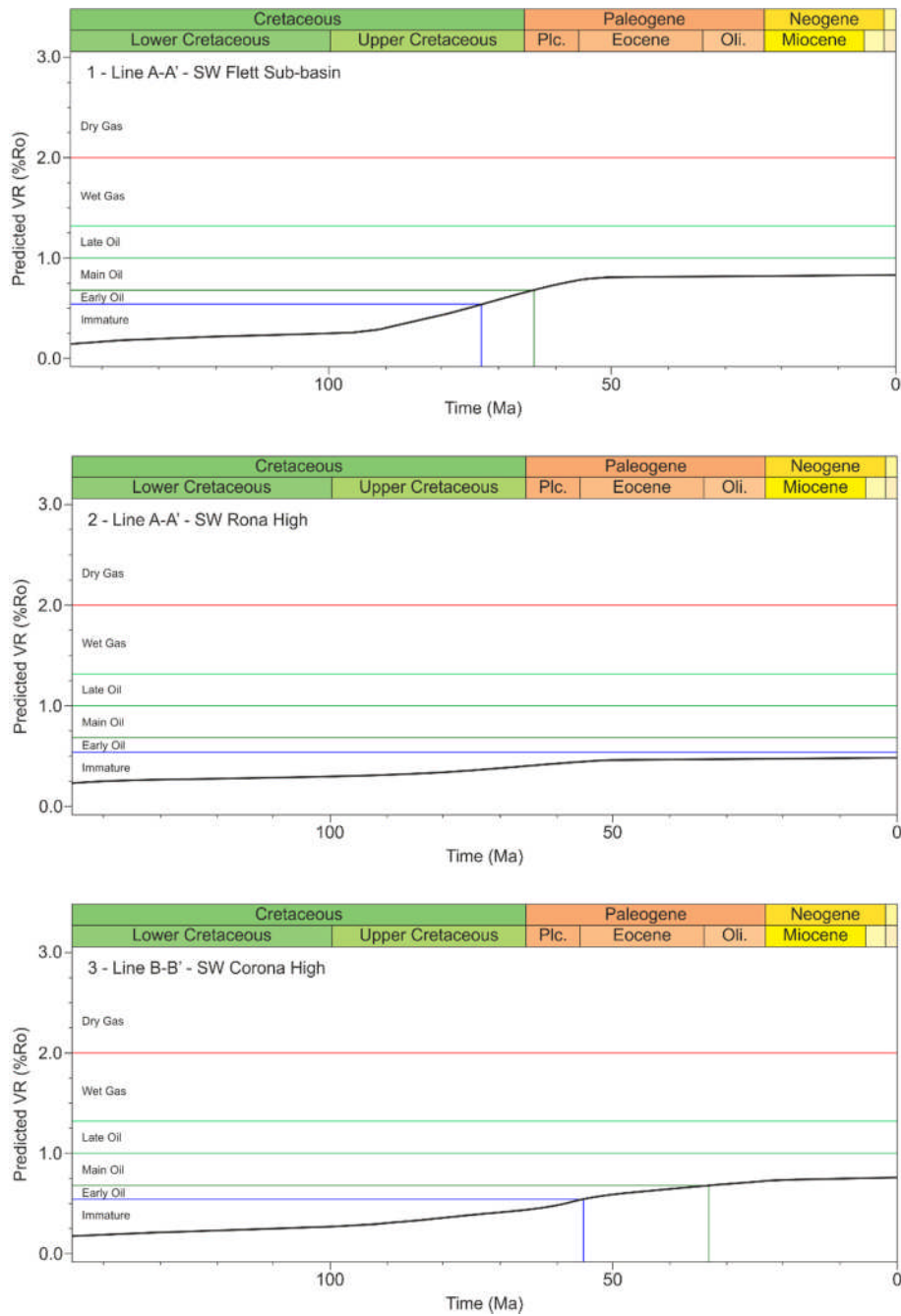


**Figure 6.25** – Time extraction plots from the Flett Sub-basin, Rona & Corona highs illustrating the maturation evolution of the Upper Jurassic source rock, shown as predicted vitrinite reflectance (%Ro). Plot numbers refer to the localities shown on the map in Figure 6.24.

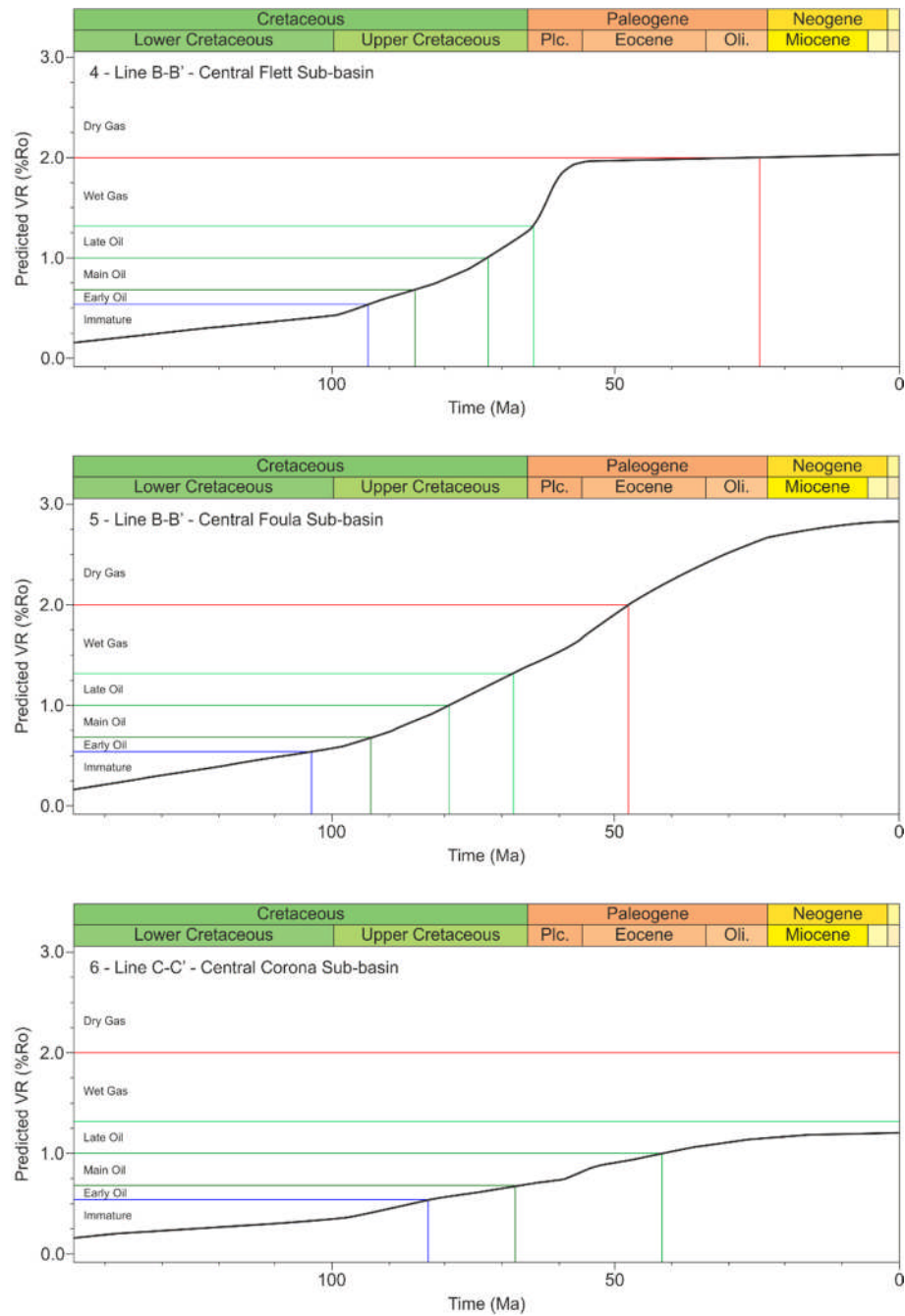


**Figure 6.26** - Time extraction plots from the Flett, Foula and Corona Sub-basins illustrating the maturation evolution of the Upper Jurassic source rock, shown as predicted vitrinite reflectance (%Ro). Plot numbers refer to the localities shown on the map in Figure 6.24.

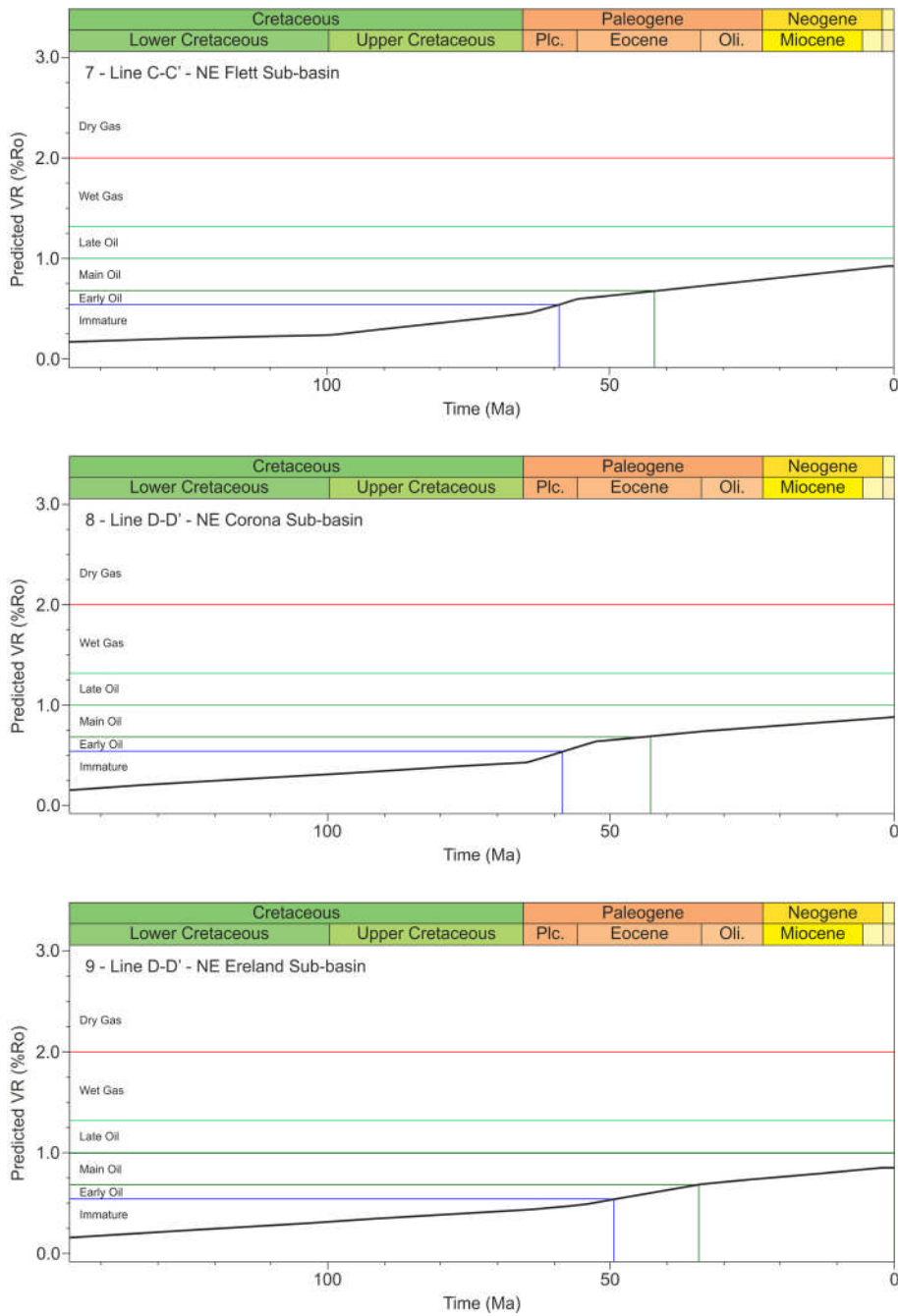


**Figure 6.27** - Time extraction plots from the Flett, Corona and Ereland Sub-basins illustrating the maturation evolution of the Upper Jurassic source rock, shown as predicted vitrinite reflectance (%Ro). Plot numbers refer to the localities shown on the map in Figure 6.24.

The central Corona Sub-basin first entered the early oil window in the mid Late Cretaceous (~83 Ma), rapidly progressing to the main oil window by the end Late Cretaceous (~67 Ma) and into the late oil window by the mid Eocene (~42 Ma, Plot 6 - Figure 6.26). Further northeast, the Corona Sub-basin did not begin generation oil until the mid Paleocene (~58 Ma, Plot 8 - Figure 6.27). Along the southwest Rona High, although there is an increase in the rate of maturation during the Paleocene (~67 Ma) the area remained immature for hydrocarbon generation until the present day (Plot 2 - Figure 6.25). The Ereland Sub-basin, much like other north-eastern areas of the basin, underwent late maturation and took until the Early Eocene (~50 Ma) to enter the early oil window and the Late Eocene (~35 Ma) to enter the main oil window (Plot 9 - Figure 6.27).

Overall, the earliest hydrocarbon generation occurred in the late Early Cretaceous to early Late Cretaceous (~95 – 105 Ma) in the Foula and central Flett Sub-basins, the majority of the other depocentres were generating oil by the Late Cretaceous with the latest beginning in the Early Eocene. Only the deep central areas of the basin reach sufficient maturity to produce gas, with the flanks and basin highs either mature for oil generation or remaining immature.

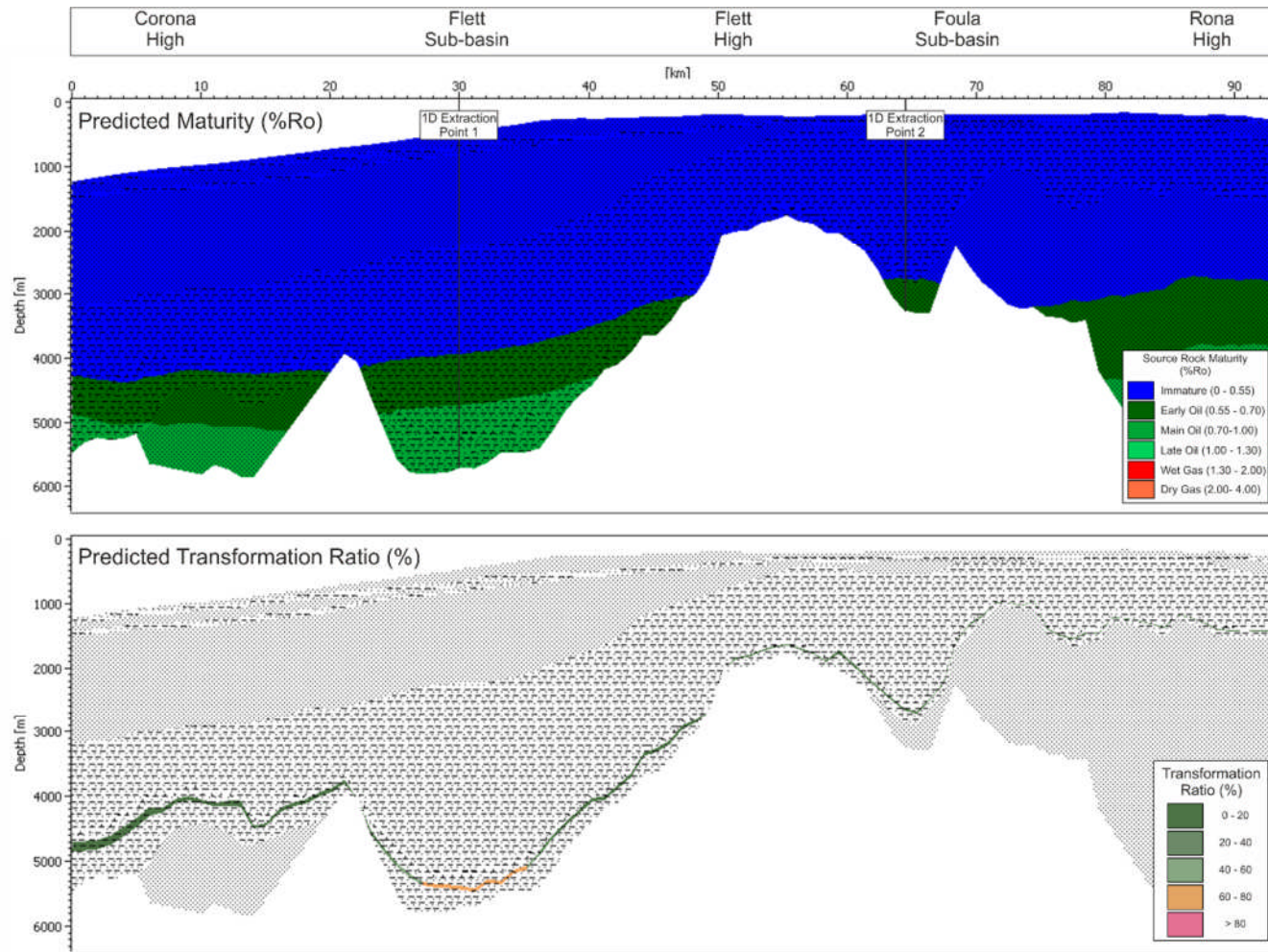


Figure 6.28 – Modelled hydrocarbon maturation potential and predicted transformation ratio for Line A-A'.

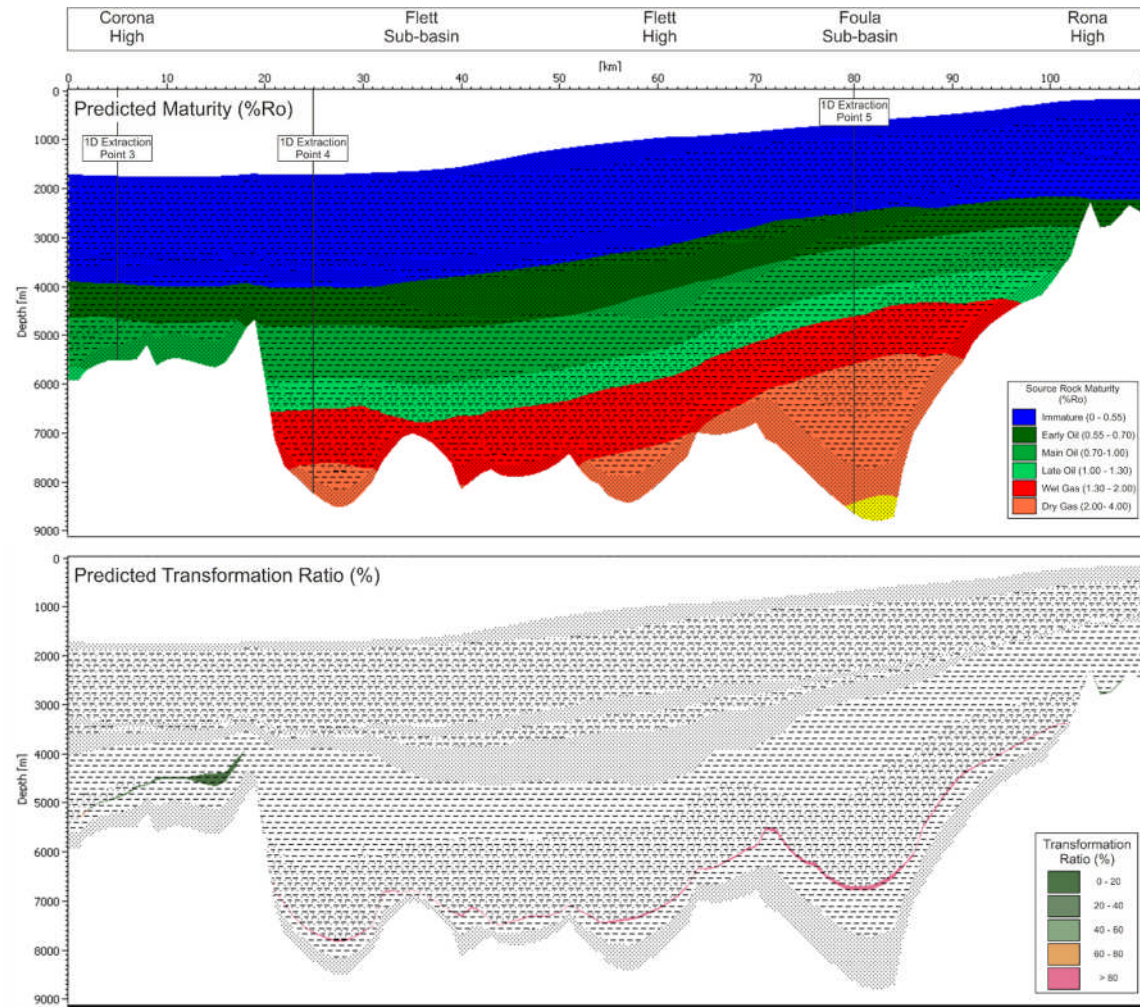


Figure 6.29 - Modelled hydrocarbon maturation potential and predicted transformation ratio for Line B-B'

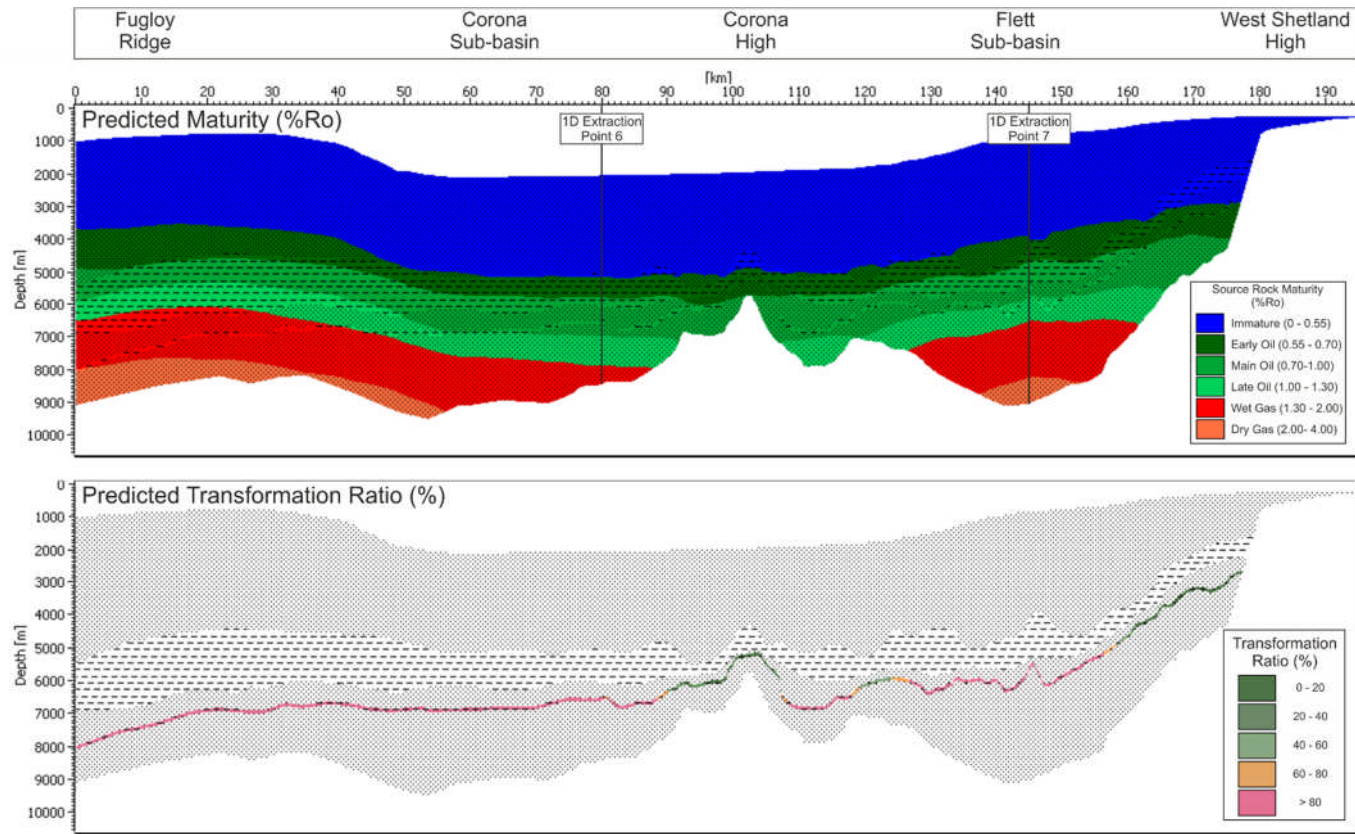


Figure 6.30 - Modelled hydrocarbon maturation potential and predicted transformation ratio for Line C-C'.

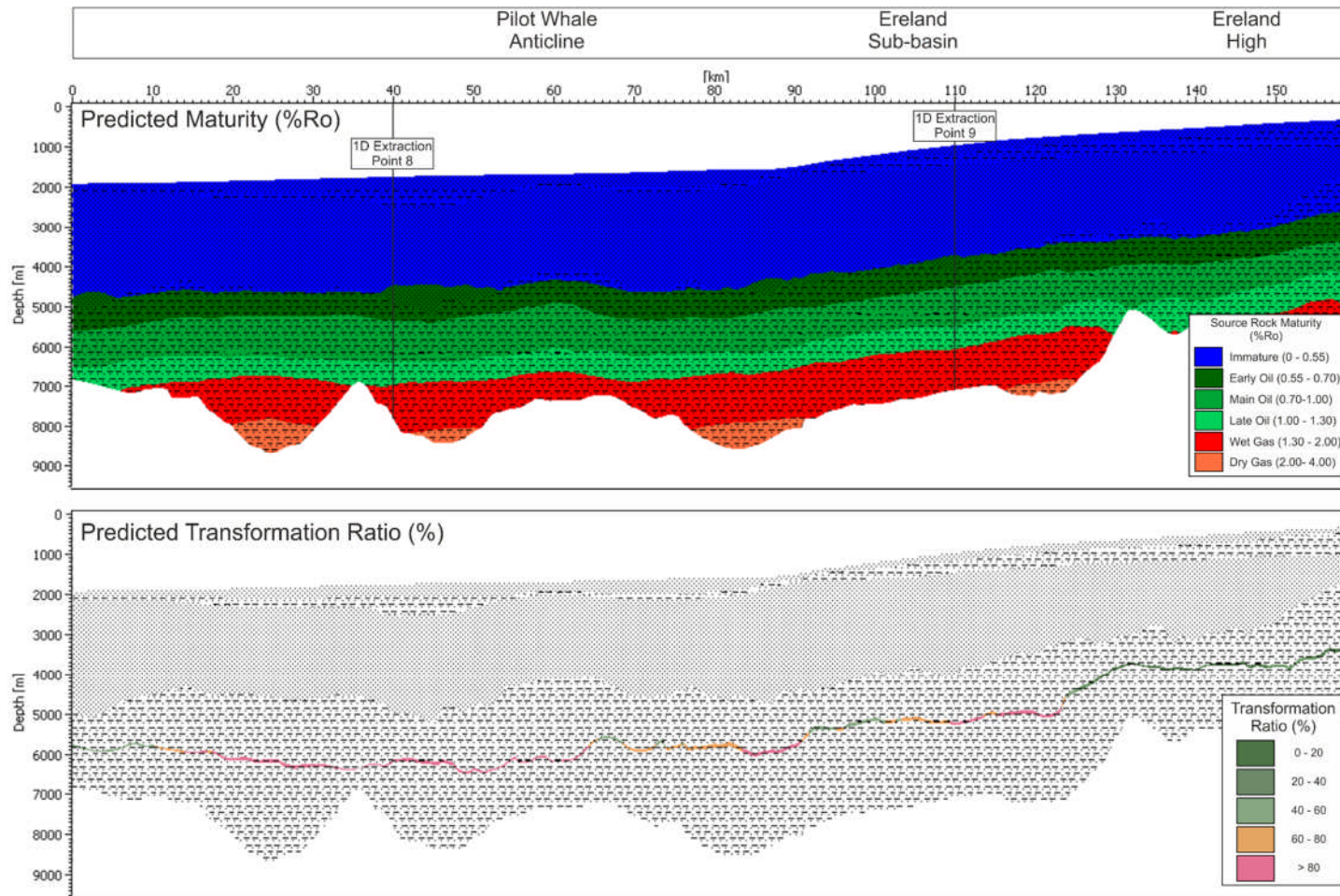


Figure 6.31 - Modelled hydrocarbon maturation potential and predicted transformation ratio for Line D-D'.

### 6.9.2 Transformation Ratio (TR)

The maturation of a source rock can be expressed as the transformation ratio (TR), which is a measure of the actual hydrocarbons generated in relation to the total hydrocarbon generation potential for that given kerogen (Goff, 1983). The present day transformation ratio map (Figure 6.32) shows that much of the central axis of the basin has reached 100% TR with respect including the Corona, Flett and Foula Sub-basins. Structural highs such as the West Shetland and Rona Highs have much lower transformation ratios, with some areas yet to start hydrocarbon generation.

Viewing the change in transformation ratio over time can help to identify critical periods in the hydrocarbon generation history such as initiation (10% TR), peak generation (50% TR) and over maturity (>80% TR). 1D time extraction plots taken from representative points along the modelled transects illustrate the spatial variation of hydrocarbon generation with time (Figure 6.33 & Figure 6.34) the localities of which are shown in Figure 6.32.

In the southwest Flett Sub-basin, hydrocarbon generation began by the End Upper Cretaceous (~65 Ma) and rapidly progresses to peak generation by the Mid Paleocene (~58 Ma). The rate of generation then slowed by the End Paleocene (55 Ma) and remained steady to the present day (Plot 1 - Figure 6.33). In contrast, the centre of the sub-basin underwent initiation much earlier (~88 Ma), peak generation occurred shortly afterwards (~82 Ma), before the area rapidly became overmature (>80% TR, ~79 Ma). Therefore, in the centre of the sub-basin, the transition from immature to over mature occurred entirely during the Late Cretaceous (Plot 4 - Figure 6.33). The source rocks in the north-eastern portion of the Flett Sub-basin did not begin generating hydrocarbons until the Early Eocene (~52 Ma), from then there was a steady increase in generation, reaching peak oil by the Mid Oligocene (~28 Ma) and over maturity by the Late Miocene (~12 Ma) (Plots 7 - Figure 6.34). A similar trend is observed in the Ereland Sub-basin Plots 9 - Figure 6.34).

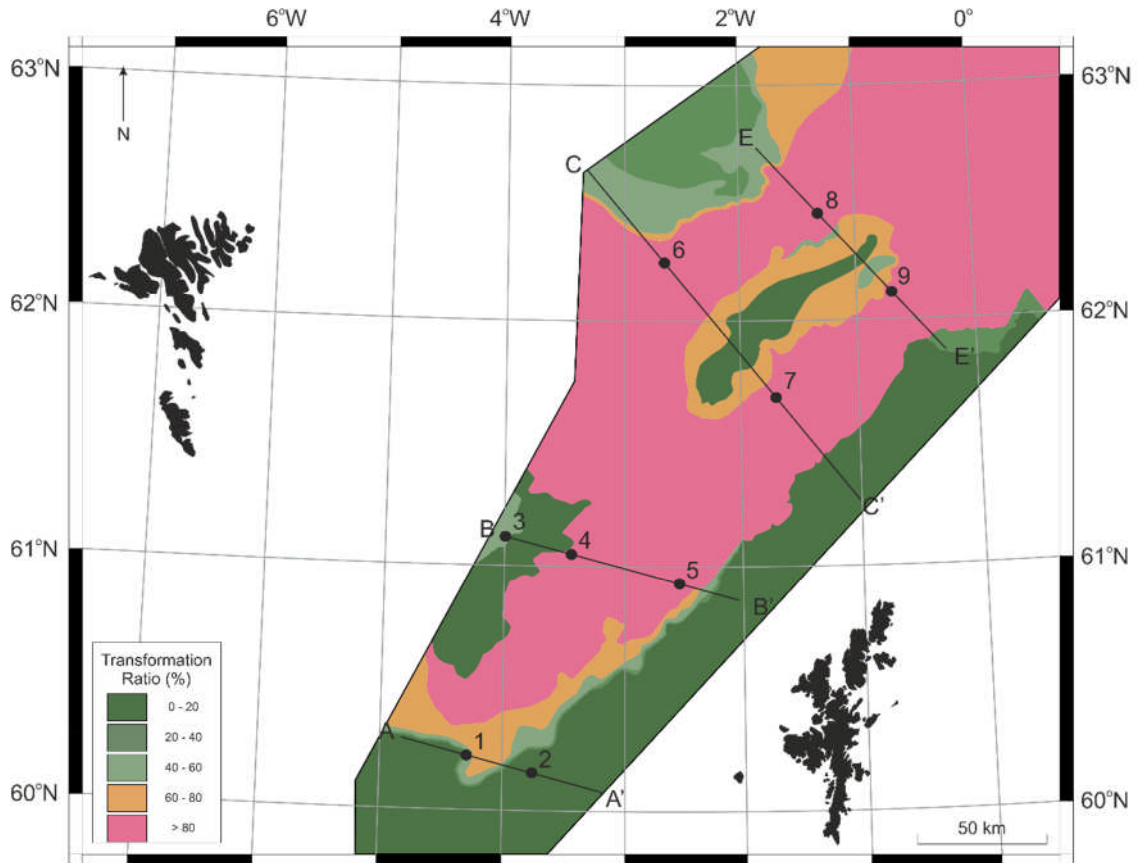


**Figure 6.32** – Present day predicted transformation ratio (%) of the Upper Jurassic source rock. Data is extrapolated between modelled 2D lines using present day source depth contour maps.

In the southwest Flett Sub-basin, hydrocarbon generation began by the end Late Cretaceous (~65 Ma) and rapidly progressed to peak generation by the Mid Paleocene (~58 Ma). The rate of generation then slowed by the End Paleocene (55 Ma) and remained steady until the present day (Plot 1 - Figure 6.33). In contrast, the centre of the sub-basin underwent initiation much earlier (~88 Ma), with peak generation occurring shortly afterwards (~82 Ma), before the area rapidly became overmature (>80% TR, ~79 Ma). Therefore, in the centre of the sub-basin, the transition from immature to over mature occurred entirely during the Late Cretaceous (Plot 4 - Figure 6.33). The source rocks in the north-eastern portion of the Flett Sub-basin did not begin generating hydrocarbons until the Early Eocene (~52 Ma), from then there was a steady increase in generation, reaching peak oil by the Mid Oligocene (~28 Ma) and over maturity by the Late Miocene (~12 Ma) (Plots

7 - Figure 6.34). A similar trend is observed in the Ereland Sub-basin Plots 9 - Figure 6.34).

The central Foula Sub-basin was over mature by the mid Late Cretaceous (~85 Ma), hydrocarbons were first generated in this area around the early Late Cretaceous (~96 Ma) and peak generation occurred in the mid-early Late Cretaceous (~90 Ma) (Plot 5 - Figure 6.33). In the Corona Sub-basin hydrocarbon generation initiated in the Early Eocene (~50 Ma) and increased at a constant rate until it peaked in the Mid Oligocene (~30 Ma), all source rocks being over-mature by the Late Miocene (~8 Ma) (Plots 6 & 8 - Figure 6.34). Source rocks overlying structural high such as those at the southwest edge of the Corona High underwent hydrocarbon generation much later than the surrounding depocentres, with initiation occurring in the Late Eocene (~35 Ma) and never reaching peak oil generation (Plot 3 - Figure 6.33).

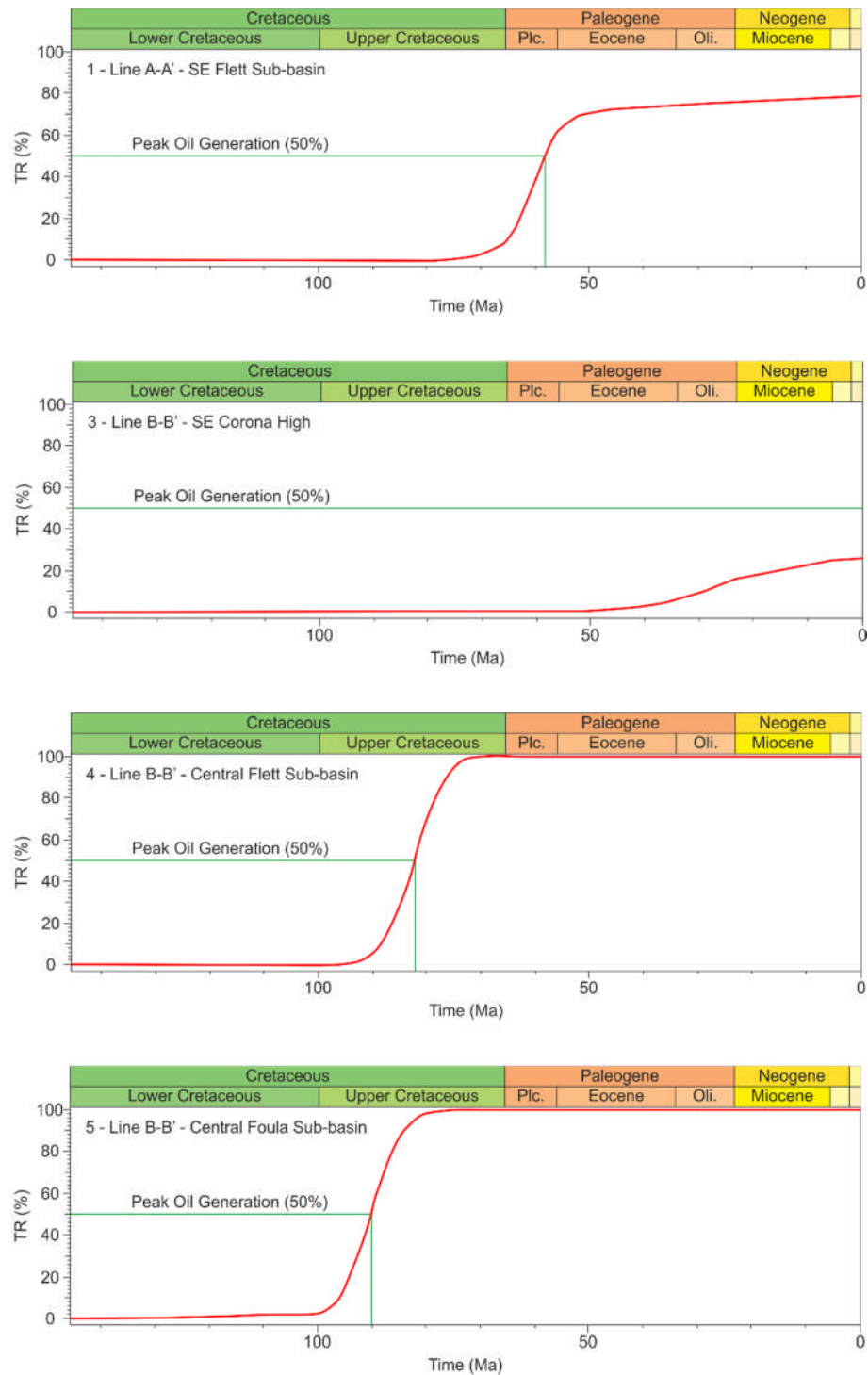


**Figure 6.33** – Time extraction plots from the Flett and Foula Sub-basins and the Corona High illustrating the hydrocarbon generation history of the Upper Jurassic source rock, shown as predicted transformation ratio (%). Peak oil generation (50% TR) is highlighted. Plot numbers refer to the localities shown on the map in Figure 6.32.

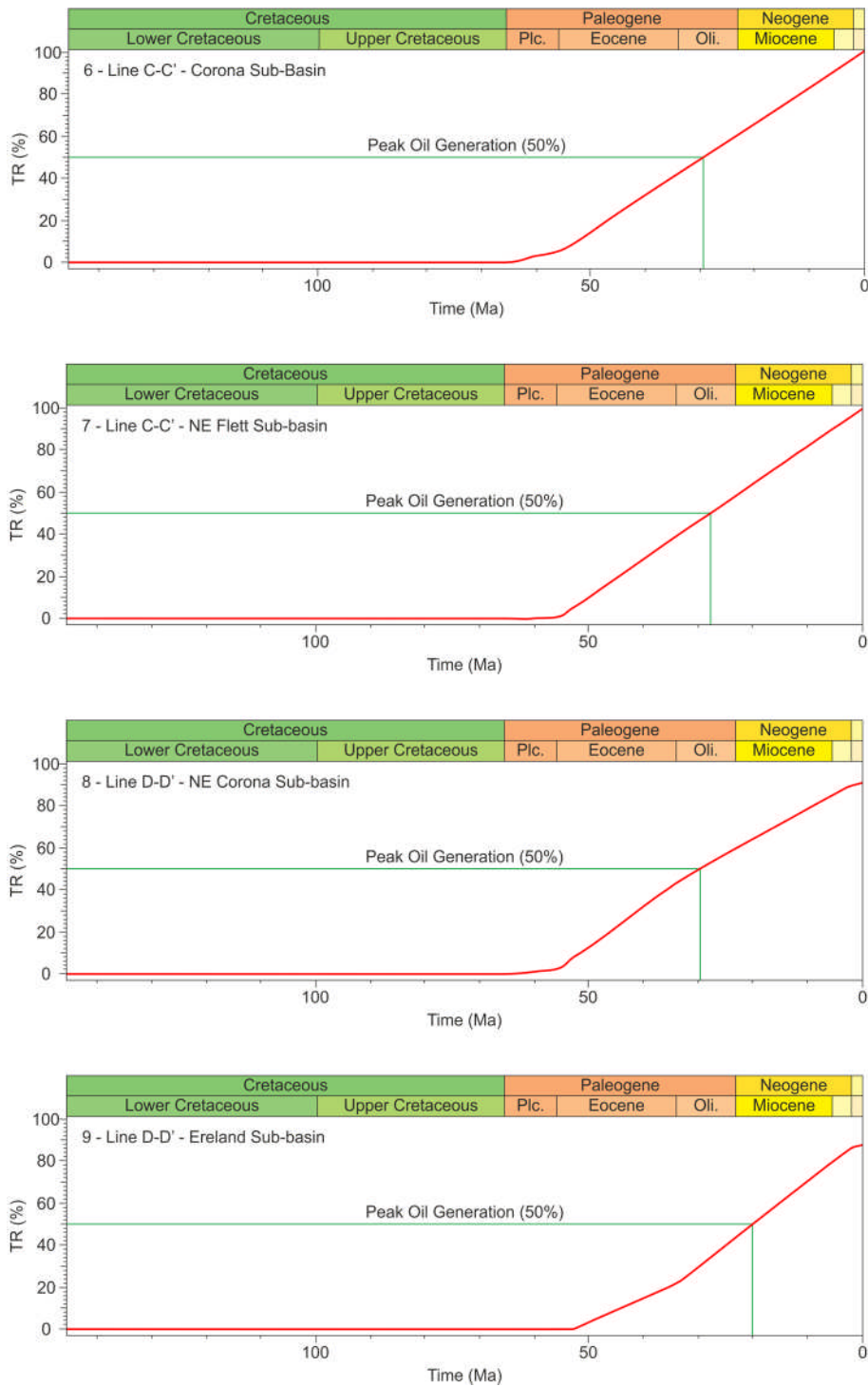


**Figure 6.34** - Time extraction plots from the Flett, Foula and Ereland Sub-basins illustrating the hydrocarbon generation history of the Upper Jurassic source rock, shown as predicted transformation ratio (%). Peak oil generation (50% TR) is highlighted. Plot numbers refer to the localities shown on the map in Figure 6.32.

### 6.9.3 Overpressure & Temperature

A series of combined time extraction plots have been generated to illustrate the development of overpressure and temperature in the source rock horizon with respect to burial. The transformation ratios from the previous section have been added to show how these factors coincide with hydrocarbon generation (Figure 6.35, Figure 6.36 & Figure 6.37), the localities are shown on the maps in Figure 6.24 & Figure 6.32).

The highest levels of overpressure occurred in the central Flett and Foula Sub-basins and developed as a response to rapid burial during Early Cretaceous rifting and subsequent Late Cretaceous subsidence (Plots 4 & 5). Elsewhere overpressure was substantially lower during the Cretaceous and did not begin to develop until the latest Cretaceous (~65 Ma) to Late Eocene (~32 Ma) (Plot 1 – Figure 6.35, Plot 6 – Figure 3.36 and Plots 7, 8 & 9 – Figure 3.37).

Areas that have developed overpressure by the end of the Cretaceous such as the central Flett, Foula, and NE Corona Sub-basins saw overpressure drop due to regional uplift in the Paleocene (~65 Ma), however renewed subsidence following Paleocene rifting caused overpressure to rise shortly after (Plots 4 & 5 Figure 3.36 and Plot 8 Figure 3.37). Overpressure typically increased in all areas of the basin until the Early Oligocene (~30 Ma), at which point substantial regional uplift during Cenozoic inversion caused it to decline. Over structural highs, overpressure remains low or does not develop at all (Plots 2 & 3 – 6.35).

Temperature within the source rock horizon was closely correlated to the rate and depth of burial. The temperature gradient steepened during Late Cretaceous subsidence and again during subsidence following Paleocene rifting. Spikes in source rock temperature can be observed towards the end Paleocene (~55 Ma) due to a heat influx from stretching of the whole mantle lithosphere (Plot 2 – 6.35 and Plots 4 & 5 - 6.36).

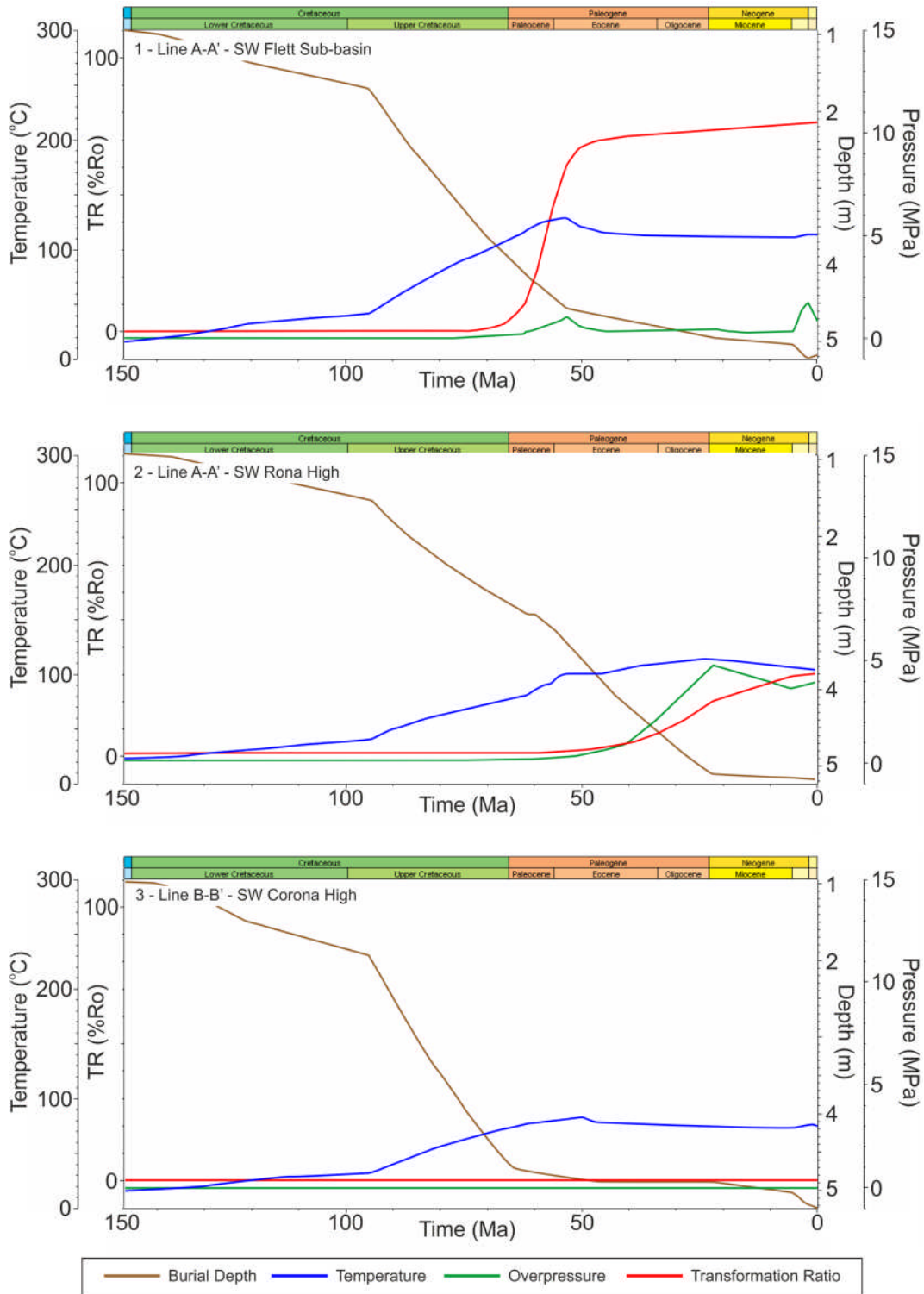


**Figure 6.35** – Compiled time extraction plots for the Flett Sub-basin and Rona & Corona Highs illustrating the development of overpressure and heat flow evolution in the Upper Jurassic source rock horizon in relation to burial depth and transformation ratio. Plot localities are shown in Figure 6.24 & Figure 6.32.

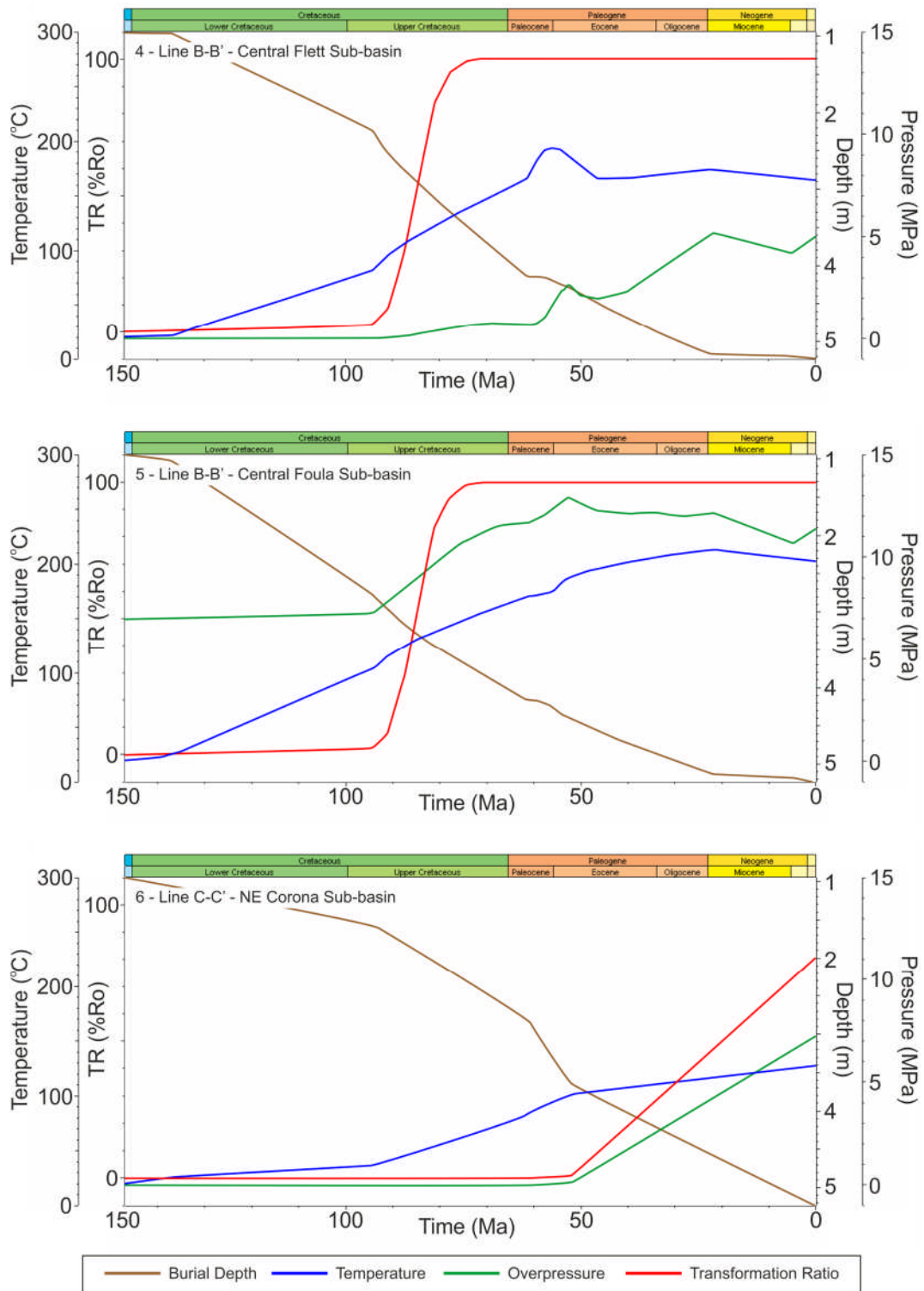


**Figure 6.36** - Compiled time extraction plots for the Flett Sub-basin and Rona & Corona Highs illustrating the development of overpressure and heat flow evolution in the Upper Jurassic source rock horizon in relation to burial depth and transformation ratio. Plot localities are shown in Figure 6.24 & Figure 6.32.

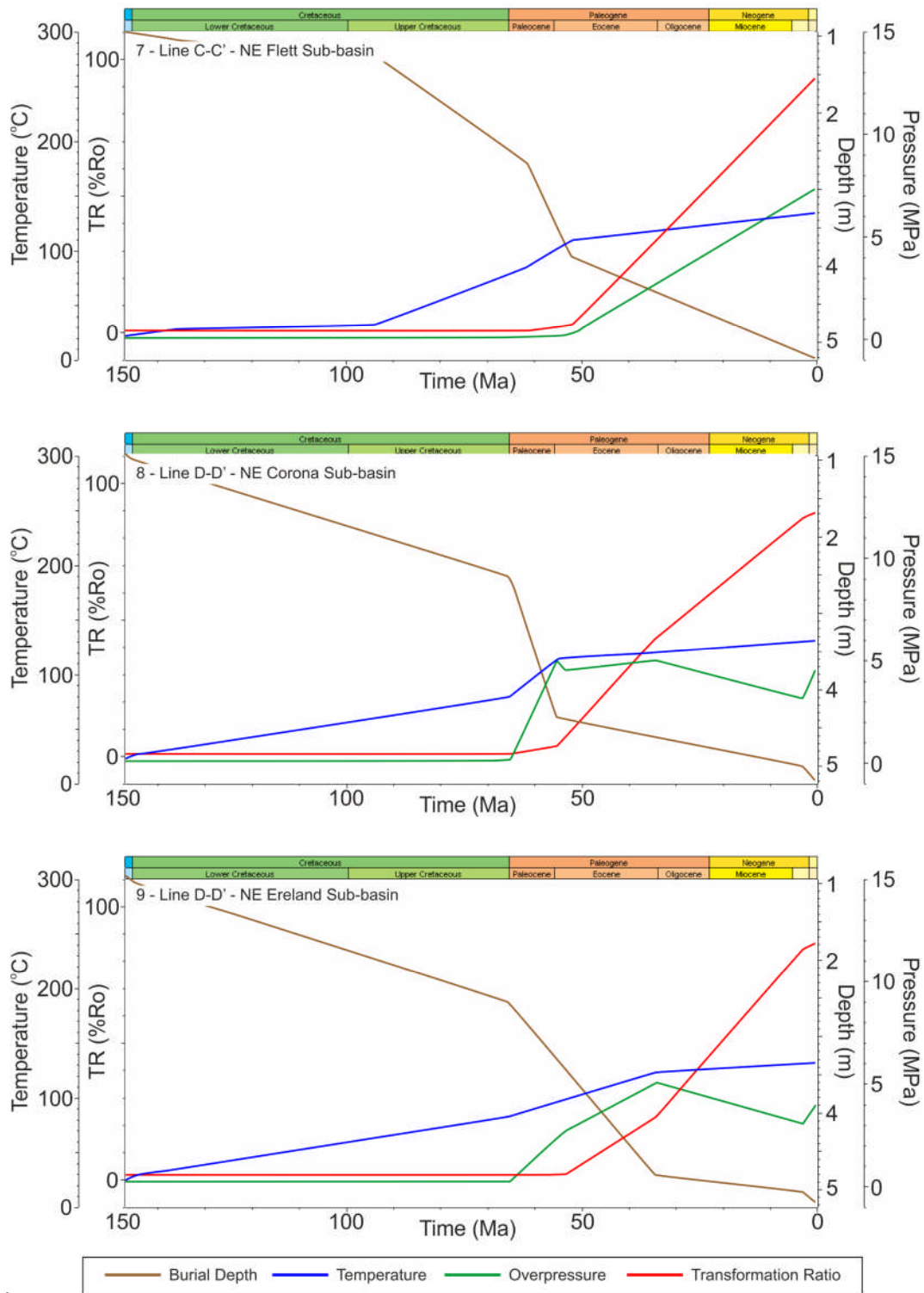


**Figure 6.37** - Compiled time extraction plots for the Flett Sub-basin and Rona & Corona Highs illustrating the development of overpressure and heat flow evolution in the Upper Jurassic source rock horizon in relation to burial depth and transformation ratio. Plot localities are shown in Figure 6.24 & Figure 6.32.

## 6.10 Discussion

The results of petroleum system modelling indicate that hydrocarbon maturation in the Faroe-Shetland Basin was controlled by a complex relationship between post-rift subsidence, rift-related heat flow anomalies and overpressure within the source rock horizon.

The majority of the basin is mature for hydrocarbon generation, with the deepest central areas, including parts of the Flett and Foula Sub-basins, mature for gas generation. Modelled transformation ratios suggest the majority of the basin was overmature with the only remaining generation potential on the flanks of the basin and overlying structural highs.

In the most mature areas of the basin, such as the central Flett and Foula sub-basins (Line B-B'), the source rock was rapidly buried by up to 2 km during Late Cretaceous subsidence. The increased heat flow associated with burial was sufficient to initiate maturation of the source rock such that it was producing oil by the early Late Cretaceous and gas by the mid Late Cretaceous and the source rock was overmature by the late Late Cretaceous. Despite substantial overpressure developing within the source rock at this time, it was not sufficient to retard hydrocarbon generation.

Comparable rates of Late Cretaceous subsidence occurred in the southwest Flett Sub-basin (Line A-A') (Figure 6.38), however, overall burial depth remained marginally shallower than in the central areas of the basin, whilst the modelled temperatures are significantly lower. Hydrocarbon maturation in this area was initiated during the Early Paleocene due to increased heat flow attributed to Paleocene rifting, with the source rock rapidly reaching peak generation by the end Paleocene. Burial during Paleocene rifting developed overpressure in the source rock horizon, reducing the rate of generation. Lower burial rates and a decline in heat flow during the Eocene and Oligocene ensured that the area continued to produce oil rather than progress to gas generation.

In the far northeast of the basin, including the Ereland and Corona Sub-basins (Line E-E') there was a slow, constant, rate of subsidence and increasing temperatures

during the Late Cretaceous allowed the area to remain immature. Rapid subsidence during the Paleocene significantly increased burial depth, however, the development of overpressure prevented maturation proceeding. As burial depth and temperatures increased, the area became mature for oil generation by the Early Eocene. It is, however, not until a drop in overpressure during the Late Eocene (as a consequence of Cenozoic inversion) that the area was able to reach peak oil generation.

The principal control on hydrocarbon maturation is depth of source rock burial, which is regulated by the rate of post-rift subsidence following the major Cretaceous and Paleocene rift events. Isochron maps of the Late Cretaceous and Eocene/Oligocene successions show the distribution and thickness of post-rift overburden deposition accumulated following these rift events (Figure 6.38). Late Cretaceous subsidence was focused in the central Flett and Foula Sub-basins with much of the NE Flett, Corona and Ereland Sub-basins undergoing significantly less subsidence. Post-Paleocene subsidence occurred across the margin but was greatest in the northeast of the basin.

In general Cretaceous subsidence appears to have occurred within small blocks and segmented sub-basins causing rapid maturation of hydrocarbons in these localised areas. Post-Paleocene subsidence, however, occurred across the entire Faroe-Shetland Basin and is highest towards the basin axis, declining towards the flanks, causing a regional increase in maturation in areas which are not already mature. The nature of post-rift subsidence strongly reflects the difference in the style of rifting between the two discrete events. In the Paleocene where the mantle-lithosphere was extended to a greater extent than the upper crust there is greater, regional-scale subsidence as opposed to the shallow upper crustal stretching of the Early Cretaceous which created moderate subsidence.

Whilst significant overpressure developed in the source rock horizon as a result of subsidence during the Late Cretaceous and Paleocene, it has been shown to have a limited effect on maturation where burial depths and temperatures were already sufficiently high. In shallower or cooler areas overpressure has been shown to have either inhibited the progression of maturation allowing source rocks to remain in

the oil window or delayed the initiation of maturation until later in the basin's evolution. This may explain why oil is still the primary hydrocarbon discovered in areas predicted to be overmature and is consistent with the findings of Scotchman et al (2006).

Previous studies suggest that volcanic heat flow played a role in increasing the maturity of source rocks during the Paleogene volcanic events (Iliffe et al., 1999, Parnell et al., 1999, Green, 2002, Scotchman et al., 2006). Modelling here shows the effect of subsidence alone is enough to induce maturation without any implication of volcanic heat flow although it is not known what, if any, influence volcanism would have on the model. Therefore the local and regional impact of volcanic heat flow will be examined further in Chapter 7.

### 6.11 Conclusions

- Sensitivity analysis identifies heat flow and source rock depth as the most influential uncertainties in the modelling process.
- Flexural backstripping shows depth-dependant stretching models successfully explain Paleocene rifting in the Faroe-Shetland Basin, whilst depth uniform-stretching can explain Cretaceous rifting.
- The majority of the basin is currently overmature for the generation of hydrocarbons.
- The earliest generated hydrocarbons occurred in the central Flett and Foula Sub-basins during the late Early Cretaceous, these areas are over mature by the end Late Cretaceous.
- The rest of the basin underwent a steady increase in maturation during post-Paleocene thermal subsidence.
- Overpressure developed as a response to both Cretaceous and Paleocene rifting; the reduction in overpressure during Cenozoic inversion enhanced maturation in the northeast of the basin.
- There is remaining generation potential on the flanks of the basin and over some structural highs.

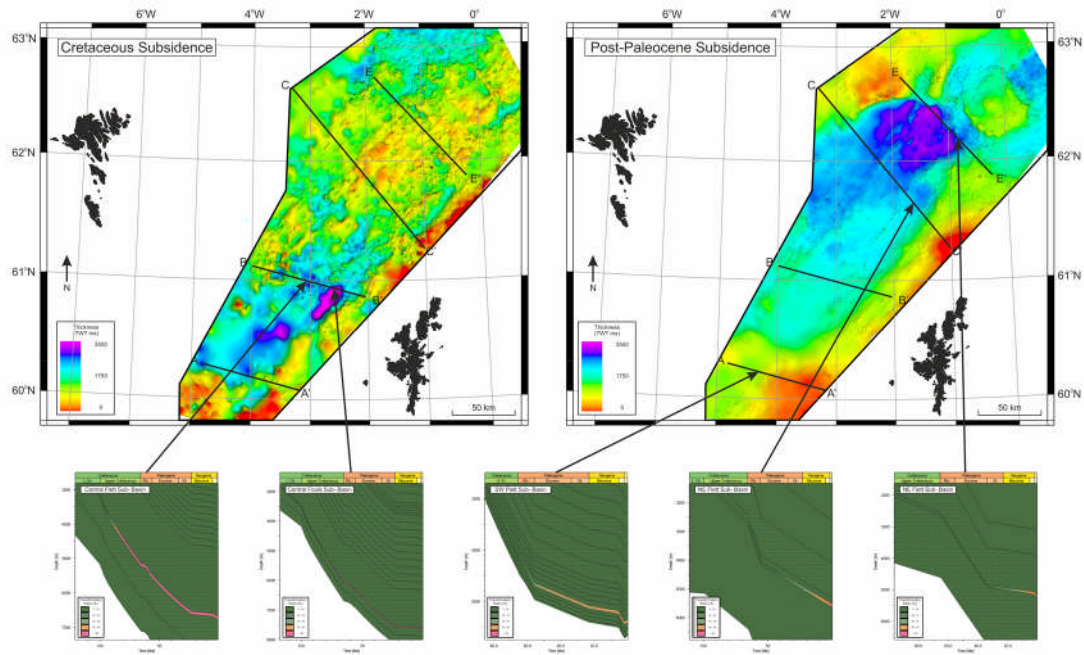


**Figure 6.38** – Isochron maps of the Upper Cretaceous and Eocene/Oligocene packages alongside transformation ratio burial plots showing hydrocarbon generation during these periods. The areas of hydrocarbon generation strongly correlate with the areas of deposition.

## Chapter 7 The Implications of Sill Intrusion for Hydrocarbon Prospectivity.

### 7.1 Abstract

This chapter integrates the findings of Chapters 4, 5 and 6 to assess the impact of the Faroe-Shetland Sill complex on the hydrocarbon prospectivity of the margin.

The petroleum system modelling techniques and parameters established in Chapter 6 provide the basis for the models used in this chapter. Regional two-dimensional profiles were modified by incorporating the intrusion of igneous rock during the Early Cenozoic volcanic event. The impact of the igneous intrusions and associated heat flow anomalies on regional and local hydrocarbon maturation were assessed.

Intrusion modelling demonstrates that the individual and cumulative heat flow effect of sill intrusion is a sharp, localised, short-lived phenomenon. Given the stratigraphic context and distribution of sills throughout the basin, the associated heat flow elevation during emplacement is not considered a significant factor in regional maturation profiles. Despite this, sill intrusion is capable of elevating maturation profiles in local settings where the distance between intrusion and source rock is sufficiently small, such as the northeast Corona and Ereland Sub-basins.

Given the timing of hydrocarbon maturation and expulsion demonstrated in Chapter 6, there is potential for hydrocarbon accumulation within Upper Cretaceous, Paleocene and Lower Eocene reservoirs during the time over which the sill complex was intruded. The heat flow implications of igneous intrusions are such that localised secondary maturation is a possibility where migrated hydrocarbons lay within close proximity of the igneous bodies.

## 7.2 Introduction

In a typical sedimentary basin, the maturation of organic matter is a function of progressive burial and thermal alteration throughout basin evolution (Clayton and Bostick, 1986), however, in areas of intense volcanic activity, such as volcanic passive margins, igneous systems have the potential to modify both regional and local heat flow gradients, thus influencing maturation (Fjeldskaar et al., 2008).

The Faroe-Shetland Basin is located on the NE Atlantic margin and has undergone intense volcanism during the Early Cenozoic prior to continental break-up (Skogseid et al., 2000). Much of the northwestern and central areas of the basin are covered by extensive flood basalts (Passey and Hitchen, 2011) and a widespread intrusive igneous suite, known as the Faroe-Shetland Sill Complex, has been intruded throughout the Cretaceous and Paleocene sub-basins (Bell and Butcher, 2002)

The thermal implications of igneous intrusions on the maturation of organic matter have been extensively studied through numerical modelling (Jaeger, 1964, Galushkin, 1997), physical observations (Simonet et al., 1981, Dennis et al., 1982, Hutton and Henstridge, 1985, Clayton and Bostick, 1986, Saxby and Stephenson, 1987, George, 1992, Gurba and Weber, 2001, Rimmer et al., 2009) and petroleum system modelling (Fjeldskaar et al., 2008). Despite this, the impact of the Faroe-Shetland Sill Complex on Upper Jurassic source rock maturation in the Faroe-Shetland Basin is poorly understood and largely overlooked in published petroleum system modelling studies (Holmes et al., 1999, Jowitt et al., 1999, Iliffe et al., 1999).

The intrusion of sills into sedimentary successions causes an elevation in heat flow within the surrounding country rock, the area affected by this thermal field is known as the thermal aureole (Raymond and Murchison, 1988) (Figure 7.1).

Vitrinite reflectance data suggest country rock temperatures within the thermal aureole of an intruded body may increase by between 200-500°C up to kilometres from the intrusion (Clayton and Bostick, 1986). Depending on the magnitude and length of heat flow elevation, a pulse of additional heat can induce physical and chemical changes to the host rock, either through recrystallization of metamorphism of its constituent minerals (Aarnes et al., 2011). The conversion of kerogens to hydrocarbons occurs over a small temperature window and the

difference between immature, mature and post-mature is often less than 100°C (Hunt, 1996). Thus, thermal and metamorphic aureoles produced by sill intrusion have the potential to induce or enhance hydrocarbon generation, conversely, in areas of established maturity it may cause otherwise prospective areas to become post-mature.

In this chapter, predictive forward modelling is used to assess the potential implications of the Faroe-Shetland Sill Complex on hydrocarbon prospectivity in the Faroe-Shetland Basin. Using the 2D petroleum system models produced in Chapter 6, the heat flow anomalies associated with sill intrusions are simulated to determine their local and regional impact on heat flow, organic maturation and other aspects of prospectivity.

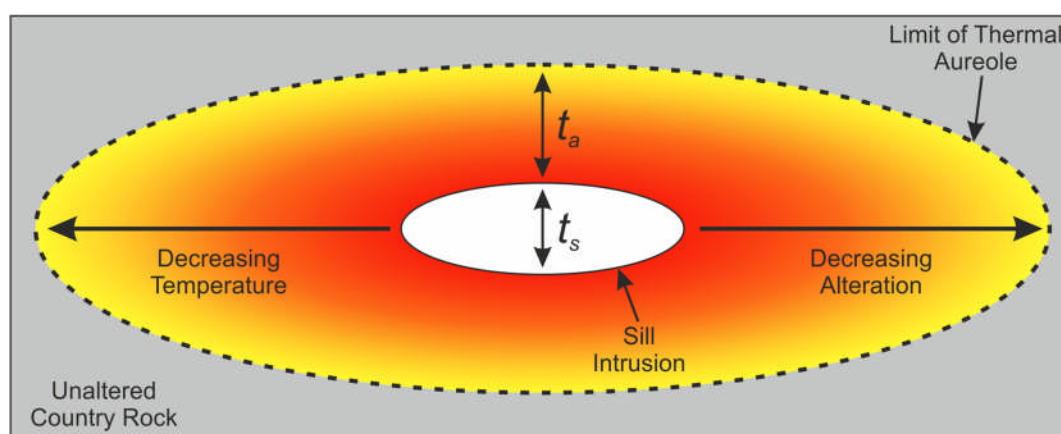


**Figure 7.1** – Schematic illustration of the thermal aureole surrounding a sill intrusion, showing the zone of thermal alteration. Common observations suggest the thickness of the thermal aureole ( $t_a$ ) is related to the thickness of the sill intrusion ( $t_s$ ) (Galushkin (1997) and references therein).

### 7.3 The Thermal Implications of Sill Intrusion

The extent of thermal alteration caused by an intrusive body is often expressed as a ratio of sill thickness with typical values varying between 0.5 and 5 depending on the study (Galushkin, 1997). The highest published estimates suggest the size of the aureole can be up to five times the intrusion thickness (Dutcher et al., 1966), more

commonly it is around twice the thickness of the intrusion (Correia and Maury, 1975, Dow, 1977, Kendrick et al., 1978, Senger et al., 2014) or around half the intrusion thickness (Bostick, 1971, Perregaard and Schiener, 1979, Simonet et al., 1981). Regardless of distance studies unanimously indicate that the severity of source rock alteration decreases with distance from the intrusion contact (Saxby and Stephenson, 1987). Studies do, however, suggest that thermal effects of intrusions are greater in areas of multiple intrusion (Fjeldskaar et al., 2008), indeed, numerical modelling of intrusion in the Karoo Basin, South Africa suggests the intrusion of multiple sills can influence the maturation of organic matter several hundred metres from the site of intrusion and initial thermal aureole (Aarnes et al., 2011).

The intrusion of sills, has the ability to increase the maturation of surrounding organic matter. Geochemical analysis by Clayton and Bostick (1986) show that a 130 cm sill alters the vitrinite reflectance values (%R<sub>o</sub>) of the Pierre Shale, Walcott, Colorado, from 0.4 % (170 cm from the contact) to 3.3 % immediately adjacent to it, equivalent to the difference between immature organic matter and the generation of gas. The 1D and 2D modelling by Jones et al. (2007) indicates that the thermal impact of sill intrusion is significant enough to enable renewed gas generation from shallow source rocks in the Sverdrup Basin, Canadian Arctic Islands. Similarly Fjeldskaar et al. (2008) show that sill intrusion in the Gjallar Rudge, Norwegian Sea increases the transformation ratio of in-situ organic material from 70% to 100% during intrusion.

#### **7.4 Sill Intrusion in the Faroe-Shetland Basin**

The Faroe-Shetland Basin, NE Atlantic underwent intense volcanism during the final stages of continental break-up in the Early Paleogene (Doré et al., 1999). This resulted in emplacement of extensive flood basalts and the intrusion of the Faroe-Shetland Sill Complex (FSSC) (Passey and Hitchen, 2011).

The FSSC has been extensively studied using seismic data (e.g. Bell and Butcher, 2002, Smallwood and Maresh, 2002, Hansen and Cartwright, 2006, Thomson and

Schofield, 2008), which has significantly enhanced our understanding of sill emplacement, evolution and regional distribution. More recently, however, studies have begun to consider what impact sill intrusion may have on hydrocarbon systems in the area (Rateau et al., 2013, Schofield et al., 2015). These studies are largely concerned with the migration and trapping of hydrocarbons and as such, overlook the thermal implications of intrusion. As a consequence, the impact of sill intrusion on the thermal evolution of the basin and the surrounding petroleum plays remains poorly understood.

Dramatic increases in maturity have been observed where sill intrusions come into contact with Kimmeridgean source rocks in the basin (Ilfie et al., 1999). This is demonstrated by an increase in vitrinite reflectance measured in wells close to igneous intrusions (Holmes et al., 1999) and attributed to the heating and hydrothermal circulation initiated by the intrusion events. At a basin scale, however, the effects of sill intrusion are neither uniform or well understood and are considered unlikely to impact the regional heat flow history of the basin (Holmes et al., 1999).

## **7.5 Methods**

### **7.5.1 Data**

In order to investigate the thermal effects of sill intrusion, modelling is undertaken on three, 2D seismic profiles from across the basin. Using the petroleum system models constructed in Chapter 6, Line B-B' (southern Flett Sub-basin), Line C-C' (Corona and Flett Sub-basins) and Line D-D' (Corona and Ereland Sub-basins) are modified to incorporate sill intrusion during the Paleogene volcanic event (see Figure 7.2 for location).

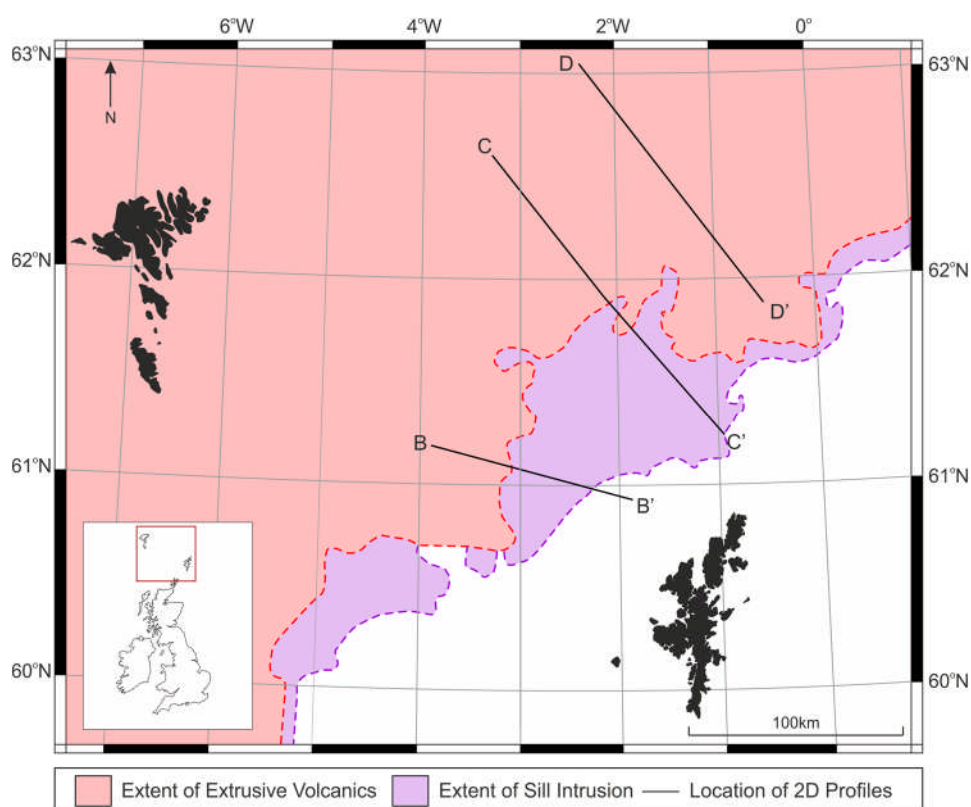


**Figure 7.2** – Map of the Faroe-Shetland Basin showing the location of 2D seismic profiles used for intrusion modelling. The lines are modified from the petroleum system modelling undertaken in Chapter 6.

The selected lines provide three distinct scenarios of sill intrusion, which have either a low, moderate or high number of sills. Line B-B' represents a low intrusion scenario with a single sill emplaced within the Upper Cretaceous sediments (Figure 7.3). Line C-C' represents a moderate intrusion scenario with multiple sills emplaced into the Upper Cretaceous and Lower Paleocene strata (Figure 7.4). Finally, Line E-E' represents a high intrusion scenario with extensive, high-density sill emplacement throughout the Cretaceous and Paleocene sediments (Figure 7.5). The depth of the source rock varies with respect to intrusion depth across the three profiles. The data provide the opportunity to study both the isolated and cumulative heat flow anomalies associated with sill intrusion and their impact potential impact on source rock maturation.

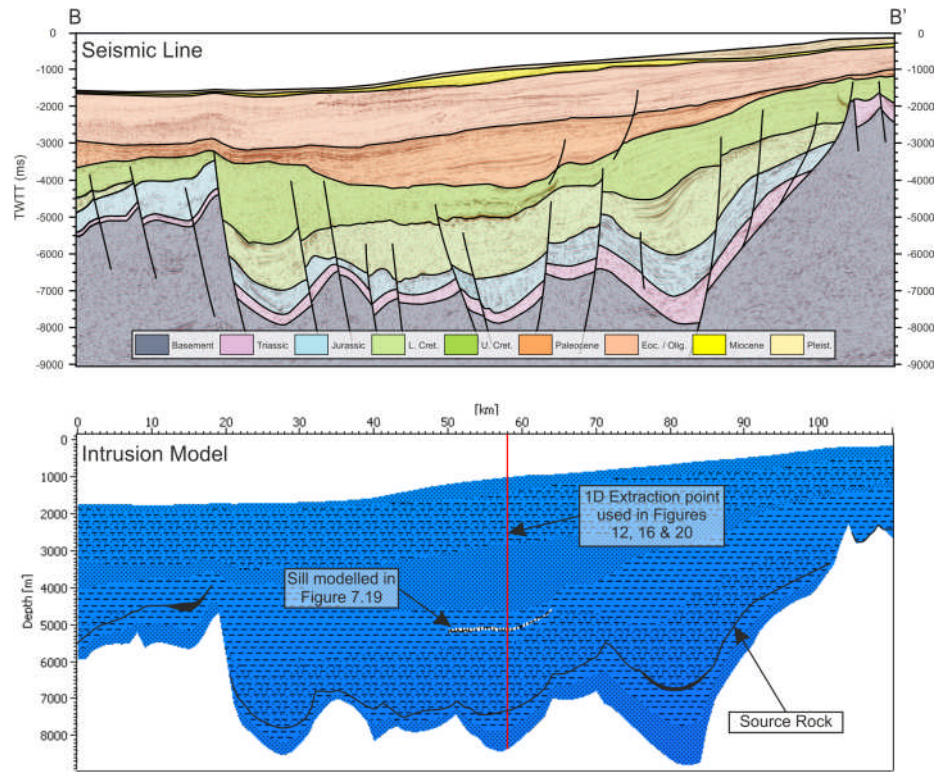


**Figure 7.3** – Line B-B’- 2D seismic profile and petroleum system model showing the location of the modelled sill. The 1D extraction points and individual sills used for analysis in this chapter are highlighted.

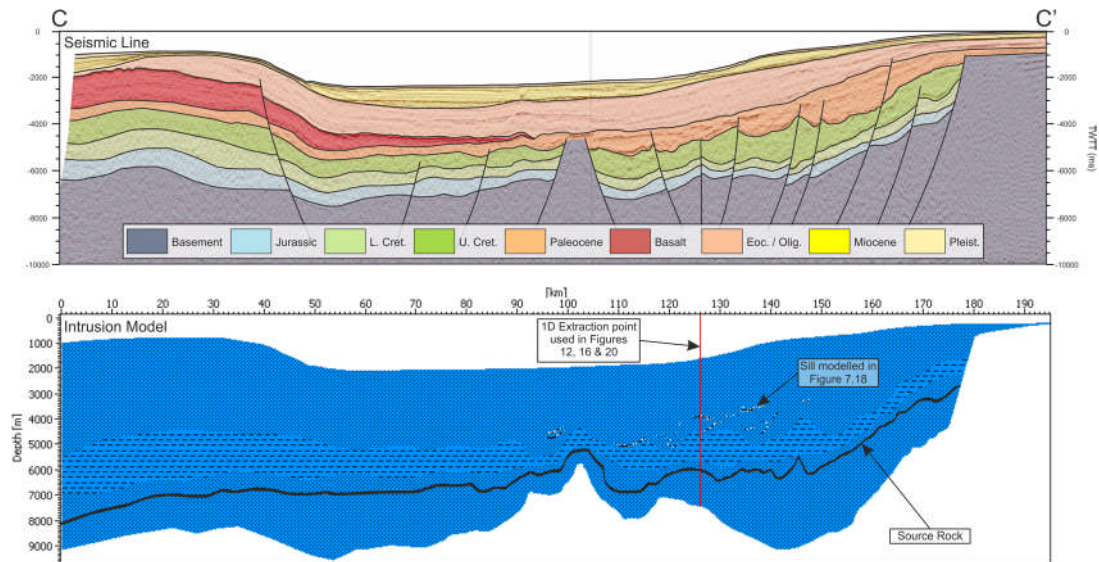


**Figure 7.4** - Line C-C’- 2D seismic profile and petroleum system model showing the location of the modelled sills. The 1D extraction points and individual sills used for analysis in this chapter are highlighted.

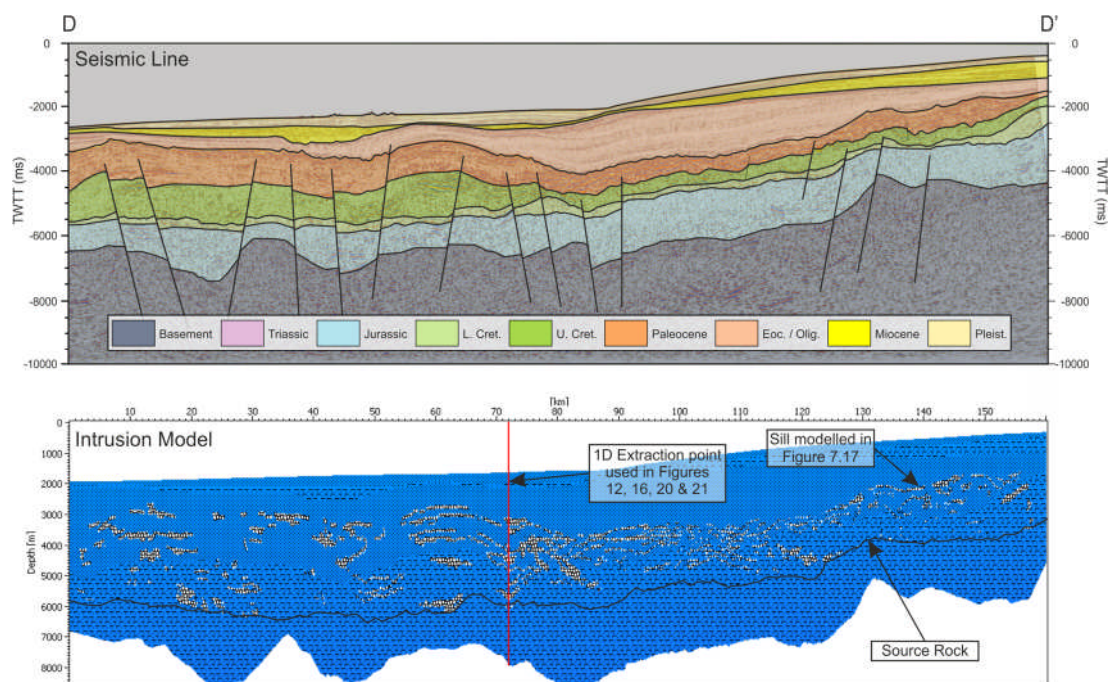


**Figure 7.5** - Line D-D' - 2D seismic profile and petroleum system model showing the location of the modelled sill(s). The 1D extraction points and individual sills used for analysis in this chapter are highlighted.

### 7.5.2 Intrusion Modelling Workflow

*Intrusion Model* within *Petromod*<sup>®</sup> (2014.1 from Schlumberger) was used to model the heat flow implications of sills. The software simulates magma emplacement by replacing an assigned sedimentary facies within pre-defined model cells with igneous rock at a given time interval. The thermal and physical parameters assigned to the igneous rock dictate the amount and rate of heat dissipation from intrusion into the surrounding sediments. The regional petroleum system modelling undertaken in Chapter 6 provides the basis for all models in this chapter, which are then modified using *Intrusion Model* to reproduce the heat flow anomalies associated with sill intrusion. The workflow for intrusion modelling used for intrusion modelling is shown in Figure 7.6.

The ability to replicate the intricate sill geometries observed in seismic data is limited by the model's grid resolution of the model. The model resolution is defined vertically by grid spacing and horizontally by the stratigraphic layers; coarse spacing of this grid can often lead to blocky or pixelated sill geometries, however, this issue

is not considered significant in the context of the final modelling results. Within all models, the horizontal grid resolution is typically between 40-120 m, this is dependent on the stratigraphy of that particular model, whilst vertical grid spacing is fixed at 1 km.

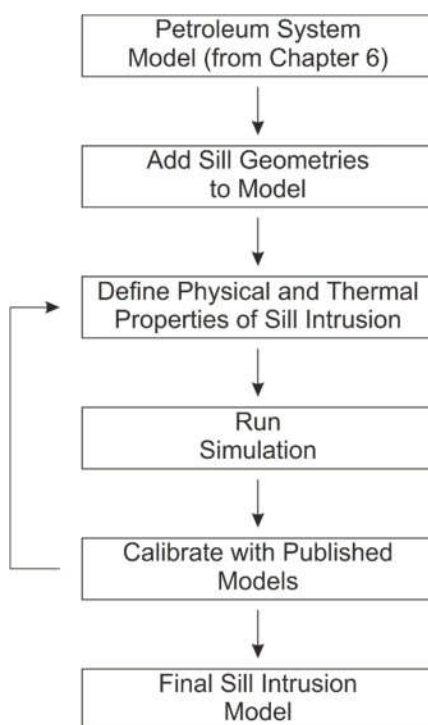


**Figure 7.6** – Flowchart illustrating the workflow used to undertake sill intrusion modelling.

### 7.5.3 Uncertainties and Limitations

In addition to the emplacement of the FSSC, up to 40,000 km<sup>2</sup> of thick flood basalt sequences were extruded across the Faroe-Shetland Basin during Early Paleogene volcanism (Naylor et al., 1999, Schofield and Jolley, 2013). The thermal effects of the flood basalts are not considered in this study for two reasons, firstly sub-aerial emplacement and the associated thermo-dynamic complications of heat flow dissipation in water are beyond the limits of the software, and secondly, their impact on underlying hydrocarbon plays is considered to be negligible (Fjeldskaar et al., 2008).

For the purposes of modelling it is assumed that all intrusions are instantaneous and synchronous. With the absence of direct well data, only relative dating techniques such as cross-cutting relationships (Hansen et al., 2004) and forced fold onlap relationships (Hansen and Cartwright, 2006, Trude et al., 2003) are available to constrain the timing of intrusion. Even by applying such techniques, the absolute date of intrusion cannot be defined and any dates assigned are likely to be speculative; consequently a regional area average age of intrusion (53 Ma) obtained from radiometric dating (Passey and Hitchen, 2011) was used for all sills. In the context of regional heat flow the absolute timing of intrusions is considered to be an unconstrained but minor variable. Whilst instantaneous intrusion modelling is considered to overestimate temperatures and therefore any potential maturation effects (Galushkin, 1997), other studies have deemed it suitable and sufficient for use in petroleum system modelling (Fjeldskaar et al., 2008).

It is noted that the thermodynamics of the *Intrusion Model* software rely entirely on conductive heat flow for the dissipation of energy away from the sill intrusion. Some authors have suggested that the effects of hydrothermal convection are insignificant, especially in low permeability rocks (Galushkin, 1997, Wang et al., 2007, Fjeldskaar et al., 2008, Aarnes et al., 2010) however, observed asymmetry in thermal alteration zones, (Galushkin, 1997, Wang et al., 2007), suggests convection may play a role. This is further supported by abnormally high geothermal gradients above the sill compared to below (Peters et al., 1978), a phenomenon that cannot be accounted for through a purely conductive system (Wang and Manga, 2015). Any role of convection, however, becomes less important with distance from the intrusion contact (Jaeger, 1964). The software is unable to incorporate hydrothermal circulation and therefore heat transfer through convection is beyond the scope of this study. It is predicted that the thermodynamic implications of convection would accelerate the rate of heat flow away from the sill bodies (Galushkin, 1997) particularly above the intrusion (Wang and Manga, 2015) as such any modelling results presented here represent a conservative scenario. The influence of convection is thought to significantly reduce with distance from the sill

body (Jaeger, 1964) and would therefore have a smaller impact on overall regional scale modelling compared to local heat fields associated with individual intrusions.

#### 7.5.4 Heat Flow Calibration

To ensure realistic heat flow anomalies are produced during intrusion modelling, calibration of heat flow profiles and predicted maturity (vitrinite reflectance - %Ro) were undertaken. In the absence of any suitable well data available in the study area the model was calibrated using published data from a variety of sources detailed below.

First, the numerical and analytical models presented by Fjeldskaar et al. (2008) are tested before the modelling results are compared to maturity aureole field observations from the Midland Valley Sill, Scotland (Raymond and Murchison, 1988). This two-phase approach demonstrates that the modelling parameters are able to reproduce established time - heat flow scenarios associated with sill intrusion as well as predicting realistic final maturation profiles as constrained by field data.

##### ***Numerical and Analytical Calibration***

The time-temperature profiles from a single 50 m thick sill emplaced at 4000 m depth are presented by Fjeldskaar et al. (2008). The 2 km long sill has an intrusion temperature of 1000°C and was emplaced within a regional temperature gradient of 20°C km<sup>-1</sup>. The subsequent heat flow from numerical modelling and software based analytical modelling are shown in Figure 7.7. The data show that the magnitude and extent of the heat flow anomaly decreases sharply in the first 500 years after intrusion, with a gradual decline thereafter. This model can be used to validate the software and workflows used in this chapter. Using *Intrusion Model* within *Petromod*® the model of Fjeldskaar et al. (2008) was reproduced, applying all published parameters; the results from *Petromod*® are plotted against the original published models (Figure 7.7).

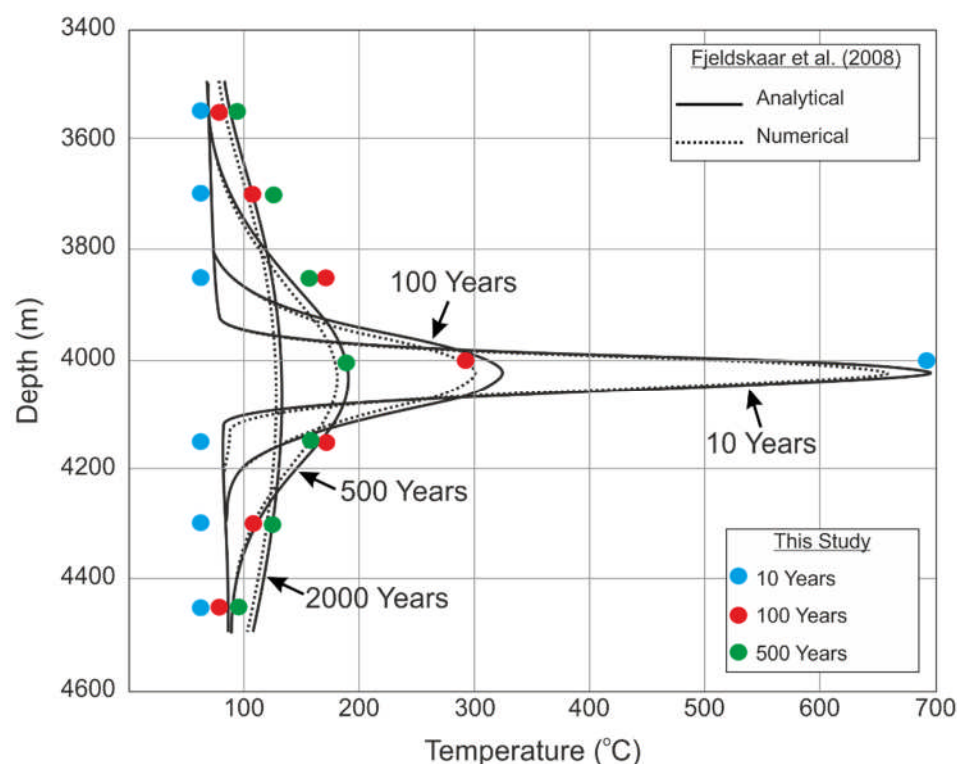


**Figure 7.7** – Calibration of sill intrusion modelling using the numerical and analytical solutions of Fjeldskaar et al. (2008). A good match can be observed between the published data and that generated using the techniques of this study.

Results show that *Intrusion model* software is capable of reproducing the numerical and analytical solutions defined by Fjeldskaar et al. (2008). Whilst excellent correlation can be observed 10 years after of intrusion, the model over-predicts temperature between 100 to 500 years after intrusion. Between 200-400m above the intrusion temperature profiles are up to 20°C higher than expected although correlation is much better below the sill. These small discrepancies in correlation could be due to a number of undefined parameters, which are not published and therefore cannot be replicated, a fluctuation in heat capacity is most likely; the ratio of heat capacities (e.g. energy densities) between basalt and country rock will directly and proportionately affect temperatures in the aureole. The porosity will also play a major role, as even immobile pore-fluid has a significant heat capacity. Overall the correlation between the results produced using Petromod<sup>®</sup> and the published numerical and analytical models of Fjeldskaar et al. (2008) is strong

enough to suggest the methods of this study are sufficient to produce realistic heat flow scenarios associated with sill intrusions.

### ***Measured Vitrinite Reflection (VR) Calibration***

Additional calibration is undertaken on published VR data from the thermal aureole above the Midland Valley Sill, Scotland (Raymond and Murchison, 1988). Using *Intrusion Model* within Petromod® the Midland Valley Sill, Scotland, is replicated by emplacing a 115m thick intrusion at 500 m depth, further thermal and physical parameters required for modelling are predicted using data from Robertson (1988) and Clauser and Huenges (1995). The results are plotted in Figure 7.8 along with the observed VR values from the Midland Valley Sill and additional numerical modelling of the same sill by Galushkin (1997).

The predicted VR reflectance profile shows excellent correlation >150 m from the intrusion contact. Poor correlation is observed <100m from the sill contact which under-predicts VR values by around 20 m. A number of parameters are undefined in the original study (Raymond and Murchison, 1988), which may account for this.

One possible explanation is the influence of convective heat flow and hot fluid circulation. This becomes increasingly relevant when considering field data as these processes have almost certainly occurred. Assuming convection accelerates heat dissipation away from the sill body and that convection is considered to have the greatest influence close to the sill-sediment contact (Jaeger, 1964), it would be expected that the measured field data shows higher temperatures in the areas closest to the sill than Petromod® model which do not consider convection at all.

This small discrepancy between field data and simulated models may also be attributed to other physical and thermal properties, which are not defined in the original study. It is anticipated that when considering the regional thermal effects of multiple intrusions, such small discrepancies between modelled and observed data will not have a significant impact on the overall result.

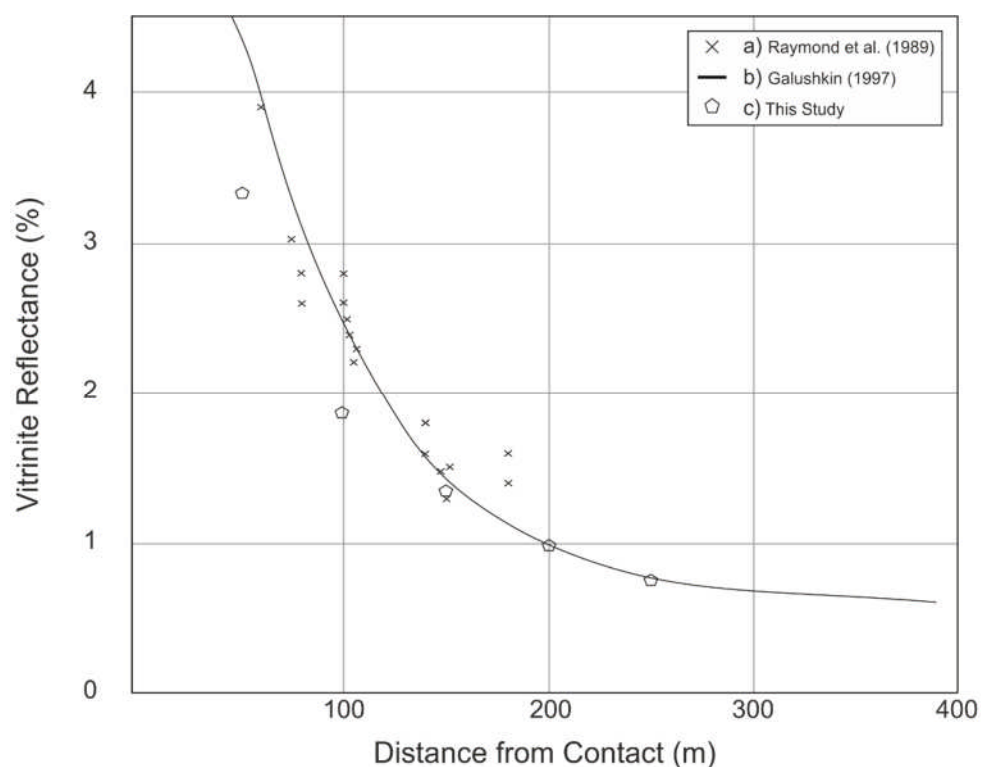


**Figure 7.8** – Heat flow calibration using measured vitrinite reflectance data from the maturity aureole above the Midland Valley Sill (Scotland). (a) Observed data (Raymond and Murchison, 1988) (b) calculated data (Galushkin, 1997) (c) modelled data from this study using *Intrusion Model* within *Petromod*<sup>®</sup>. An excellent correlation is observed >100 m from the sills, the underestimation <100 m from the sill is attributed to the effects of convective heat flow.

### ***Thermal and Physical Parameters***

The final thermal and physical parameters used for sill intrusion modelling as defined by calibration are shown in Table 7.1. These values are applied to all intrusions across all seismic profiles.

Facies	Intrusion Lithotype	Age (Ma)	Intrusion Temperature (°C)	Solidus Temperature (°C)	Magma Density (kg/m <sup>3</sup> )	Magma Thermal Conductivity (W/m/K)	Magma Heat Capacity (kcal/kg/K)	Crystallization Heat (KJ/m <sup>3</sup> )
Sill	Basalt	53	1200	920	2750	2	27	43

**Table 7.1** – The thermal and physical parameters used for intrusion modelling, values are predicted from Robertson (1988), Clauser and Huenges (1995) and are calibrated using published analytical models (Fjeldskaar et al., 2008) and field data (Raymond and Murchison, 1988).

## 7.6 Results

All igneous intrusions modelled resulted in an increase in temperature and predicted maturity in the immediately adjacent country rock. The magnitude and time scale over which this change occurs varies with emplacement depth, host rock lithology, sill thickness and sill frequency. This section presents the modelled temperature changes associated with sill intrusion, and what impact they have on predicted maturity. In addition the secondary implications of intrusion such as porosity and permeability reduction are considered.

### 7.6.1 The Thermal Impact of Sill Intrusion

#### *Regional Thermal Impact of Sill Intrusion*

The thermal impact of sill intrusion is illustrated through a series of sequential time-steps from 0 to 0.05 Ma after the intrusion event for each of the modelled profiles (Figure 7.9, Figure 7.10 & Figure 7.11). In the low density intrusion scenario (Line B-B' – Figure 7.9) the heat generated from the intrusion gradually dissipates away from the sill body with time. Immediately after the intrusion there is a substantial (500 - 800°C) increase in temperature in the area immediately surrounding the sill. As the heat dissipates the thermal aureole spreads to 2 – 3 times the sill thickness and temperatures anomalies drop to between 200 – 300°C. At 0.05 Ma the heat has dissipated such that the thermal effects can be measured up to 1km below the sill,

although the magnitude of the heat flow anomaly is only slightly above the regional geothermal gradient.

In the moderate intrusion scenario (Line C-C' - Figure 7.10) upon intrusion a substantial thermal aureole develops immediately surrounding the intrusions with temperatures reaching 500 – 800°C a distance of around 1 – 1.5 times the sill thickness. After 0.001 Ma the heat has dissipated so that temperatures are around 300 -500°C 2 – 3 times the sill thickness and 100 - 200°C 4 -5 times the sill thickness. At 0.010 Ma after the intrusion the temperature in the host sediments has increased by around 50°C a distance of 8 times the sill thickness, at which stage the cumulative effect of emplacement becomes apparent, the thermal aureoles of nearby sills began to merge and the elevated heat flow is sustained. The cumulative effect of the high density sill intrusion on Line D-D' (Figure 7.11) is so significant that temperatures of up to 500°C are maintained through to 0.05 Ma after the intrusion, long after the thermal effects of individual intrusions have all but subsided.

### ***The Thermal Impact of Sill Intrusion on In-Situ Source Rock***

In order to assess the thermal impact of sill intrusion on the Upper Jurassic source rock horizon, time – temperature plots ( Figure 7.12) were constructed for each of the 2D profiles using the 1D extraction points shown in Figure 7.3, Figure 7.4 & Figure 7.5.

The plots show that the source rock horizon in each of the three profiles experiences some degree of heating during sill intrusion, but that the magnitude of the heating event varies between profiles. Both Line B-B' and Line C-C' experience small increases in source rock temperature of < 10°C, which rapidly subsides back to the regional geotherm shortly after intrusion event. In contrast, however, the source rock sampled from Line E-E' experiences increases of up to 100 °C.

The 1D extraction points used to construct the plots have been taken from the areas of highest intrusion along each profile, and therefore, the numbers presented here represent the maximum possible thermal impact sill intrusion has on the in-

situ source rock. Analysis of the 2D profiles (Figure 7.9, Figure 7.10 & Figure 7.11) show the lateral extent of heating is limited (typically between 200 - 400 m), therefore the observed increases in source rock temperature are highly localised (typically less than 500 m laterally from the sill body), with much of the horizon remaining within the regional geothermal gradient.

### **Summary**

- Sill intrusion causes an increase in temperature of the surrounding country rock.
- The magnitude and extent of temperature increase typically increases with sill thickness, which increases the amount of heat energy into the system. It also increases with depth, due to the increased regional geotherm.
- The cumulative heating effects of multiple sill intrusions means the elevated temperatures are higher and can be sustained for longer.
- The thermal effects of sill emplacement can be measured at significant distances from the intrusion (over 1 km) although in such areas the temperature increase is small (< 50°C).

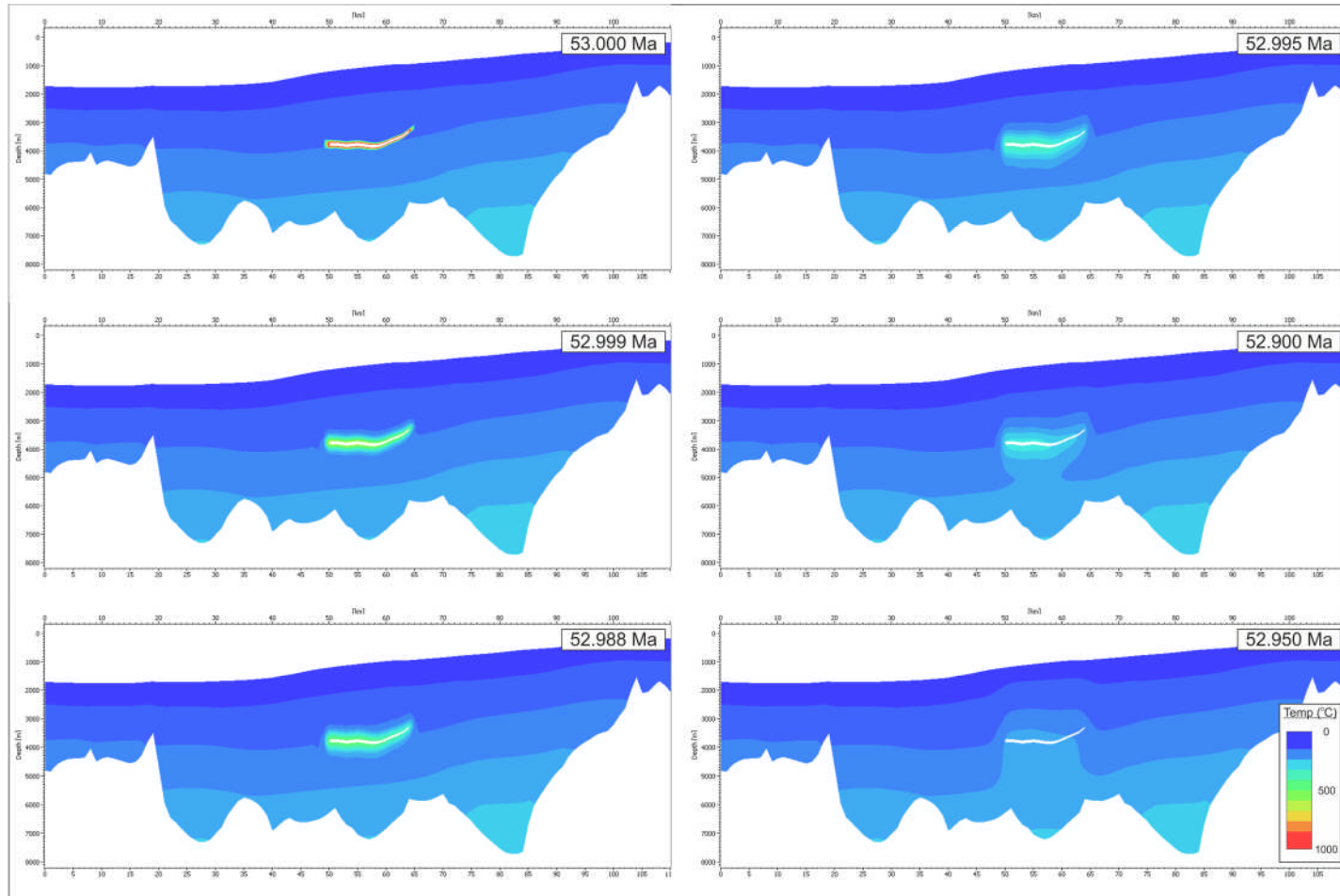


**Figure 7.9** – Sequential predicted temperature plots for Line B-B' up to 0.05 Ma after the intrusion event.

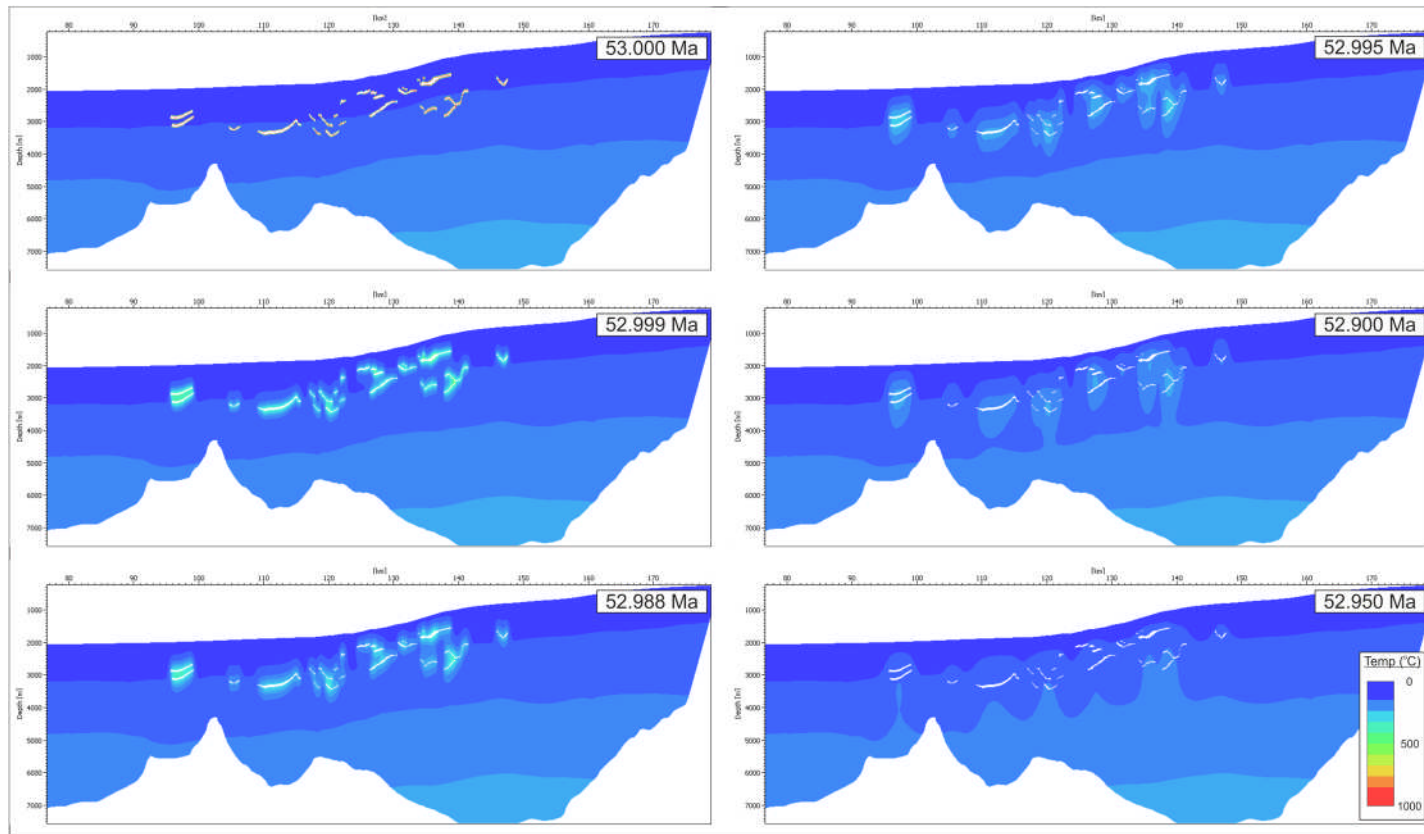


**Figure 7.10** – Sequential predicted temperature plots for Line C-C' up to 0.05 Ma after the intrusion event.

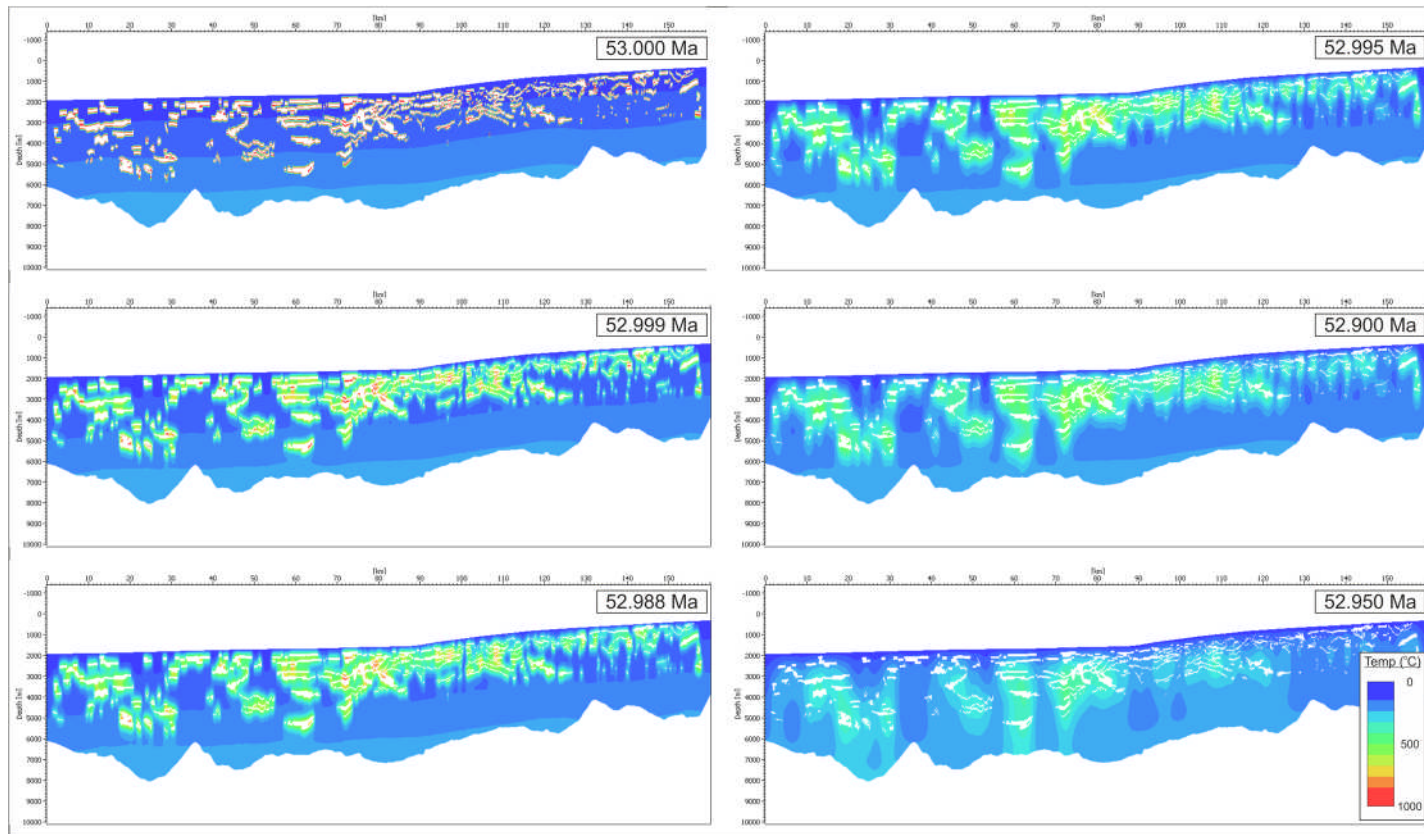


**Figure 7.11** – Sequential predicted temperature plots for Line D-D' up to 0.05 Ma after the intrusion event.

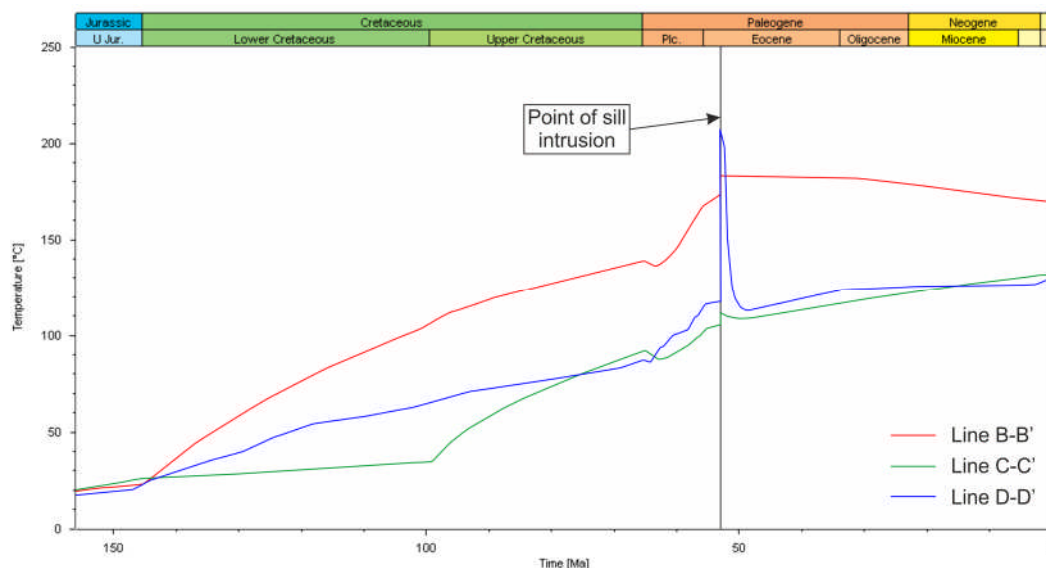


**Figure 7.12** – Time – temperature plots from the 1D extraction points (shown in Figure 7.3, Figure 7.4 & Figure 7.5) illustrating the increase in in-situ source rock temperature during the intrusion event.

## 7.6.2 The Impact of Sill Intrusion on Maturation

### *Impact of Sill Intrusion on Regional Maturation*

The impact of sill intrusion on predicted maturity (vitrinite reflectance - %Ro) is illustrated through a series of sequential time-steps from 0 to 0.05 Ma after the intrusion event for each of the modelled profiles (Figure 7.13, 7.14 & 7.15). The profiles show that each intrusion creates an area of increased maturity in the metamorphic aureole that surrounds it, which can be up to 6 times the sill thickness, although is more typically 1 -2 times the sill thickness. The level of maturity progresses from over mature (> 4 %Ro) in the areas immediately adjacent to (< 100 m) the sill through to oil mature (0.55 – 1.30 %Ro) on the fringes of the aureole (up to 500 m away). The size of the metamorphic aureole varies significantly but is generally larger around thicker and/or deeper sills.

The largest impact on predicted maturity appears to be the number of sills emplaced in a particular area, the cumulative effect of layered intrusions can be observed in Line C-C' (Figure 7.14) where the aureole around closely spaced sills amalgamates and is significantly larger than that observed around individual sills of the same thickness emplaced at the same depth. This is further demonstrated in

Line D-D' (Figure 7.15) where the high density of intrusion results in the majority of the Cretaceous and Paleocene stratigraphy being predicted to be over mature.

### ***Impact of Sill Intrusion on In-Situ Source Rock***

The time – maturation plot shown in Figure 7.16 illustrates the predicted change maturity of the Upper Jurassic source rock horizon at the 1D extraction points shown in Figure 7.3, Figure 7.4 & Figure 7.5. The plot demonstrates that for both Line B-B' and Line C-C' the thermal impact of sill intrusion is not significant enough to affect the maturation of in-situ source rock. Both profiles show an increase in source rock maturation around the time of the intrusion event, although this is attributed to the heat flow associated with lithospheric extension in the Paleocene and Early Eocene and not the intrusions (see petroleum system modelling in Chapter 6), the increase in maturation initiates before the intrusion occurs and the gradient of the line does not change during the intrusion event. In contrast, however, Line D-D' shows a substantial increase in source rock maturation associated with the intrusion of sills, the profile shifts near instantaneously from immature to over mature at the point of intrusion. Analysis of the 2D profiles (Figure 7.15), however, shows that this is a highly localised phenomenon, and only occurs in areas with the deepest sills. Elsewhere on along the 2D profile, even in areas of high sill intrusion, the in-situ source rock remains unaffected.

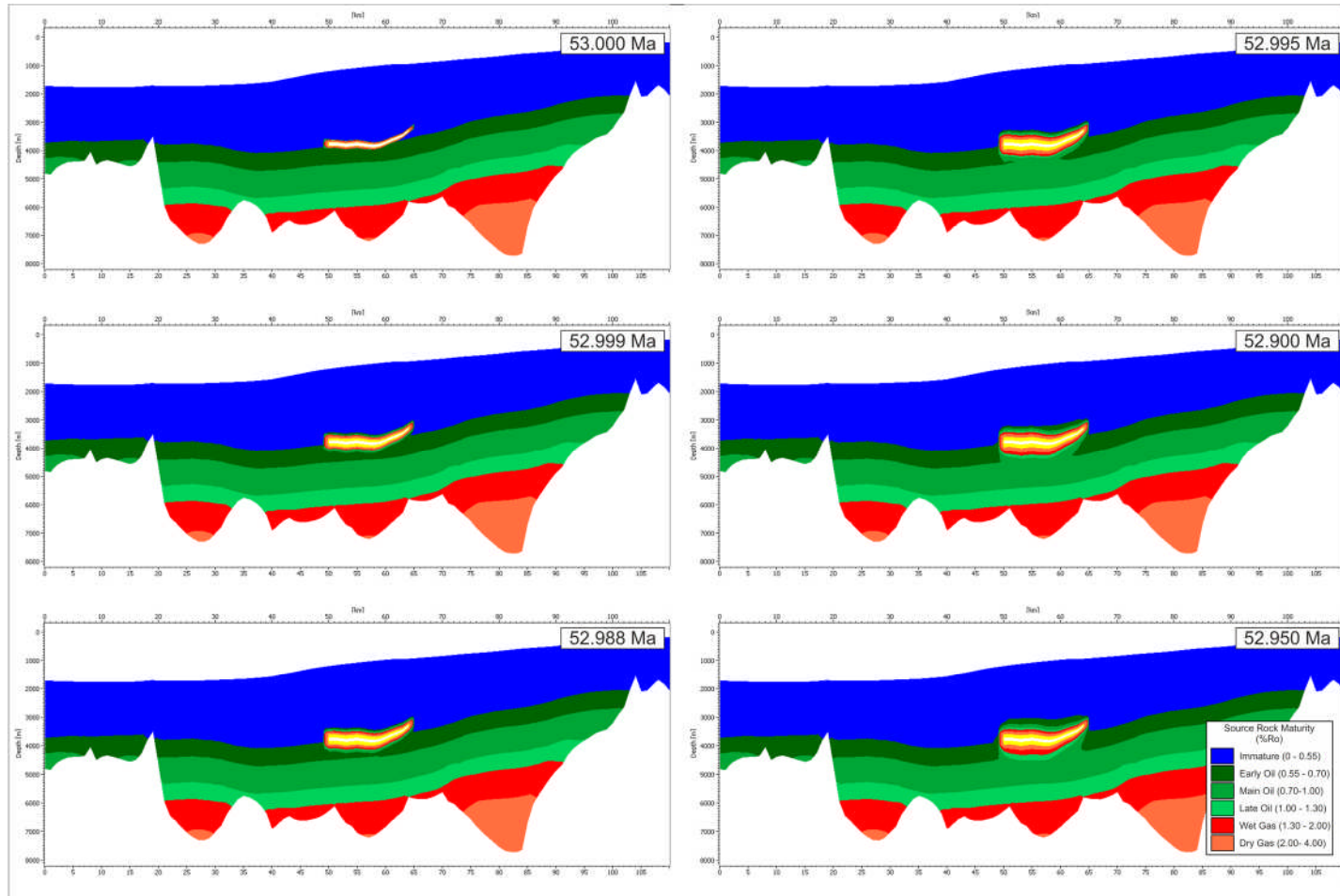


Figure 7.13 – Sequential predicted vitrinite reflectance plots for Line B-B' up to 0.05 Ma after the intrusion event.

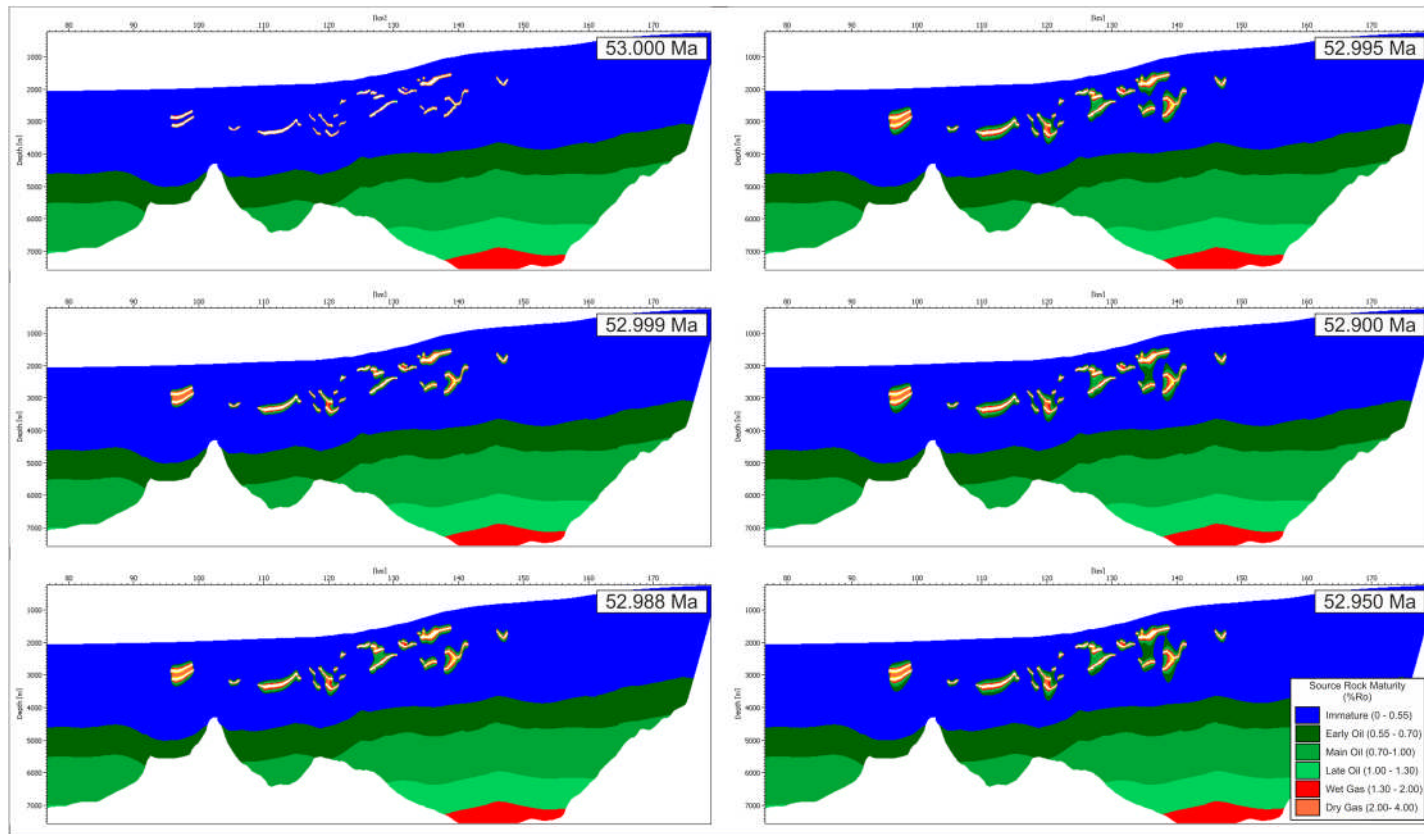


Figure 7.14 – Sequential predicted vitrinite reflectance plots for Line C-C' up to 0.05 Ma after the intrusion event.

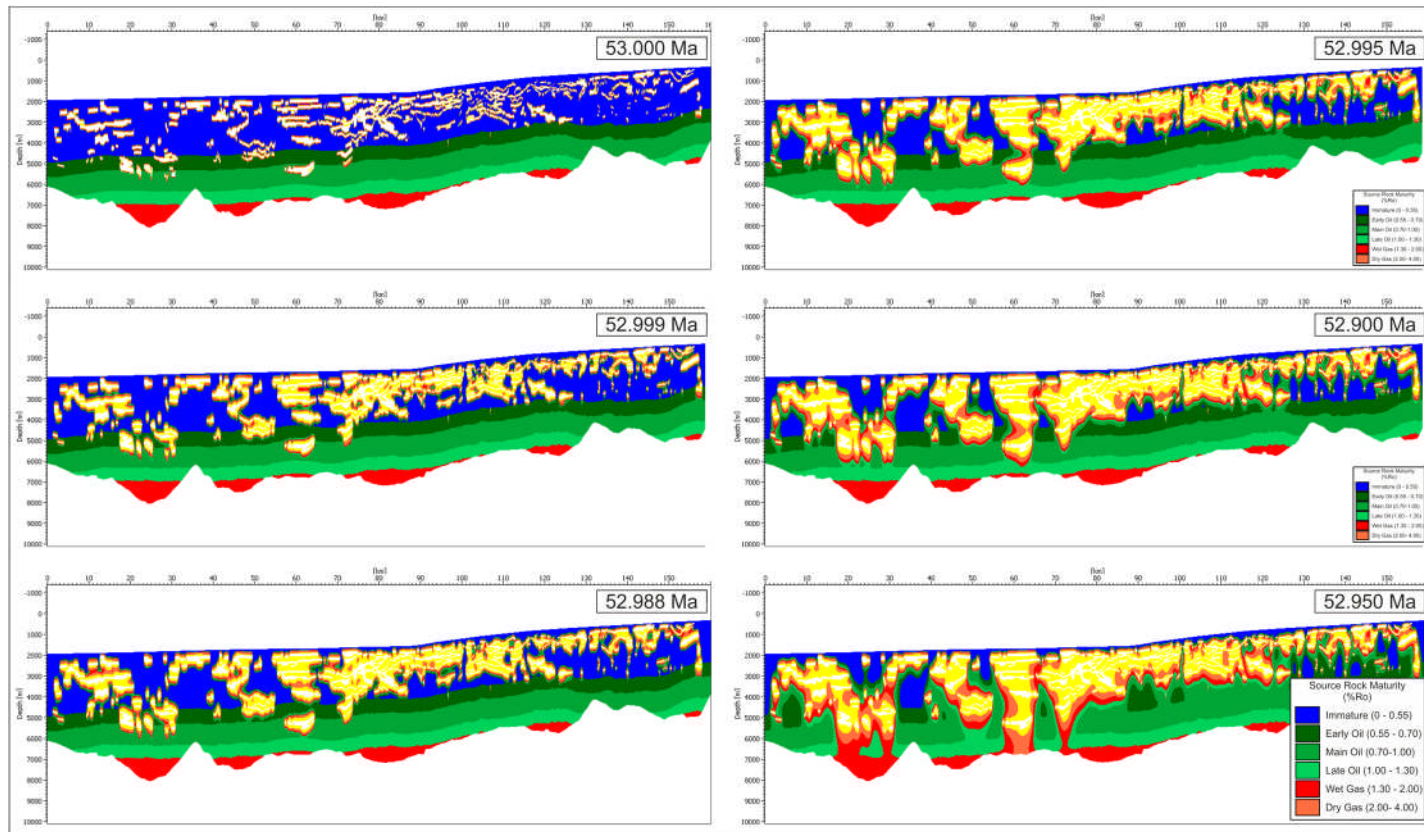
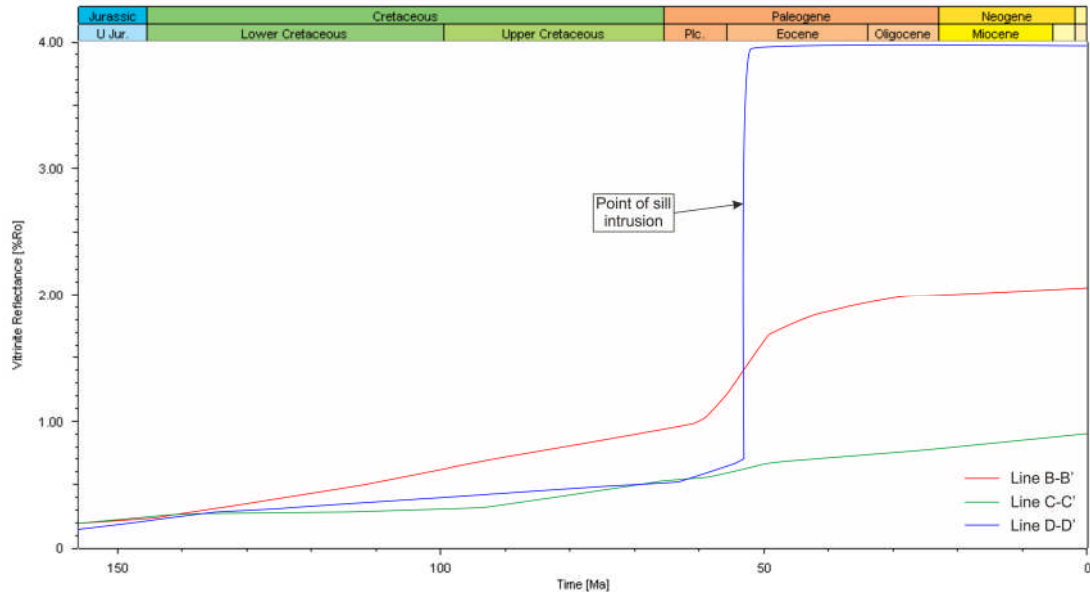


Figure 7.15 – Sequential predicted vitrinite reflectance plots for Line D-D' up to 0.05 Ma after the intrusion event.



**Figure 7.16** – Time – temperature plots from the 1D extraction points (shown in Figure 7.3, Figure 7.4 & Figure 7.5) illustrating the increase in predicted maturity of the source rock during the intrusion event.

### ***Extent of Maturation Aureole***

The relationship between the thickness of the sill and the extent of maturation is not uniform and is demonstrated through a series of plots, which illustrate the change in maturation with distance from an individual sill body (see Figure 7.17, Figure 7.18 & Figure 7.19). Measurements taken from a 40 m sill emplaced at around 200 m depth on Line D-D' (Figure 7.17) show that the predicted maturity of the surrounding host stratigraphy is affected as much as 180 m from the sill body, a distance of 4.5 times the sill thickness. Prior to emplacement, the host sediments are predicted to be immature ( $< 0.55 \%R_o$ ), immediately after emplacement an aureole of over maturity ( $> 4.00 \%R_o$ ) develops 5 m from the sill body. This is surrounded by an aureole of gas maturity ( $1.30 - 4.00 \%R_o$ ) up to 50 m from the sill body. The remaining maturation aureole is within various oil windows ( $0.55 - 1.30 \%R_o$ ) up to a distance of 180 m from the sill body, after which the original regional maturity is restored.

The sill modelled on Line C-C' is around 80 m thick and is emplaced into host sediments, which are predicted to be immature ( $< 0.55 \%R_o$ ) (Figure 7.18). After emplacement, a 25m aureole develops around the sill, within which all sediments

become overmature ( $> 4.00 \%R_o$ ). Between 25 m and 125 m from the sill the sediments are in the gas window ( $1.30 - 4.00 \%R_o$ ) and between 125 m and 200 m they are within the oil window ( $0.55 - 1.30 \%R_o$ ). Therefore, total extent of the aureole is around 200 m, beyond which there is no measured change in predicted maturity, the total aureole size is around 2.5 times the original sill thickness.

The thickest sill analysed is the single 110 m thick intrusion from Line B-B' which has a present day depth of 3771 m (Figure 7.19). The maturation profile indicates that the sediments within 150 m were over mature (1.3 times the sill thickness), the gas window is up to 440 m from the point of intrusion (4 times the sill thickness) and the oil window is 750 m from the sill contact (6.8 times the sill thickness).

Based on the examples shown in Figure 7.17, Figure 7.18 & Figure 7.19, the aureole for over maturity is between 0.16 and 1.3 times the sill thickness, the aureole for gas generation is between 1.25 and 4 times the sill thickness and the aureole for oil generation is between 2.5 and 6.8 times the sill thickness.

30 m Thick Sill Intruded at 2050 m Depth

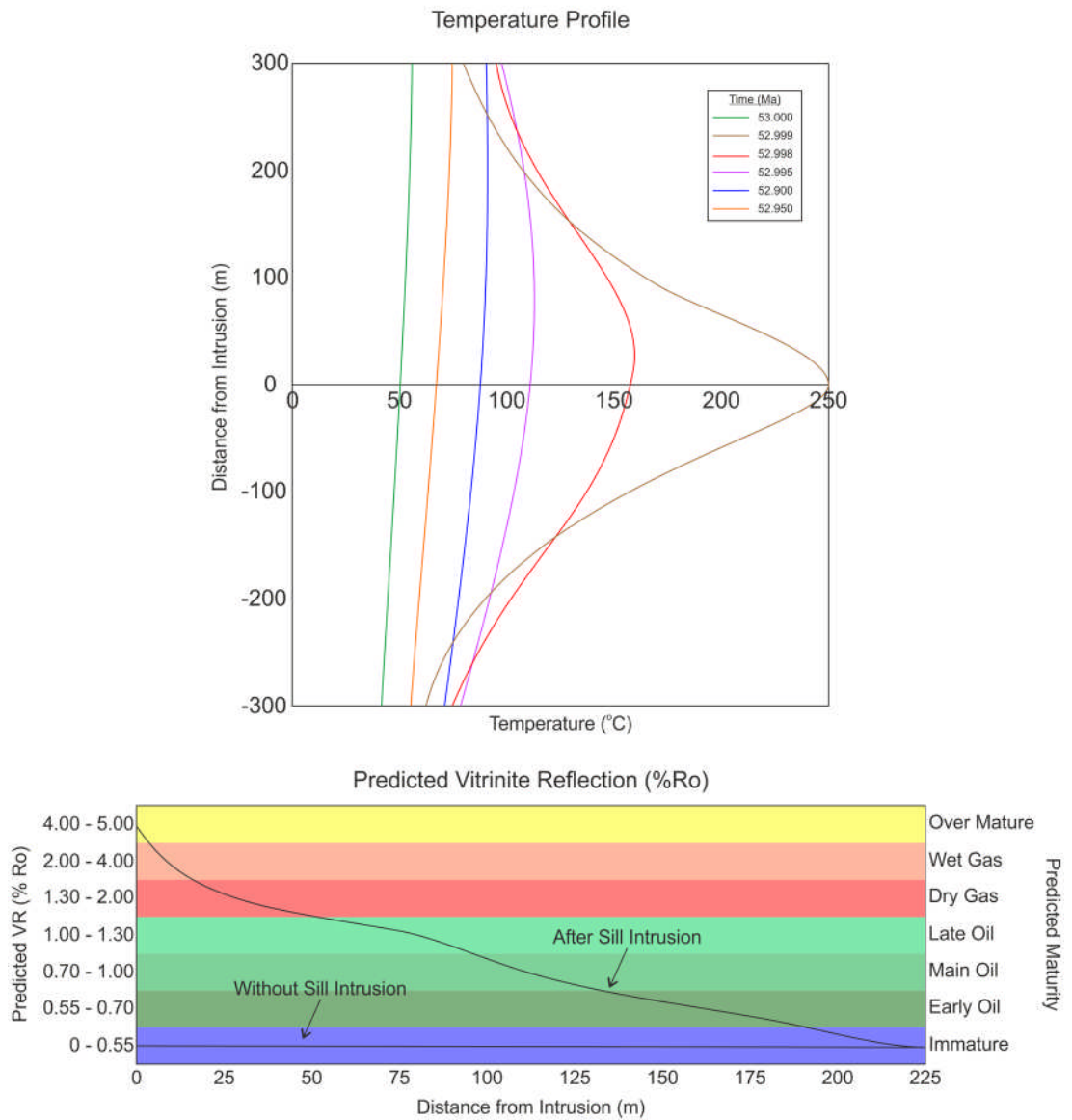


**Figure 7.17** – Time-temperature plot and predicted vitrinite reflectance profile for a 30 m thick sill intruded at 2050 m depth from Line C-C' (see Figure 7.4 for location).

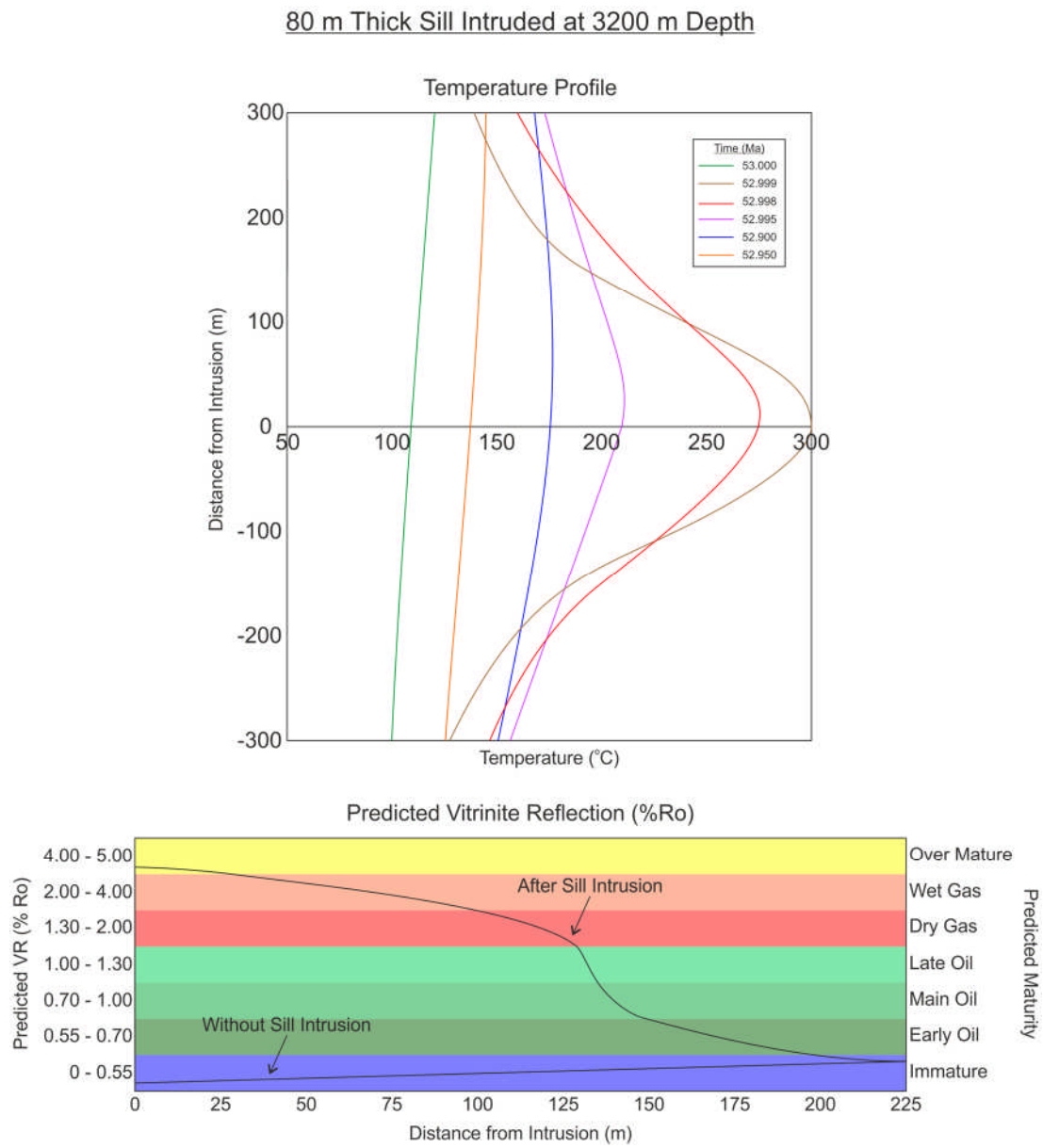


**Figure 7.18** - Time-temperature plot and predicted vitrinite reflectance profile for a 80 m thick sill intruded at 3200 m depth from Line C-C' (see Figure 7.4 for location).

110 m Thick Sill Intruded at 3771 m Depth

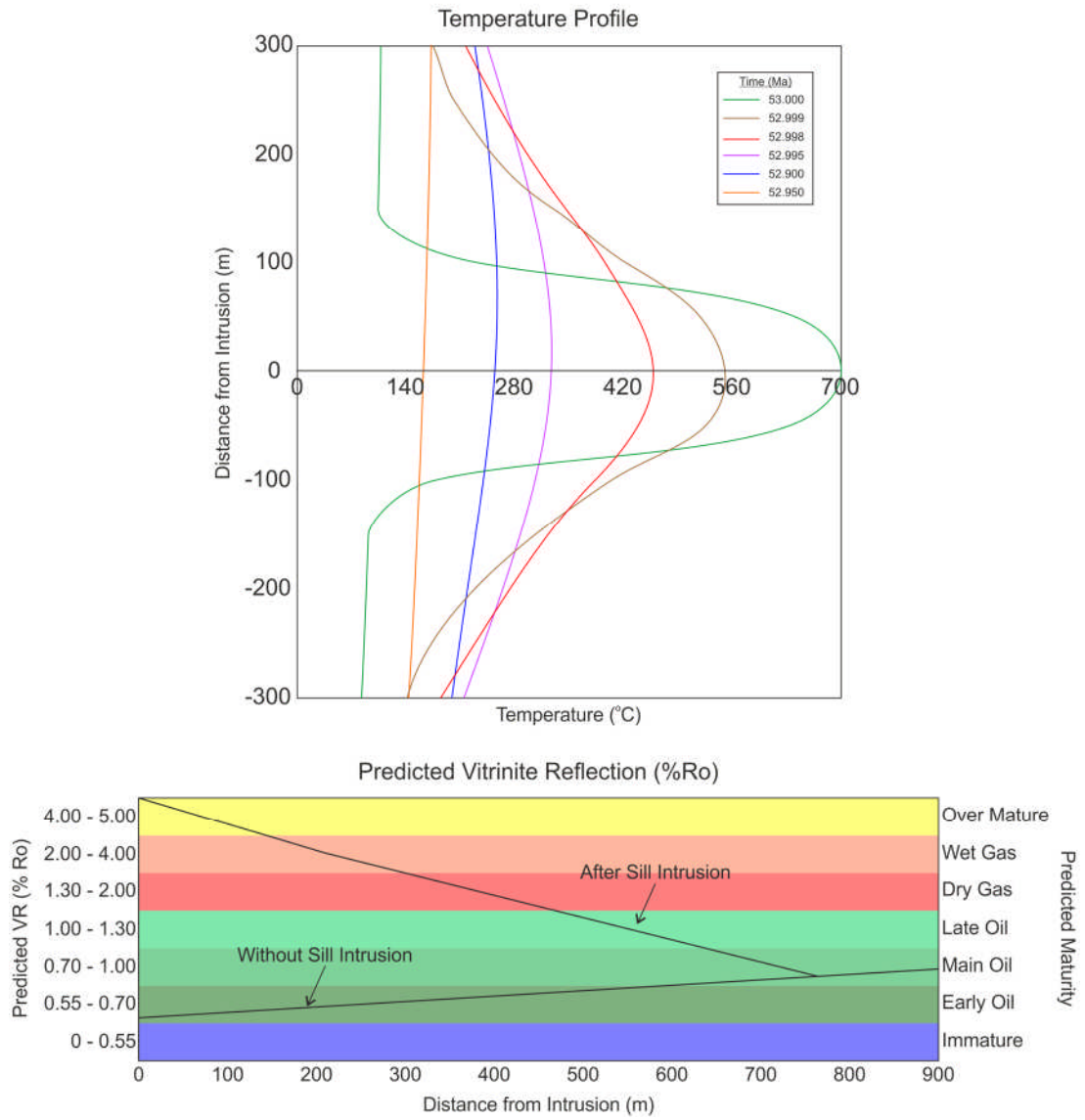


**Figure 7.19** - Time-temperature plot and predicted vitrinite reflectance profile for a 110 m thick sill intruded at 3771 m depth from Line B-B' (see Figure 7.3).

**Summary**

- All sills develop a metamorphic aureole, within which there is a notable increase in predicted maturity (vitrinite reflection - %Ro).
- The size of the metamorphic aureole is highly variable but is typically between 2 and 7 times the sill thickness.
- The size of the metamorphic aureole typically increases with thickness of sill and depth of emplacement.
- The cumulative effect of emplacement is substantial, with areas of multiple sill emplacement showing significantly larger areas of increased maturity.

**7.6.3 The Porosity and Permeability Implications of Sill Intrusion**

To evaluate the impact that sill intrusion has on the porosity and permeability of host stratigraphy, a number of 1D extractions were taken from the modelled 2D profiles (Figure 7.20). The results show that the intruded sill bodies have drastically lower porosity and permeability than the surrounding sediments. The porosity of the igneous rocks is up to 22 % lower than the host stratigraphy, whilst permeability drops by as much as 20 mD (from around 40 mD to 20 mD). The thickness of the sill and the depth at which it is intruded has little bearing on the porosity and permeability values modelled, however, the relative magnitude of porosity and permeability reduction becomes more apparent at shallow depths, where the initial values are typically higher.

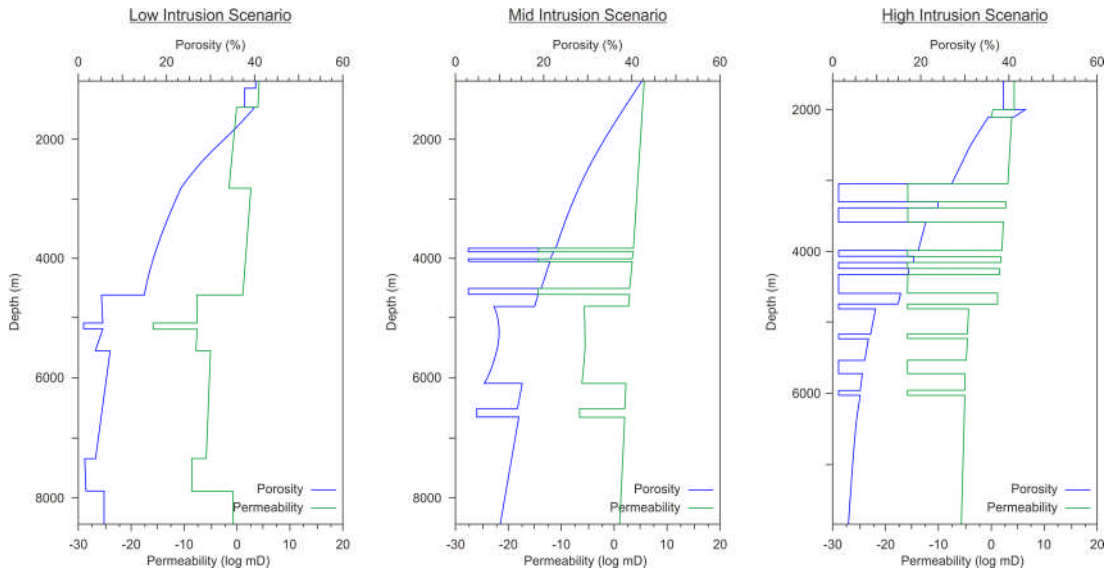


**Figure 7.20** – Porosity and permeability plots for a low (Line B-B'), mid (Line C-C') and high (Line E-E') intrusion scenario (the location of 1D extraction is shown in Figure 7.3, Figure 7.4 & Figure 7.5). The plots illustrate a dramatic reduction in both porosity and permeability between the intruded igneous rock and the host stratigraphy.

Observations show that the emplacement of igneous rock, especially areas with multiple intrusions, introduces a series of low porosity, low permeability horizons, which segment host stratigraphy, potentially acting as baffles or barriers to fluid flow. It is worth noting, however, that all observations made here are using 1D data and that actual impact on flow will also be dependent on the 3D geometry and lateral extent of the sill body.

The emplacement of sills also has implications for the porosity of the host lithology. The heat flow associated with intrusion causes contact metamorphism, which reduces the porosity of the host stratigraphy within the sill's metamorphic aureole due to recrystallization.

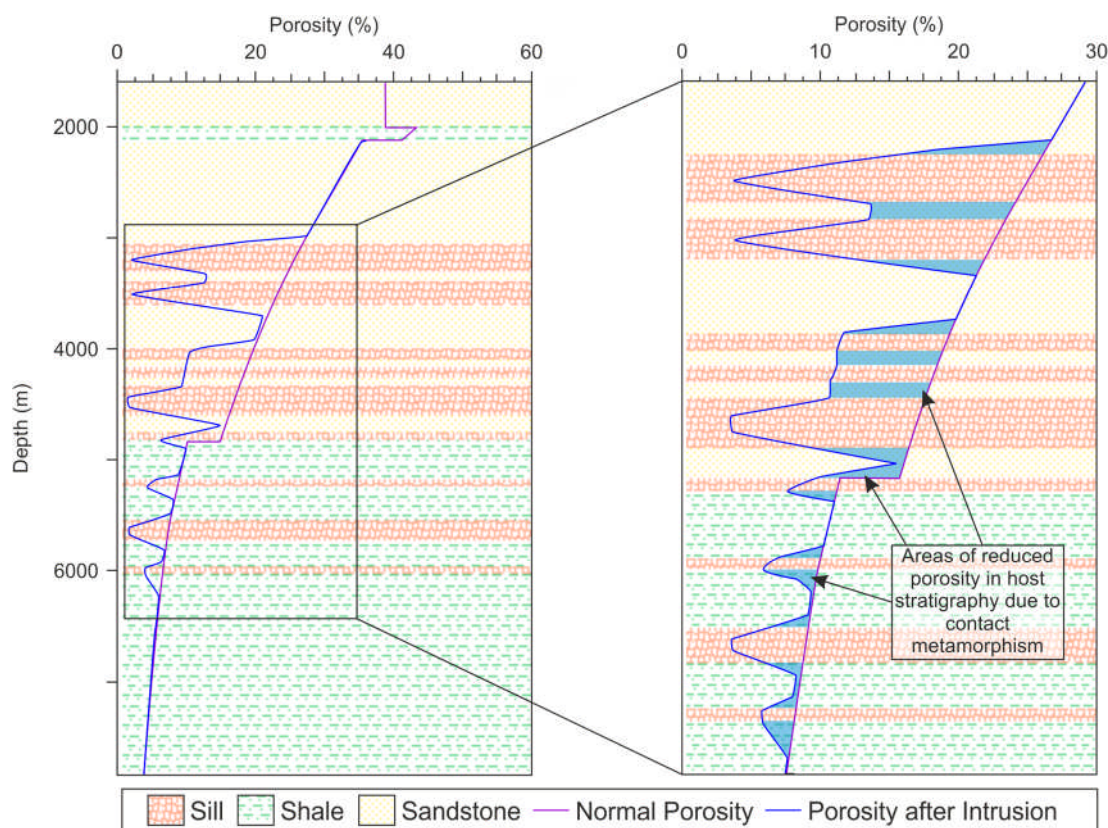


**Figure 7.21** – The effect of sill intrusion on the porosity of the host stratigraphy. Porosity is reduced by up to 20% within the metamorphic aureole of the intrusion. Sandstone lithologies experience greater porosity reduction than shale.

Comparisons between the pre-intrusion and post-intrusion porosity of sediments in this study show that contact metamorphism can reduce overall porosity of sediments by as much as 50% (Figure 7.21). The modelling results suggest that the extent to which porosity is reduced through contact metamorphism is dependent on the lithology of the host stratigraphy. Indeed, the porosity reduction in sandstone is significantly higher than in shale, as is the size of the metamorphic aureole. In the example shown in Figure 7.21, the porosity of the sandstone is between 15-30% but is reduced to between 10-15% within the metamorphic aureoles of the sills. By contrast, the porosity of shale is around 10% but drops to between 5-9% within the aureoles. The size of the metamorphic aureole is typically 1 to 1.5 times the thickness of the sill within the sandstones, although in a heavily

intruded section such as the one shown in Figure 7.21, the aureole of one sill is often overlapped by that of a nearby sill. The size of the metamorphic aureole in shale is typically between 0.3 and 1 times the sill thickness.

### **Summary**

- Sill intrusions have significantly lower porosity and permeability than the surrounding sedimentary host units.
- Contact metamorphism can reduce the porosity of the sediments adjacent to intruded sill bodies by up to 50%.
- The size of the alteration aureole varies between 0.3 and 1.5 times the thickness of sill body.
- The lithology of the host stratigraphy strongly influences the amount and extent of porosity reduction; it is typically greater within sandstones compared to shales.

## **7.7 Discussion**

### **7.7.1 The Impact of Sill Intrusion on Hydrocarbon Maturation**

#### ***The Thermal Impact of Intrusion***

The modelling presented in this chapter demonstrates that the emplacement of sills into sedimentary successions can produce a significant and widespread increase in host rock temperature. Initial temperature increases can be up to 500-800°C within the immediate vicinity of the sill decreasing to around 20°C up to 1-2 km away.

The rate of heat dissipation away from the sill body and the size of the thermal aureole are strongly influenced by the depth of emplacement, thickness of the sill and the number of other sill bodies intruded in the immediate area.

The depth at which the sill is intruded is critical, as the background temperature strongly influences the size of the thermal aureole that develops and the rate of heat dissipation from the sill body. The regional geothermal gradient naturally increases with depth, so the sills, which are emplaced into the deeper host

stratigraphy, are intruding into higher temperatures than the shallower sills. Thus the geothermal gradient between the sill intrusion and host rock is smaller as a result the intrusions cool slower (Aarnes et al., 2010).

Sills modelled in this study that have been emplaced at shallow depths (< 300 m) often lack a significant or sustained thermal aureole. This can be attributed to the rapid dissipation of heat due to large geothermal gradient associated with shallow emplacement (Galushkin, 1997) or the presence of surface water which accelerates heat flow away from the sill bodies (Raymond and Murchison, 1988).

The thermal anomaly associated with multiple sill intrusion is significantly higher and sustained for longer than with single intrusion events. This can be attributed to the cumulative heat flow of multiple sills collectively reducing the rate of heat dissipation by reducing the geothermal gradient between an individual sill and the surrounding country rock (Fjeldskaar et al., 2008, Aarnes et al., 2011).

The magma, which feeds the sill complexes observed in the area is likely to be sourced from mid-crustal magma bodies. Given the volume of sill intrusion the size of these bodies may be substantial. Although the identification and interpretation of these bodies is beyond the scope of this study it is possible they have additional thermal implications for the region.

### ***The Impact of Intrusion on Maturation***

Despite demonstrating significant heat flow potential, the actual impact of igneous intrusions on in-situ source rock maturation appears minimal. The vast majority of sills are emplaced into the uppermost Cretaceous and Palaeocene strata, which in places is over 1km shallower than the source rock horizon. As such, the short-lived heat flow anomalies associated with sill intrusion often fail to affect the maturation of source rock at depth.

The depth at which the sill is intruded is important for two reasons, the first is that the deeper the point of intrusion, the closer thermal anomalies are to the in-situ source rock and thus the more impact they can have. The second is that the background temperature strongly influences the size of the metamorphic aureole.

The geothermal gradient naturally increases with depth; at higher temperatures the gradient between the sill intrusion and host rock is smaller and so the intrusion cools more slowly (Aarnes et al., 2010), allowing a larger metamorphic aureole to develop inevitably increases the potential impact on source rock maturation.

What is apparent is that the magnitude of heat flow and thus the maturation potential of sills become significantly greater in areas of multiple intrusions, indeed, where there are many, closely spaced intrusions along Line D-D' the thermal anomaly is higher, is sustained longer and has greater impact on the source rock than elsewhere along the profile. This has been observed in other areas such as the Karoo Basin, South Africa, where the gas generation potential of the organic rich Ecca Group is up to 35% higher when the vertical spacing between two sills is less than 7 times the sill thickness (Aarnes et al., 2011).

The average zone of alteration observed during modelling as derived from predicted vitrinite reflectance profiles is 2-4 times the sill thickness; this is typically much higher than many of the published examples, which typically suggest values of less than 2 (Correia and Maury, 1975, Dow, 1977, Kendrick et al., 1978, Senger et al., 2014). The discrepancy between observations may arise from the difference in sill thickness within the published studies and those observed in seismic data. The average published sill thickness is less than 5 m with only a few notable exceptions (up to 120 m) (e.g. Raymond and Murchison, 1988), in comparison the average modelled sill thickness in this study is around 120 m. The thickness of the sill body increases the heat capacity allowing the intrusion to maintain elevated temperatures for longer (Galushkin, 1997) and thus have great influence on the predicted maturity of the surrounding sediments.

Petroleum system modelling (Chapter 6) indicates that transformation ratios of the Upper Jurassic source rock in the Central Flett Sub-basin (Line B-B') were 100% by the time of sill emplacement and so any sill intrusion in this area had no impact on maturation. In contrast, peak oil generation (50% transformation ratio) in the Corona and Ereland Sub-basins (Line C-C' and Line D-D') did not occur until the Early Oligocene to Early Miocene and therefore intrusion could potentially influence maturation. Given the modelling undertaken in this chapter it is suggested that any

impact of sill intrusion on maturation in these areas was severely localised and that the heat flow anomalies associated with sill intrusion have not significantly affected regional maturation.

### **7.7.2 Implications for Hydrocarbon Migration**

#### ***Porosity and Permeability Reduction***

Modelling in this chapter demonstrates that the sills are low porosity, low permeability bodies, and so when emplaced into sedimentary sequences have the potential to act as barriers to fluid migration. This has been demonstrated previously in areas such as the Gunnwedah Basin, Australia (Gurba and Weber, 2001), the Phetchabun Basin, Thailand (Schutter, 2003) and the Solimoes Basin Brazil (Filho et al., 2008). This is not to say, however, that all sills are always barriers to flow, indeed Rateau et al. (2013) show that sills may also act as conduits to flow, although this requires an understanding of other factors such as fracture intensity and diagenesis, which are beyond the scope of this study.

The Upper Jurassic, Kimmeridgean mudstones are considered to be the most prolific source rocks in the Faroe-Shetland Basin (Scotchman et al., 1998), which feed a number of deep water Paleocene sandstone and Eocene basin-floor fan reservoirs that form producing fields such as Foinaven, Schiehallion/Loyal and undeveloped discoveries such as Cambo, Rosebank and Laggan (Ritchie et al., 2011). The charging of these reservoirs indicates that hydrocarbon migration was occurring from below the level of sill intrusion after the time of sill emplacement and therefore must have travelled through areas of intrusion to reach the overlying reservoirs.

The emplacement of sills has been shown to reduce the porosity of the host stratigraphy by up to 20% through contact metamorphism; this in itself has implications for reduced migration but is also important when considering reservoir quality in exploration areas where sills act as prospective hydrocarbon traps (Schutter, 2003). The composition and previous burial history play an important role in controlling the extent of contact metamorphism and thus porosity reduction

during intrusion (Senger et al., 2014). Moderate to highly porous siliciclastic lithologies with limited burial or prior heating will undergo significantly greater metamorphism than shale which has been sufficiently buried and/or heated prior to intrusion (Barker and Bone, 1995).

### ***Secondary Maturation***

Observations made from the modelling undertaken in this chapter suggest that the overall impact of sill intrusion on the maturation of in-situ Upper Jurassic source rock is low, even in areas where heating is sufficient to influence maturation, as the effects are highly localised. However, the petroleum system modelling undertaken in Chapter 6 demonstrates that the Upper Jurassic source rock across much of the Flett and Corona Sub-basins began generating hydrocarbons in the Late Cretaceous and Early Paleocene and that migration pathways were established from the source rock to the surface during this time. Should migrating hydrocarbons pass through the Cretaceous and Paleocene stratigraphy during the time of emplacement then the significant local heat flow increases associated with intrusion have the potential to further increase maturity, possibly making those in the immediate vicinity over mature.

Whilst porosity and permeability reduction in the host stratigraphy has the ability to affect the migration of hydrocarbons long after sill emplacement has occurred, the thermal implications for secondary maturation are much more short-lived. The overall impact of secondary maturation is dependent on timing of hydrocarbon migration with respect to sill emplacement; even then the thermal effects are severely localised therefore the effect of secondary maturation on the overall petroleum system evolution of the basin is considered negligible.

### 7.7.3 Other Factors to Consider

Chapter 5 in this thesis makes a number of observations on the FSSC that have important implications when assessing the thermal impact of sill intrusion on regional hydrocarbon maturation, these are considered below.

#### *Seismically Resolvable Sills*

Whilst we are able to successfully model the implications of seismically-resolvable sills, data published by Schofield et al. (2015) suggests that up to 88% of the total sills intruded in the Faroe-Shetland Basin are less than 40 m thick and therefore below conventional seismic resolution. This implies that the sills modelled in this study actually only represent a portion of the total intruded magma volume. Despite not modelling a large number of the sills, those which are modelled are likely to contribute most of the bulk magma volume given their substantial thickness and surface area.

This has implications for heat flow, permeability and porosity, all of which are likely to be underestimated in the modelling presented here. Given that both this study and previous studies (Annen and Sparks, 2002, Aarnes et al., 2011) have shown that multiple, closely spaced intrusions produce larger heat flow anomalies, which are sustained for longer periods of time, the actual impact of sill intrusion in the Faroe-Shetland basin may be significantly greater than indicated by the results of this study.

#### *Magma Source and Feeding Mechanisms*

Observations of the magma source and feeding mechanisms of sills in the basin suggest that vertical dykes are an important component of the magma plumbing system. Dykes act as conduits transporting magma from deep crustal levels to the point of sill emplacement, in doing so they cross cut underlying country rock, including source rock horizons. The thermal implications of dykes have been described by previous authors (e.g. George, 1992, Cooper et al., 2007), and like sills,

are predicted to have a thermal impact on the surrounding country rock. Therefore, in areas of sill emplacement we must assume that additional heating occurs below the sills associated with the underlying dykes.

Studies have shown that the amount of heating caused by dykes can be considerably less than that associated with sills. Observations in the Raton Basin, USA, suggest that sills have a greater impact on the maturation of organic matter than dykes (Cooper et al., 2007). This has been attributed to the thermal insulation of the sills by the coal horizons into which they are intruded, the thermal conductivity of coal is low, and as such that rate of heat dissipation low. In contrast dykes cross cut through various lithologies and so have higher rates of heat dissipation. Dykes, although conduits for large volumes of magma, are relatively thin bodies compared to sills and as such, have much smaller volumes. This results in a significantly lower heat flow from dykes when compared to sills. This may have implications in the Faroe-Shetland basin where sills are predominantly intruded into Cretaceous and Paleocene shale, which will have a low thermal conductivity, in comparison dykes may travel through a series of lithologies during emplacement, including Triassic and Jurassic Sandstones, which would have a much higher thermal conductivity.

The impact of dykes may also extend to porosity and permeability reduction in host stratigraphy and the reduction in lateral migration due to segmentation of the sediments which they cross cut (Lee et al., 2006).

The feeding mechanisms identified in Chapter 5 suggest that dykes may exploit pre-existing faults to feed the overlying sill complexes, therefore in addition to the thermal and physical implications for the host rock they may also impact potential migration pathways from the source rock to any overlying plays.

## 7.8 Conclusions

- Predictive forward modelling can be used to estimate the thermal implications of sill intrusion on the maturation of organic matter.
- Modelling shows that sills have a short lived, but significant impact on the maturation of immediately adjacent sediments (< 500 m).
- The regional thermal effects of sill emplacement are small and localised.
- Sill emplacement can significantly reduce the permeability and porosity of host sediments, which has implications for hydrocarbon migration and reservoir quality.

## Chapter 8 Discussion & Conclusions

### 8.1 Introduction

The preceding chapters have discussed the controls on sill emplacement, the regional hydrocarbon maturation and the heat flow implications of sill intrusion across the Faroe-Shetland Basin. This chapter provides a synthesis of the work undertaken and assesses the potential implications that sill complexes have for regional hydrocarbon plays, addressing the data and resolution issues associated with volcanic basins. The chapter then finishes with a broader discussion on the issues of uncertainty that this project poses, and on the results of this study that are applicable to other frontier exploration regions.

The chapter is divided into three sections. The first section synthesises the tectonic, volcanic and petroleum system evolution of the Faroe-Shetland Basin. The second section considers the research questions proposed at the start of the thesis and discusses them in context of the findings. The third and final section considers the implications of this study for other volcanic passive margins and frontier exploration areas.

### 8.2 The Petroleum System Evolution of the Faroe-Shetland Basin.

The petroleum system of the Faroe-Shetland Basin was modelled with the aim of determining the maturation history of the Upper Jurassic (Kimmeridgian) source rock. The modelling results indicate that there is significant variation in present day maturity, and that maturity increases from the basin flanks towards the Flett and Foula Sub-basins in the centre of the basin (See Figure 8.1).

The principal control on the timing of maturation in the basin was the depth of source rock burial, which was determined by the rate of post-rift subsidence following Cretaceous and Paleocene rifting events. Subsidence following the Cretaceous rift event was highly localised, with the highest rates observed in the central Flett and Foula Sub-basins. As a consequence, source rocks here begin

generating oil by the early late Cretaceous and gas by late Cretaceous, which is consistent with previous observations (e.g. Holmes et al., 1999). By the onset of Paleocene rifting, many of the early areas of generation were either within the gas window or over mature and so the substantial thermal anomaly associated with depth-dependent stretching of the lithosphere during this time had little influence on maturation in these areas (See Figure 8.1).

There were, however, areas of the basin that were immature at the start of the Paleocene, such as the southwest and northeast Flett Sub-basin and the Corona and Ereland Sub-basins. The heat flow anomaly associated with Paleocene rifting was sufficient to induce maturation in the southeast Flett Sub-basin, with subsequent subsidence causing maturation of the Corona and Ereland Sub-basins shortly afterwards.

The maturation history of the Upper Jurassic rock source is currently poorly understood in the northeastern areas of the basin and has largely been overlooked in previous basin modelling studies (e.g. Holmes et al., 1999, Iliffe et al., 1999, Jowitt et al., 1999, Scotchman et al., 2006). The data and resolution issues associated with igneous complexes in the area make modelling highly uncertain, however, the application of sensitivity analysis and the production of regional scale heat flow models in this study have helped produce a more constrained model for hydrocarbon maturation in the area, within certain limits of confidence.

Sill intrusion is not believed to have any significant impact on the overall regional maturation patterns in the basin, although modelling suggests it may have local implications in the Ereland Sub-basin. The importance of sill intrusion to the prospectivity of hydrocarbon plays in the area is discussed in Section 8.3.3.

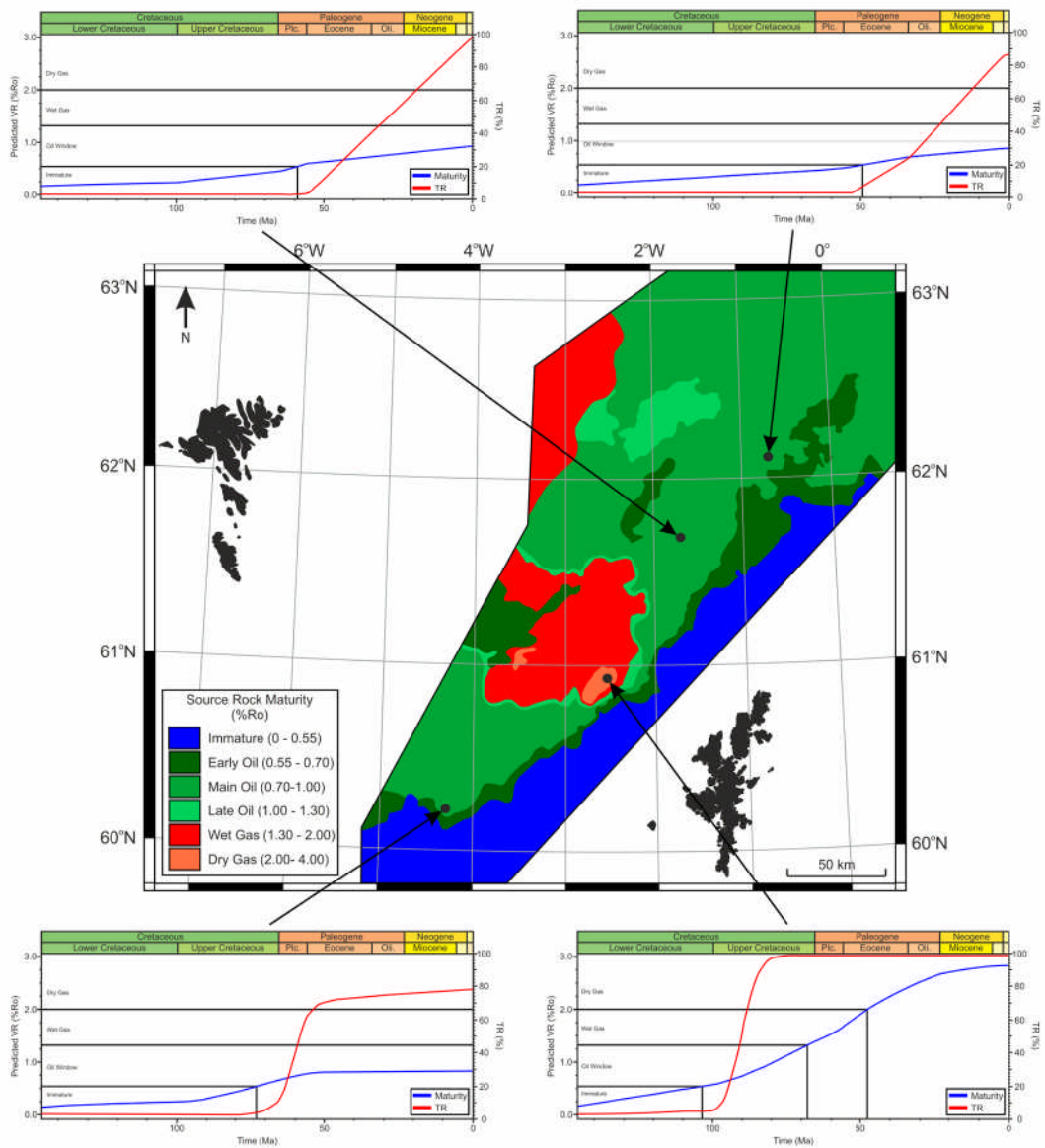


**Figure 8.1** – Map showing the present day maturity of the Faroe-Shetland Basin, with maturation and transformation ratio plots illustrating the hydrocarbon generation history in different areas of the basin.

### 8.3 Research Questions

This section considers the key findings from the preceding chapters and places them into the context of the research questions proposed in Chapter 1.

#### 8.3.1 Question 1 – How does regional basin structure and magma supply affect the emplacement of sill complexes along passive-margins?

Observations of the Faroe-Shetland Sill Complex (Chapters 4 & 5) suggest that not only does pre-existing basin structure control the location of sill intrusion, but that it also influences the style of emplacement and the geometry of individual sill bodies.

Intrusive igneous complexes are one of the earliest volcanic products to form in the stages preceding continental break-up (Planke et al., 2000), and observations suggest that this early phase of magmatic activity is strongly influenced by pre-existing basin structure, with the NE-SW trending Lewisian basement ridges and Mesozoic rift faults controlling the distribution of magma into the basin. As the sill complex develops, away from the future spreading centre the style of sill emplacement evolves, both in response to reduced magma supply and to the changing structural regime into which it is emplaced (See Figure 5.21 – Chapter 5).

It is likely that the preferential thinning of the lithosphere during multiple Mesozoic rift events (Permo-Triassic to Cretaceous) has focused the upward migration of mantle derived magma (Thompson and Gibson, 1991), controlling the site of sill emplacement. Indeed, the alignment of igneous complexes with structural discontinuities has been observed by various authors (e.g. Sykes, 1978, Jacques and Reavy, 1994). In this study these structures are parallel to the final break-up orientation, however, other authors have demonstrated igneous complexes may also form along trends which are either sub-parallel (Archer et al., 2005) or even perpendicular (Marsh, 1973) to the line of incipient break-up. This may in part be a function of the oblique orientation of rifting and eventual continental break-up (Mohammed et al., 2016).

In the northeast Corona Ridge region of the Faroe-Shetland Basin, the main points of magma input into the basin are the northern splay of the Corona Ridge and the Flett Sub-basin. In the Flett Sub-basin, magma input is predominantly through vertical dykes in the deepest grabens and through large basement-bound faults towards the southeast. These points of magma input are all sites of preferential thinning during rifting. Other studies suggest that the Flett Sub-basin continues to feed sills along the flank of the southern splay of the Corona Ridge many kilometres south (Schofield et al., 2015).

Once the magma has reached the depth of emplacement, the pre-existing structure still exerts significant influence. Faults within the area of emplacement are key in controlling the size and morphology of the intruded body, as demonstrated by the different sill facies observed in different structural regimes in Chapter 4.

It is therefore concluded that the Mesozoic rift architecture of the Faroe-Shetland Basin plays a key role in the distribution and emplacement of intrusive igneous complexes across the area.

### **8.3.2 Question 2 – How can we reduce uncertainty in the interpretation of sill complexes and petroleum system modelling in frontier exploration regions?**

The concept of uncertainty is critical when undertaking petroleum system modelling on a regional scale or in areas with limited data. Understanding how sensitive such a model is to each input parameter and how accurately that parameter can be defined with the data available is the key to producing robust, realistic models.

The decision matrix in Figure 8.2 shows the main work elements from each chapter in this thesis, providing a qualitative ranking of uncertainty for the data and methods used to undertake each work element, what impact this has on the final modelling results, and the confidence with which the conclusions can be presented.

Overall, the seismic and well data used in the study were sufficient to undertake all tasks with either a low or moderate level of uncertainty. The data, however, becomes increasingly uncertain when performing interpretation or calibration at depth.

The issue of seismic resolution at depth, especially around the source rock horizon is primarily due to the widespread presence of igneous rock, which covers much of the central and northeast areas of the basin (Passey and Hitchen, 2011). Accurately determining the depth of the source rock is critical to predicting the timing and extent of maturation in the basin. Whilst it is also hard to predict the thickness of the source rock this is not considered to affect the timing of maturation, although source rock thickness may strongly influence volumetric calculations. The modelling undertaken in Chapter 6 demonstrates that source rock burial due to post-rift subsidence is one of the major controls on maturation in the area and so understanding the depth of present day source rock burial is essential. As a consequence, the petroleum system in the southeast area of the basin, which is free from intrusion, is not only better studied, but substantially better understood (Holmes et al., 1999, Iliffe et al., 1999, Jowitt et al., 1999, Scotchman et al., 2006).

Well data in the basin are largely restricted to the flanks of the basin and structural highs; very few wells penetrate the source rock in the deeper, more central areas of the basin. As such, the wells used in this study had limited control on the source rock horizon. The spacing of the wells also limited the extrapolation of lithological facies across regional 2D lines, although it can be considered that such a lack of data is typical of most, if not all, frontier exploration regions. Ultimately, the number of wells within the Faroe-Shetland Basin is significantly higher than in true frontier regions such the West Greenland Margin (Alsulami, 2014), offshore South Africa (Paton et al., 2007), East African margin (Schull, 1988), however, the restriction of wells to basin flanks and structural highs combined with their limited penetration depth means few are genuinely useful for identifying source rock at depth or calibrating the heat flow models within the source rock horizon.

Predicting heat flow in frontier or data-limited basins remains one of the greatest uncertainties, especially on a regional scale. As discussed in Chapter 6 the

application of constant heat flow or simple depth-uniform stretching models may be appealing, given that they can be confidently constructed with little to no data. In the Faroe-Shetland Basin, however, these models fail to account for the increased heat flow associated with depth-dependent stretching during the Paleocene (Fletcher et al., 2013). Preferential stretching of the mantle lithosphere in comparison to the upper crust results in a higher than expected heat flow during rifting than through depth-uniform stretching alone (Kusznir et al., 2005) and is required to successfully explain the thermal evolution of the Faroe-Shetland Basin. Through flexural backstripping, variable stretching factors can be established across individual profiles, producing a heat flow model consistent with the tectonic evolution of the basin. The technique is strongly recommended for data-limited areas where constraining heat flow is otherwise problematic, at present published studies do not consider risking uncertainty in such basins.

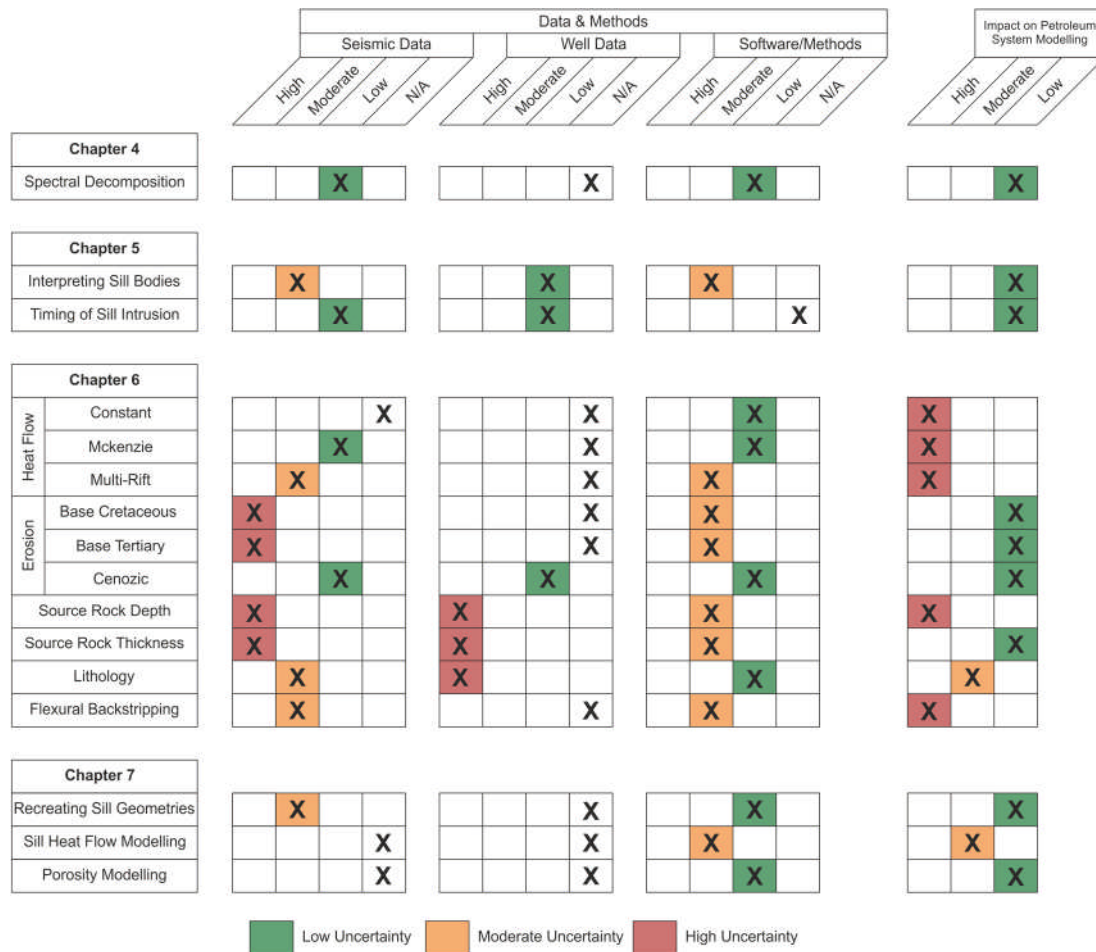


**Figure 8.2** – Decision matrix illustrating the level of uncertainty associated with the different data types, methods and software used to undertake key tasks in each chapter of this thesis. The overall level uncertainty is then assessed with regards to its impact on petroleum system modelling.

### 8.3.3 Question 3 – How has the intrusion of the Faroe-Shetland Sill Complex impacted hydrocarbon systems in the Faroe-Shetland Basin?

The map shown in Figure 8.3 illustrates the distribution of potential hydrocarbon plays and areas of sill intrusion within the Faroe-Shetland Basin. The majority of the Mesozoic plays, including the Otter Bank Formation, Rona Member Sandstone, Victory Formation Sandstone and the Solan Sandstone Member plays are found in southwestern sub-basins or towards the southeast shelf. These areas are free from igneous intrusion and therefore the impact of the Faroe-Shetland Sill Complex on the prospectivity of these plays is considered to be zero.

There are, however, a number of plays that occur in areas of sill intrusion including the Commodore Formation, Paleocene Sandstone and Eocene Fan plays, which may potentially be influenced by the intrusion of the Faroe-Shetland Sill Complex.

From the sill intrusion modelling undertaken in Chapter 7, it seems unlikely that the emplacement of sills has caused any substantial thermal impact on hydrocarbon maturation associated with these plays. The source rocks across much of the central areas of the basin were mature and in some areas even over mature for hydrocarbon generation before the main phase of sill intrusion. Furthermore, the relative depth between the sills and source rock horizon was large enough that any potential heat flow implications on the in-situ source rock were minimal and localised.

There are, however, still a number of implications that sill intrusion may have on these plays as illustrated in Figure 8.4. Sill intrusion has the potential to influence migration, reservoir compartmentalisation, seal integrity and trap formation.

Indeed, sills are believed to have influenced the migration of hydrocarbons associated with both Paleocene Sandstone (Schofield et al., 2015) and Eocene Fan Plays (Ritchie et al., 2011). In addition, the modelling undertaken in Chapter 7 shows the significant role that sill intrusion can play in the porosity reduction of host stratigraphy; this can have further implications for migration as well as the reduction of reservoir quality when sills are emplaced close to or around potential plays.

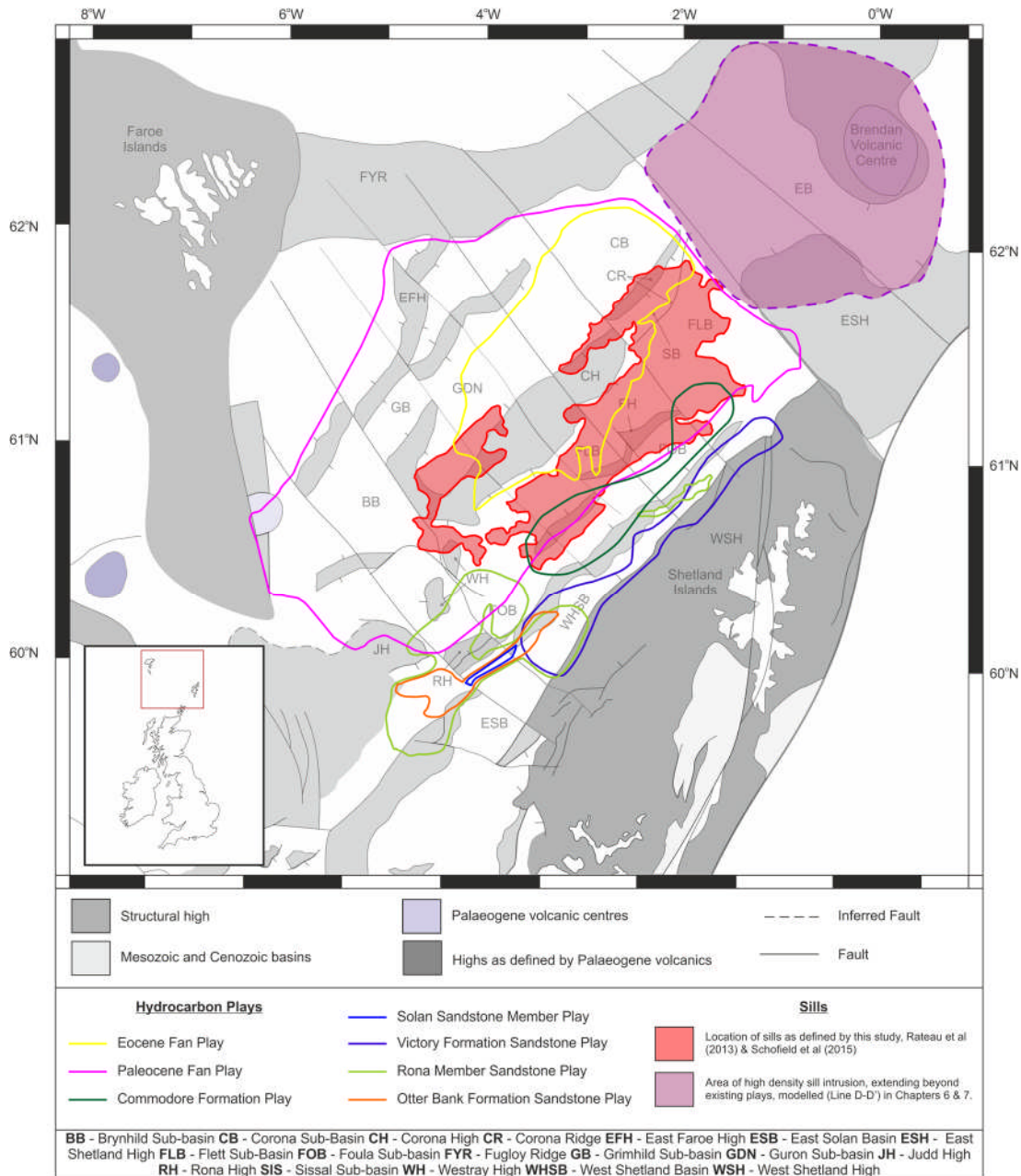


**Figure 8.3** – Map of the Faroe-Shetland Basin showing the distribution of hydrocarbon plays (after Ritchie et al., 2011) and the distribution of sills as observed in this study and in other published studies (Rateau et al., 2013, Schofield et al., 2015). The spatial correlation suggests the impact of sill intrusion on prospectivity is only a consideration in the Eocene Fan, Paleocene Sands and Commodore Formation Plays.

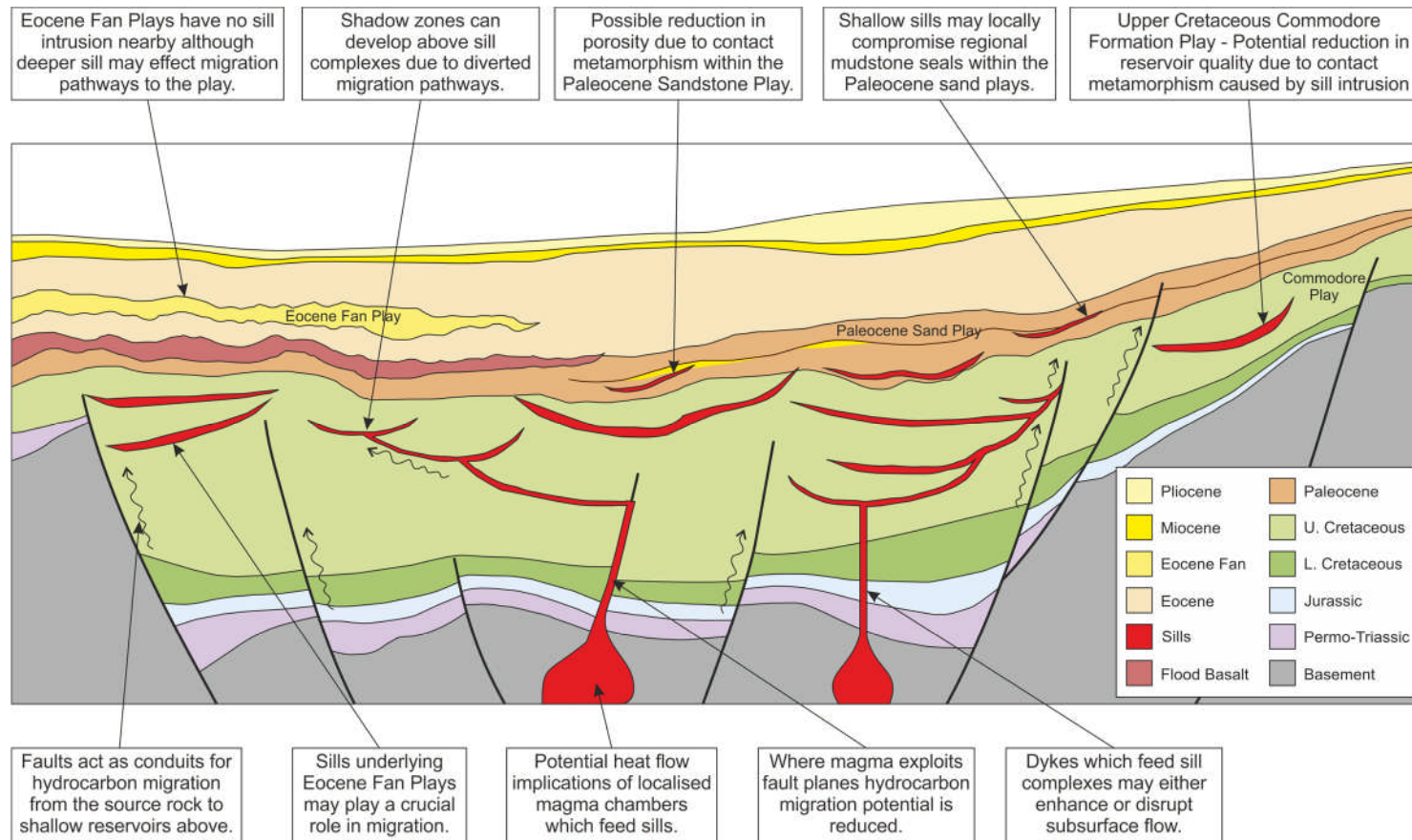


**Figure 8.4** – A schematic illustration of some of the potential implications of sill intrusion on the Commodore Formation, Paleocene Sandstone and Eocene Fan Plays.

The northeast area, around the NE Corona and Ereland Sub-basins, is largely under-explored with respect to hydrocarbon prospectivity (Ritchie et al., 2011). There is theoretically potential in these regions for Paleocene Sandstone or Eocene Fan plays, although the impact of intrusion is substantially greater here than across the rest of the basin, as demonstrated by the modelling shown in Chapter 7. As such, any exploration would carry a significantly higher risk than that undertaken in the central or indeed southeast areas of the basin.

#### **8.4 Applications to Other Areas**

The Faroe-Shetland Basin is but one of a number of volcanic basins with hydrocarbon potential, indeed, active exploration is ongoing in volcanic basins worldwide (Magee et al., 2016). The preceding chapters demonstrate that the thermal influence of the sill intrusion on hydrocarbon maturation in the Faroe-Shetland Basin is minimal, largely due to the distribution of the intrusive bodies, the depth of emplacement and the relative timing between regional maturation and emplacement. Despite this, however, the modelling undertaken indicates that given the correct conditions the heat flow implications of intrusion are entirely sufficient to cause maturation of a given source rock, consistent with observations noted elsewhere (eg. Aarnes et al., 2011).

There are a number of volcanic regions worldwide in which sills are intruded around and within source or reservoir intervals, where the potential impact of sill intrusion may be significantly greater than that predicted in the Faroe-Shetland Basin. One such area is the Western Australian Continental Margin, in particular, the Exmouth Plateau and Browse Basin, which has a series of intrusions within the Triassic – Jurassic stratigraphy (Barber, 1988). The source rocks in the area include the Lower Triassic Locker Shale and the Upper Triassic Mungaroo Formation, the later containing fluvio-deltaic reservoir sands (Exon and Willcox, 1978, Holford et al., 2013). Although burial depth alone (up to 5-6 km) is sufficient to explain the present day hydrocarbon maturation of the source rock, the potential influence of sills in the timing and development of maturation has not been fully explored

(Rohrman, 2012). Furthermore, intrusion into the siliciclastic reservoir has additional implications for migration, porosity, permeability and seal integrity.

Another example is the Vøring Basin, Norwegian Sea. The Jurassic source rocks in the area are unproven due to the thick Cretaceous successions but are considered to be over mature (Aram, 1999). There are, however, potential source rock horizons within the Cretaceous succession, which has been subjected to intense sill intrusion (Planke et al., 2005). It has already been demonstrated that sills in the area have the potential to significantly enhance the transformation ratio of the Cretaceous succession into which they are emplaced (Fjeldskaar et al., 2008), therefore further consideration should be giving to the relative timing of regional maturation and sill emplacement in the context of the petroleum system evolution of the area.

Aside from the examples given above, there are further potential areas which merit additional investigation including offshore East and West Greenland, Brazil, Angola, Senegal, and China (see Figure 8.5). The techniques and workflows presented in this thesis show that even in data-limited, frontier exploration regions the risks associated with igneous intrusions can be greatly reduced by considering and modelling their influence of regional petroleum systems.

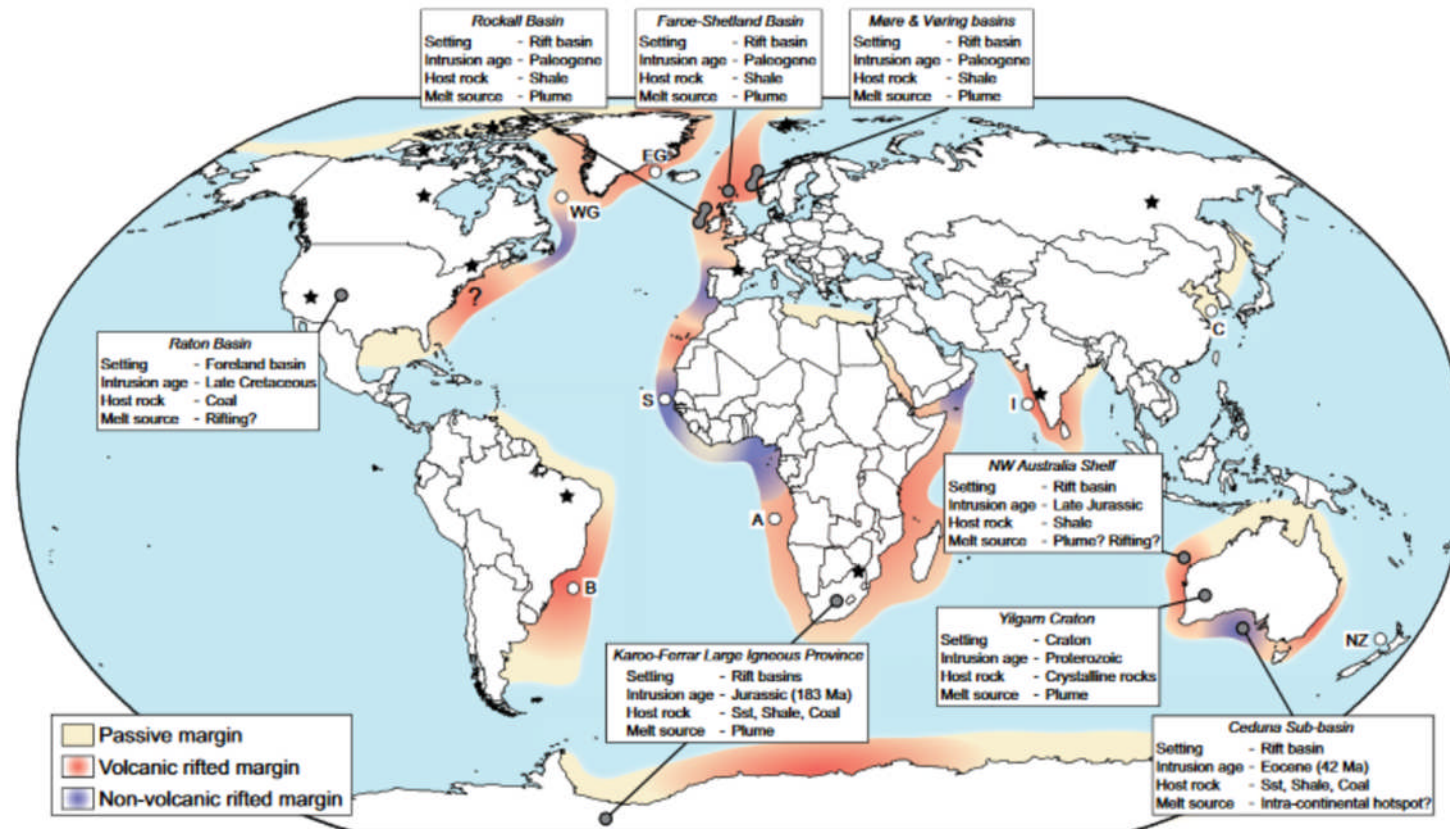


**Figure 8.5** – The global distribution of offshore sill complexes, including East Greenland, West Greenland, Brazil, Angola, Senegal, and China, from Magee et al. (2016). The techniques and workflows established in this thesis are transferable and can be used to study the impact of igneous intrusions on the potential and proven hydrocarbon systems in these regions.

## 8.5 Conclusions

Each chapter contains a number of conclusions specific to the work therein, here these points are reiterated.

- Converting seismic data in the frequency-amplitude domain can enhance the imaging of igneous intrusions compared to time-amplitude data alone, this can be achieved using standard spectral decomposition algorithms found in commercial software packages.
- The application of spectral decomposition to igneous bodies can aid in the interpretation of closely spaced, vertically stacked sills and the identification of discontinuities/faults within individual sills bodies.
- Re-interpreting sills using frequency-amplitude data helps to delineate ridges on the sill's surface, which can be used to infer magma flow directions. Understanding magma flow directions in turn helps to determine the magma source and emplacement direction.
- The intrusions and intrusion styles within the Faroe-Shetland Sill Complex vary significantly over a distance of less than 50 km around the NE Corona Ridge. The intrusions can be categorised into broad facies based on similarities in morphology, distribution and emplacement style.
- The pre-existing basin structure strongly influences magma supply and sill emplacement style. The northern splay of the Corona Ridge and other basement-bound faults are the main points of magma input into the area.
- Vertical dykes also provide a major mechanism for magma input into the basin and are concentrated in the main sediment depocentres such as the Flett Sub-basin.
- There is a noticeable reduction in magma supply from the northeast to southwest, which is reflected in the size and style of intrusion.
- Sensitivity analysis can help identify and quantify uncertainty when undertaking regional petroleum system modelling in frontier or data limited areas. In the case of the Faroe-Shetland Basin the greatest uncertainty is

attributed to the heat flow scenarios and the exact depth of the source rock beneath the basalt.

- Standard depth-uniform stretching models cannot account for anomalously high levels of post-rift subsidence following Paleocene rifting in the Faroe-Shetland Basin. It can however be explained using depth dependent stretching models.
- The application of flexural backstripping can help produce heat flow models which successfully account for depth-dependent stretching.
- Hydrocarbon maturation across the basin is strongly influenced by the depth of source rock burial, which is predominantly controlled by post-rift subsidence.
- Rapid, localised subsidence following Cretaceous rifting resulted in the Central Flett and Foula Sub-basins becoming over mature by the end Upper Cretaceous.
- Elevated heat flows during Paleocene rifting and the subsequent post-rift subsidence were responsible for increasing maturation across much of the Corona, NE Flett and Erelund Sub-basins.
- Overpressure develops as a response to both Cretaceous and Paleocene subsidence. Towards the northeast of the basin, a reduction in overpressure during Cenozoic inversion is attributed to enhanced maturation.
- Sill intrusions are capable of producing significant thermal aureoles, which raise the regional geotherm within rocks over 1 km away.
- The actual altered aureole is significantly smaller and is typically less than six times the sill thickness, within this aureole the heating effects of the sill are sufficient to cause significant maturation of organic matter.
- The timing and depth of sill emplacement across much of the basin is such that the heat flow anomalies associated with intrusion do not influence in-situ source rock maturation.
- Contact metamorphism due to sill intrusion can reduce the porosity of the host stratigraphy by up to 20%, which has potential implications for migration and reservoir quality.

- Overall the impact of the Faroe-Shetland Sill Complex on the petroleum system evolution of the Faroe-Shetland Basin is considered to be low.

## 8.6 Further Work

During the course of producing this thesis a number of ideas were formulated, which due to time or data constraints we not perused further, these ideas are briefly outlined below and provide a scope for further work.

- Whilst the interpretation of the Faroe-Shetland Sill Complex over the Corona Ridge yielded some interesting results, this still represents a relatively small study area when compared to the total distribution of sills across the basin. In order to fully appreciate the basin-wide controls on sill emplacement a similar study should be conducted towards the centre of the Corona Ridge and the Guron Sub-basin. This could also be used to test the emplacement model proposed in Chapter 5.
- It is clear from the intrusion modelling undertaken in Chapter 7 that the thermal impact of sill intrusion on the petroleum systems in the basin is minimal, except perhaps in the currently under-explored northeast Corona and Ereland Sub-basins. In contrast, the modelled porosity and permeability reduction associated with intrusion has important implications for hydrocarbon migration. In order to fully understand how sill intrusion influences migration, further modelling is required, in order to fully appreciate the impact of migration any future modelling should be 3D.
- The work in this thesis presents a case study, which demonstrates the structural controls on sill distribution and emplacement in the Faroe-Shetland Basin. It would be beneficial to conduct similar investigations on other volcanic margins across the world, such as the Norwegian Margin and offshore NW Australia. This would allow us to evaluate the model for sill emplacement presented here and determine if pre-existing basin structure is indeed a key factor in the emplacement of all sill complexes, or just a process which occurs in the highly segmented Faroe-Shetland Basin.

- As mentioned in Section 8.4 there are a number of other volcanic basins that are the site of active hydrocarbon exploration. The techniques established in Chapters 6 and 7 are transferable and can be used to assess the potential impact of sill intrusion on the hydrocarbon systems in those areas.

## References

### A

- AARNES, I., SVENSEN, H., CONNOLLY, J. A. & PODLADCHIKOV, Y. Y. 2010.** How contact metamorphism can trigger global climate changes: Modeling gas generation around igneous sills in sedimentary basins. *Geochimica et Cosmochimica Acta*, 74, 7179-7195.
- AARNES, I., SVENSEN, H., POLTEAU, S. & PLANKE, S. 2011.** Contact metamorphic devolatilization of shales in the Karoo Basin, South Africa, and the effects of multiple sill intrusions. *Chemical Geology*, 281, 181-194.
- ADDA, G. W. 2012.** Hydrocarbon generation and migration from Jurassic source rocks in the northern North Sea. Master of Sciences Thesis. Norwegian University of Science and Technology.
- AKI, K. & RICHARDS, P. G. 2002.** Quantitative seismology, 2nd. University Science Books.
- AL-HAJERI, M. M., AL SAEED, M., DERKS, J., FUCHS, T., HANTSCH, T., KAUEAUF, A., NEUMAIER, M., SCHENK, O., SWIENTEK, O. & TESSEN, N. 2009.** Basin and petroleum system modeling. *Oilfield Review*, 21, 14-29.
- ALLEN, P. A. & ALLEN, J. R. 2013.** Basin analysis: Principles and application to petroleum play assessment, John Wiley & Sons.
- ALSULAMI, S. L. 2014.** Tectonic Variation and Structural Evolution of the West Greenland Continental Margin. PhD Thesis.
- ANDERSON, D. L. 1994.** The sublithospheric mantle as the source of continental flood basalts; the case against the continental lithosphere and plume head reservoirs. *Earth and Planetary Science Letters*, 123, 269-280.
- ANNEN, C. & SPARKS, R. S. J. 2002.** Effects of repetitive emplacement of basaltic intrusions on thermal evolution and melt generation in the crust. *Earth and Planetary Science Letters*, 203, 937-955.
- ARAM, R. 1999.** West Greenland versus Vøring Basin: comparison of two deepwater frontier exploration plays. Geological Society, London, Petroleum Geology Conference series, 1999. Geological Society of London, 315-324.
- ARCHER, S. G., BERGMAN, S. C., ILIFFE, J., MURPHY, C. M. & THORNTON, M. 2005.** Palaeogene igneous rocks reveal new insights into the geodynamic evolution and petroleum potential of the Rockall Trough, NE Atlantic Margin. *Basin Research*, 17, 171-201.
- ASHCROFT, W. 2011.** A petroleum geologist's guide to seismic reflection, John Wiley & Sons.
- ASQUITH, G. B., KRYGOWSKI, D. & GIBSON, C. R. 2004.** Basic well log analysis, American Association of Petroleum Geologists Tulsa, OK.
- AYDIN, A. 2000.** Fractures, faults, and hydrocarbon entrapment, migration and flow. *Marine and petroleum geology*, 17, 797-814.

### B

- BACON, M., SIMM, R. & REDSHAW, T. 2007.** 3-D seismic interpretation, Cambridge University Press.
- BAILEY, N., BURWOOD, R. & HARRIMAN, G. 1990.** Application of pyrolysate carbon isotope and biomarker technology to organofacies definition and oil correlation problems in North Sea basins. *Organic Geochemistry*, 16, 1157-1172.

- BAILEY, N., WALKO, P. & SAUER, M. 1987.** Geochemistry and source rock potential of the west of Shetlands. *Petroleum Geology of North West Europe*. Graham & Trotman, London, 711-721.
- BARBER, P. 1988.** The Exmouth Plateau deep water frontier: a case history. *The North West Shelf, Australia: Proc. Pet. Expl. Soc. Aust. Symp*, 1988. 173-187.
- BARKER, C. & BONE, Y. 1995.** The minimal response to contact metamorphism by the Devonian Buchan Caves Limestone, Buchan Rift, Victoria, Australia. *Organic geochemistry*, 22, 151-164.
- BARR, D., SAVORY, K. E., FOWLER, S. R., ARMAN, K. & MCGARRITY, J. P. 2007.** Pre-development fracture modelling in the Clair field, west of Shetland. *Geological Society, London, Special Publications*, 270, 205-225.
- BARTON, C. A., ZOBACK, M. D. & MOOS, D. 1995.** Fluid flow along potentially active faults in crystalline rock. *Geology*, 23, 683-686.
- BELL, B. & BUTCHER, H. 2002.** On the emplacement of sill complexes: evidence from the Faroe-Shetland Basin. *Geological Society, London, Special Publications*, 197, 307-329.
- BELLIENI, G., COMIN-CHIARAMONTI, P., MARQUES, L., MELFI, A., PICCIRILLO, E. & STOLFA, D. 1984.** Low-pressure evolution of basalt sills from bore-holes in the Paraná Basin, Brazil. *Tschermaks mineralogische und petrographische Mitteilungen*, 33, 25-47.
- BELOTTI, H., REBORI, L. & IBANEZ, G. 1995.** Igneous reservoirs in triangle zones, Neuquén Basin, Argentina. *American Association of Petroleum Geologists*, 8.
- BEN-AWUAH, J., ANDRIAMIAJA, S., MIJINYAWA, A., ALI, A., SIDDIQUI, N. A. & ADDA, G. W. 2014.** Effect of Some Input Parameters on 3D Basin and Petroleum Systems Modelling: A Case Study of the Norwegian Section of the Northern North Sea. *Research Journal of Applied Sciences, Engineering and Technology*, 7, 3746-3762.
- BOND, G., KOMINZ, M. & SHERIDAN, R. 1995.** Continental terraces and rises. *Tectonics of sedimentary basins: Oxford, Blackwell Science*, 149-178.
- BOSTICK, N. H. 1971.** Thermal alteration of clastic organic particles as an indicator of contact and burial metamorphism in sedimentary rocks. *Geoscience and Man*, 3, 83-92.
- BRADLEY, J. 1965.** Intrusion of major dolerite sills. *Transactions of The Royal Society of New Zealand Geology*, 4, 27.
- BROWN, R., GALLAGHER, K. & DUANE, M. 1994.** A quantitative assessment of the effects of magmatism on the thermal history of the Karoo sedimentary sequence. *Journal of African Earth Sciences*, 18, 227-243.
- BRYAN, S. E. & ERNST, R. E. 2008.** Revised definition of large igneous provinces (LIPs). *Earth-Science Reviews*, 86, 175-202.
- BURNHAM, A. 1989.** A simple kinetic model of petroleum formation and cracking. Lawrence Livermore National Lab., CA (USA).
- BURNHAM, A. K. & SWEENEY, J. J. 1989.** A chemical kinetic model of vitrinite maturation and reflectance. *Geochimica et Cosmochimica Acta*, 53, 2649-2657.

## C

- CALLOT, J. P., GRIGNÉ, C., GEOFFROY, L. & BRUN, J. P. 2001.** Development of volcanic passive margins: Two-dimensional laboratory models. *Tectonics*, 20, 148-159.
- CAMPBELL, I. H. & GRIFFITHS, R. W. 1990.** Implications of mantle plume structure for the evolution of flood basalts. *Earth and Planetary Science Letters*, 99, 79-93.

- CARDOTT, B. 2014.** Thermal Maturity Assessment Of Early Oil Production From The Woodford Shale, Oklahoma, USA. *Abstracts of the 31st Annual Meeting of the Society for Organic Petrology: 2014*, 31.
- CARRUTH, A. 2003.** The Foinaven Field, Blocks 204/19 and 204/24a, UK North Sea. *Geological Society, London, Memoirs*, 20, 121-130.
- CARSLAW, H. S. & JAEGER, J. C. 1959.** Conduction of heat in solids. *Oxford: Clarendon Press, 1959, 2nd ed.*
- CARTWRIGHT, J. & HANSEN, D. M. 2006.** Magma transport through the crust via interconnected sill complexes. *Geology*, 34, 929-932.
- CARTWRIGHT, J., HUUSE, M. & APLIN, A. 2007.** Seal bypass systems. *AAPG bulletin*, 91, 1141-1166.
- CATHLES, L. M., ERENDI, A. & BARRIE, T. 1997.** How long can a hydrothermal system be sustained by a single intrusive event? *Economic Geology*, 92, 766-771.
- CHEN, Z., YAN, H., LI, J., ZHANG, G., ZHANG, Z. & LIU, B. 1999.** Relationship between Tertiary volcanic rocks and hydrocarbons in the Liaohe Basin, People's Republic of China. *AAPG bulletin*, 83, 1004-1014.
- CHEVALLIER, L. & WOODFORD, A. 1999.** Morpho-tectonics and mechanism of emplacement of the dolerite rings and sills of the western Karoo, South Africa. *South African Journal of Geology*, 102, 43-54.
- CHOPRA, S. & MARFURT, K. J. 2007.** Seismic attributes for prospect identification and reservoir characterization. *Society of Exploration Geophysicists and European Association of Geoscientists and Engineers.*
- CLAUSER, C. & HUENGES, E. 1995.** Thermal conductivity of rocks and minerals. *Rock physics & phase relations: A handbook of physical constants*, 105-126.
- CLAYTON, J. & BOSTICK, N. 1986.** Temperature effects on kerogen and on molecular and isotopic composition of organic matter in Pierre Shale near an igneous dike. *Organic geochemistry*, 10, 135-143.
- CLIFT, P. & LIN, J. 2001.** Preferential mantle lithospheric extension under the South China margin. *Marine and Petroleum Geology*, 18, 929-945.
- CLIFT, P. D. & TURNER, J. 1998.** Paleogene igneous underplating and subsidence anomalies in the Rockall-Faeroe-Shetland area. *Marine and Petroleum Geology*, 15, 223-243.
- COE, A. L. 2003.** *The sedimentary record of sea-level change*, Cambridge University Press.
- COFFIN, M. F. & ELDHOLM, O. 1992.** Volcanism and continental break-up: a global compilation of large igneous provinces. *Geological Society, London, Special Publications*, 68, 17-30.
- COFFIN, M. F. & ELDHOLM, O. 1994.** Large igneous provinces: crustal structure, dimensions, and external consequences. *Reviews of Geophysics*, 32, 1-36.
- CONEY, D., FYFE, T. B., RETAIL, P. & SMITH, P. J. 1993.** Clair appraisal: the benefits of a co-operative approach. 4, 1409-1420.
- COOPER, J. R., CRELLING, J. C., RIMMER, S. M. & WHITTINGTON, A. G. 2007.** Coal metamorphism by igneous intrusion in the Raton Basin, CO and NM: implications for generation of volatiles. *International Journal of Coal Geology*, 71, 15-27.
- COOPER, M., EVANS, A., LYNCH, D., NEVILLE, G. & NEWLEY, T. 1999.** The Foinaven Field: managing reservoir development uncertainty prior to start-up. Geological Society, London, Petroleum Geology Conference series, 1999. Geological Society of London, 675-682.
- CORREIA, M. & MAURY, R. 1975.** Thermal, mineralogical, and chemical effects of the intrusion of a basaltic dike in the Toarcian of the Causses. *Bull. Cent. Rech. Pau*, 9, 245-259.

- COURTILLOT, V., JAUPART, C., MANIGHETTI, I., TAPPONNIER, P. & BESSE, J. 1999.** On causal links between flood basalts and continental breakup. *Earth and Planetary Science Letters*, 166, 177-195.
- COWARD, M. 1990.** The Precambrian, Caledonian and Variscan framework to NW Europe. *Geological Society, London, Special Publications*, 55, 1-34.
- COWARD, M. 1995.** Structural and tectonic setting of the Permo-Triassic basins of northwest Europe. *Geological Society, London, Special Publications*, 91, 7-39.
- COWARD, M., ENFIELD, M. & FISCHER, M. 1989.** Devonian basins of Northern Scotland: extension and inversion related to Late Caledonian—Variscan tectonics. *Geological Society, London, Special Publications*, 44, 275-308.

## D

- DAVIES, R., BELL, B. R., CARTWRIGHT, J. A. & SHOULDERS, S. 2002.** Three-dimensional seismic imaging of Paleogene dike-fed submarine volcanoes from the northeast Atlantic margin. *Geology*, 30, 223-226.
- DAVIES, R., CLOKE, I., CARTWRIGHT, J., ROBINSON, A. & FERRERO, C. 2004.** Post-breakup compression of a passive margin and its impact on hydrocarbon prospectivity: An example from the Tertiary of the Faeroe-Shetland Basin, United Kingdom. *AAPG bulletin*, 88, 1-20.
- DEAN, K., MCLACHLAN, K. & CHAMBERS, A. 1999.** Rifting and the development of the Faeroe-Shetland Basin. Geological Society, London, Petroleum Geology Conference series, 1999. Geological Society of London, 533-544.
- DENNIS, L. W., MACIEL, G. E., HATCHER, P. G. & SIMONEIT, B. R. 1982.** <sup>13</sup>C nuclear magnetic resonance studies of kerogen from Cretaceous black shales thermally altered by basaltic intrusions and laboratory simulations. *Geochimica et Cosmochimica Acta*, 46, 901-907.
- DORÉ, A. 1992.** Synoptic palaeogeography of the northeast Atlantic seaway: Late Permian to Cretaceous. Geological Society, London, Special Publications, 62, 421-446.
- DORÉ, A. & LUNDIN, E. 1996.** Cenozoic compressional structures on the NE Atlantic margin; nature, origin and potential significance for hydrocarbon exploration. *Petroleum Geoscience*, 2, 299-311.
- DORÉ, A., LUNDIN, E., FICHLER, C. & OLESEN, O. 1997.** Patterns of basement structure and reactivation along the NE Atlantic margin. *Journal of the Geological Society*, 154, 85-92.
- DORÉ, A., LUNDIN, E., JENSEN, L., BIRKELAND, Ø., ELIASSEN, P. & FICHLER, C. 1999.** Principal tectonic events in the evolution of the northwest European Atlantic margin. Geological Society, London, Petroleum Geology Conference series, 1999. Geological Society of London, 41-61.
- DOW, W. G. 1977.** Kerogen studies and geological interpretations. *Journal of Geochemical Exploration*, 7, 79-99.
- DU TOIT, A. 1920.** The Karoo dolerites of South Africa: a study in hypabyssal injection. *Transactions of the Geological Society of South Africa*, 23, 1-42.
- DUTCHER, R. R., CAMPBELL, D. L. & THORNTON, C. P. 1966.** Coal metamorphism and igneous intrusives in Colorado.

## E

- EINSELE, G., GIESKES, J. M., CURRAY, J., MOORE, D. M., AGUAYO, E., AUBRY, M.-P., FORNARI, D., GUERRERO, J., KASTNER, M. & KELTS, K. 1980.** Intrusion of basaltic sills into highly porous sediments, and resulting hydrothermal activity. *Nature*, 283(5746), 441-445.

- ELDHOLM, O., SKOGSEID, J., PLANKE, S. & GLADCZENKO, T. P. 1995.** Volcanic margin concepts. *Rifted Ocean-Continent Boundaries*. Springer.
- ELDHOLM, O., THIEDE, J. & TAYLOR, E. 1989.** Evolution of the Vøring volcanic margin. *Proceedings of the ocean drilling program, scientific results, 1989*. 1033-1065.
- ELLIS, D., PASSEY, S., JOLLEY, D. & BELL, B. 2009.** Transfer zones: The application of new geological information from the Faroe Islands applied to the offshore exploration of intra basalt and sub-basalt strata. *Faroe Islands Exploration Conference: Proceedings of the 2nd Conference*. *Annales Societatis Scientiarum Færoensis, Tórshavn, 2009*. 205-226.
- ELLIS, D. & STOKER, M. S. 2014.** The Faroe–Shetland Basin: a regional perspective from the Paleocene to the present day and its relationship to the opening of the North Atlantic Ocean. *Geological Society, London, Special Publications, 397*, 11-31.
- EMERY, D. & MYERS, K. 2009.** *Sequence stratigraphy*, John Wiley & Sons.
- EPPELBAUM, L., KUTASOV, I. & PILCHIN, A. 2014.** Thermal properties of rocks and density of fluids. *Applied Geothermics*. Springer.
- EXON, N. & WILLCOX, J. 1978.** Geology and petroleum potential of Exmouth Plateau area off Western Australia. *AAPG Bulletin*, 62, 40-72.

## F

- FILHO, MIZUSAKI A, PIMENTEL AM & A, L. 2008.** Magmatism and petroleum exploration in the Brazilian Paleozoic basins. *Marine and petroleum geology*, 25, 143-151.
- FJELDSKAAR, W., HELSET, H., JOHANSEN, H., GRUNNALEITE, I. & HORSTAD, I. 2008.** Thermal modelling of magmatic intrusions in the Gjallar Ridge, Norwegian Sea: implications for vitrinite reflectance and hydrocarbon maturation. *Basin Research*, 20, 143-159.
- FLEITOUT, L., FROIDEVAUX, C. & YUEN, D. 1986.** Active lithospheric thinning. *Tectonophysics*, 132, 271-278.
- FLETCHER, R., KUSZNIR, N., ROBERTS, A. & HUNSDALE, R. 2013.** The formation of a failed continental breakup basin: The Cenozoic development of the Faroe-Shetland Basin. *Basin Research*, 25, 532-553.
- FRANCIS, E. 1982.** Magma and sediment-I Emplacement mechanism of late Carboniferous tholeiite sills in northern Britain President's anniversary address 1981. *Journal of the Geological Society*, 139, 1-20.

## G

- GALERNE, C. Y., GALLAND, O., NEUMANN, E.-R. & PLANKE, S. 2011.** 3D relationships between sills and their feeders: evidence from the Golden Valley Sill Complex (Karoo Basin) and experimental modelling. *Journal of Volcanology and Geothermal Research*, 202, 189-199.
- GALUSHKIN, Y. I. 1997.** Thermal effects of igneous intrusions on maturity of organic matter: A possible mechanism of intrusion. *Organic Geochemistry*, 26, 645-658.
- GANINO, C. & ARNDT, N. T. 2009.** Climate changes caused by degassing of sediments during the emplacement of large igneous provinces. *Geology*, 37, 323-326.
- GEOFFROY, L. 2005.** Volcanic passive margins. *Comptes Rendus Geoscience*, 337, 1395-1408.
- GEORGE, S. 1992.** Effect of igneous intrusion on the organic geochemistry of a siltstone and an oil shale horizon in the Midland Valley of Scotland. *Organic Geochemistry*, 18, 705-723.

- GOFF, J. 1983.** Hydrocarbon generation and migration from Jurassic source rocks in the E Shetland Basin and Viking Graben of the northern North Sea. *Journal of the Geological Society*, 140, 445-474.
- GOODCHILD, M., HENRY, K., HINKLEY, R. & IMBUS, S. 1999.** The Victory gas field, west of Shetland. Geological Society, London, Petroleum Geology Conference series, 1999. Geological Society of London, 713-724.
- GOULTY, N. & SCHOFIELD, N. 2008.** Implications of simple flexure theory for the formation of saucer-shaped sills. *Journal of Structural Geology*, 30, 812-817.
- GREEN, P., DUDDY, I., HEGARTY, K. & BRAY, R. 1999.** Early Tertiary heat flow along the UK Atlantic margin and adjacent areas. Geological Society, London, Petroleum Geology Conference series, 1999. Geological Society of London, 349-357.
- GREEN, P. F. 2002.** Early Tertiary paleo-thermal effects in Northern England: reconciling results from apatite fission track analysis with geological evidence. *Tectonophysics*, 349, 131-144.
- GRETENER, P. 1969.** On the mechanics of the intrusion of sills. *Canadian Journal of Earth Sciences*, 6, 1415-1419.
- GRIDLEY, J. & PARTYKA, G. 1997.** Processing and interpretational aspects of spectral decomposition. *SEG Technical Program Expanded Abstracts, Dallas*, 1055-1058.
- GUDMUNDSSON, A. 2011.** Deflection of dykes into sills at discontinuities and magma-chamber formation. *Tectonophysics*, 500, 50-64.
- GURBA, L. W. & WEBER, C. R. 2001.** Effects of igneous intrusions on coalbed methane potential, Gunnedah Basin, Australia. *International Journal of Coal Geology*, 46, 113-131.

## H

- HALL, M. & TROUILLOT, E. 2004.** Predicting stratigraphy with spectral decomposition. CSEG National Convention, Landmark Graphics, Calgary, Canada, 2004.
- HANSEN, D. M. 2006.** The morphology of intrusion-related vent structures and their implications for constraining the timing of intrusive events along the NE Atlantic margin. *Journal of the Geological Society*, 163, 789-800.
- HANSEN, D. M. & CARTWRIGHT, J. 2006a.** Saucer-shaped sill with lobate morphology revealed by 3D seismic data: implications for resolving a shallow-level sill emplacement mechanism. *Journal of the Geological Society*, 163, 509-523.
- HANSEN, D. M. & CARTWRIGHT, J. 2006b.** The three-dimensional geometry and growth of forced folds above saucer-shaped igneous sills. *Journal of Structural Geology*, 28, 1520-1535.
- HANSEN, D. M., CARTWRIGHT, J. A. & THOMAS, D. 2004.** 3D seismic analysis of the geometry of igneous sills and sill junction relationships. *Geological Society, London, Memoirs*, 29, 199-208.
- HANTSCH, T. & KAUERAUF, A. I. 2009.** *Fundamentals of basin and petroleum systems modeling*, Springer Science & Business Media.
- HAQ, B. U., HARDENBOL, J. & VAIL, P. R. 1987.** Chronology of fluctuating sea levels since the Triassic. *Science*, 235, 1156-1167.
- HART, B. S. 1999.** Definition of subsurface stratigraphy, structure and rock properties from 3-D seismic data. *Earth-Science Reviews*, 47, 189-218.
- HEDBERG, H. D. 1964.** Geologic aspects of origin of petroleum. *AAPG Bulletin*, 48, 1755-1803.
- HELLAND-HANSEN, D. 2009.** Rosebank—challenges to development from a subsurface perspective. Faroe Islands Exploration Conference, 2nd Conference Annales Societatis Scientiarum, Proceedings, Supplementum, 2009. 241-245.

- HERRIES, R., PODDUBIUK, R. & WILCOCKSON, P. 1999.** Solan, Strathmore and the back basin play, west of Shetland. Geological Society, London, Petroleum Geology Conference series, 1999. Geological Society of London, 693-712.
- HILL, R. I. 1991.** Starting plumes and continental break-up. *Earth and Planetary Science Letters*, 104, 398-416.
- HINDLE, A. D. 1997.** Petroleum migration pathways and charge concentration: A three-dimensional model. *AAPG bulletin*, 81, 1451-1481.
- HOLBROOK, W. & KELEMEN, P. 1993.** Large igneous province on the US Atlantic margin and implications for magmatism. *Nature*, 364, 29.
- HOLFORD, S., SCHOFIELD, N., JACKSON, C., MAGEE, C., GREEN, P. & DUDDY, I. 2013.** Impacts of Igneous Intrusions on Source and Reservoir Potential in Prospective Sedimentary Basins Along the Western Australian Continental Margin. West Australian Basins Symposium 18–21 August 2013, 2013.
- HOLFORD, S., SCHOFIELD, N., MACDONALD, J., DUDDY, I. & GREEN, P. 2012.** Seismic analysis of igneous systems in sedimentary basins and their impacts on hydrocarbon prospectivity: Examples from the southern Australian margin.
- HOLMES, A., GRIFFITH, C. & SCOTCHMAN, I. 1999.** The Jurassic petroleum system of the West of Britain Atlantic margin—an integration of tectonics, geochemistry and basin modelling. Geological Society, London, Petroleum Geology Conference series, 1999. Geological Society of London, 1351-1365.
- HOSHI, K. & OKUBO, S. 2010.** Hydrothermally dissolved dolerite reservoir in the Akita Basin, Japan. AAPG International Conference and Exhibition, 2010. 12-15.
- HUNT, J. 1996.** Petroleum geology and geochemistry. *Freeman, New York*.
- HUTTON, A. C. & HENSTRIDGE, D. A. 1985.** Pyrolysis of Tertiary oil shale by a dolerite intrusion, Stuart Deposit, Queensland, Australia. *Fuel*, 64, 546-552.

## I

- ILIFFE, J., ROBERTSON, A., WARD, G., WYNN, C., PEAD, S. & CAMERON, N. 1999.** The importance of fluid pressures and migration to the hydrocarbon prospectivity of the Faeroe–Shetland White Zone. Geological Society, London, Petroleum Geology Conference series, 1999. Geological Society of London, 601-611.

## J

- JACKSON, C. A., SCHOFIELD, N. & GOLENKOV, B. 2013.** Geometry and controls on the development of igneous sill-related forced folds: A 2-D seismic reflection case study from offshore southern Australia. *Geological Society of America Bulletin*, 125, 1874-1890.
- JACQUES, J. & REAVY, R. 1994.** Caledonian plutonism and major lineaments in the SW Scottish Highlands. *Journal of the Geological Society*, 151, 955-969.
- JAEGER, J. 1964.** Thermal effects of intrusions. *Reviews of Geophysics*, 2, 443-466.
- JAMTVEIT, B., SVENSEN, H., PODLADCHIKOV, Y. Y. & PLANKE, S. 2004.** Hydrothermal vent complexes associated with sill intrusions in sedimentary basins. *Physical geology of high-level magmatic systems*, 234, 233-241.
- JARVIS, G. T. & MCKENZIE, D. P. 1980.** Sedimentary basin formation with finite extension rates. *Earth and Planetary Science Letters*, 48, 42-52.

- JOLLEY, D., MORTON, A. & PRINCE, I. 2005.** Volcanogenic impact on phytogeography and sediment dispersal patterns in the NE Atlantic. Geological Society, London, Petroleum Geology Conference series, 2005. Geological Society of London, 969-975.
- JOLLEY, D. W. & BELL, B. R. 2002.** The evolution of the North Atlantic Igneous Province and the opening of the NE Atlantic rift. *Geological Society, London, Special Publications*, 197, 1-13.
- JOLLEY, D. W. & MORTON, A. C. 2007.** Understanding basin sedimentary provenance: evidence from allied phytogeographic and heavy mineral analysis of the Palaeocene of the NE Atlantic. *Journal of the Geological Society*, 164, 553-563.
- JONES, S., WIELENS, H., WILLIAMSON, M. C. & ZENTILLI, M. 2007.** Impact of magmatism on petroleum systems in the Sverdrup Basin, Canadian Arctic Islands, Nunavut: a numerical modelling study. *Journal of Petroleum Geology*, 30, 237-256.
- JOWITT, R., HINDLE, A., JONES, D. & ROSE, P. 1999.** Petroleum systems analysis of the Paleocene play in the West of Shetland area. Geological Society, London, Petroleum Geology Conference series, 1999. Geological Society of London, 1367-1381.

## K

- KAVANAGH, J. L., MENAND, T. & SPARKS, R. S. J. 2006.** An experimental investigation of sill formation and propagation in layered elastic media. *Earth and Planetary Science Letters*, 245, 799-813.
- KEAREY, P., BROOKS, M. & HILL, I. 2013.** *An introduction to geophysical exploration*, John Wiley & Sons.
- KEEN, C. 1985.** The dynamics of rifting: deformation of the lithosphere by active and passive driving forces. *Geophysical Journal International*, 80, 95-120.
- KENDRICK, J., HOOD, A. & CASTANO, J. 1978.** Petroleum-Generating potential of sediments from Leg 41, Deep sea drilling project.
- KERR, A. D. & POLLARD, D. D. 1998.** Toward more realistic formulations for the analysis of laccoliths. *Journal of Structural Geology*, 20, 1783-1793.
- KING, S. D. & ANDERSON, D. L. 1995.** An alternative mechanism of flood basalt formation. *Earth and Planetary Science Letters*, 136, 269-279.
- KUSZNIR, N., HUNSDALE, R. & ROBERTS, A. 2005.** Timing and magnitude of depth-dependent lithosphere stretching on the southern Lofoten and northern Vøring continental margins offshore mid-Norway: implications for subsidence and hydrocarbon maturation at volcanic rifted margins. Geological Society, London, Petroleum Geology Conference series, 2005. Geological Society of London, 767-783.
- KUSZNIR, N. & KARNER, G. 2007.** Continental lithospheric thinning and breakup in response to upwelling divergent mantle flow: application to the Woodlark, Newfoundland and Iberia margins. *Geological Society, London, Special Publications*, 282, 389-419.
- KUSZNIR, N. J., ROBERTS, A. M. & MORLEY, C. K. 1995.** Forward and reverse modelling of rift basin formation. *Geological Society, London, Special Publications*, 80, 33-56.

## L

- LAMERS, E. & CARMICHAEL, S. 1999.** The Paleocene deepwater sandstone play West of Shetland. Geological Society, London, Petroleum Geology Conference series, 1999. Geological Society of London, 645-659.
- LARSEN, M., RASMUSSEN, T. & HJELM, L. 2010.** Cretaceous revisited: exploring the syn-rift play of the Faroe–Shetland Basin. Geological Society, London, Petroleum Geology Conference series, 2010. Geological Society of London, 953-962.

- LEACH, H., HERBERT, N., LOS, A. & SMITH, R. 1999.** The Schiehallion development. Geological Society, London, Petroleum Geology Conference series, 1999. Geological Society of London, 683-692.
- LEAMAN, D. 1975.** Form, mechanism, and control of dolerite intrusion near Hobart, Tasmania. *Journal of the Geological Society of Australia*, 22, 175-186.
- LEE, G. H., KWON, Y. I., YOON, C. S., KIM, H. J. & YOO, H. S. 2006.** Igneous complexes in the eastern Northern South Yellow Sea Basin and their implications for hydrocarbon systems. *Marine and Petroleum Geology*, 23, 631-645.
- LEROY, M., GUEYDAN, F. & DAUTEUIL, O. 2008.** Uplift and strength evolution of passive margins inferred from 2-D conductive modelling. *Geophysical Journal International*, 172, 464-476.
- LEVELL, B., ARGENT, J., DORÉ, A. & FRASER, S. 2010.** Passive margins: overview. Geological Society, London, Petroleum Geology Conference series, 2010. Geological Society of London, 823-830.
- LOIZOU, N. 2005.** West of Shetland exploration unravelled—an indication of what the future may hold. *First Break*, 23, 53-59.
- LOIZOU, N. 2007.** Improving Exploration Success for Paleocene Vaila Formation Stratigraphic Traps West of Shetland. 69th EAGE Conference & Exhibition, 2007.
- LOIZOU, N. 2014.** Success in exploring for reliable, robust Paleocene traps west of Shetland. Geological Society, London, Special Publications, 397, 59-79.
- LONG, D., HOULT, R., HAFLIDASON, H., STEVENSON, A., RITCHIE, J., JOHNSON, H., DE HAAS, H., VAN WEERING, T. & MIENERT, J. 2003.** Mud mound? diapiric features in the Faroe-Shetland Channel. EGS-AGU-EUG Joint Assembly, 2003. 11201.

## M

- MACCAFERRI, F., BONAFEDE, M. & RIVALTA, E. 2011.** A quantitative study of the mechanisms governing dike propagation, dike arrest and sill formation. *Journal of Volcanology and Geothermal Research*, 208, 39-50.
- MAGEE, C., JACKSON, C. A.-L. & SCHOFIELD, N. 2013.** The influence of normal fault geometry on igneous sill emplacement and morphology. *Geology*, 41, 407-410.
- MAGEE, C., MUIRHEAD, J. D., KARVELAS, A., HOLFORD, S. P., JACKSON, C. A., BASTOW, I. D., SCHOFIELD, N., STEVENSON, C. T., MCLEAN, C. & MCCARTHY, W. 2016.** Lateral magma flow in mafic sill complexes. *Geosphere*, 12, 809-841.
- MALTHE-SØRENSEN, A., PLANKE, S., SVENSEN, H. & JAMTVEIT, B. 2004.** Formation of saucer-shaped sills. *Physical geology of high-level magmatic systems*. Geological Society, London, Special Publications, 234, 215-227.
- MANN, P., GAHAGAN, L. & GORDON, M. B. 2003.** Tectonic setting of the world's giant oil and gas fields. *AAPG Special Volumes*, 15-105.
- MARESH, J. & WHITE, R. S. 2005.** Seeing through a glass, darkly: strategies for imaging through basalt. *First Break*, 23, 27-33.
- MARSH, B. 2004.** A magmatic mush column rosetta stone: the McMurdo Dry Valleys of Antarctica. *Eos, Transactions American Geophysical Union*, 85, 497-502.
- MARSH, J. 1973.** Relationships between transform directions and alkaline igneous rock lineaments in Africa and South America. *Earth and Planetary Science Letters*, 18, 317-323.
- MASTERS, J. 2000.** The slow discovery of Dineh-bi-Keyah. *Mountain Geologist*, 37, 91-100.
- MATTER, J. M., GOLDBERG, D., MORIN, R. H. & STUTE, M. 2006.** Contact zone permeability at intrusion boundaries: new results from hydraulic testing and geophysical logging in the Newark Rift Basin, New York, USA. *Hydrogeology Journal*, 14, 689-699.

- MCKENZIE, D. 1978.** Some remarks on the development of sedimentary basins. *Earth and Planetary science letters*, 40, 25-32.
- MCKENZIE, D. 1984.** The generation and compaction of partially molten rock. *Journal of Petrology*, 25, 713-765.
- MENAND, T. 2008.** The mechanics and dynamics of sills in layered elastic rocks and their implications for the growth of laccoliths and other igneous complexes. *Earth and Planetary Science Letters*, 267, 93-99.
- MENAND, T., DE SAINT-BLANQUAT, M. & ANNEN, C. 2011.** Emplacement of magma pulses and growth of magma bodies. *Tectonophysics*, 500, 1-2.
- MENZIES, M. A. 2002.** Volcanic rifted margins, Geological Society of America.
- MEYERHOFF, A. A. 1980.** Geology and petroleum fields in Proterozoic and Lower Cambrian strata, Lena-Tunguska petroleum province, eastern Siberia, USSR. AAPG Special Volumes, 362.
- MILANI, E. J. & ZALAN, P. V. 1999.** An outline of the geology and petroleum systems of the Paleozoic interior basins of South America. *Episodes*, 22, 199-205.
- MILES, A. & CARTWRIGHT, J. 2010.** Hybrid flow sills: A new mode of igneous sheet intrusion. *Geology*, 38, 343-346.
- MITCHELL, S., BEAMISH, G., WOOD, M., MALACEK, S., ARMENTROUT, J., DAMUTH, J. & OLSON, H. 1993.** Paleogene sequence stratigraphic framework of the Faeroe Basin. Geological Society, London, Petroleum Geology Conference series, 1993. Geological Society of London, 1011-1023.
- MOHAMMED, M., PATON, D., COLLIER, R., HODGSON, N. & NEGONGA, M. 2016.** Interaction of crustal heterogeneity and lithospheric processes in determining passive margin architecture on the southern Namibian margin. Geological Society, London, Special Publications, 438, SP438. 9.
- MORGAN, P. 1983.** Constraints on rift thermal processes from heat flow and uplift. *Tectonophysics*, 94, 277-298.
- MOY, D. & IMBER, J. 2009.** A critical analysis of the structure and tectonic significance of rift-oblique lineaments ('transfer zones') in the Mesozoic–Cenozoic succession of the Faroe–Shetland Basin, NE Atlantic margin. *Journal of the Geological Society*, 166, 831-844.

## N

- NADIN, P., KUSZNIR, N. & CHEADLE, M. 1997.** Early Tertiary plume uplift of the North Sea and Faeroe-Shetland basins. *Earth and Planetary Science Letters*, 148, 109-127.
- NAYLOR, P., BELL, B., JOLLEY, D., DURNALL, P. & FREDSTED, R. 1999.** Palaeogene magmatism in the Faeroe–Shetland Basin: influences on uplift history and sedimentation. Geological Society, London, Petroleum Geology Conference series, 1999. Geological Society of London, 545-558.
- NELSON, C. E. 2010.** Understanding the offshore flood basalt sequence using onshore volcanic facies analogues: an example from the Faroe–Shetland basin. *Geol. Mag.*, 146, 353-367.

## O

- OLSON, P., SCHUBERT, G., ANDERSON, C. & GOLDMAN, P. 1988.** Plume formation and lithosphere erosion: A comparison of laboratory and numerical experiments. *Journal of Geophysical Research: Solid Earth*, 93, 15065-15084.

## P

- PÁLFY, J. & SMITH, P. L. 2000.** Synchrony between Early Jurassic extinction, oceanic anoxic event, and the Karoo-Ferrar flood basalt volcanism. *Geology*, 28, 747-750.
- PARNELL, J., CAREY, P., GREEN, P. & DUNCAN, W. 1999.** Hydrocarbon migration history, West of Shetland: integrated fluid inclusion and fission track studies. Geological Society, London, Petroleum Geology Conference series, 1999. Geological Society of London, 613-625.
- PARTYKA, G., GRIDLEY, J. & LOPEZ, J. 1999.** Interpretational applications of spectral decomposition in reservoir characterization. *The Leading Edge*, 18, 353-360.
- PASSEY, S. & HITCHEN, K. 2011.** Cenozoic (igneous). *Geology of the Faroe–Shetland Basin and Adjacent Areas*. British Geological Survey and Jarøfeingi Research Report, RR/11/01, 209-228.
- PASSEY, S. R. & JOLLEY, D. W. 2008.** A revised lithostratigraphic nomenclature for the Palaeogene Faroe Islands Basalt group, NE Atlantic Ocean. *Earth and Environmental Science Transactions of the Royal Society of Edinburgh*, 99, 127-158.
- PASSEY, S. R. & VARMING, T. 2010.** Surface interpolation within a continental flood basalt province: An example from the Palaeogene Faroe Islands Basalt Group. *Journal of Structural Geology*, 32, 709-723.
- PATON, D. A., DI PRIMIO, R., KUHLMANN, G., VAN DER SPUY, D. & HORSFIELD, B. 2007.** Insights into the petroleum system evolution of the southern Orange Basin, South Africa. *South African Journal of Geology*, 110, 261-274.
- PÉRON-PINVIDIC, G., MANATSCHAL, G., MINSHULL, T. A. & SAWYER, D. S. 2007.** Tectonosedimentary evolution of the deep Iberia-Newfoundland margins: Evidence for a complex breakup history. *Tectonics*, 26.
- PERREGAARD, J. & SCHIENER, E. 1979.** Thermal alteration of sedimentary organic matter by a basalt intrusive (Kimmeridgian shales, Milne Land, East Greenland). *Chemical Geology*, 26, 331-343.
- PETERS, K., SIMONEIT, B., BRENNER, S. & KAPLAN, I. 1978.** Vitrinite reflectance-temperature determinations for intruded Cretaceous black shale in the Eastern Atlantic. The AAPG/Datapages Combined Publications Database, Pacific Section SEPM, 53-58.
- PETFORD, N. & MCCAFFREY, K. 2003.** Hydrocarbons in crystalline rocks: an introduction. Geological Society, London, Special Publications, 214, 1-5.
- PETTINGILL, H. S. & WEIMER, P. 2002.** Worldwide deepwater exploration and production: Past, present, and future. *The Leading Edge*, 21, 371-376.
- PLANKE, S., ALVESTAD, E. & ELDHOLM, O. 1999.** Seismic characteristics of basaltic extrusive and intrusive rocks. *The Leading Edge*, 18, 342-348.
- PLANKE, S., RASMUSSEN, T., REY, S. & MYKLEBUST, R. 2005.** Seismic characteristics and distribution of volcanic intrusions and hydrothermal vent complexes in the Vøring and Møre basins. Geological Society, London, Petroleum Geology Conference series, 2005. Geological Society of London, 833-844.
- PLANKE, S., SYMONDS, P. A., ALVESTAD, E. & SKOGSEID, J. 2000.** Seismic volcanostratigraphy of large-volume basaltic extrusive complexes on rifted margins. *Journal of Geophysical Research: Solid Earth* (1978–2012), 105, 19335-19351.
- POLLARD, D. D. & JOHNSON, A. M. 1973.** Mechanics of growth of some laccolithic intrusions in the Henry Mountains, Utah, II: bending and failure of overburden layers and sill formation. *Tectonophysics*, 18, 311-354.
- POLTEAU, S., MAZZINI, A., GALLAND, O., PLANKE, S. & MALTHE-SØRENSEN, A. 2008.** Saucer-shaped intrusions: occurrences, emplacement and implications. *Earth and Planetary Science Letters*, 266, 195-204.

**PRAPTONO, S. H., MURTI, B. & MAIR, D. 2003.** Spectral Decomposition: Extending the Limits of Seismic Resolution for Reservoir Delineation. The AAPG/Datapages Combined Publications Database, Indonesian Petroleum Association.

**PRATSCH, J. C. 1978.** Future hydrocarbon exploration on continental margins and plate tectonics. *Journal of Petroleum Geology*, 1, 95-105.

**PUJOL, J. & SMITHSON, S. 1991.** Seismic wave attenuation in volcanic rocks from VSP experiments. *Geophysics*, 56, 1441-1455.

## Q

**QINGPING, L. 2006.** The situation and challenges for deepwater oil and gas exploration and exploitation in China. *China Offshore Oil and Gas*, 2, 130-133.

## R

**RATEAU, R., SCHOFIELD, N. & SMITH, M. 2013.** The potential role of igneous intrusions on hydrocarbon migration, West of Shetland. *Petroleum Geoscience*, 19, 259-272.

**RAY, R. 1989.** Seismic expressions of igneous sills in San Juan Sag, south central Colorado. *Am Assoc Pet Geol Bull*, 73, 1159.

**RAYMOND, A. C. & MURCHISON, D. G. 1988.** Development of organic maturation in the thermal aureoles of sills and its relation to sediment compaction. *Fuel*, 67, 1599-1608.

**RIDER, M. H. 1986.** The geological interpretation of well logs. John Wiley and Sons.

**RIMMER, S. M., YOKSOULIAN, L. E. & HOWER, J. C. 2009.** Anatomy of an intruded coal, I: effect of contact metamorphism on whole-coal geochemistry, Springfield (No. 5)(Pennsylvanian) coal, Illinois Basin. *International Journal of Coal Geology*, 79, 74-82.

**RITCHIE, J., GATLIFF, R. & RICHARDS, P. 1999.** Early Tertiary magmatism in the offshore NW UK margin and surrounds. Geological Society, London, *Petroleum Geology Conference series*, 1999. Geological Society of London, 573-584.

**RITCHIE, J., GATLIFF, R. & RIDING, J. 1996.** Stratigraphic nomenclature of the UK north west margin, 1. Pre-Tertiary lithostratigraphy: British Geological Survey, 193p.

**RITCHIE, J. & HITCHEN, K. 1996.** Early Paleogene offshore igneous activity to the northwest of the UK and its relationship to the North Atlantic Igneous Province. Geological Society, London, *Special Publications*, 101, 63-78.

**RITCHIE, J., JOHNSON, H. & KIMBELL, G. 2003.** The nature and age of Cenozoic contractional deformation within the NE Faroe-Shetland Basin. *Marine and Petroleum Geology*, 20, 399-409.

**RITCHIE, J., ZISKA, H., JOHNSON, H. & EVANS, D. 2011.** Geology of the Faroe-Shetland Basin and adjacent areas.

**ROBERTS, A., WHITE, R., LUNNON, Z., CHRISTIE, P. & SPITZER, R.** Imaging magmatic rocks on the Faroes Margin. Geological Society, London, *Petroleum Geology Conference series*, 2005. Geological Society of London, 755-766.

**ROBERTS, A. M., KUSZNIR, N. J., YIELDING, G. & STYLES, P. 1998.** 2D flexural backstripping of extensional basins: the need for a sideways glance. *Petroleum Geoscience*, 4, 327-338.

**ROBERTS, J. R. 1970.** The intrusion of magma into brittle rocks. In: NEWALL, G. & RAST, N. (eds), 287-338. Mechanism of igneous intrusion, *Geol. J. Spec. Issue No. Geol. J. Spec.*, 380.

- ROBERTSON, E. C. 1988.** Thermal properties of rocks. Open-File Report. US Geological Survey. 88-441.
- RODNOVA, E. 1976.** Change in collector attributes of sediments in contact zone of traps in central part of Tungussian syncline. *Voprosy geologii i neftegasonosnosti Tungusskoy sineklize*. Trudy VSEGEI Leningrad.
- ROHRMAN, M. 2007.** Prospectivity of volcanic basins: Trap delineation and acreage de-risking. *AAPG bulletin*, 91, 915-939.
- ROHRMAN, M. 2012.** Seismic Delineation of Igneous Sheet Complexes on the Exmouth Plateau (NW Australia): Origin, Emplacement Mechanism and Implications for Petroleum Generation. *Search and Discovery Article*, 10444.
- ROSE, P. R. 1987.** Dealing with risk and uncertainty in exploration: how can we improve? *AAPG Bulletin*, 71, 1-16.
- ROSS, P.-S., PEATE, I. U., MCCLINTOCK, M., XU, Y. G., SKILLING, I. P., WHITE, J. D. & HOUGHTON, B. F. 2005.** Mafic volcanoclastic deposits in flood basalt provinces: a review. *Journal of Volcanology and Geothermal Research*, 145, 281-314.
- ROYDEN, L. & KEEN, C. 1980.** Rifting process and thermal evolution of the continental margin of eastern Canada determined from subsidence curves. *Earth and Planetary Science Letters*, 51, 343-361.
- RUMPH, B., REAVES, C., ORANGE, V. & ROBINSON, D. 1993.** Structuring and transfer zones in the Faeroe Basin in a regional tectonic context. *Geological Society, London, Petroleum Geology Conference series*, 1993. Geological Society of London, 999-1009.
- RYAN, P. & DEWEY, J. 1997.** Continental eclogites and the Wilson Cycle. *Journal of the Geological Society*, 154, 437-442.

## S

- SAUNDERS, A., FITTON, J., KERR, A. C., NORRY, M. & KENT, R. 1997.** The north Atlantic igneous province. *Large igneous provinces: Continental, oceanic, and planetary flood volcanism*, 45-93.
- SAXBY, J. & STEPHENSON, L. 1987.** Effect of an igneous intrusion on oil shale at Rundle (Australia). *Chemical geology*, 63, 1-16.
- SCHOFIELD, N., HOLFORD, S., MILLETT, J., BROWN, D., JOLLEY, D., PASSEY, S., MUIRHEAD, D., GROVE, C., MAGEE, C. & MURRAY, J. 2015.** Regional Magma Plumbing and emplacement mechanisms of the Faroe-Shetland Sill Complex: Implications for magma transport and petroleum systems within sedimentary basins. *Basin Research*.
- SCHOFIELD, N. & JOLLEY, D. W. 2013.** Development of intra-basaltic lava-field drainage systems within the Faroe-Shetland Basin. *Petroleum Geoscience*, 19, 273-288.
- SCHOFIELD, N., STEVENSON, C. & RESTON, T. 2010.** Magma fingers and host rock fluidization in the emplacement of sills. *Geology*, 38, 63-66.
- SCHOFIELD, N. J., BROWN, D. J., MAGEE, C. & STEVENSON, C. T. 2012.** Sill morphology and comparison of brittle and non-brittle emplacement mechanisms. *Journal of the Geological Society*, 169, 127-141.
- SCHULL, T. J. 1988.** Rift basins of interior Sudan: petroleum exploration and discovery. *AAPG bulletin*, 72, 1128-1142.
- SCHUTTER, S. R. 2003.** Hydrocarbon occurrence and exploration in and around igneous rocks. *Geological Society, London, Special Publications*, 214, 7-33.
- SCOTCHMAN, I., CARR, A. & PARNELL, J. 2006.** Hydrocarbon generation modelling in a multiple rifted and volcanic basin: a case study in the Foinaven Sub-basin, Faroe-Shetland Basin, UK Atlantic margin. *Scottish Journal of Geology*, 42, 1-19.

- SCOTCHMAN, I. & DORÉ, A. 1995.** A regional appraisal of source rocks north and west of Britain and Ireland. *AAPG Bulletin*, 79.
- SCOTCHMAN, I., GRIFFITH, C., HOLMES, A. & JONES, D. 1998.** The Jurassic petroleum system north and west of Britain: a geochemical oil-source correlation study. *Organic Geochemistry*, 29, 671-700.
- SCOTCHMAN, I. & THOMAS, J. 1995.** Maturity and hydrocarbon generation in the Slyne Trough, northwest Ireland. Geological Society, London, Special Publications, 93, 385-411.
- SENGER, K., PLANKE, S., POLTEAU, S., OGATA, K. & SVENSEN, H. 2014.** Sill emplacement and contact metamorphism in a siliciclastic reservoir on Svalbard, Arctic Norway. *NORWEGIAN JOURNAL OF GEOLOGY*, 94, 155-169.
- SERRA, O. 1983.** Fundamentals of well-log interpretation.
- SHAW, F., WORTHINGTON, M., WHITE, R., ANDERSEN, M. & PETERSEN, U. 2008.** Seismic attenuation in Faroe Islands basalts. *Geophysical Prospecting*, 56, 5-20.
- SHERIFF, R. E. & GELDART, L. P. 1995.** Exploration seismology, Cambridge university press.
- SIMONET, B. R., BRENNER, S., PETERS, K. & KAPLAN, I. 1981.** Thermal alteration of Cretaceous black shale by diabase intrusions in the Eastern Atlantic—II. Effects on bitumen and kerogen. *Geochimica et Cosmochimica Acta*, 45, 1581-1602.
- SINHA, S., ROUTH, P. S., ANNO, P. D. & CASTAGNA, J. P. 2005.** Spectral decomposition of seismic data with continuous-wavelet transform. *Geophysics*, 70, P19-P25.
- SKOGSEID, J., PLANKE, S., FALEIDE, J. I., PEDERSEN, T., ELDHOLM, O. & NEVERDAL, F. 2000.** NE Atlantic continental rifting and volcanic margin formation. *SPECIAL PUBLICATION-GEOLOGICAL SOCIETY OF LONDON*, 167, 295-326.
- SMALLWOOD, J. & KIRK, W. 2005.** Paleocene exploration in the Faroe–Shetland Channel: disappointments and discoveries. Geological Society, London, Petroleum Geology Conference series, 2005. Geological Society of London, 977-991.
- SMALLWOOD, J. & WHITE, R. 2002.** Ridge-plume interaction in the North Atlantic and its influence on continental breakup and seafloor spreading. Geological Society, London, Special Publications, 197, 15-37.
- SMALLWOOD, J. R. 2009.** Back-stripped 3D seismic data: A new tool applied to testing sill emplacement models. *Petroleum Geoscience*, 15, 259-268.
- SMALLWOOD, J. R. & MARESH, J. 2002.** The properties, morphology and distribution of igneous sills: modelling, borehole data and 3D seismic from the Faroe-Shetland area. Geological Society, London, Special Publications, 197, 271-306.
- SØRENSEN, A. B. 2003.** Cenozoic basin development and stratigraphy of the Faroes area. *Petroleum Geoscience*, 9, 189-207.
- SPENCER, A., BIRKELAND, Ø., KNAG, G. & FREDSTED, R. 1999.** Petroleum systems of the Atlantic margin of northwest Europe. Geological Society, London, Petroleum Geology Conference series, 1999. Geological Society of London, 231-246.
- STOKER, M., HOULT, R., NIELSEN, T., HJELSTUEN, B., LABERG, J., SHANNON, P., PRAEG, D., MATHIESEN, A., VAN WEERING, T. & MCDONNELL, A. 2005.** Sedimentary and oceanographic responses to early Neogene compression on the NW European margin. *Marine and Petroleum Geology*, 22, 1031-1044.
- SUN, S., CASTAGNA, J. P. & SIEGFRIED, R. W. 2002.** Examples of wavelet transform time-frequency analysis in direct hydrocarbon detection. 2002 SEG Annual Meeting, 2002. Society of Exploration Geophysicists.
- SVENSEN, H., JAMTVEIT, B., PLANKE, S. & CHEVALLIER, L. 2006.** Structure and evolution of hydrothermal vent complexes in the Karoo Basin, South Africa. *Journal of the Geological Society*, 163, 671-682.

**SVENSEN, H., PLANKE, S., MALTHER-SØRENSEN, A., JAMTVEIT, B., MYKLEBUST, R., EIDEM, T. R. & REY, S. S. 2004.** Release of methane from a volcanic basin as a mechanism for initial Eocene global warming. *Nature*, 429, 542-545.

**SWEENEY, J. J. & BURNHAM, A. K. 1990.** Evaluation of a simple model of vitrinite reflectance based on chemical kinetics (1). *AAPG Bulletin*, 74, 1559-1570.

**SYKES, L. R. 1978.** Intraplate seismicity, reactivation of preexisting zones of weakness, alkaline magmatism, and other tectonism postdating continental fragmentation. *Reviews of Geophysics*, 16, 621-688.

## T

**THOMPSON, R. N. & GIBSON, S. A. 1991.** Subcontinental mantle plumes, hotspots and pre-existing thinspots. *Journal of the Geological Society*, 148, 973-977.

**THOMSON, K. 2004.** Sill complex geometry and internal architecture: a 3D seismic perspective. *Physical geology of high-level magmatic systems*. Geological Society, London, Special Publications, 234, 229-232.

**THOMSON, K. 2007.** Determining magma flow in sills, dykes and laccoliths and their implications for sill emplacement mechanisms. *Bulletin of Volcanology*, 70, 183-201.

**THOMSON, K. & SCHOFIELD, N. 2008.** Lithological and structural controls on the emplacement and morphology of sills in sedimentary basins. *Geological Society, London, Special Publications*, 302, 31-44.

**TRUDE, J., CARTWRIGHT, J., DAVIES, R. J. & SMALLWOOD, J. 2003.** New technique for dating igneous sills. *Geology*, 31, 813-816.

**TRUDE, K. 2004.** Kinematic Indicators for Shallow Level Igneous Intrusions from 3D Seismic Data: Evidence of Flow Direction and Feeder Location. *Geological Society, London, Memoirs*, 29, 209-218.

**TURNER, J. & SCRUTTON, R. 1993.** Subsidence patterns in western margin basins: evidence from the Faeroe–Shetland Basin. *Geological Society, London, Petroleum Geology Conference series*, 1993. Geological Society of London, 975-983.

**TWETO, O. 1951.** Form and structure of sills near Pando, Colorado. *Geological Society of America Bulletin*, 62, 507-532.

## V

**VALENTINE, G. A. & KROGH, K. E. 2006.** Emplacement of shallow dikes and sills beneath a small basaltic volcanic center—The role of pre-existing structure (Paiute Ridge, southern Nevada, USA). *Earth and Planetary Science Letters*, 246, 217-230.

## W

**WANG, D., LU, X., ZHANG, X., XU, S., HU, W. & WANG, L. 2007.** Heat-model analysis of wall rocks below a diabase sill in Huimin Sag, China compared with thermal alteration of mudstone to carbargillite and hornfels and with increase of vitrinite reflectance. *Geophysical Research Letters*, 34.

**WANG, D. & MANGA, M. 2015.** Organic matter maturation in the contact aureole of an igneous sill as a tracer of hydrothermal convection. *Journal of Geophysical Research: Solid Earth*, 120, 4102-4112.

- WELTE, D. H., HORSFIELD, B. & BAKER, D. R. 2012.** Petroleum and basin evolution: insights from petroleum geochemistry, geology and basin modeling, Springer Science & Business Media.
- WELTE, D. H. & YALÇIN, M. N. 1988.** Basin modelling—A new comprehensive method in petroleum geology. *Organic Geochemistry*, 13, 141-151.
- WERNICKE, B. 1985.** Uniform-sense normal simple shear of the continental lithosphere. *Canadian Journal of Earth Sciences*, 22, 108-125.
- WHITE, N., THOMPSON, M. & BARWISE, T. 2003a.** Understanding the thermal evolution of deep-water continental margins. *Nature*, 426, 334-343.
- WHITE, R. 1988.** A hot-spot model for early Tertiary volcanism in the N Atlantic. Geological Society, London, Special Publications, 39, 3-13.
- WHITE, R. & MCKENZIE, D. 1989.** Magmatism at rift zones: the generation of volcanic continental margins and flood basalts. *Journal of Geophysical Research: Solid Earth*, 94, 7685-7729.
- WHITE, R. S., SMALLWOOD, J. R., FLIEDNER, M. M., BOSLAUGH, B., MARESH, J. & FRUEHN, J. 2003b.** Imaging and regional distribution of basalt flows in the Faeroe-Shetland Basin. *Geophysical Prospecting*, 51, 215-231.
- WHITE, R. S., SPITZER, R., CHRISTIE, P., ROBERTS, A., LUNNON, Z., MARESH, J. & GROUP, I. W. 2005.** Seismic imaging through basalt flows on the Faroes Shelf. *Proceedings of the 1st Faroe Islands Exploration Conference: Annal. Soc. Scient. Færoensis, Supplementum*, 2005. 11-31.
- WITTE, J., BONORA, M., CARBONE, C. & ONCKEN, O. 2012.** Fracture evolution in oil-producing sills of the Rio Grande Valley, northern Neuquen Basin, Argentina. *AAPG bulletin*, 96, 1253-1277.
- WOOD, A. M., PATON, D. A. & COLLIER, R. E. L. 2015.** The missing complexity in seismically imaged normal faults: what are the implications for geometry and production response? Geological Society, London, Special Publications, 421, 213-230.
- WRIGHT, K., A.M. 2012.** Seismic Stratigraphy and Geomorphology of Palaeocene Volcanic Rocks, Faroe-Shetland Basin. PhD.
- WYGRALA, B. 1989.** Integrated study of an oil field in the southern Po basin, northern Italy. *Publikationen vor 2000*.

## X

- XIA, L. 1999.** Spectral Analysis of seismic data using wavelet transform, Thesis, University of Oklahoma.

## Z

- ZIEGLER, P. A. 1988.** Evolution of the Arctic-North Atlantic and the Western Tethys--A Visual Presentation of a Series of Paleogeographic-Paleotectonic Maps. *Mem.-Am. Assoc. Pet. Geol*, 43, 164-196.



